# Designing Multiphase Step-Growth Polymers for Advanced Technologies: From Electromechanical Transducers to Additive Manufacturing

Benjamin Tyler White

Dissertation submitted to the faculty of the Virginia Polytechnic Institute and State University in partial fulfillment of the requirements for the degree of

Doctor of Philosophy

In

Macromolecular Science and Engineering

Timothy E. Long, Chair

Christopher B. Williams

Michael J. Bortner

John B. Matson

Robert B. Moore

April 23, 2021

Blacksburg, VA

Keywords: step-growth polymerization, ionic liquids, additive manufacturing, electromechanical transducers, polyurethanes, polyureas

# Designing Multiphase Step-Growth Polymers for Advanced Technologies: From Electromechanical Transducers to Additive Manufacturing

B. Tyler White

## Abstract

The synthesis and characterization of step-growth polymers with novel monomers provided materials with tailored properties for emerging technologies. Specifically, multiphase materials (i.e., microphase separated block copolymers) exploit the synergistic relationship of combining polymers with disparate thermal and mechanical properties. The introduction of intramolecular interactions such as hydrogen and ionic bonding into these polymers further tailored their properties for applications including elastomers, electromechanical transducers, and additive manufacturing (AM). A review of recent literature revealed the material properties required for polymeric materials in electromechanical transducers, which aided in the design of polymers for this application.

An isocyanate-, catalyst-, and solvent-free approach facilitated the synthesis of segmented polyureas with tunable thermal and mechanical properties. These materials found use as high dielectric elastomers and water-soluble polymers for extrusion-based AM dependent on the backbone composition. Vat photopolymerization (VP) AM served as a technique to 3D printed novel unsaturated polyester resins (UPR). Incorporating a phosphonium ionic liquid as a reactive diluent replaced styrene and reduced the volatility of commonly used UPRs. VP successfully provided 3D structures from these UPRs that demonstrated limited ionic conductivities. An extensive review of the literature surrounding the structure-property relationships of charged block copolymers with varying architectures helped to inform the synthesis of novel, cationic step-

growth polymers. The synthesis of a new phosphonium IL facilitated the synthesis of a segmented polyurethane containing a phosphonium-functionalized soft segment for the first time. This phosphonium polyurethane exhibited ionic conductivities comparable to literature examples of block copolymers used for ionic polymer transducers, which suggests that these materials may serve for this application as well. Carbonyldiimidazole provides a novel route towards synthesizing imidazolium ionenes with unique backbone structures. The coupling of poly(ethylene glycol) dibromides with a bis-carbonylimidazole monomer and a commercial aliphatic dibromide led to the formation of segmented imidazolium ionenes. These polymers exhibited significant atmospheric water uptake as well as water solubility. However, the physical properties of the materials suggested that the synthetic procedure resulted in low molecular weights. Suggested future work provides methods for circumventing this issue and proposes next steps for all the projects discussed herein.

# Designing Multiphase Step-Growth Polymers for Advanced Technologies: From Electromechanical Transducers to Additive Manufacturing

B. Tyler White

## General Audience Abstract

Emerging technologies require new polymeric materials with intentionally designed properties. Step-growth polymers such as polyesters, polyurethanes, and polyureas find use in many applications of our everyday lives. Although these materials have served mainly as commodity plastics historically, a reimagining of their syntheses and chemical structures makes them accessible for modern technologies. For example, applying green chemistry principles to the synthesis of polyureas resulted in a less toxic synthetic procedure. Polyureas synthesized through this method exhibited elastic properties comparable to classical polyureas and displayed high dielectric constants, which lend them towards use in dielectric elastomer actuators. This chemistry also allowed for the synthesis of water-soluble polyureas, which served as a material for low temperature extrusion additive manufacturing, colloquially known as 3D printing. Vat photopolymerization describes another type of 3D printing that involves the selective curing of liquid resins with light to form a 3D structure. Employing a reactive ionic liquid monomer with a commercially-relevant unsaturated polyester allowed for a nontoxic method of printing these materials, which also imparted ionic conductivity. Finally, the synthesis of positively charged polyurethanes and ionenes led to the production of ionically conductive materials that may find use in polymeric transducers.

To my wife, Natalie, and my son, Asa, for whom this taxing endeavor was undertaken.

# Acknowledgements

I must first express my profound gratitude to Prof. Tim Long for allowing me the privilege of working in his research group. Over the past five years, he has continually pushed me beyond my limitations, and I am undoubtedly an immeasurably better scientist today because of it. I am continually inspired by his passion for science and his innovative outlook on the future polymers and polymer education. Working alongside Prof. Long has convinced me to whole-heartedly embrace his philosophy of performing "use inspired basic research", which I believe has positioned me perfectly for a career in industry. I am beyond grateful for the countless opportunities I have been presented with while working in this group from peer reviewing papers to leading industrially funded projects to traveling to Japan to present my research. These opportunities have forced me to become a better writer, presenter, and overall critical thinker. Without doubt, these skills will continue to serve me well throughout my career, and I owe a considerable amount of my progress in these areas to Prof. Long. I also want to thank the members of my committee: Prof. Chris Williams, Prof. John Matson, Prof. Bob Moore, and Prof. Michael Bortner. The guidance they have given me both in my research and in the classroom has been instrumental during my time as a graduate student.

I consider myself extremely fortunate to have had the opportunity to work with so many bright and talented scientists in the Long group. I must first thank my mentor Dr. Phil Scott for being both an excellent mentor and a close friend throughout graduate school. I sincerely valued our in-depth discussions ranging from politics to Marvel movies (and sometimes science) as well as the countless hours we spent playing video/board games. His constant support and advice helped me prevail through many difficult times during graduate school, and for that I am the most grateful of

all. I also benefited from the guidance of many of the senior students during my early years in graduate school including Drs. Justin Sirrine, Mingtao Chen, Joe Dennis and Allison Pekkanen. Their willingness to pass down their collective knowledge and support the younger students in our group drastically enhanced my ability to succeed in this group. I hope that I have continued to pass along that legacy within the group. Emily Wilts, Clay Arrington, and Josh Wolfgang entered the group with me at the same time, and I continually leaned on them for support throughout graduate school in both classes and research. Emily was one of the first friends I made when coming to Virginia Tech. I will always remember fondly the times that we spent studying for (and complaining about) classes with Ryan Carrazzone and Priya Venkatraman over the first several years of graduate school. Clay Arrington remains one of the most intelligent and interesting people I have met to this day. I never grew tired of hearing his unique perspectives on almost any issue and talking with him about shared interests such as fantasy novels and video games. His keen knowledge of chemistry has served the group well and has likewise assisted me in many projects. I became close with Josh Wolfgang through our many shared interests and through our time living together over the summer while we interned at Sabic. Josh always provided good conversation and I value the time that I was able to spend hanging out with him. Of course, the rest of the Long group both past and present has contributed to my education in some way. These members include, but are not limited to: Dr. Katie Heifferon, Dr. Ryan Mondschein, Dr. Nick Moon, Dr. Xi Chen, Dr. Bruce Orler, Kevin Drummey, Boer Liu, Mark Cashman, James Brown, Ren Bean, Johanna Vandenbrande, Ben Stovall, Jose Sintas, Cody Weyhrich, and Jianheng Wen. I feel that our group was very tight-knit, and I will never forget the kindness that the whole group and Prof. Long showed me after my father passed away.

I need to thank many others outside of the Long group as well. Cam Chatham from the Williams' group became a dear friend to Natalie and I quickly after we moved to Blacksburg. I enjoyed getting to know him through the bible study that he led, and I have him to thank for my newfound love of D&D! I also had the pleasure of collaborating with several other graduate students from the Williams' group and the Moore group including: Dr. Viswanath Meenakshisundaram, Dr. Callie Zawaski, Keyton Feller, Danny Rau, Glenn Spiering, and Melissa Novy. Working with these students truly enriched my research and reinforced the interdisciplinary nature of my degree. I also want to acknowledge the endless support Natalie and I have received from both of our families. My mom has been a continuous source of encouragement to me throughout my entire education and has always made me believe that it was possible for me to pursue my love of science in the form of an advanced degree. Natalie's family, especially her mom, spent a considerable amount of time visiting us in Blacksburg in order to help us balance the craziness of taking care of our newborn child while finishing experiments, teaching, and writing our dissertations. It is hard to overstate the impact that has had on allowing us to finish our degrees on time.

I have also benefitted from the instruction of many mentors during my time as an undergraduate at the University of Tennessee, Knoxville. Carrying out undergraduate research in Prof. Jimmy Mays' group was my first foray into the exciting field of polymer chemistry and working with him and his group inspired me to pursue a Ph.D. in this field. Weiyu Wang and Dr. Namgoo Kang were both excellent mentors throughout my time as an undergraduate researcher, and I owe them for teaching me all the fundamentals of carrying out research in a chemistry lab. I also owe a huge thanks to Dr. Tomonori Saito at Oak Ridge National Lab for taking me on as a summer intern and subsequently a post-baccalaureate research associate. I am extremely grateful

that he saw potential in me as a researcher at that time and allowed me to gain experience working at a national lab. Tomonori taught me so much about polymer synthesis and collaborating on interdisciplinary projects, which prepared me well for graduate school.

I have saved the most important acknowledgements for last. Words are scarcely able to describe the amount of love and care that my incredible wife, Natalie, has shown me over the past five years of our marriage. We both entered graduate school as newlyweds unaware of the mental and physical strain it would exert on us both. Despite that, she has always been there to support me through even the most challenging times in graduate school. Without question, I would never have made it this far in my degree without her by my side. Her work ethic continuously inspires me to improve, and it will never cease to amaze me how successful she is at everything she puts her mind to. On top of everything, the greatest gift she has given me is that of our son, Asa. Somehow, she has managed the seemingly impossible task of excelling as a mother while simultaneously completing her Ph.D in Electrical Engineering and supporting me as I searched for jobs and wrote my dissertation. Over the past seven months, Asa has filled my life with an inexpressible joy. The unparalleled love I feel for him has driven me forward even when there were days when finishing my degree seemed like an impossible task. I hope that one day he understands how much he means to me and how honored I feel to be his father. Overall, I am excited to start our lives together as a family and I am forever grateful to a merciful and loving God that has blessed me beyond all imagination.

# Attributions

**Prof. Timothy E. Long** is a professor and director of the Biodesign Center for Sustainable Macromolecular Materials and Manufacturing at Arizona State University. He was previously a professor in the Department of Chemistry at Virginia Tech. He is the author's research advisor and primary mentor.

**Prof. Christopher B. Williams** is a professor in the Department of Mechanical Engineering and is the assistant director of the Macromolecules Innovation Institute (MII) at Virginia Tech. He was a collaborator on Chapters 4 and 6.

**Prof. Joshua R. Sangoro** is a professor in the Department of Chemical and Biomolecular Engineering at the University of Tennessee, Knoxville. He was a collaborator on Chapter 3.

**Dr. Callie Zawaski** was a graduate student in Prof. Williams' group and was a collaborator on Chapter 4.

**Dr. Emmanuel U. Mapesa** is a post-doctoral researcher in Prof. Joshua Sangoro's research group at the University of Tennessee, Knoxville. He was a collaborator on Chapter 3.

**Dr. Xi Chen** was a graduate student in Prof. Long's research group and was a collaborator on Chapter 5.

**Dr. Viswanath Meenakshisundaram** was a graduate student in Prof. Williams' research group and was a collaborator on Chapter 6.

**Kevin J. Drummey** was a graduate student in Prof. Long's group and was a collaborater on Chapter 5.

**Josh D. Wolfgang** is a graduate student in Prof. Long's research group and was a collaborator on Chapters 3 and 8.

**Boer Liu** is a graduate student in Prof. Long's research group and was a collaborator on Chapter 5.

**John M. Migliore** was an REU summer student in Prof. Long's research group and a collaborator on Chapter 3.

**Keyton D. Feller** is a graduate student in Prof. Williams' research group and was a collaborator on Chapter 6.

**Jose Sintas** is a graduate student in Prof. Long's research group and is a collaborator on Chapter 8.

# Table of Contents

# List of Figures

# List of Tables

# List of Schemes

# Chapter 1: **Introduction**

## 1.1 Dissertation Overview

This dissertation focuses on the synthesis and characterization of step-growth polymers such as polyureas, polyurethanes, polyesters, and ionenes. Special attention is given to the structure-property relationships of segmented block copolymers as they relate to applications in advanced technologies (i.e., additive manufacturing and electromechanical transducers). Chapter 2 provides a review of the major advances in the design of polymeric materials for electromechanical transducers. The first section discusses ionic polymer-metal composites and provides a summary of polymer types and material properties needed for low voltage transduction. The second section deals with polymers for dielectric elastomer actuators including polysiloxane and acrylic elastomers. Specifically, this part of the review covers techniques for increasing the dielectric permittivity of elastomers as a method of driving down the required operating voltages for these actuators. A final perspective describes potential future directions in polymers for electromechanical transducers including additive manufacturing approaches and producing polymeric electrodes for dielectric elastomer actuators.

Chapter 3 describes a strategy for producing isocyanate-free, segmented polyurea elastomers using a catalyst- and solvent-free melt polycondensation reaction. The elastomers exhibited tunable thermal, mechanical, and dielectric properties dependent on the structural composition of the polymer. High dielectric permittivities in some of the elastomers point towards utilizing variations of these materials for dielectric elastomer applications. Chapter 4 expands on this isocyanate-free chemistry to produce water-soluble poly(ether urea)s (PEUs) for low-temperature extrusion-based additive manufacturing. Modulating the molecular weight of a commercial, water-

soluble polyether diamine resulted in PEUs with varying thermal properties. This approach facilitated the extrusion 3D printing of a water-soluble PEU at low temperatures.

Chapter 5 provides a detailed review of the structure-property relationships in charged block copolymers. This review categorizes recent literature by polymer architecture including linear, branched, segmented, and multiply charged block copolymers. The polymer architectures are compared in terms of their effect on properties, and applications for these materials are highlighted. Chapter 6 reports a new method for 3D printing unsaturated polyester resins using vat photopolymerization. A polymerizable phosphonium ionic liquid serves as a non-volatile reactive diluent to replace the volatile and toxic monomer styrene. Photorheological experiments elucidated the photocuring properties of a variety of resin compositions to determine the most suitable formulation for 3D printing. Vat photopolymerization produced high resolution 3D structures and the cured resins displayed ionic conductivity at elevated temperatures.

Chapters 7 and 8 describe the synthesis and characterization of charged segmented block copolymers. Chapter 7 describes a poly(siloxane urethane) (PSiU) containing a phosphonium-functionalized soft segment. The synthesis of this polymer allows for the insertion of a novel phosphonium ionic liquid into the low $T_g$ poly(dimethyl siloxane) phase of a polyurethane. The charged PSiU formed flexible films and demonstrated ionic conductivities comparable to those of other phase separated block copolymers in literature. Chapter 8 presents preliminary studies on a new method of producing imidazolium ionenes through the reaction of dihalides with a biscarbonylimidazole monomer. Initial studies demonstrate the formation of low molecular weight polymers, and experiments on small-molecule analogues suggest that the issue may lie in the incomplete conversion of the imidazoles to imidazolium. However, the formation of low molecular weight polymers suggests that future work on this method may produce imidazolium ionenes with

an interesting new structure. Finally, Chapters 9 and 10 detail the overall conclusions of the dissertation and suggest avenues for future work. Chapter 10 describes promising preliminary data for some projects in progress as well as suggested work that expands on the research presented herein.

# Chapter 2: **Advances in Polymeric Materials for Electromechanical Devices**

Published in *Macromolecular Rapid Communication* **2019,** *40* (1), 1800521

B. Tyler White and Timothy E. Long*

Department of Chemistry, Macromolecules Innovation Institute, Virginia Tech, Blacksburg, VA, 24061

**Keywords:** ionic polymer metal composite, dielectric elastomer, electroactive actuator, polymer transducer

*Address correspondence to: Timothy.E.Long@asu.edu

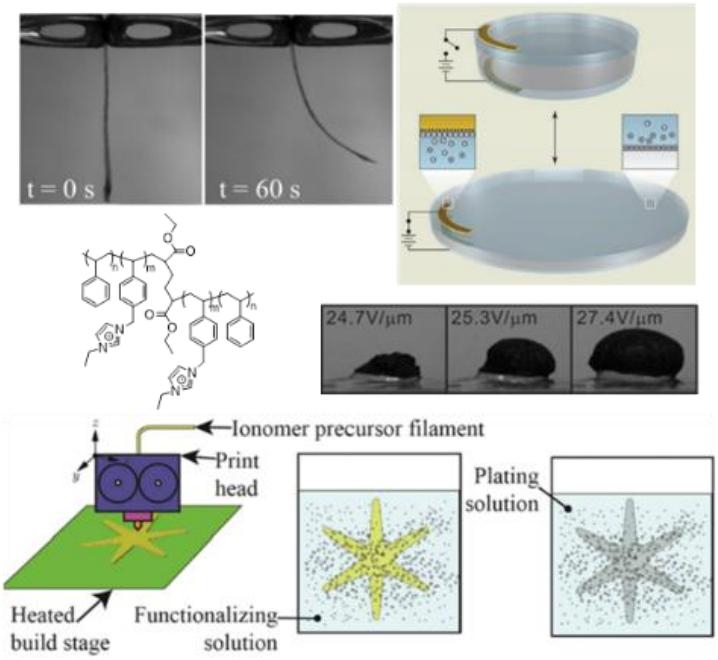


## 2.1 Abstract

Electroactive polymers (EAP) provide lightweight and cost-effective materials that enable the next generation of electromechanical devices. Commercial polymers have historically dominated research in EAP devices due to their availability. However, several drawbacks of these materials have limited their commercial applications, necessitating new materials for the commercial success of future EAP devices. This review highlights recent advances in novel electroactive polymers for ionic polymer-metal composites (IPMC) and dielectric elastomer actuators (DEA).

Ion-containing block copolymers and charged segmented condensation polymers have demonstrated suitable electromechanical properties competitive with Nafion™-based IPMCs. In addition, swelling ionic polymer membranes with free ionic liquid enhanced ionic conductivity and promoted electromechanical actuation. Synthetic approaches to increasing permittivity in dielectric elastomers were also explored as a method of producing more efficient DEAs. Incorporating polar functional groups into siloxane and acrylic elastomers through grafting or blending provided high-dielectric elastomers for use in DEAs with low driving voltages.

## 2.2 Introduction

Actuators are a type of electromechanical transducers, which convert an electrical signal into a mechanical force. Over the past two decades, electroactive polymers (EAP) have garnered much interest as candidates for actuators, which is attributed to their lightweight, flexibility, and low cost.[1] EAP actuators enable various applications including artificial muscles,[2] soft robotics,[3] and sensors.[4] There are two main categories of EAP actuators based on their modes of actuation: ionic (regarding the diffusion and mobility of ions) and electronic (electric field driven) actuation. Ionic EAPs include ionic polymer-metal composites (IPMC), conductive polymers, and carbon nanotubes; electronic EAPs consist of dielectric elastomers (DE), electrostrictive polymers, ferroelectric polymers, and liquid crystal elastomers.[5] The most commonly investigated EAPs for actuators are DEs and IPMCs, and earlier reviews have captured their broad impact.[2-4]

DEs especially exhibit potential for mimicking human muscles due to their high strain capacity and work density.[6] Polymers used for DEs often include siloxanes or acrylic elastomers, and the optimal DE actuators (DEA) in literature are surprisingly comprised of a commercial acrylic adhesive from 3M.[7] However, these DEs require prestretching and large driving voltages

to achieve large actuation strains, which limit their impact. The past decade has seen a plethora of research dedicated to finding materials to circumvent these limitations.

Nafion™ has long served as the benchmark material for IPMCs due to its commercial availability and superior actuation performance at low voltages. Nafion™ actuators, however, have several drawbacks such as: low bending performance at low humidity, processing difficulties, and back relaxation. Due to these limitations, interest in new ionic polymers for IPMCs continues to grow in the literature.[8] This review aims to summarize the progress made in materials for electroactive polymer actuators over the past decade, focusing on IPMCs and DEAs, which comprise a significant fraction of the recent advances.

## 2.3 Ionic Polymer-Metal Composites

Ionic polymer-metal composites (IPMC) consist of an ion exchange membrane sandwiched between high surface area electrodes such as gold nanoparticles or ionic polymer nanocomposites containing carbon nanotubes. Nafion™ exemplifies the criteria for an ionic polymer for IPMC actuators. Nafion™, a perfluorinated polymer, contains sulfonated pendant groups with bound, monovalent counterion such as $Na^+$ (**Figure 2.1b**). The polymer usually requires a certain amount of water or organic solvent to facilitate the motion of the counterion through plasticization.[6] The metal electrodes charge upon application of a voltage, and the hydrated, free counterions migrate toward the oppositely charged electrode. The migration of ions and water causes the film to swell on one side and contract on the other, which results in the actuator bending.[6, 9] Many IPMCs also experience back relaxation, which occurs when the mobile ions saturate the oppositely charged electrode and reverse the polarity of the device. The polarity change causes the ions to migrate in the opposite direction of the applied potential and the device relaxes.[8, 10-12] Actuators based on hydrated polymers such as Nafion™ also experience back relaxation due to the diffusion of the

free water molecules toward the opposite side of the membrane. **Figure 2.1** elaborates on the basic actuation mechanism of an IPMC, and Pugal et al. provided a more detailed explanation of the IPMC transduction mechanism in a recent review paper.[13]

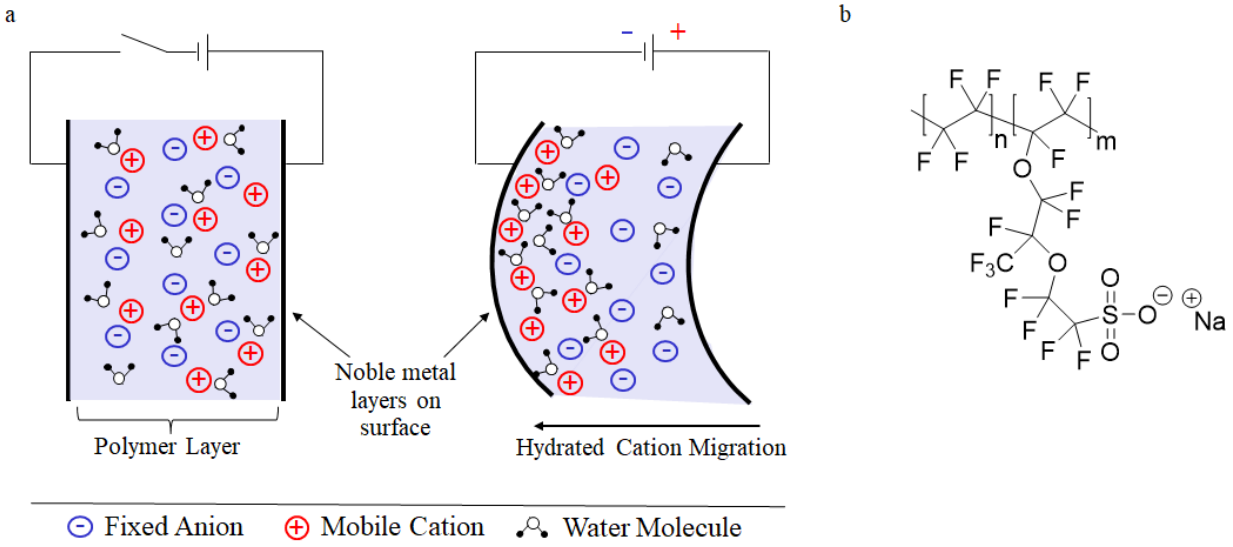


**Figure 2.1:** (a) Schematic depicting the basic actuation mechanism of an IPMC. Hydrated cations move towards the anode under an applied voltage causing the membrane to swell on one side and contract on the other. (b) Structure of Nafion™ containing a sodium counterion.

IPMCs excel in low power electronics applications due to their relatively low operating voltages of < 7 volts; however, these materials typically have low strains on the order of 0.5-3% and suffer from low efficiencies. Furthermore, slow ion diffusion in undoped ionic polymers and in the nanocomposite electrodes ultimately results in slow response times.[6, 9] Common parameters for evaluating IPMC performance include bending (tip) displacement, blocking force, and actuation speed. These parameters relate directly to the conductivity and mechanical properties of the polymer. Furthermore, optimizing the IPMC performance often requires a compromise between the polymer modulus and ionic conductivity. Thus, most recent research focuses on increasing the conductivity of novel or commercial polymers to match or exceed Nafion™, while simultaneously maintaining flexibility.

### 2.3.1 Ion-Containing Block Copolymers

The high conductivity in Nafion™ stems in part from its unique, semi-crystalline morphology, which allows efficient transport of ions through the amorphous domains while crystallites provide mechanical integrity through physical crosslinking.[14] In order to mimic this structure, the rational design of IPMCs includes polymer morphologies that promote ion diffusion through the membrane. Block copolymers provide a convenient method for tailoring the microphase morphologies of a polymeric membrane. Changing the volume fraction of each phase enables several microphase morphologies such as: spheres, cylinders, bicontinuous networks, and lamellae. Bicontinuous networks form adequate ion conducting channels while cylinders and lamellae are only efficient if properly oriented; ionic-phase spheres, conversely, lack a continuous conductive phase and therefore do not conduct well.[15-16] Ionic conductivity generally increases with decreasing $T_g$ while mechanical properties scale inversely. Consequently, high ionic conductivities are often sacrificed to satisfy the mechanical properties required for IPMCs or vice versa. Another benefit of utilizing block copolymers arises from the ability to effectively decouple the ionic conductivity from the mechanical properties. For example, phase separated block copolymers consisting of rigid reinforcing domains dispersed in a low $T_g$ conductive phase provides adequate mechanical properties while maintaining acceptable ionic conductivities.[17]

Zheng and Cornelius recently reported a sulfonated penta-block copolymer (**Figure 2.2a**), with a tunable morphology dependent on casting solvent.[18] Films cast from cyclohexane (CH) and THF mixtures containing high CH content resulted in a discontinuous ionic phase, which lead to low conductivity and, consequently, low electromechanical bending. As the content of THF increased, the morphology changed from random to lamella/hexagonal, and the polymer exhibited nearly a 1000% increase in room temperature proton conductivity in the parallel direction. The films also exhibited anisotropy in the measured conductivity as expected for lamellae or hexagonal morphologies. **Figure 2.2b** shows a graph of conductivity vs. solvent composition measured parallel and perpendicular to the film. Conductivities measured in the perpendicular direction revealed circa 70% decrease for all solvent compositions. The bending displacement over time (**Figure 2.2c**) for each morphology correlated well with the increase in conductivity. The films cast from THF demonstrated the highest room temperature conductivity in the parallel direction with a conductivity of 47.8 mS/cm while submerged in DI water; however, the conductivity in the perpendicular direction fell to 19.6

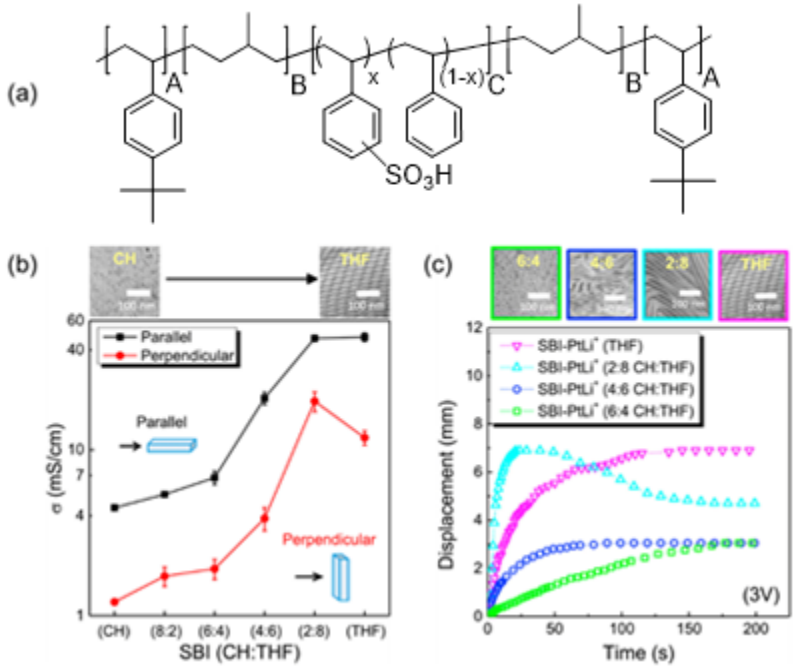


**Figure 2.2:** (a) Structure of a sulfonated pentablock copolymer used in an IPMC (b) graph of conductivity, σ, vs. solvent composition measured in the parallel and perpendicular directions of IPMCs (c) displacement vs. time measured at 3V for pentablocks cast from different solvents. Adapted with permission from Zheng et al.[18] Copyright 2016, Elsevier.

mS/cm, which is the more pertinent value for actuation. The THF cast film of also displayed the lowest elastic modulus of the series at approximately 80 MPa. IPMCs fabricated from this film displayed the best electromechanical performance with a maximum and constant bending displacement of 6.9 mm at 3V. Vargantwar and coworkers previously reported a similar increase in conductivity for the same penta-block copolymer after swelling with polar solvents.[19]

Long et al. previously intensively investigated the utilization of polymerized ionic liquids (PIL) in block copolymers for IPMCs.[11, 17, 20-22] For example, Green and Long et al. synthesized the first cationic triblock copolymer for electromechanical transducers, which incorporated an imidazolium-based PIL.[11] The triblock consisted of a poly(ethylvinylbenzyl imidazolium) central block with external polystyrene blocks, and showed microphase separation between the charged block and the reinforcing polystyrene blocks. The $T_g$ of the central block varied with counterion selection from 148 °C for $Br^-$ down to 29 °C for the bulky $Tf_2N^-$ counterion. The triblock containing the $Tf_2N$ counterion exhibited a storage modulus of 100 MPa at room temperature, comparable to that of Nafion (~120 MPa) demonstrating a strong matrix capable of supporting actuation. However, this copolymer exhibited a low room temperature ionic conductivity (< $1x10^{-6}$ S/cm) compared to Nafion™ ($1.1x10^{-1}$ S/cm) attributed to the relatively high $T_g$ of the conductive phase. Moreover, Green et al. showed that the conductivity decreased by 2.5 orders of magnitude with a two decade increase in storage modulus demonstrating the important interplay between modulus and conductivity. Despite the low conductivity, IPMCs fabricated from this triblock demonstrated a curvature 2.5 times greater than Nafion™ under an applied voltage of 4V at room temperature (**Figure 2.3**). These IPMCs also did not show any back relaxation, which commonly affects Nafion™-based actuators. Although these block copolymers demonstrate potential to

compete with Nafion™ as conductive materials in IPMCs, increasing their conductivities to values comparable with hydrated Nafion™ remains a challenge critical to improving IPMC performance.

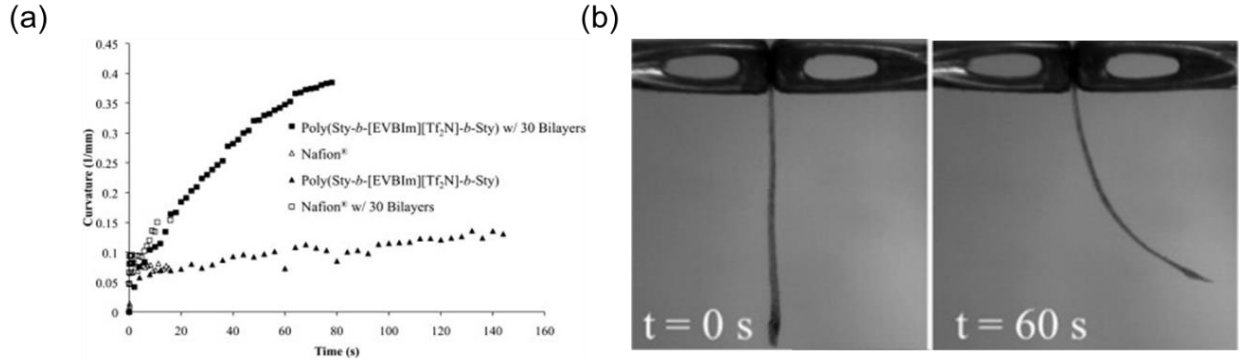


**Figure 2.3:** (a) Graph of IPMC curvature for the triblock copolymer compared to Nafion™. (b) Time lapse photo of triblock IPMC under an applied voltage. Adapted with permission from Long et al. [11] Copyright 2012, Elsevier.

## 2.3.2 Ionic-liquid-containing Polymers

Swelling ionic polymers with ionic liquids (ILs) often provides a convenient method to increase the conductivity in polymer membranes.[16, 23-31] The mobility of the added free ions in the polymer increases the conductivity, which depends strongly on temperature.[30] Furthermore, IL plasticizes the membrane, which decreases the $T_g$ of the polymer and consequently increases the conductivity. The hard segment (normally not conductive) of the block copolymer also must not be miscible with the free IL such that only the continuous, ionic phase contains IL. This prevents plasticization of the hard segment as well as phase mixing, which diminishes the mechanical properties. Incorporation of free IL also has the benefit of tuning the morphology of the polymer. Gwee and coworkers demonstrated that the morphology of a poly(styrene-*b*-methyl methacrylate) diblock copolymer changed from a non-continuous lamella to cylinders upon the addition of 35 wt.% of an imidazolium IL.[16] The change in morphology also promoted a substantial increase in the measured in-plane conductivity. This provides yet another control for tuning the conductivity of a polymer membrane with free IL.

The counterion selected for the IL also affects the actuation performance of the IPMC. Kim et al. studied the effect of the size of the 1-hexyl-3-methylimidazolium (HMIm) counterion in sulfonated diblock and triblock copolymers.[23] They discovered that the counterion size affects conductivity, modulus, and actuated strain in the swollen polymer membranes. The imidazolium with a large bis(trifluromethylsulfonyl)imide ($Tf_2N$) counterion showed the highest conductivity compared to smaller tetrafluoroborate ($BF_4$) and hexafluorophosphate ($PF_6$) anions. Similarly, the Young's modulus decreased with the size of the counter ion from $Tf_2N$ to $BF_4$. On account of these desirable properties, IPMCs made from triblock copolymers containing 70 wt.% [HMIm][$Tf_2N$] exhibited the greatest actuated strain of 1.5% at 3V. These actuators also exhibited long-term durability without noticeable changes in actuation after 13,000 cycles.

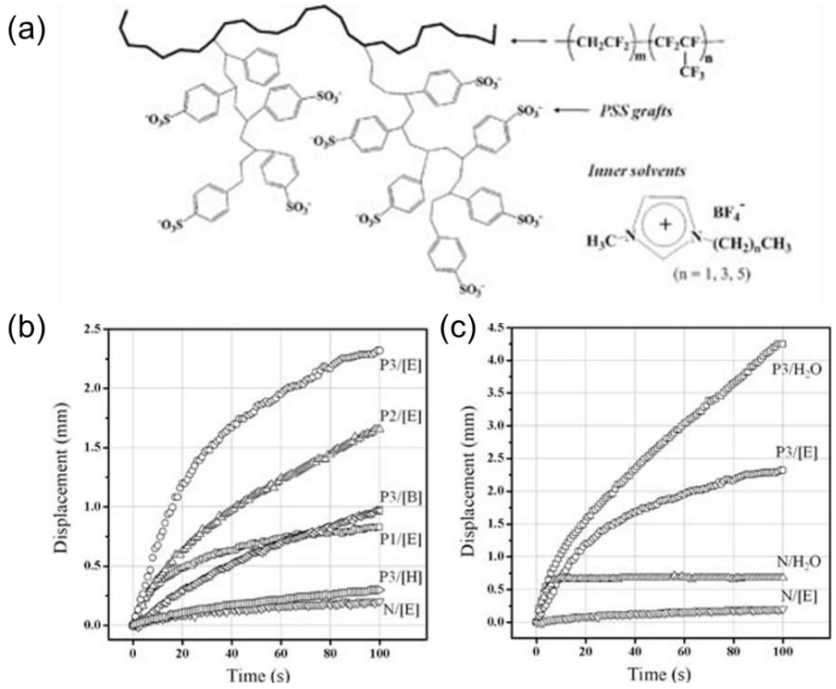


**Figure 2.4:** (a) structure of PSS grafted fluoropolymers (b) graph of displacement vs time for ionic liquid swollen PSS grafted fluoropolymers compared to Nafion™ where P1,2 and 3 correspond to grafting densities of 35, 85, and 125 wt.% respectively. [E], [B], and [H] represent ethyl, butyl, and hexyl MIm $BF_4$ respectively. (c)Hydrated P3 displacement vs hydrated Nafion™.[27]

Lee and coworkers reported a sulfonated polystyrene (PSS) graft fluoropolymer containing ILs as a high-performance actuator.[27] The graft polymer (**Figure 2.4a**) showed the highest conductivity at a PSS graft density of 125 wt.%. This graft copolymer exhibited a maximum conductivity of 4.23 mS/cm when swollen in 1-*ethyl*-3-

methylimidazolium tetrafluoroborate ([EMIm][$BF_4$]), while the hydrated polymer displayed a conductivity of 79.61 mS/cm. These values are higher than both dry and hydrated Nafion™ (0.21 and 13.83 mS/cm, respectively). Consequently, the prepared ionomers exhibited much higher bending displacements than Nafion™, with the largest displacement at an order of magnitude higher (**Figure 2.4b, c**). However, actuators made from Nafion™ exhibited blocking forces between 2-3 times higher than the graft fluoropolymers. This result was attributed to the inferior moduli of the fluoropolymers compared to Nafion™.

### 2.3.3 Charged Condensation Polymers

Although block copolymers are now commonly investigated for IPMCs, sulfonated condensation polymers such as polyimides,[32-35] polysulfones,[36-38] polyphenylsulfone,[39] poly(ether ketone)s,[40-41] and polybenzimidazoles[42] also show potential as new materials for IPMCs. Similar to block copolymers, condensation polymers have the ability to microphase separate into hard and soft segments based on the monomers chosen for the polymerization. However, segmented condensation polymers lack the variety of possible morphologies and topologies afforded by block copolymers typically prepared using living and controlled polymerization processes. Condensation polymerizations also scale more easily whereas block copolymer synthesis typically involves the more precise synthetic methods associated with living or controlled radical polymerizations, which are not as readily amenable to large scale manufacturing.

Wang and coworkers produced sulfonated poly(arylene thioether sulfone) (SPTES) crosslinked with poly(vinyl alcohol) (PVA) (**Figure 2.5**).[38] The SPTES/PVA network absorbed 60 wt.% of water compared to 30 wt.% in a Nafion-117™ membrane. Furthermore, the hydrated network exhibited a comparable proton conductivity to the hydrated Nafion-117™ at $1.36 \times 10^{-2}$

S/cm despite taking up twice as much water. Mechanical analysis revealed that the elongation at break and Young's modulus of the hydrated

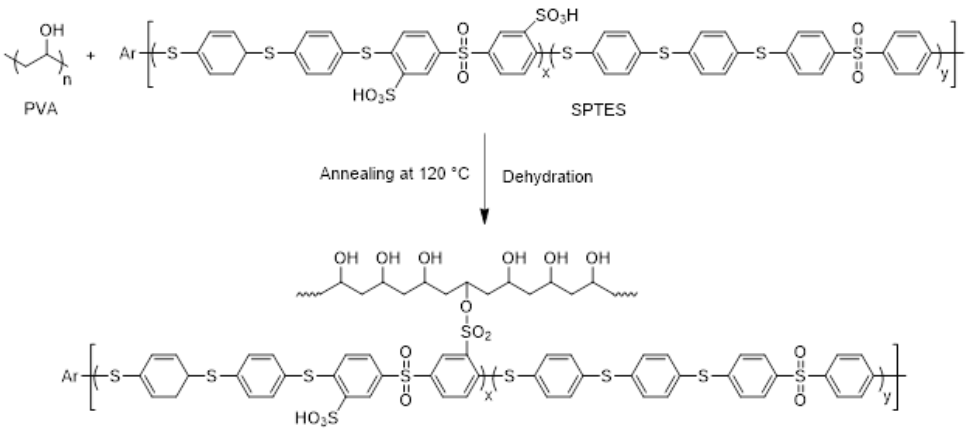


**Figure 2.5**: Synthesis of SPTES/PVA crosslinked membranes through a dehydration reaction.[38]

SPTES/PVA network (11.6% and 140.3 MPa, respectively) was significantly lower than those of the hydrated Nafion-117™ membrane (137.3% and 267.7 MPa). However, the modulus of the network remained suitable for the fabrication and actuation of an IPMC. The IPMC based on the hydrated SPTES/PVA network exhibited tip displacements up to 2.5 mm at 2V. This displacement outperformed hydrated Nafion-117™, which reached a maximum at 1.5 mm. Moreover, SPTES/PVA did not show back relaxation, which was prevalent in the Nafion-117™ actuators. Although this material has a low onset of thermal degradation (~100 °C), it remains suitable for room temperature applications.

Tang and Xie et al. also recently fabricated IPMCs using sulfonated polyphenylsulfones (SPPSU) with varying degrees of sulfonation from 91% - 109%.[39] The SPPSU membranes took up ~2-4 times more water than a Nafion-117™ membrane with water uptake increasing with degree of sulfonation. SPPSU membranes exhibited comparable room temperature proton conductivities to Nafion-117™ (0.081 S/cm) in the hydrated state, with the most highly sulfonated membrane displaying the highest conductivity at 0.074 S/cm. As expected, the elastic modulus dropped substantially when hydrated. However, even the SPPSU membrane with the highest water

uptake maintained a higher modulus (296 MPa) than hydrated Nafion-117™ (92 MPa), suggesting the potential to form IPMCs. IPMC actuators fabricated from the SPPSU with the highest degree of sulfonation displayed a maximum bending strain nearly identical to that of the Nafion-117™ based IPMC under an applied voltage of 3V. Moreover, the SPPSU achieved the maximum bending strain almost 7 times faster than the Nafion-117™ actuator. Although these IPMC actuators demonstrate good electromechanical properties, they still suffer from significant back relaxation similar to Nafion™.

Fillers are frequently used to try to increase conductivity in IPMCs.[24, 34, 36] Kwon et al. recently achieved nanocomposites from sulfonated poly(arylene ether sulfone) (SPAES) and copper(II) phthalocyanine tetrasulfonic acid (CuPCSA).[36] The sulfonate groups on the CuPSCA nanofillers allowed for uniform dispersion throughout the ion channels, and thus increased the conductivity. The SPAES mixed with 5% CuPCSA provided a very high conductivity at >100 mS/cm compared to Nafion™, which had a conductivity of 75 mS/cm. This material outperforms Nafion™ in every regard including modulus, blocking force, ion exchange capacity, displacement retention, and mechanical power density. Additionally, these SPAES nanocomposites offer much faster displacement rates than most IPMCs at 12 mm/s. Although most IPMCs produced from condensation polymers still have particularly low tip displacements, these materials show potential as cost effective alternatives to Nafion™ as their properties continue to improve.

### 2.3.4 Polysaccharide Actuators

Producing electromechanical devices from natural polymers provides several practical advantages such as: biocompatibility, biodegradability, and a renewable feedstock. One such natural polymer, an amino polysaccharide derived from shrimp shells known as chitosan, finds use in electromechanical actuators mostly due to its low cost, biocompatibility, and good

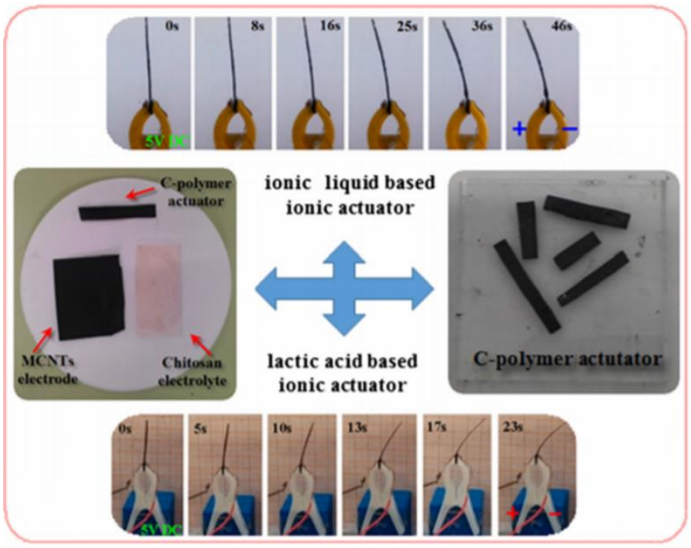


**Figure 2.6:** Chitosan-based actuators consist of chitosan mixed with either an ionic liquid or an acidic electrolyte solution. Carbon nanotubes coat the surfaces to form electrodes. Reproduced with permission from Sun et al.[45] Copyright 2017, Springer.

miscibility with ILs.[43-47] Chitosan-based actuators commonly contain a blend of chitosan and an IL or acidic electrolyte solution, coated with carbon nanotubes as the electrodes as shown in **Figure 2.6.**[45] The actuators bend due to ion migration from either the IL present in the membrane, or the counterion in the acidic electrolyte solution, which quaternizes the amine group on chitosan. Actuators based on chitosan show decent bending deformations at low voltages (<7V) and relatively large blocking forces with a maximum force of 7.5 mN.[45]

Cellulose represents another polysaccharide suitable for actuator applications.[48-56] Cellulose is one of the most abundant natural polymers in the world and makes up about 1.5 trillion tons of the biomass produced each year.[51] Cellulose actuators, also known as electroactive paper actuators, show good actuation performance at low voltages, but demonstrate extreme moisture sensitivity and suffer from diminished performance over time. Blending cellulose with chitosan improved the actuator performance, but simultaneously increased the sensitivity to humidity.[51, 55] Incorporating PEG into cellulosic actuators doped with IL improved the maximum bending displacement up to 5 mm, and significantly decreased the power consumption of the actuators.[52-53] Furthermore, blending cellulose derivatives with electroactive fillers such as poly(3-hydroxybutyrate)[49], fullerenol[54], and polyaniline[56] increased the bending displacement at low

humidity, and decreased the power consumption. Other less common biopolymers such as gelatin[57] and soy protein [58] also show potential for use in electroactive actuators. Although these natural polymers are inexpensive, biocompatible, and biodegradable on their own, the electrodes still require the use of noble metals or nanomaterials, which effectively negates these advantages. Biological applications for these devices necessitate the discovery of biofriendly electrodes to increase the likelihood of commercial success.

**Table 2.1** compiles key material properties for selected IPMCs. Converting tip displacement (d) to % strain (ε) (Equation 2.1) allows for a direct comparison of actuator performance between samples independent of sample length (L) and thickness (t). In general, ionic polymers exhibiting storage moduli on the order of 100 MPa are suitable for IPMC fabrication and actuation. Conversely, there is no apparent correlation between Young's modulus and actuation performance indicating that this parameter may not provide a suitable metric for predicting actuation ability. Although polymers with ionic conductivities as low as $1x10^{-8}$ mS/cm have demonstrated actuation under an applied voltage, higher conductivities generally lead to faster response time.

$$\varepsilon\ (\%) = \frac{2dt}{L^2+d^2} \text{ x } 100 \qquad (2.1)$$

**Table 2.1:** Ionic conductivity, glass transition temperature. modulus, operating voltage, and bending strain or curvature of selected IPMCs

| Ionic Polymer | σ (mS/cm)[a] | $T_g$ (°C)[b] | Modulus (MPa)[c] | Voltage (V) | Bending Strain (%) | \|Curvature\| ($mm^{-1}$) |
|---|---|---|---|---|---|---|
| **PS-PEVBIm triblock copolymer** | $5.0x10^{-4}$ | 17, 107 | 100 | 4 | - | 0.38 |
| **Sulfonated PS pentablock copolymer** | 48 | - | 80 | 3 | 1.8 | - |

| | | | | | | | |
|---|---|---|---|---|---|---|---|
| **PS-PMVBIm triblock copolymer** | $1.1x10^{-8}$ | 13, 102 | 100 | 4 | - | 0.15 | 20 |
| **PS-PMVBIm-co-DEGMEMA triblock copolymer** | ~$1.0x10^{-6}$ | 40, 96 | - | 4 | - | 0.60 | 21 |
| **PS-PAA(MeIm) triblock copolymer/ IL** | $1.0x10^{-4}$ | -15, 106 | 100 | 4 | - | 0.30 | 22 |
| **Sulfonated PS-poly(methyl-buytlene) triblock copolymer** | - | - | 700[d] | 3 | 1.5 | - | 23 |
| **Sulfonated PS pentablock/ silicate/ IL composite** | ~$7.0x10^{-2}$ | - | 4.1[d] | 2 | 0.9 | - | 24 |
| **Sulfonated PS-poly(methyl-buytlene) block copolymer** | 30 | - | 3,200[d] | 3 | 4.0 | - | 25 |
| **PVDF-co-HFP graft sulfonated PS** | 80 | - | - | 2 | 4.9 | - | 27 |
| **P(VDF-CTFE)/ PMMA crosslinked blend** | $7.0x10^{-2}$ [e] | -20, 105 | 150[d] | 4 | - | 0.75 | 28 |
| **sPS Pentablock copolymer/ IL** | - | -35, 110 | 700 | 4 | - | 0.70 | 29 |
| **Sulfonated polysulfone/ sulfonated CuPCSA composite** | 102 | - | 208[d] | 2 | 1.2 | - | 36 |
| **Sulfonated poly(arylene thioether sulfone)/ PVA** | 14 | - | 140[d] | 2 | 0.2 | - | 38 |

| | | | | | | | |
|---|---|---|---|---|---|---|---|
| **Cellulose/ fullerenol composite** | 1.8 | 221 | - | 3 | ~0.008 | - | 54 |

[a] measured at room temperature unless otherwise noted
[b] measured with differential scanning calorimetry (DSC) unless otherwise noted
[c] refers to storage modulus (E') unless otherwise noted
[d] refers to Young's modulus (E)
[e] measured at $T_g$

## 2.4 Dielectric Elastomer Actuators

Dielectric elastomer actuators (DEA) consist of an elastic polymer film with compliant electrodes coated on the top and bottom. Unlike other electroactive polymers, DEs are not ionically or electrically conductive, and behave as electrical insulators. Thus, DEs act as capacitors, storing charge instead of conducting.[6] The ability of a DE to act as a good capacitor depends primarily on its permittivity (ε), or ability to resist an electric field. A high permittivity relates proportionally to high capacitance and indicates that the material stores charge efficiently. The actuated strain of a DEA relates to the permittivity as described in Equation 2.2 where s is the thickness strain, ε' is the relative permittivity (the ratio of the absolute permittivity to vacuum permittivity), $\varepsilon_0$ is the vacuum permittivity constant, Y is the Young's modulus, and E is the electric field strength.[59]

$$s = -\frac{\varepsilon' \varepsilon_0}{Y} E^2 \tag{2.2}$$

DEAs have a fundamentally different mechanism of actuation than IPMCs. **Figure 2.7** shows the basic structure of a DEA.[7] Upon application of a voltage across the device, the Coulombic attraction between the oppositely charged electrodes generates an electrostatic Maxwell stress on the polymer in the thickness direction.[7] As a result, the elastic film expands in area, and contracts back to its original shape and size when the voltage is removed.

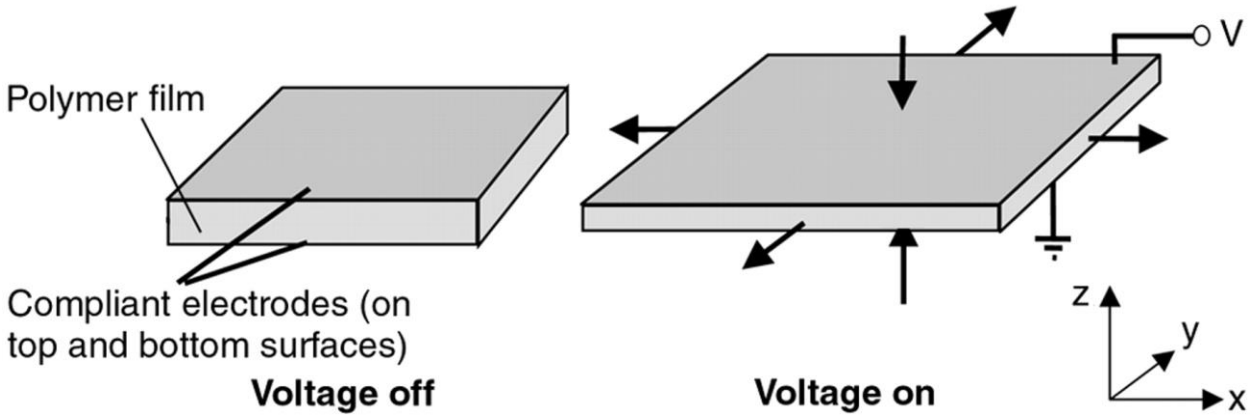


**Figure 2.7:** Basic actuation mechanism of dielectric elastomer actuators. A polymer film coated with compliant electrodes on the top and the bottom. Upon application of an applied voltage, the oppositely charged electrodes apply a Maxwell stress on the polymer film, resulting in a strain in the x direction. Reproduced with permission from Pelrine et al.[7] Copyright 2000, The American Association for the Advancement of Science

DEAs enjoy several advantages over other types of electroactive polymer actuators, including fast electromechanical response and large areal deformations.[1, 6-7, 60] However, DEAs typically require high operating voltages (between 500V and 10kV) owing to the low relative permittivity of many common DEs.[61] The breakdown voltage, or the minimum applied voltage that causes a polymer to electrically conduct due to degradation, therefore limits the materials selection for DEAs.[1] Increasing the breakdown voltage or decreasing the required operating voltage remain the primary interests for improving DEA performance. Equation 2 implies that, at a constant strain, the operating voltage (electric field strength) decreases with increasing relative permittivity or with decreasing Young's modulus in the DE. Hence, the most common materials used in DEAs are poly(dimethyl siloxane)s and acrylic-based elastomers, which typically exhibit low Young's moduli. Recent literature has focused on modifying these materials to improve their electromechanical performance.

### 2.4.1 Siloxane Elastomers

DEAs often utilize crosslinked polysiloxanes, also known as silicone rubber for poly(dimethyl siloxanes), due to their low $T_g$, high breakdown voltage, and low water uptake. However, silicones typically have low dielectric permittivity (< 3), which leads to high operating voltages.[1, 62] Functionalizing silicone elastomers with pendant polar groups represents one method for increasing permittivity. Silicones have been synthesized containing trifluoropropyl,[62] nitrile,[63-64] alkyl chloride,[65] nitroaniline,[66] nitrobenzene,[67] and cyanopropyl[68] pendant groups, which resulted in a modest increase in the permittivity of the silicones at high frequencies. A representative example of these materials comes from Dünki et al. who synthesized silicone elastomers functionalized with polar nitrile groups as shown in **Figure 2.8**.[59] DEAs made from these silicones had a maximum relative permittivity of 10.1 (10 kHz) and exhibited room temperature strains of 20.5% at electric fields of 10.8 V $\mu m^{-1}$. The electric field required for these strains fell between 3-8.5 times lower than required for commercial DEAs. Similarly, Dünki and coworkers recently reported the synthesis of polysiloxanes bearing sulfonyl pendant groups using efficient thiol-ene chemistry.[69] They tuned the relative permittivity between 4.9 to 22.7 while maintaining low glass transition temperatures between -100 and 9 °C.

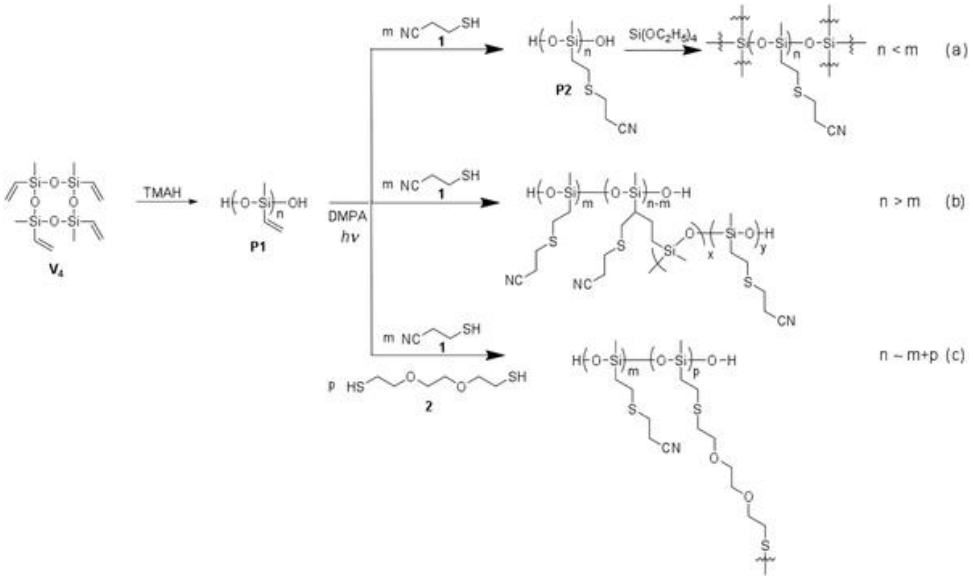


**Figure 2.8**: Synthesis of polysiloxane networks bearing polar nitrile groups. Post-polymerization functionalization of polymethylvinylsiloxane via thiol-ene chemistry yields silicones with nitrile pendant groups.[59]

The preparation of composites or blends with high permittivity fillers represents another strategy for increasing the permittivity of silicones. Ceramic fillers such as titanium dioxide,[70-72] barium titanate,[73] zirconium dioxide,[74] and lead zirconate [74] dispersed in a silicone matrix showed minor improvements in permittivity. Unfortunately, the stiffness of the ceramic fillers typically resulted in a higher Young's modulus for the elastomer, which increases the operating voltage as mentioned previously (Equation 2). Furthermore, the breakdown voltage in silicone composites often decreases as a function of increased particle loading, severely limiting the use of composites for DEAs.

Blending silicones with conductive or highly dielectric polymeric fillers affords an alternative approach to increasing permittivity.[75-77] For example, Carpi and coworkers blended polydimethylsiloxane rubber with 1-6 wt.% of conductive poly(3-hexylthiophene) (PHT).[78] At 6 wt.% of PHT, the blend exhibited high relative permittivity (13.8 at 1Hz) and a Young's modulus (69 kPa) lower than that of the unblended silicone. SEM images revealed a lack of phase separation, which suggested good compatibility between the rubber and PHT. Although these parameters are ideal for decreasing the driving voltage, the transverse strain of actuation diminished as PHT content increased above 1 wt.%, likely due to the increasing Young's modulus. Incorporating poly(ethylene glycol) (PEG) into a silicone matrix also enabled a significant increase in dielectric permittivity.[79-81] Razak and coworkers synthesized PDMS-PEG multiblock copolymers and used them as fillers in a commercial PDMS matrix.[79] Incorporating PDMS blocks into the PEG filler enhanced the dispersibility and promoted homogeneous films at 5 wt.% of filler content. The films containing 5 wt.% of the filler exhibited a 60% increase in relative permittivity at ambient temperature while maintaining a high dielectric breakdown strength of 100 V $\mu m^{-1}$. As the filler content increased from 5-20 wt.%, SEM images revealed the presence of increasing

spherical PEG domains. Although the higher filler content demonstrated increased relative permittivity, the Young's modulus and dielectric loss factor (electromagnetic energy dissipation) also increased suggesting that macrophase separation in these blends may diminish actuator performance and lifetime.

### 2.4.2 Acrylic Elastomers

Acrylic elastomers typically have a slightly higher relative permittivity and have the capability to produce much larger actuation strains than silicone elastomers. However, acrylic DEAs suffer from slow response times, and are often sensitive to humidity and lower temperature ranges when compared to silicone DEAs.[82-83] Nevertheless, Pelrine and coworkers showed that a commercial acrylic elastomer known as VHB 4910 from 3M achieved up to 215% actuated strain after prestretching the polymer.[7] Although prestretching the acrylic elastomers leads to a major improvement in actuated strain, it also limits applications and lowers the lifetime of the DEA due to stress relaxation and fatigue in the film. This has lead researchers to explore materials that do not require prestretching to reach large actuation strains.[84-85] Niu et al. synthesized new acrylic elastomers through the UV curing of eight different commercial acrylate and diacrylate formulations such as: CN9021 (a difunctional acrylic esters resin), isobornyl acrylate (IBOA), 1,6-hexanediol diacrylate (HDDA), isodecyl acrylate (IDA), trimethylolpropane triacrylate (TMPTA), and dibutoxyethoxyethyl formal (DBEF).[84] **Figure 2.9a** shows DEAs made from three different formulations, and actuated at five electric field strengths. The formulation with the lowest amount of HDDA crosslinker demonstrated a high areal strain of 318% at 27.4 V $\mu m^{-1}$ without prestretching. This acrylic elastomer composition exhibited a two-fold increase in actuated strain at one quarter of the electric field strength compared to a sample of biaxially prestretched VHB4905 (**Figure 2.9b**).

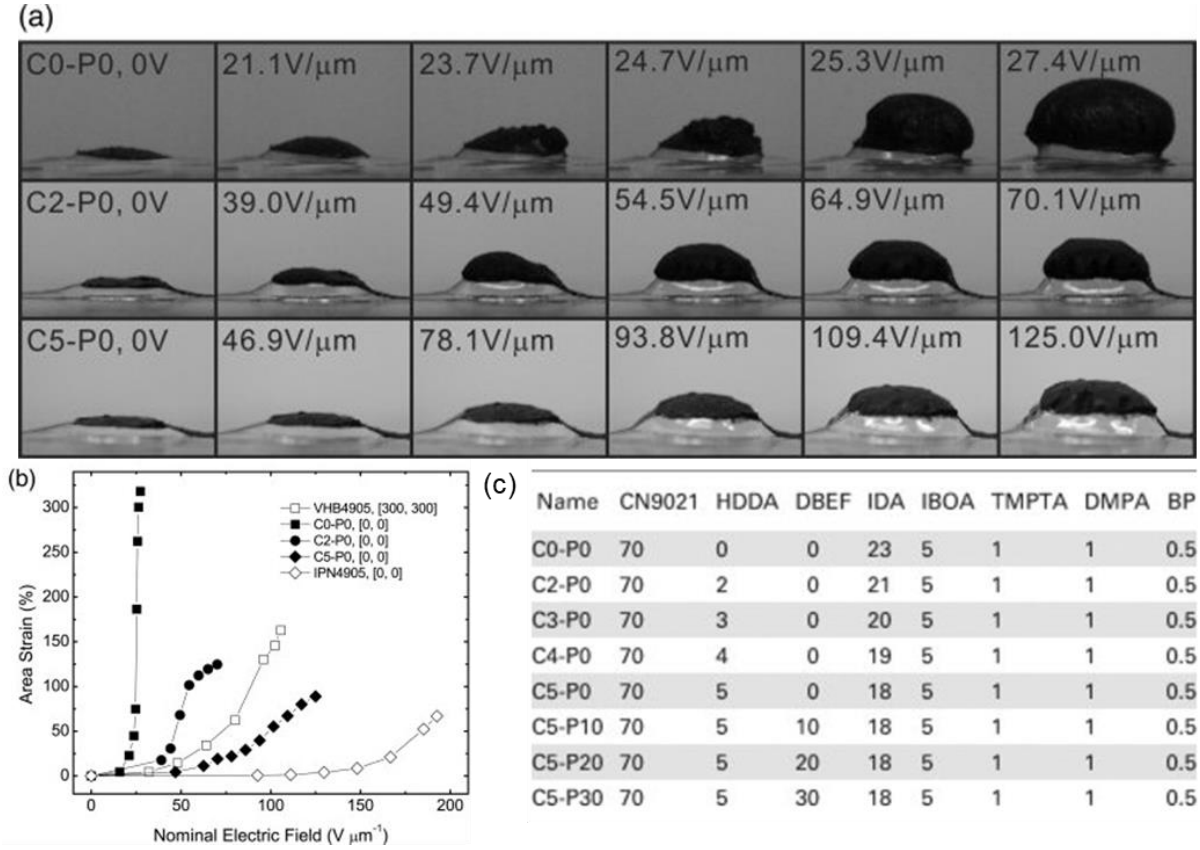


| Name | CN9021 | HDDA | DBEF | IDA | IBOA | TMPTA | DMPA | BP |
|---|---|---|---|---|---|---|---|---|
| C0-P0 | 70 | 0 | 0 | 23 | 5 | 1 | 1 | 0.5 |
| C2-P0 | 70 | 2 | 0 | 21 | 5 | 1 | 1 | 0.5 |
| C3-P0 | 70 | 3 | 0 | 20 | 5 | 1 | 1 | 0.5 |
| C4-P0 | 70 | 4 | 0 | 19 | 5 | 1 | 1 | 0.5 |
| C5-P0 | 70 | 5 | 0 | 18 | 5 | 1 | 1 | 0.5 |
| C5-P10 | 70 | 5 | 10 | 18 | 5 | 1 | 1 | 0.5 |
| C5-P20 | 70 | 5 | 20 | 18 | 5 | 1 | 1 | 0.5 |
| C5-P30 | 70 | 5 | 30 | 18 | 5 | 1 | 1 | 0.5 |

**Figure 2.9:** (a) Three acrylic elastomer DEA compositions actuated at various electric field strengths. (b) Actuated strain vs. electric field strength for three DEA formulations compared to standard VHB and IPN DEAs. (c) Composition information of acrylic elastomers.[84]

Although these materials have excellent electromechanical properties, they still required large electric fields to actuate due to the inherently low dielectric permittivity of acrylic elastomers. Zhang and coworkers recently reported acrylic elastomers with grafted copper phthalocyanine oligomer (CuPC) (**Figure 2.10b**) pendant groups, which formed highly dielectric nanocomposites.[86-88] The reaction of -OH groups from the acrylic copolymer with toluene diisocyante yielded functional isocyanate pendant groups as shown in **Figure 2.10a**.[86] This allowed the terminal carboxylic acid groups from the CuPC to form covalent linkages with the polymer, effectively forming a crosslinked network.[86] The acrylic elastomers containing 15 wt.% of grafted CuPC achieved an enormous room temperature relative permittivity of 303 at 100 Hz, 60 times higher than the pure acrylic elastomer. All the elastomers also exhibited low dielectric

(a)

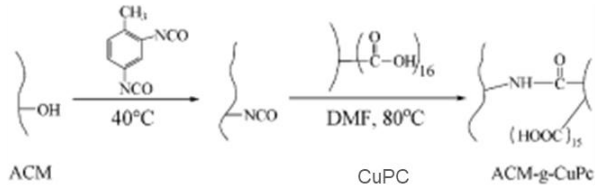


(b)

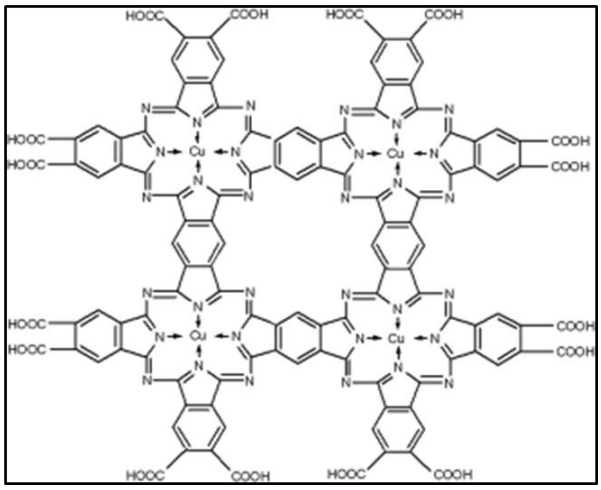


**Figure 2.9:** (a) Synthesis of ACM-graft-CuPC starting from an acrylic elastomer (ACM) (b) structure of copper phthalocyanine oligomer.[86]

loss (< 0.4). The elastomer displayed a relatively high Young's modulus (2.97 MPa for 15% grafted) and showed an actuated strain of 8.7% at 8.18 V $\mu m^{-1}$. Despite these excellent results, the elastomers have low breakdown voltages of 20.6 V $\mu m^{-1}$. Furthermore, the synthetic method utilized potentially suffers from poor reproducibility and a complicated synthetic procedure involving isocyanates, although others have confirmed the formation of the amide bond under appropriate reaction conditions. Wang et al. later simplified the synthesis using a simple esterification to graft the CuPC.[88] These acrylics containing 11 wt.% of grafted CuPC exhibited a room temperature relative permittivity of 173 at 100 Hz, resembling that of the 10 wt.% graft acrylic reported by Wang et al. (192 at 100 Hz).

Hu et al. synthesized UV curable acrylic elastomers from formulations of n-butyl acrylate, acrylic acid, and two commercial Sartomer diacrylates.[89] They discovered that varying the content of acrylic acid in each formation had a large effect on the electromechanical properties of the actuator. For example, Young's modulus and the dielectric constant increased as a function of acrylic acid content between 0-20 wt.%. Compositions with 13 wt.% of acrylic acid showed the best electromechanical properties with a relative permittivity of 6.0, breakdown voltage of 222 V $\mu m^{-1}$, and maximum areal strain at 186% (300% pre-strain). Most properties of the material started

to decrease at acrylic acid concentrations greater than 13% except for the dielectric constant, which the authors attributed to an increase in current leakage at higher acrylic acid contents.

### 2.4.3 Other Dielectric Elastomers

Silicones and acrylics comprise a majority of the DEA literature, however, other elastomeric materials have emerged as well. Thermoplastic elastomers (TPE) are triblock copolymers, which consist of a low $T_g$ inner block capped at either end with high $T_g$ external blocks. The immiscibility of the hard and soft phase causes these materials to phase separate into nanostructured morphologies, creating physical crosslinks. These crosslinks induce a shape memory effect in TPEs, which endows them with high strain capabilities for DEAs.[90] Recent examples of TPEs for DEs include poly[styrene-*b*-(ethylene-*co*-butylene)-*b*-styrene] (SEBS),[91] poly[styrene-*b*-(*n*-butyl acrylate)-*b*-styrene] (SBAS),[92] and poly[(methyl methacrylate)-*b*-(n-butyl acrylate)-*b*-(methyl methacrylate)] (PMMA-PBA-PMMA)[93-94]. Pèrez-Madrigal and coworkers demonstrated the dielectric properties of SEBS composites containing poly(3-methylthiophene acetate) (P3TMA).[91] They found that increasing the amount of P3HT loading from 0-20 wt.% afforded an increase in the relative permittivity from 2.9-6.7, respectively. SEM and AFM images revealed increased P3TMA aggregate sizes with increased filler content, especially above 5% loading. As a result, nanocomposites containing less than 5 wt.% of P3TMA all showed similar values for Young's modulus while those with higher loadings experienced a moderate increase. These nanocomposites have the benefit of easy processing as well as decent dielectric properties, which makes them a promising candidate for DEAs.

Another example of non-silicone or acrylic elastomers comes from Poikelispää et al. who discuss the potential of high actuation from commercially available diene-based rubbers.[95] Acrylonitrile-butadiene rubbers (NBR) exhibit increasingly large relative permittivity with

increasing acrylonitrile content. Despite this fact, NBR with lower acrylonitrile contents exhibited better electromechanical strain due to their lower Young's moduli. Introducing plasticizer with the rubber further increased the electromechanical properties and allowed NBR to strain 1.8% at the low electric field strength of 7 V $\mu m^{-1}$. The ability to tune the electromechanical properties of commercial polydiene rubbers makes them attractive candidates for DEA applications. **Table 2.2** summarizes the properties of selected DEAs.

**Table 2.2:** Polymer backbone, polar group structure, relative permittivity, Young's modulus, breakdown electric field ($E_b$), electric field during testing (E), and strain for selected DEAs

| Polymer Backbone | Polar Group | ε' [a] | Y (kPa) | $E_b$ (V $\mu m^{-1}$) | E (V $\mu m^{-1}$) | Strain[h] (%) | Ref |
|---|---|---|---|---|---|---|---|
| Siloxane | 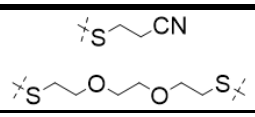 | 10.1 | 154[b] | 10.8 | 10.0 | 17.4 | 59 |
| Siloxane | 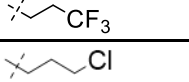 | 6.20 | 19.0[b] | 7.80 | 7.80 | 5.40 | 62 |
| Siloxane |  | 4.70[c] | 1.00x10[3] [d] | 94.4 | - | - | 65 |
| Siloxane | 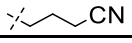 | 3.50 | 712 | 42.0 | 42.0 | 11.8 | 68 |
| Siloxane | 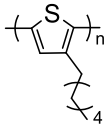 (blend) | 5.60[e] | 20.0[f] | 8.20 | 8.00 | 7.70 | 75, 78 |
| Siloxane | 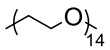 (blend) | ~5.00 | ~450[d] | - | 40.0 | 11.5[i] | 80 |
| Acrylic | - | ~5.0 | - | 114 | 27.4 | 318[j] | 84 |
| Acrylic | CuPC | 303[c] | 2.97x10[3] | 20.6 | 8.18 | 8.70 | 86 |
| Acrylic |  (copolymer) | 6.00 | - | 222 | 222 | 65.0[g] | 89 |
| Acrylic Triblock Copolymer | 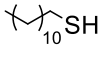 (plasticizer) | ~7.00[k] | 10.0 | - | 5.00x10[3] | ~6.00[j] | 94 |

[a] measured at 10 kHz unless otherwise noted
[b] measured at 10% strain
[c] measured at 100 Hz

[d] measured at 5% strain
[e] measured at 10 Hz
[f] measured at 100% pre-strain
[g] 300% biaxial prestrain
[h] lateral strain unless otherwise noted
[i] planar strain
[j] area strain
[k] measured at 1 Hz

## 2.5 Future Directions and Perspectives

Employing EAPs in electromechanical devices remains a central focus of research for the advancement of soft robotics, artificial muscles, and sensors. Recent literature has predominantly focused on improving ionic polymers and DEs for these devices in lieu of other EAPs such as conductive or electrostrictive polymers, likely due to their synthetic diversity and commercial availability. The design of novel ionic polymers for IPMCs currently tends toward phase separated morphologies that contain a low $T_g$, continuous charged phase. The inherently low conductivity of these polymers so far necessitates the incorporation of free ionic liquids to endow them with suitable conductivities for fast actuation. Conversely, research into novel DEAs tends toward modifying commercially available DEs to improve their permittivity and modulus as opposed to synthesizing novel structures. Covalently attaching or physically blending high dielectric materials into a DE network provides the simplest route toward improving permittivity and thus lowering operating voltages in DEAs; however, increasing DE permittivity without sacrificing compliance remains a challenge in the field.

A large majority of the ionic polymers studied for IPMCs are either sulfonated or contain an imidazolium-based polymerized IL due to the wide availability of these monomers. Likewise, ILs used to swell IPMC membranes overwhelmingly contain imidazolium. Incorporating other free or polymerized ILs such as ammonium, sulfonium, or phosphonium based ILs presents an

opportunity to explore an even wider variety of IPMCs.[96] Although these types of ILs are commercially available at only research quantities, their unique properties (e.g., high thermal stability, higher conductivities compared to ammonium analogues[97]) will have a significant impact on the conductivities and mechanical properties of IPMCs.

EAPs are attractive materials for electromechanical actuators due to their low cost and light weight; however, the high-cost and difficult processing conditions of electrodes severely limits the commercial viability of polymeric actuators. Most electrodes for polymeric actuators consist of noble metals (i.e., gold, silver, and platinum) or carbon nanomaterials (i.e., graphene and carbon nanotubes) plated onto the polymer using either vapor deposition or a chemical reduction. These electrode materials are expensive, and the deposition process suffers from irreproducibility. Moreover, the rigid electrodes can limit the mechanical properties and response times of the actuator. Keplinger showed that electrodes made from hydrogels have the capacity to deliver potentials of several kilovolts through the formation of a charged double layer at the interface of the hydrogel and a dielectric elastomer under an applied voltage (**Figure 2.11**).[98-99] The use of hydrogel or ionogel[100] electrodes allows for the production of completely optically clear, flexible electromechanical devices, and has the potential to replace metal electrodes in future DEAs. Furthermore, improving the lifetime of DEAs remains an obstacle to widespread

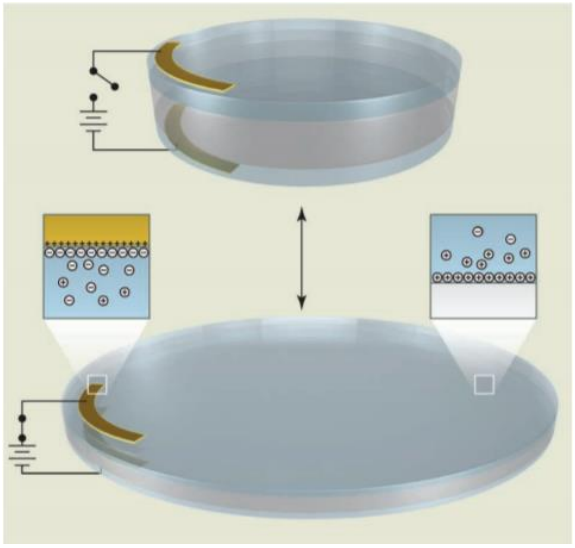

**Figure 2.10:** Hydrogels transport ions to the interface of a dielectric elastomer forming a charged double layer. Subsequently, the double layer produces a large potential, which causes actuation. Reproduced with permission from Rogers.[98] Copyright 2013, The American Association for the advancement of Science.

commercialization of DEA devices. Incorporating ionic or hydrogen bonds into DEA materials promotes self-healing after a breakdown event, which helps to improve the lifetime of the DEA.[59,101]

As mentioned previously, polymeric electromechanical devices are suitable materials for sensors and biomimetic actuators. However, the difficulty in processing Nafion™ into three-dimensional structures prevents the fabrication of complex devices. Carrico et al. demonstrated the 3D printing of Nafion™ IPMCs using fused deposition modeling.[102-103] This process involved extruding a Nafion™ precursor filament into the desired 3D shape, functionalizing the precursor to give the final Nafion™ structure, and then plating the structure with platinum using a reduction process shown in **Figure 2.12.**[103] Designing conductive or dielectric polymers suitable for 3D printing opens the door for a new generation of 3D IPMCs and DEAs.

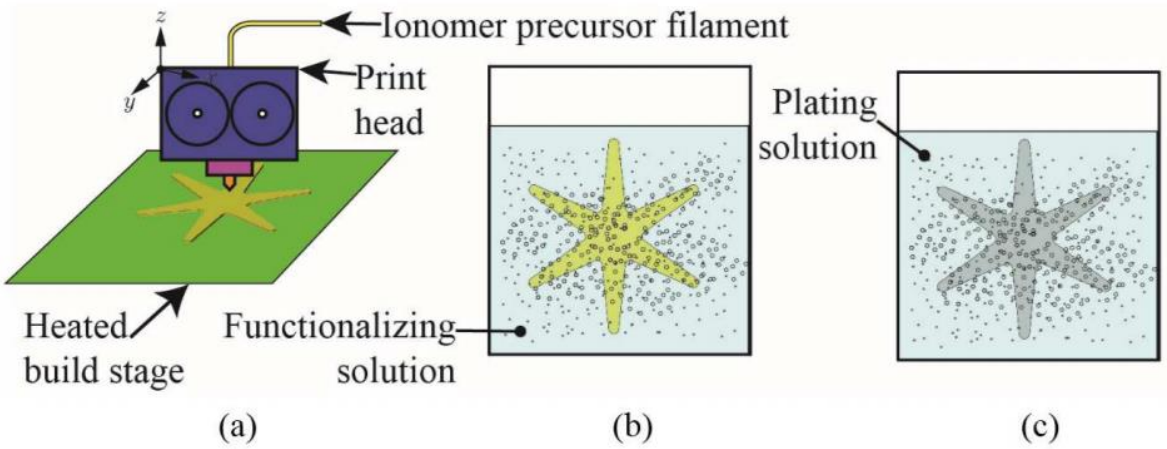


**Figure 2.11:** (a) extrusion of Nafion™ precursor from a customized 3D printer (b) functionalization of precursor to form Nafion™ (c) platinum plating solution to form final IPMC structure. Reproduced with permission from Carrico et al. [103] Copyright 2017, Society of Photo-Optical Instrumentation Engineers (SPIE).

## 2.6 Conclusions

This review covered the recent advances in materials for EAP actuators. A need to produce low voltage, high strain actuators for applications in soft robotics, artificial muscles, and sensors

presents itself in the field. The morphology of Nafion™ actuators inspired the design of a new generation of high performance IPMCs. New ionic polymers based on block copolymers, ILs, condensation polymers, and polysaccharides showed competitive actuation performances with Nafion™. These new materials provide several advantages over Nafion™ such as: easy processing, tunable electromechanical properties, and the potential to limit back relaxation. This review also highlighted the electrical and mechanical properties necessary for ionic polymer membranes to form IPMCs. In general, IPMCs demonstrated the best electromechanical performance when the ionic polymers exhibited storage moduli on the order of 100MPa and conductivities greater than $10^{-6}$ S/cm. These empirical values offer general guidelines for the design of future high-performance IPMCs.

The advances in DEAs have come primarily in the form of decreasing the operating voltages in these devices. The modification of siloxanes and acrylic elastomers with high dielectric pendant groups or fillers increased the permittivity and decreased the operating voltages DEA actuators. Increasing the dielectric permittivity above 3 while maintaining compliance was crucial to lowering the driving voltages in DEA actuators. In addition to decreasing the voltage, eliminating the need for prestretching in DEAs represents another critical improvement over commercial materials. DEAs utilizing hydrogels and ionogels as electrodes exhibited excellent actuation properties and represent a new class of completely transparent DEAs for the future.

## 2.7 Acknowledgements

The authors would like to thank Dr. Mingtao Chen for his editorial input and technical expertise especially regarding ionic polymer-metal composites.

## 2.8 References


1. Madsen, F. B.; Daugaard, A. E.; Hvilsted, S.; Skov, A. L., *Macromol. Rapid Commun.* **2016,** *37* (5), 378-413.
2. Mirfakhrai, T.; Madden, J. D. W.; Baughman, R. H., *Mater. Today* **2007,** *10* (4), 30-38.
3. Bahramzadeh, Y.; Shahinpoor, M., *Soft Robotics* **2014,** *1* (1), 38-52.
4. Shahinpoor, M., *Electrochim. Acta* **2003,** *48* (14), 2343-2353.
5. Bar-Cohen, Y.; *Artificial muscles using electroactive polymers (EAP): capabilities, challenges and potential*; NASA technical report; **2005**.
6. Madden, J. D. W., Dielectric Elastomers as Electromechanical Transducers: Fundamentals, Materials, Devices, Models and Applications of an Emerging Electroactive Polymer Technology. Elsevier: Oxford, **2008**, pp 13-21.
7. Pelrine, R.; Kornbluh, R.; Pei, Q.; Joseph, J., *Science* **2000,** *287* (5454), 836-839.
8. Duncan, A. J.; Leo, D. J.; Long, T. E., *Macromolecules* **2008,** *41* (21), 7765-7775.
9. Graziani, S., Ionic Polymer Metal Composites as Post-silicon Transducers for the Realisation of Smart Systems. Royal Society of Chemistry: Cambridge, **2016**; Vol. 2, pp 158-214.
10. Nemat-Nasser, S.; Li, J. Y., *J. Appl. Phys.* **2000,** *87* (7), 3321-3331.
11. Green, M. D.; Wang, D.; Hemp, S. T.; Choi, J.-H.; Winey, K. I.; Heflin, J. R.; Long, T. E., *Polymer* **2012,** *53* (17), 3677-3686.
12. Chen, Z.; Tan, X., *IEEE/ASME Trans. Mechatronics* **2008,** *13* (5), 519-529.
13. Pugal, D.; Jung, K.; Aabloo, A.; Kim, K. J., *Polym. Int.* **2010,** *59* (3), 279-289.
14. Eisenberg, A.; Hird, B.; Moore, R. B., *Macromolecules* **1990,** *23* (18), 4098-4107.
15. Weber, R. L.; Ye, Y.; Schmitt, A. L.; Banik, S. M.; Elabd, Y. A.; Mahanthappa, M. K., *Macromolecules* **2011,** *44* (14), 5727-5735.
16. Gwee, L.; Choi, J.-H.; Winey, K. I.; Elabd, Y. A., *Polymer* **2010,** *51* (23), 5516-5524.
17. Green, M. D.; Choi, J.-H.; Winey, K. I.; Long, T. E., *Macromolecules* **2012,** *45* (11), 4749-4757.
18. Zheng, W.; Cornelius, C. J., *Polymer* **2016,** *103*, 104-111.
19. Vargantwar, P. H.; Roskov, K. E.; Ghosh, T. K.; Spontak, R. J., *Macromol. Rapid Commun.* **2012,** *33* (1), 61-68.
20. Jangu, C.; Wang, J. H. H.; Wang, D.; Sharick, S.; Heflin, J. R.; Winey, K. I.; Colby, R. H.; Long, T. E., *Macromol. Chem. Phys.* **2014,** *215* (13), 1319-1331.
21. Jangu, C.; Wang, J.-H. H.; Wang, D.; Fahs, G.; Heflin, J. R.; Moore, R. B.; Colby, R. H.; Long, T. E., *J. Mater. Chem. C* **2015,** *3* (16), 3891-3901.
22. Margaretta, E.; Fahs, G. B.; Inglefield Jr, D. L.; Jangu, C.; Wang, D.; Heflin, J. R.; Moore, R. B.; Long, T. E., *ACS Appl. Mater. Interfaces* **2016,** *8* (2), 1280-1288.
23. Kim, O.; Kim, S. Y.; Park, B.; Hwang, W.; Park, M. J., *Macromolecules* **2014,** *47* (13), 4357-4368.
24. Lee, J.-W.; Yu, S.; Hong, S. M.; Koo, C. M., *J. Mater. Chem. C* **2013,** *1* (24), 3784-3793.
25. Kim, O.; Shin, T. J.; Park, M. J., *Nat. Commun.* **2013,** *4*, 9.
26. Wang, Z. P.; He, B.; Liu, X. H.; Wang, Q. G., *J. Intell. Mater. Syst. Struct.* **2017,** *28* (15), 2036-2050.
27. Lee, J. Y.; Wang, H. S.; Yoon, B. R.; Han, M. J.; Jho, J. Y., *Macromol. Rapid Commun.* **2010,** *31* (21), 1897-1902.
28. Liu, Y.; Ghaffari, M.; Zhao, R.; Lin, J. H.; Lin, M. R.; Zhang, Q. M., *Macromolecules* **2012,** *45* (12), 5128-5133.
29. Gao, R.; Wang, D.; Heflin, J. R.; Long, T. E., *J. Mater. Chem.* **2012,** *22* (27), 13473-13476.

30. Almomani, A.; Hong, W. Y. J.; Hong, W.; Montazami, R., *Polymers* **2017,** *9* (8), 13.
31. Ishii, S.; Kokubo, H.; Hashimoto, K.; Imaizumi, S.; Watanabe, M., *Macromolecules* **2017,** *50* (7), 2906-2915.
32. Song, J.; Jeon, J. H.; Oh, I. K.; Park, K. C., *Macromol. Rapid Commun.* **2011,** *32* (19), 1583-1587.
33. Rajagopalan, M.; Jeon, J.-H.; Oh, I.-K., *Sensors Actuators B: Chem.* **2010,** *151* (1), 198-204.
34. Rajagopalan, M.; Oh, I.-K., *ACS Nano* **2011,** *5* (3), 2248-2256.
35. Imaizumi, S.; Ohtsuki, Y.; Yasuda, T.; Kokubo, H.; Watanabe, M., *ACS Appl. Mater. Interfaces* **2013,** *5* (13), 6307-6315.
36. Kwon, T.; Cho, H.; Lee, J.-W.; Henkensmeier, D.; Kang, Y.; Koo, C. M., *ACS Appl. Mater. Interfaces* **2017,** *9* (34), 29063-29070.
37. Duncan, A. J.; Layman, J. M.; Cashion, M. P.; Leo, D. J.; Long, T. E., *Polym. Int.* **2010,** *59* (1), 25-35.
38. Wang, X.-L.; Oh, I.-K.; Lee, S., *Sensors Actuators B: Chem.* **2010,** *150* (1), 57-64.
39. Tang, Y. J.; Chen, C.; Ye, Y. S.; Xue, Z. G.; Zhou, X. P.; Xie, X. L., *Polym. Chem.* **2014,** *5* (20), 6097-6107.
40. Tas, S.; Zoetebier, B.; Sukas, O. S.; Bayraktar, M.; Hempenius, M.; Vancso, G. J.; Nijmeijer, K., *Macromol. Mater. Eng.* **2017,** *302* (4), 6.
41. Jeon, J.-H.; Kang, S.-P.; Lee, S.; Oh, I.-K., *Sensors Actuators B: Chem.* **2009,** *143* (1), 357-364.
42. Kwon, T.; Lee, J. W.; Cho, H.; Henkensmeier, D.; Kang, Y.; Hong, S. M.; Koo, C. M., *Sensors Actuators B: Chem.l* **2015,** *214*, 43-49.
43. Lu, L.; Chen, W., *Adv. Mater.* **2010,** *22* (33), 3745-3748.
44. Zhao, G.; Sun, Z. Z.; Wang, J.; Xu, Y.; Muhammad, F., *Polym. Compos.* **2017,** *38* (8), 1609-1615.
45. Sun, Z. Z.; Zhao, G.; Song, W. L., *Cellulose* **2017,** *24* (2), 441-445.
46. Shang, J.; Shao, Z. Z.; Chen, X., *Polymer* **2008,** *49* (25), 5520-5525.
47. Altınkaya, E.; Seki, Y.; Yılmaz, Ö. C.; Çetin, L.; Özdemir, O.; Şen, İ.; Sever, K.; Gürses, B. O.; Sarıkanat, M., *Composites Sci. Technol.* **2016,** *129*, 108-115.
48. Jeon, J.-H.; Oh, I.-K.; Kee, C.-D.; Kim, S.-J., *Sensors Actuators B: Chem.* **2010,** *146* (1), 307-313.
49. Cai, Z. J.; Hou, C. W.; Yang, G., *Carbohydr. Polym.* **2012,** *87* (1), 650-657.
50. Cai, Z.; Kim, J., *J. Appl. Polym. Sci.* **2008,** *109* (6), 3689-3695.
51. Cai, Z.; Kim, J., *J. Appl. Polym. Sci.* **2010,** *115* (4), 2044-2049.
52. Mahadeva, S. K.; Kim, J.; Kang, K. S.; Kim, H. S.; Park, J. M., *J. Appl. Polym. Sci.* **2009,** *114* (2), 847-852.
53. Ozdemir, O.; Karakuzu, R.; Sarikanat, M.; Akar, E.; Seki, Y.; Cetin, L.; Sen, I.; Gurses, B. O.; Yilmaz, O. C.; Sever, K.; Mermer, O., *Cellulose* **2015,** *22* (3), 1873-1881.
54. Li, J.; Vadahanambi, S.; Kee, C. D.; Oh, I. K., *Biomacromolecules* **2011,** *12* (6), 2048-2054.
55. Cai, Z.; Kim, J., *Smart Mater. Struct.* **2008,** *17* (3), 035028.
56. Hong, C.-H.; Ki, S.-J.; Jeon, J.-H.; Che, H.-l.; Park, I.-K.; Kee, C.-D.; Oh, I.-K., *Composites Sci. Technol.* **2013,** *87*, 135-141.
57. Tungkavet, T.; Seetapan, N.; Pattavarakorn, D.; Sirivat, A., *Polymer* **2015,** *70*, 242-251.
58. Tian, K.; Shao, Z. Z.; Chen, X., *Biomacromolecules* **2010,** *11* (12), 3638-3643.

59. Dünki, S. J.; Ko, Y. S.; Nüesch, F. A.; Opris, D. M., *Adv. Funct. Mater.* **2015,** *25* (16), 2467-2475.
60. Pelrine, R.; Kornbluh, R.; Kofod, G., *Adv. Mater.* **2000,** *12* (16), 1223-1225.
61. Brochu, P.; Pei, Q., *Macromol. Rapid Commun.* **2010,** *31* (1), 10-36.
62. Dascalu, M.; Dünki, S. J.; Quinsaat, J.-E. Q.; Ko, Y. S.; Opris, D. M., *RSC Adv.* **2015,** *5* (126), 104516-104523.
63. Racles, C.; Alexandru, M.; Bele, A.; Musteata, V. E.; Cazacu, M.; Opris, D. M., *RSC Adv.* **2014,** *4* (71), 37620-37628.
64. Dünki, S. J.; Tress, M.; Kremer, F.; Ko, S. Y.; Nüesch, F. A.; Varganici, C.-D.; Racles, C.; Opris, D. M., *RSC Adv.* **2015,** *5* (62), 50054-50062.
65. Madsen, F. B.; Yu, L.; Daugaard, A. E.; Hvilsted, S.; Skov, A. L., *RSC Adv.* **2015,** *5* (14), 10254-10259.
66. Kussmaul, B.; Risse, S.; Kofod, G.; Wache, R.; Wegener, M.; McCarthy, D. N.; Kruger, H.; Gerhard, R., *Adv. Funct. Mater.* **2011,** *21* (23), 4589-4594.
67. Madsen, F. B.; Yu, L. Y.; Daugaard, A. E.; Hvilsted, S.; Skov, A. L., *Polymer* **2014,** *55* (24), 6212-6219.
68. Racles, C.; Cazacu, M.; Fischer, B.; Opris, D. M., *Smart Mater. Struct.* **2013,** *22* (10), 104004.
69. Dunki, S. J.; Cuervo-Reyes, E.; Opris, D. M., *Polym. Chem.* **2017,** *8* (4), 715-724.
70. Liu, H.; Zhang, L.; Yang, D.; Yu, Y.; Yao, L.; Tian, M., *Soft Mater.* **2013,** *11* (3), 363-370.
71. Stoyanov, H.; Brochu, P.; Niu, X.; Della Gaspera, E.; Pei, Q., *Appl. Phys. Lett.* **2012,** *100* (26), 262902.
72. Vudayagiri, S.; Zakaria, S.; Yu, L.; Hassouneh, S. S.; Benslimane, M.; Skov, A. L., *Smart Mater. Struct.* **2014,** *23* (10), 105017.
73. Bele, A.; Cazacu, M.; Stiubianu, G.; Vlad, S.; Ignat, M., *Composites Part B* **2015,** *68*, 237-245.
74. Stiubianu, G.; Bele, A.; Cazacu, M.; Racles, C.; Vlad, S.; Ignat, M., *Mater. Res. Bull.* **2015,** *71*, 67-74.
75. Gallone, G.; Galantini, F.; Carpi, F., *Polym. Int.* **2010,** *59* (3), 400-406.
76. Böse, H.; Uhl, D.; Rabindranath, R. In *Novel DEA with organically modified silicone elastomer for permittivity enhancement*, SPIE Smart Structures and Materials+ Nondestructive Evaluation and Health Monitoring, International Society for Optics and Photonics: **2012**; pp 83402E-83402E-83410.
77. Risse, S.; Kussmaul, B.; Krüger, H.; Kofod, G., *Adv. Funct. Mater.* **2012,** *22* (18), 3958-3962.
78. Carpi, F.; Gallone, G.; Galantini, F.; De Rossi, D., *Adv. Funct. Mater.* **2008,** *18* (2), 235-241.
79. Razak, A. H. A.; Szabo, P.; Skov, A. L., *RSC Adv.* **2015,** *5* (65), 53054-53062.
80. Liu, H.; Zhang, L.; Yang, D.; Ning, N.; Yu, Y.; Yao, L.; Yan, B.; Tian, M., *J. Phys. D: Appl. Phys.* **2012,** *45* (48), 485303.
81. Wang, G. L.; Zhang, Y. Y.; Zhang, J.; Ding, K. H.; Wang, Z. F.; Zhang, M., *J. Appl. Polym. Sci.* **2017,** *134* (38), 6.
82. Michel, S.; Zhang, X. Q. Q.; Wissler, M.; Lowe, C.; Kovacs, G., *Polym. Int.* **2010,** *59* (3), 391-399.
83. Romasanta, L. J.; Lopez-Manchado, M. A.; Verdejo, R., *Prog. Polym. Sci.* **2015,** *51* (Supplement C), 188-211.

84. Niu, X.; Stoyanov, H.; Hu, W.; Leo, R.; Brochu, P.; Pei, Q., *J. Polym. Sci., Part B: Polym. Phys.* **2013,** *51* (3), 197-206.
85. Duduta, M.; Wood, R. J.; Clarke, D. R., *Adv. Mater.* **2016,** *28* (36), 8058-8063.
86. Liu, R. N.; Wang, J. W.; Li, Q.; Li, S. Q.; Zhang, S.; Ding, X. J., *J. Appl. Polym. Sci.* **2014,** *131* (6), 7.
87. Zhang, S.; Wang, J. W.; Ding, X. J.; Wang, J.; Liu, R. N., *Polym. Bull.* **2015,** *72* (8), 2059-2073.
88. Wang, J.; Wang, J. W.; Zhou, S. W.; Wang, G. Q.; Zhang, S., *J. Appl. Polym. Sci.* **2016,** *133* (36), 6.
89. Hu, W.; Niu, X.; Yang, X.; Zhang, N.; Pei, Q. In *Synthesis and electromechanical characterization of a new acrylic dielectric elastomer with high actuation strain and dielectric strength*, SPIE Smart Structures and Materials+ Nondestructive Evaluation and Health Monitoring, International Society for Optics and Photonics: **2013**; pp 86872U-86872U-86812.
90. El-Sonbati, A., Electroactive Thermoplastic Dielectric Elastomers as a New Generation Polymer Actuators. InTech: **2012**; pp 399-416.
91. Pérez-Madrigal, M. M.; Ochoa, D. A.; García, J. E.; Armelin, E.; Alemán, C., *J. Polym. Sci., Part B: Polym. Phys.* **2016,** *54* (18), 1896-1905.
92. Ma, Z. P.; Xie, Y. H.; Mao, J.; Yang, X. X.; Li, T. F.; Luo, Y. W., *Macromol. Rapid Commun.* **2017,** *38* (16), 6.
93. Jang, Y.; Hirai, T., *Soft Matter* **2011,** *7* (22), 10818-10823.
94. Jang, Y.; Hirai, T.; Ueki, T.; Kato, T., *Polym. Int.* **2012,** *61* (2), 228-234.
95. Poikelispaa, M.; Shakun, A.; Das, A.; Vuorinen, J., *Polym. Adv. Technol.* **2017,** *28* (1), 130-136.
96. Terasawa, N.; Asaka, K., *Sensors Actuators B: Chem.* **2014,** *193* (Supplement C), 851-856.
97. Hemp, S. T.; Zhang, M.; Allen, M. H.; Cheng, S.; Moore, R. B.; Long, T. E., Macromol. Chem. Phys. **2013**, *214* (18), 2099-2107.
98. Rogers, J. A., *Science* **2013,** *341* (6149), 968-969.
99. Keplinger, C.; Sun, J.-Y.; Foo, C. C.; Rothemund, P.; Whitesides, G. M.; Suo, Z., *Science* **2013,** *341* (6149), 984-987.
100. Chen, B.; Lu, J. J.; Yang, C. H.; Yang, J. H.; Zhou, J.; Chen, Y. M.; Suo, Z., *ACS Appl. Mater. Interfaces* **2014,** *6* (10), 7840-7845.
101. Madsen, F. B.; Yu, L.; Skov, A. L., *ACS Macro Lett.* **2016,** *5* (11), 1196-1200.
102. Carrico, J. D.; Traeden, N. W.; Aureli, M.; Leang, K. K., *Smart Mater. Struct.* **2015,** *24* (12), 125021.
103. Carrico, J. D.; Leang, K. K. In *Fused filament 3D printing of ionic polymer-metal composites for soft robotics*, Electroactive Polymer Actuators and Devices (EAPAD) 2017, International Society for Optics and Photonics: **2017**; p 101630I.

# Chapter 3: **Isocyanate- and Solvent-free Synthesis of Melt Processible Polyurea Elastomers Derived from Urea as a Monomer**

Published in *RSC Advances* **2020,** *10* (32), 18760-18768

B. Tyler White[1], John M. Migliore[1,2], Emmanuel U. Mapesa[3], Josh D. Wolfgang[1], Joshua Sangoro[3], and Timothy E. Long[1*]

[1]Department of Chemistry, Macromolecules Innovation Institute (MII), Virginia Tech, Blacksburg, VA 24061

[2]Department of Chemistry, Bethel University, St. Paul, MN 55112

[3]Department of Chemical and Biomolecular Engineering, University of Tennessee, Knoxville, TN 37996

*Address correspondence to: E-mail: Timothy.E.Long@asu.edu.

**Keywords:** Non-isocyanate polyureas, elastomers, dielectric permittivity, urea

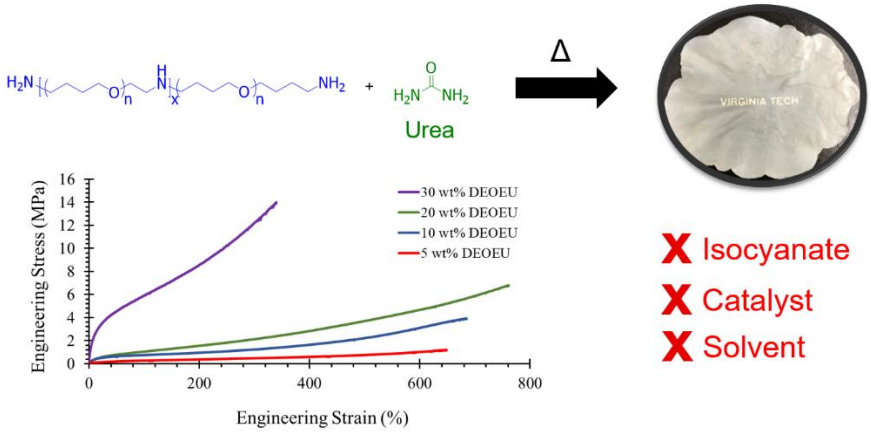


## 3.1 Abstract

Polyurea elastomers are utilized for a myriad of applications ranging from coatings and foams to dielectric materials for capacitors and actuators. However, current synthetic methods for polyureas rely on highly reactive isocyanates, solvents, and catalysts, which collectively pose serious safety considerations. This report details the synthesis and characterization of melt processible, poly(tetramethylene oxide) (PTMO)-based segmented polyurea elastomers utilizing an isocyanate-, solvent-, and catalyst-free approach. Dynamic mechanical analysis and differential

scanning calorimetry suggested microphase separation between the hard and soft segments. Tensile analysis revealed high strain at break for all segmented copolymers between 340 and 770%, and tunable modulus between 0.76 and 29.5 MPa. Dielectric spectroscopy revealed that the composition containing 20 wt.% hard segment offered the highest permittivity at 10.6 (1kHz, 300K) of the segmented copolymers, indicating potential as a dielectric elastomer.

## 3.2 Introduction

Thermoplastic polyurea elastomers (TPUr) consist of alternating, covalently linked soft segments and hard segments. A low $T_g$, flexible polymer defines the soft segments and provides flexibility to the copolymer while the hard segments act as physical crosslinks and impart mechanical strength. The most commonly employed soft segment oligomers in TPUr include amine-terminated poly(ethylene oxide) (PEO)[1], poly(propylene oxide) (PPO)[2], poly(tetramethylene oxide) (PTMO)[3-5], and poly(dimethyl siloxane) (PDMS).[6, 7] Typically, the hard segment forms from the reaction of the soft segment diamine with a diisocyanate and an optional small-molecule diamine chain extender. The resulting urea linkages in the hard segment form strong bidentate hydrogen bonds between polymer chains. The elastomeric properties of TPUr arise from microphase separation that occurs between the hard and soft segments. The degree of microphase separation largely depends on the solubility parameters between the urea units and the chosen soft segment as well as the segment length and the Flory-Huggins interaction parameter ($\chi$).[8] Segmented polyureas generally exhibit better phase separation than polyurethanes owing to the increased polarity of the urea linkage and propensity for bidentate hydrogen bonding, and thus benefit from superior mechanical properties.[9] Many microphase separated TPUr exhibit high tensile strains at break (i.e. >> 100%) while also achieving large ultimate stresses (e.g. > 15 MPa) due to the strength of the hydrogen bonding.[3, 9, 10]

As mentioned previously, the synthesis of polyureas classically involves the reaction of highly toxic diisocyanates with diamines, which poses significant human and environmental health concerns. In addition, toxic catalysts and volatile organic solvents are also frequently employed to facilitate the reaction. In response to these hazards, several isocyanate-free routes to polyureas exist in the literature. The direct incorporation of $CO_2$ with amines leveraging ionic liquids as a green catalyst affords polyureas; however, this method still requires the use of toxic solvents and high pressures, which limit its application.[11] Transurethanization between a diamine and a biscarbamate provides an alternate route towards isocyanate-free polyureas, but requires one or more additional synthetic steps before polycondensation.[12] Furthermore, this synthetic route still requires the use of organic solvents and catalysts. Leibler *et al.* previously demonstrated the ability to synthesize polyurea networks from the melt polycondensation of urea and multifunctional amine-derivatized fatty acids in the absence of a catalyst.[13, 14] This reaction utilized urea as a non-toxic, biologically derived, and relatively inexpensive substitute for isocyanates. Recently, our group also utilized this reaction to synthesize a series of semicrystalline, thermoplastic polyurea copolymers with tunable crystalline melting points.[15] Sirrine and Long *et al.* further expanded on this approach for the synthesis of segmented PDMS-based TPUr with various hard segment contents.[16] The TPUr exhibited high strain at break between 495 and 1180 % dependent on hard segment content. However, the hard segment incorporation for these materials did not exceed 4 wt.%, and thus the maximum stress at break did not exceed 1.16 MPa.

Polymers that exhibit high relative permittivity, or dielectric constant, find use in energy storage devices such as capacitors and actuators.[17, 18] Currently, polysiloxane and acrylic elastomers comprise much of the literature regarding dielectric elastomer actuators (DEA); however, these materials exhibit low relative permittivity values ranging from 3-4. Recent

literature details methods for increasing permittivity of these materials through covalent attachment of dipolar substituents or blending with high permittivity fillers, but these modifications generally result in a corresponding increase in the Young's modulus, which is detrimental to DEA performance. Similarly, biaxially oriented polypropylene (BOPP) remains the benchmark material for high energy density capacitors owing to its high breakdown strength, low dielectric loss, and ease of processability despite having a low dielectric constant (~2.2 at room temperature).[19] Polyureas and polyurethanes have an intrinsically higher dielectric permittivity than silicone and acrylic elastomers or BOPP (> 7) due to the polar nature of the urea/urethane linkage.[20] Furthermore, Lorenzini *et al.* demonstrated the ability to tune the dielectric permittivity of polyureas and polyurethanes through the incorporation of ether linkages into the polymer backbone.[21] Through careful synthetic design, polyureas and polyurethanes with both high permittivity and low modulus are achievable.

This report describes a strategy for utilizing urea as a comonomer to form PTMO-based TPUr with hard segment contents ranging from 5 to 30 wt.%. The melt polycondensation of a commercial PTMO-based diamine with urea and an ether-containing small molecule diamine in the absence of catalyst afforded a library of melt processible segmented polyureas. Thermogravimetric analysis (TGA) further confirmed the hard and soft segment content based on reaction stoichiometry while DSC revealed the thermal transitions in each polyurea. Dynamic mechanical analysis (DMA) suggested the presence of microphase separation. Tensile testing revealed high strain at break and tunable moduli for the segmented polyureas comparable to literature values for isocyanate-based polyureas. Finally, broadband dielectric spectroscopy (BDS) revealed a high dielectric permittivity and relatively low loss for the sample containing 20 wt.% hard segment, indicating the potential for this composition to act as a dielectric elastomer (DE).

## 3.3 Experimental

### 3.3.1 Materials

2,2-(ethylenedioxy)bis(ethylamine) (EBA) (98%) and urea (BioReagent, ≥99%) were purchased from Sigma Aldrich and used as received. Jeffamine® THF-170 was generously provided by the Huntsman Corporation. All reagents were dried overnight at 60 °C at reduced pressure to remove water before use.

### 3.3.2 Synthesis of poly(tetramethylene oxide urea)-co-poly(di(ethylene oxide) ethylene urea)s [poly(PTMOU)-co-poly(DEOEU)s]

The synthesis of the segmented and non-segmented polyureas follows the identical isocyanate-, solvent-, and catalyst-free melt polycondensation procedure as described in previous reports.[15, 16] The reactant amounts were calculated based on the desired hard segment content as described in detail by Sirrine and Long *et al.*[16] The amount of EBA was calculated such that there was a 1.5 mol eq. relative to urea. In a typical synthesis for a polyurea containing 30 wt.% of hard segment, Jeffamine® THF-170 (1700 g $mol^{-1}$, 16.50 g , 9.710 mmol), urea (3.172 g, 52.81 mmol), and EBA (9.580 g, 64.65 mmol) were added to a 100-mL, 1-necked, round-bottomed flask. The flask was equipped with a custom-made t-necked glass adapter with a spherical ball joint, nitrogen inlet, and spherical socket joint. The ball joint from the t-neck was connected to a glass condensing tube with a nitrogen outlet and a corresponding spherical socket joint, which was connected to a 50-mL round-bottomed collection flask. The collection flask was cooled in a bath of dry ice and isopropyl alcohol. The glass t-neck adapter allowed an overhead metal stir rod to pass through and provide mechanical stirring, which was connected by a spherical ball joint attached to Tygon® tubing. Tygon® tubing was attached to the nitrogen outlet and fed into a bubbler of 1M HCl solution to quench any urea that was not condensed in the cold bath. Three alternating vacuum and $N_2$ purge

cycles ensured that oxygen was completely removed and provided an inert atmosphere for the melt polymerization. The reaction vessel was heated under a constant flow of $N_2$ (~10 mL $min^{-1}$) to 170 °C and stirred (~80 RPM) for 1 h to provide a homogeneous melt before increasing the temperature. The presence of ammonia gas was observed within the first 1 h of the reaction.

Subsequently, the reaction mixture was heated to 200 °C for 1 h and 220 °C for 30 min while stirring under nitrogen flow. In the final step, the reaction mixture was heated to 250 °C and vacuum was applied for 2 h to remove the excess diamine generated through transureaization. The melt viscosity increased substantially during this step resulting in the polymer wrapping around the stir rod. Non-segmented poly(PTMOU) was synthesized with an identical synthetic method without incorporating EBA as a chain extender; 1 mol eq of Jeffamine® to urea was utilized for the non-segmented synthesis. The resulting polyureas were isolated and used without further purification.

### 3.3.3 Analytical Methods

The PTMO-based polyureas were dried in a vacuum oven for 18 h at 60 °C prior to melt processing. The samples were compression molded at 180 °C between two sheets of silicone-treated PET separated by 0.5 mm thick shims to obtain free-standing, creasable films. Before each experiment, the films were dried overnight in a vacuum oven at 60 °C and allowed to slow cool for at least 2 h in a dry box (< 5% RH) until utilized for analysis. Thermogravimetric analysis (TGA) was carried out on a TA Instruments Q500 TGA under nitrogen flow at a heating rate of 10 °C $min^{-1}$ to 800 °C. Stepwise isothermal TGA experiments were performed on the same instrument at a rate of 10 °C $min^{-1}$ under nitrogen. When the rate of weight change reached 1% $min^{-1}$, the TGA was held at that temperature until the rate of change dropped below 0.1% $min^{-1}$, at which time the temperature continued to ramp at 10 °C $min^{-1}$. Differential scanning calorimetry

(DSC) was performed using a TA Instruments Q200 DSC equipped with a liquid nitrogen cooling system. The thermal transitions were determined from the second heat cycle and were measured at a heating/cooling rate of 10 °C $min^{-1}$ from -120 to 200 °C under a constant helium purge. Glass transition temperatures were determined from the temperature at the half-height of the endothermic step transitions, and the melting points were taken as the peak temperature of each melting endothermic event.

Dynamic mechanical analysis (DMA) was carried out using a TA Instruments Q800 DMA equipped with a liquid nitrogen gas cooling accessory. DMA experiments were performed in oscillatory tension mode at a frequency of 1 Hz and 0.1% strain such that it remained within the linear viscoelastic region with a heating/cooling rate of 3 °C $min^{-1}$. The data collection was discontinued after the modulus dropped below 0.1 MPa or once the length of the sample, as measured by the instrument, increased more than 1%. Variable temperature Fourier transformed infrared spectroscopy (VT-FTIR) experiments were performed on a Varian 670-IR spectrometer, which was equipped with a PIKE Technologies diamond crystal variable temperature GladiATR™ attachment. Spectra were collected from 30-160 °C at every 10 °C, and every other temperature was plotted to show trends. Tensile tests and hysteresis were performed with an Instron® 5500R. Dogbone specimens were punched from films using an ASTM D638-V cutting die. Tensile tests were carried out at crosshead separation speed of 5 mm $min^{-1}$. The single depicted stress/strain curve and the corresponding tensile values for each sample were reported as an average of 5 runs. Hysteresis experiments were conducted at a maximum of 200% strain for each sample. The strain rate was 19% $min^{-1}$ for 5 cycles with a 10-minute hold at 0% strain between each cycle. The area under the curves was calculated using the trapezoid method to give % hysteresis.

For dielectric studies, polymer samples were hot-pressed in nitrogen ambience at 400 K using a Specac Mini-Film Maker to obtain 100 µm thick films. The films were then sandwiched between 20 mm stainless steel electrodes in a parallel-plate configuration with 100 µm silica rod spacers incorporated to maintain sample thickness. All dielectric measurements were carried out on a high resolution Novocontrol Alpha Analyzer (frequency range $10^{-1}$ – $10^{7}$ Hz) and the temperature control regulated by a QUATRO system (Novocontrol) using a jet of dry nitrogen, thereby ensuring relative and absolute errors better than 0.1 and 2 K, respectively. Before substantive measurements, the films were annealed at 400 K for at least 7 h to remove any possible adsorbed water. Selected permittivity data was taken at 300 K.

## 3.4 Results and Discussion

The melt condensation of amines with urea to form substituted ureas through the *in situ* formation of isocyanic acid has been described previously in the literature.[13, 15, 16, 22] **Scheme 3.1** shows the unprecedented synthesis of segmented copolyureas through the melt polycondensation of a commercial PTMO-based diamine, urea, and an optional small-molecule diamine chain extender (EBA). The reaction mixture remained heterogeneous below the melting point of urea (135 °C). The urea decomposed into isocyanic acid and ammonia above 150 °C, which allowed for the reaction with the primary amines to form the 1,3-dialkyl urea linkage. A 1.5 molar excess of the EBA chain extender to urea for the segmented copolyureas helped to account for volatilization of the small-molecule EBA at the beginning of the reaction. Additionally, a stoichiometric excess of amine over urea and heating to temperatures in excess of 200 °C limited the formation of side products such as 1,1-dialkylurea, biurets, and imidazolidone cyclics.[13, 16, 22] Initial reaction temperatures of 170 °C facilitated oligomerization and allowed for limited volatilization of the small molecule diamine in the early stages of the reaction. Increasing the

temperature incrementally to 250 °C ensured a low melt viscosity while further facilitating the reaction. The reaction proceeded under reduced pressure at 250 °C in the final stage allowing for the removal of excess EBA and the gaseous ammonia by-product. This shifted the stoichiometry towards unity and drove the reaction to completion and high molecular weight polymer. The viscosity of the polyureas increased significantly during the vacuum step resulting in high molecular weight polymers that wrapped the mechanical stir rod. Limiting the hard segment content to 30 wt.% or less ensured that the polyureas retained elastomeric properties and did not experience phase inversion resulting in a thermoplastic. Polyurea controls containing 0 wt.% and 100 wt.% of the hard segment were also synthesized for comparative purposes.

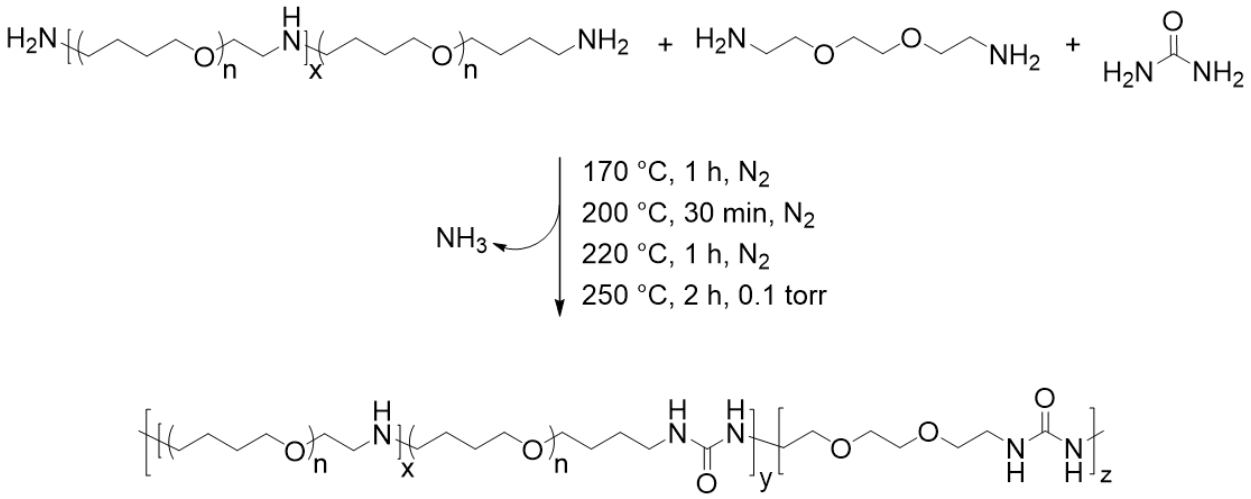


**Scheme 3.1:** Isocyanate-free synthesis of segmented polyureas utilizing melt polycondensation.

The polyurea containing 0 wt.% hard segment dissolved in common organic solvents such as chloroform and THF. Incorporation of the DEOEU hard segment rendered the segmented polyureas insoluble in most solvents due to the strongly hydrogen bonded and semi-crystalline nature of the hard segment. However, all the polyureas containing DEOEU dissolved in DMF

when heated above the hard segment melting temperature of 130 °C, indicating that the polyureas were not covalently crosslinked. Lack of solubility in common NMR and SEC solvents prevented molecular weight and structural determination. However, stepwise isothermal TGA provided a method for estimating the composition of each polyurea. Segmented polyurethanes and polyureas commonly exhibit a two-step weight loss degradation profile in TGA with the hard segment degrading in the first step.[23] As shown in **Figure 3.1**, the weight loss at each step in stepwise isothermal TGA correlated well with the targeted hard and soft segment compositions for each segmented copolyurea. Although the 5 wt.% hard segment sample did not show a sharp transition for the degradation of the hard segment as the other segmented polyureas, the weight of the sample did decrease gradually by 6% before the soft segment degradation occurred at 365 °C. **Table 3.1** displays the calculated weight loss for each degradation step of each polyurea. For simplicity, the targeted hard segment compositions are used herein to identify the polyureas instead of the measured TGA values.

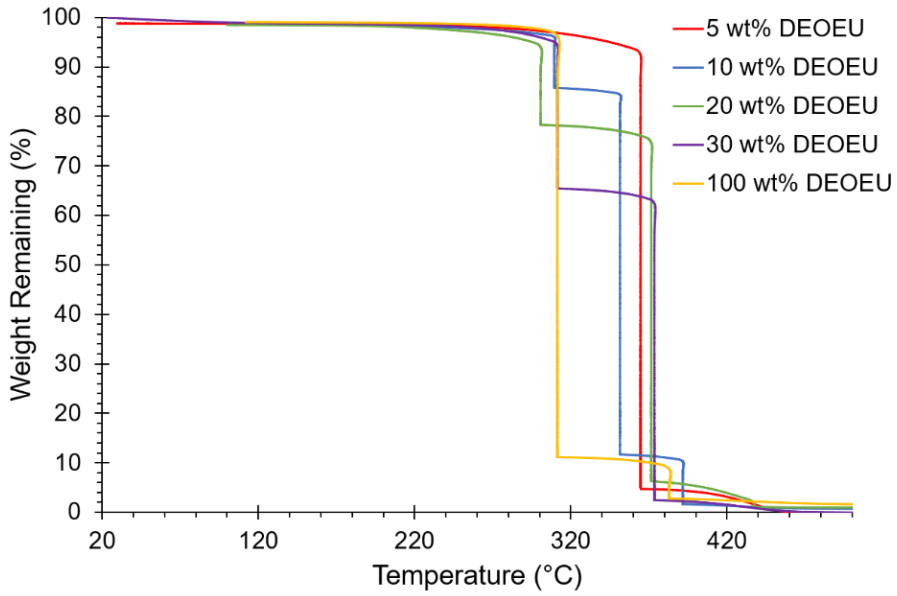


**Figure 3.1:** Stepwise isothermal TGA revealing the hard segment composition of the segmented polyureas.

Differential scanning calorimetry (DSC) revealed the thermal transitions of the polyureas as shown in **Figure 3.2**. All PTMO-containing polyureas displayed a characteristic $T_g$ at -76 °C for the soft

segment. The PTMO-based soft segment displayed a melting transition centered at 23 °C, which was consistent with the endothermic transition in the 0 wt.% DEOEU thermogram (**Figure 3.2A**). Incorporation of DEOEU hard segment into the polyureas depressed the soft segment melting point to 10-15 °C as the concentration of the soft segment domains decreased. For polyureas that contained 10 wt.% DEOEU incorporation or higher, cold crystallization of the soft segment occurred around -40 to -30 °C upon the second heating. At these compositions, the hard segment presumably provided sufficient physical crosslinking to restrict the mobility of the soft segment, which inhibited the ability of the PTMO to fully crystallize during the cooling step. Upon heating above the $T_g$, the polymer chains had sufficient mobility to continue crystallizing resulting in cold crystallization. A microphase separated polyurea typically displays two distinct $T_g$s; however, in this case, the $T_g$ for the DEOEU homopolymer (100 wt.% DEOEU) was 21 °C (**Figure 3.2B**), which overlapped with the soft segment melting endotherm and was not distinguishable. The melting enthalpy of the soft segment endotherm decreased linearly with increasing hard segment incorporation (**Figure 3.2C**) due to the decreasing concentration of soft segment domains. This trend further suggested an absence of branching in the soft segment; branching would significantly decrease the level of crystallinity in the soft segment, which would result in a non-linear trend in the melting enthalpy.[24]

Incorporation of 20 and 30 wt.% of DEOEU gave rise to two additional endothermic transitions above the soft segment melting point centered around 93 and 129 °C. The peak at 129 °C correlated with the melting point in the second heat of the 100 wt.% DEOEU and agreed with the melting point measured by Dennis *et al.*[15] The broad peak at 93 °C coincided with the peak near the same temperature in the first heat of the 100 wt.% DEOEU polyurea. This peak may indicate the presence of a polymorphic crystalline structure that arises from the DEOEU hard

segment. The presence of two distinct melting transitions in the 100 wt.% DEOEU polyurea seems to support this interpretation; however, further morphological characterization is required to definitively determine the crystal structure of these polyureas.

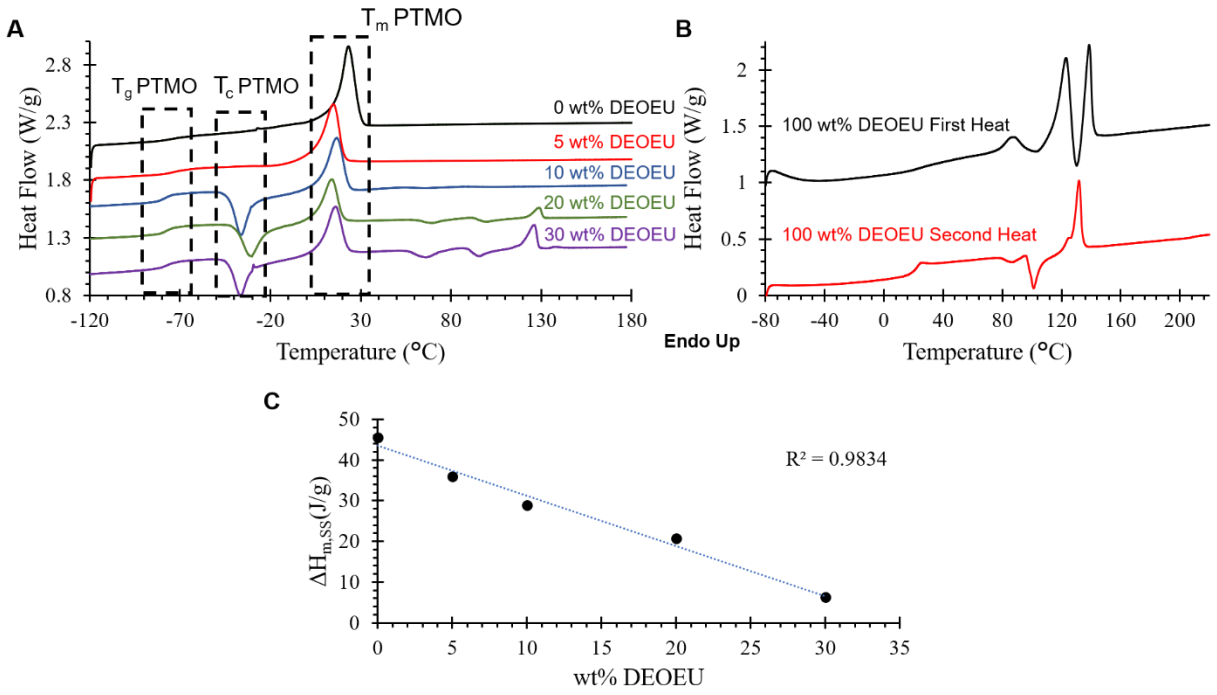


**Figure 3.2**: (A) DSC 2nd heating scans for segmented polyureas containing various amounts of DEOEU hard segment. The curves are shifted vertically for clarity. (B) 1st and 2nd heating scans for DEOEU homopolymer and (C) $\Delta H_m$ for the soft segment melting endotherm as a function of hard segment incorporation.

Dynamic mechanical analysis (DMA) revealed the storage modulus as a function of temperature between -80 and 200 °C (**Figure 3.3**). As expected, all polymers exhibited typical glassy moduli of 1-3 GPa at -80 °C. The $T_g$ for each polyurea occurred between -60 and -50 °C as indicated by a drop in the storage modulus and a broad peak in the tan δ (**Figure S3.1)**. Incorporation of hard segment resulted in further broadening of the tan δ peak, and in some cases (e.g., 30 wt.% DEOEU), induced the appearance of a second peak at higher temperatures. This behavior suggested the presence of phase mixing, which is common among low molecular weight,

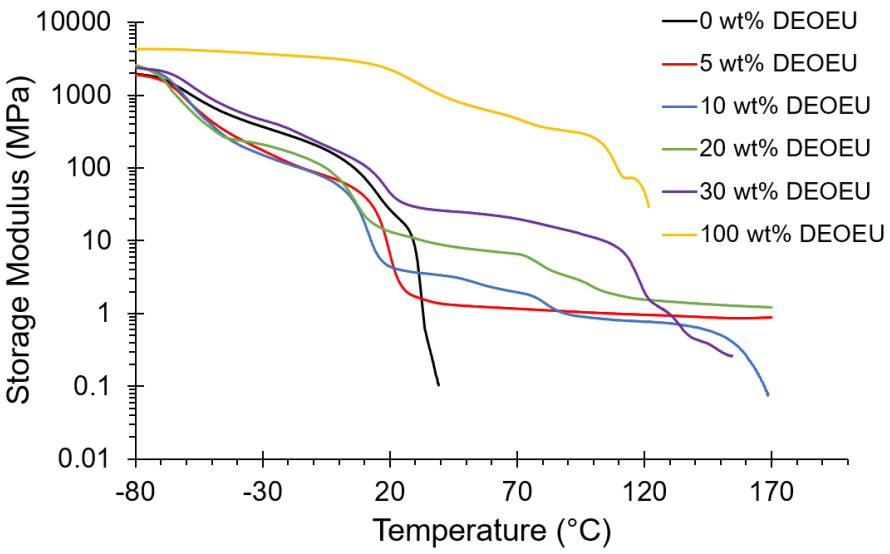


**Figure 3.3**: DMA heating trace of segmented polyurea copolymers.

ether-based soft segments.[9, 25] The soft segment melts between 10 to 20 °C resulting in an expected modulus drop. The presence of a plateau modulus after the PTMOU melting transition in the segmented copolyureas suggested microphase separation. The sample containing 0 wt.% hard segment experienced flow soon after the melting point, whereas the hydrogen bonding and crystallinity of the hard segment in the remaining samples facilitated plateaus in the moduli after soft segment melting. As expected, the plateau modulus increased as a function of increasing hard segment content (ranging from 1 to 100 MPa) due to increased hydrogen bonding and crystallinity.[26] A slight decrease in the plateau moduli near 80 °C corresponded to the endothermic transition shown in DSC near the same temperature for the higher hard segment containing polyureas. Above 100 °C, the hard segment begins to melt as apparent from a second peak in the tan δ; however, the polyureas remain physically crosslinked until 150 °C where the hydrogen bonds sufficiently dissociated to allow for flow. Variable temperature FTIR confirmed the presence of bidentate hydrogen bonding in the hard segment, and the reduction of hydrogen bonding occurred at temperatures that were consistent with the thermal transitions observed both in DSC and DMA results (**Figures S3.3-S3.4)**. **Table 3.1** summarizes the thermal properties of the polyureas.

**Table 3.1:** Summary of thermal properties for PTMO-based, segmented polyureas.

| | TGA[a] | | | | | DSC[b] | | | | | DMA[c] |
|---|---|---|---|---|---|---|---|---|---|---|---|
| DEOEU Content (wt%) | $T_{d,5\%}$[d] (°C) | $T_{d,1}$ (°C) | wt Loss (%) | $T_{d,2}$ (°C) | wt Loss (%) | $T_g$ (°C) | $T_{m,1}$ (°C) | $T_{m,2}$ (°C) | $T_{m,3}$ (°C) | $\Delta H_{m,1}$ (J/g) | $T_g$ (°C) |
| 0 | 384 | - | - | - | - | -76 | 23 | - | - | 45.5 | -56 |
| 5 | 352 | - | 6 | 365 | 94 | -76 | 15 | - | - | 36.0 | -53 |
| 10 | 335 | 316 | 12 | 351 | 88 | -76 | 12 | - | - | 28.9 | -50 |
| 20 | 323 | 300 | 20 | 371 | 80 | -76 | 14 | 92 | 129 | 20.7 | -60 |
| 30 | 326 | 311 | 34 | 373 | 66 | -76 | 10 | 94 | 129 | 6.23 | -56 |
| 100 | 311 | 311 | 90 | 383 | 10 | 21 | 123[e], 132 | 139 | - | - | 26 |

[a] Stepwise isothermal TGA, 10 °C $min^{-1}$, $N_2$

[b] Second heating cycle, -120-180 °C, 10 °C $min^{-1}$, He

[c] Oscillatory tension mode, 1 Hz, 0.1% strain, 3 °C $min^{-1}$

[d] Temperature ramp, 10 °C $min^{-1}$, $N_2$

[e] Determined from first heat

**Figure 3.4A** reveals the stress-strain behavior of the segmented, PTMO-based, polyureas. Compositions consisting of 20 wt.% DEOEU hard segment or less exhibited strains at break between 640 to 770%, consistent with or superior to isocyanate-based, segmented, polyureas and polyurethanes in the earlier literature.[3, 9, 16, 27] The ultimate stress increased systematically with increasing hard segment (**Figure 3.4B**) from 1 to 15 MPa as the amount of physical crosslinking increased. Increasing the hard segment content to 30 wt.% resulted in a significant decrease in the strain at break down to 340% as the ultimate stress increased, which was consistent with earlier literature examples.[16, 27] The mean Young's modulus also expectedly increased with increasing physical crosslinking from 0.76 MPa for 5 wt.% DEOEU to 29.5 MPa for 30 wt.% DEOEU (**Table**

**3.2**). The polyurea containing 0 wt.% hard segment melted and flowed upon handling at room temperature, and the determination of mechanical properties was impossible.

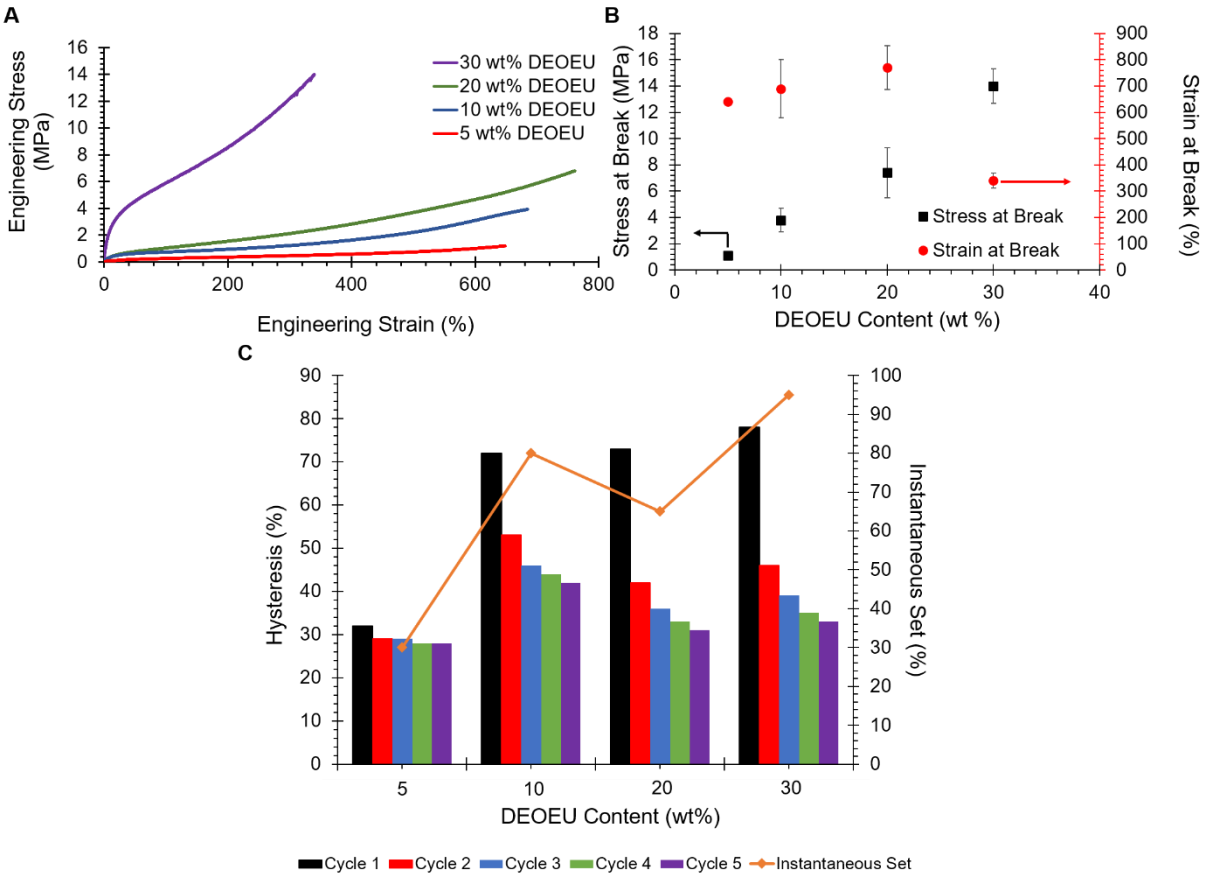


**Figure 3.4:** (A) Engineering stress vs. strain for segmented polyureas (B) stress and strain at break as a function of hard segment content and (C) five-cycle mechanical hysteresis and instantaneous set for segmented polyureas.

Tensile hysteresis results from energy lost in the form of heat as a polymer is repeatedly stretched and released. Hysteresis in segmented polyureas partly arises from the deformation of the hard segment morphology during elongation.[9] Straining the polymer disrupts the intermolecular hydrogen bonding in the hard segments. The polymer chains typically do not return to their original conformations upon unloading, which results in energy dissipation. **Figure 3.4C**

summarizes the five-cycle hysteresis measurements of the segmented polyureas strained to 200%. In all samples, the first cycles show the highest amount of hysteresis relative to the following cycles, as expected. This phenomenon presumably occurred due to an equilibrium morphology that was disrupted during the first loading and did not have sufficient time to reform between cycles, which resulted in the soft matrix sustaining the sequential loads.[7, 28] Consequently, the hysteresis increased with amount of hard segment in the polyurea.[7, 29] The first-cycle hysteresis increased substantially from the 5 wt.% DEOEU to the 10 wt.% DEOEU polyurea, and more subtly between the higher hard-segment-content polyureas. The instantaneous set, which is the strain where the stress reaches zero on the first hysteresis unloading curve, generally increased with increasing hard segment content as the disruption of the larger hard segment domains led to more unrecoverable energy loss. Given the elastomeric nature of the segmented polyureas and the presence of polarizable urea and ether linkages throughout the backbone, these materials may prove suitable for DE applications provided they also exhibit high relative permittivity.

**Table 3.2:** Summary of tensile properties for PTMO-based, segmented polyureas.

| | | | | Mechanical Hysteresis (%) | | | | | |
|---|---|---|---|---|---|---|---|---|---|
| DEOEU Content (wt%) | Modulus (MPa) | Ultimate Stress (MPa) | Strain at Break (%) | Cycle 1 | Cycle 2 | Cycle 3 | Cycle 4 | Cycle 5 | Instantaneous Set (%) |
| 5 | 0.76 ± 0.16 | 1.1 ± 0.10 | 640 ± 11 | 32 | 29 | 29 | 28 | 28 | 30 |
| 10 | 4.35 ± 0.29 | 3.8 ± 0.90 | 690 ± 110 | 72 | 53 | 46 | 44 | 42 | 80 |
| 20 | 4.54 ± 0.54 | 7.4 ± 1.9 | 770 ± 83 | 73 | 42 | 36 | 33 | 31 | 65 |
| 30 | 29.5 ± 1.13 | 14 ± 1.3 | 340 ± 29 | 78 | 46 | 39 | 35 | 33 | 95 |

Broadband dielectric spectroscopy revealed the relative permittivity and dielectric loss for each polymer. **Figure 3.5A** shows an overlay of the dielectric permittivity as a function of frequency for each composition at 300 K. At low frequencies, the permittivity increased sharply due to conductivity contributions. Therefore, the relative permittivity values were obtained at higher

frequencies (>100 Hz), which is the spectral region where minimal dispersion phenomena appear to occur in these samples. The plateaus in the dielectric permittivity spectra revealed an interesting trend. The 5 wt.% DEOEU sample displayed the lowest relative permittivity with a plateau permittivity on the order of 2.8. The permittivity initially increased with increasing hard segment as expected due to an increase in the number of ether linkages present in the backbone. However, the permittivity peaked near 10.6 for the 20 wt.% DEOEU sample and started to decline with further hard segment incorporation. The origin of this decrease in permittivity presumably stems from an increase in the hard segment crystallinity as the crystalline domains restrict the ability of the DEOEU linkages to polarize. DSC analysis appeared to support this hypothesis since the hard segment melting peaks did not appear until the 20 wt.% DEOEU sample. However, the 20 wt.% DEOEU sample displayed the highest permittivity despite also demonstrating hard segment crystallinity in the DSC. This observation suggested that the percentage of the amorphous phase

remains significantly higher than the crystalline phase at this level of DEOEU incorporation. Confirming this hypothesis will require a more in-depth morphological analysis in the future.

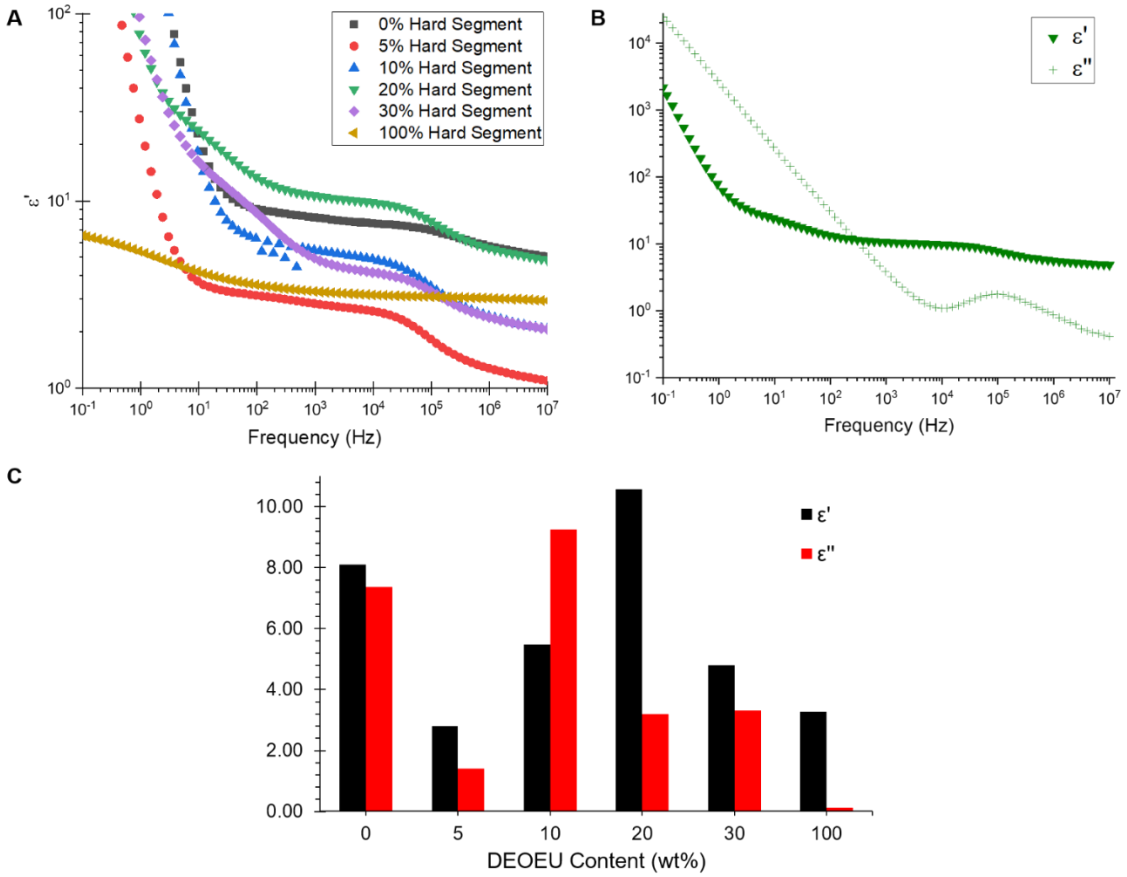


**Figure 3.5:** (A) Dielectric permittivity (ε') as a function of frequency for the synthesized polyureas. (B) permittivity and dielectric loss (ε") as a function of frequency for the polyurea containing 20 wt.% hard segment. (C) comparison of dielectric permittivity and dielectric loss at a frequency of 1kHz.

**Figure 3.5B** shows a plot of dielectric permittivity and loss as a function of frequency for the 20 wt.% DEOEU sample as a representative example. The dielectric loss quantifies the electromagnetic energy dissipated in a dielectric material, and thus should preferably remain low for DE applications. The dielectric loss starts high at low frequencies and drops to a minimum at 10 kHz before peaking again at higher frequencies. **Figure 3.5C** provides a visual representation of the relative permittivity and dielectric loss of the polyureas at 1kHz, which is a relevant frequency for DE applications. Interestingly, the graph shows no apparent trend in the dielectric

loss as a function of DEOEU hard segment content. Although the polyurea containing 0 wt.% DEOEU has a high permittivity around 8 (**Table 3.3**), it also suffers from a high dielectric loss. Additionally, this sample lacks any significant mechanical properties at room temperature as discussed previously, which excludes its use as a DE. The 100 wt.% DEOEU polymer conversely enjoys a very low dielectric loss compared to the other compositions. Despite this attribute, the permittivity remains relatively low at around 3, and this composition exhibits mechanical properties typical of a thermoplastic as shown by Dennis and Long *et al.*[15]

As for the segmented copolymers, the 20 wt.% DEOEU sample demonstrated the highest permittivity at 10.6. This permittivity sits significantly higher than many functionalized silicone and acrylics utilized in literature for DEs; however, this permittivity increase also corresponds with an increased Young's modulus compared to conventional DEA materials.[18] This composition also exhibits a relatively high dielectric loss when considering its application as a dielectric material.[30] Regardless, with more tuning, this composition may function effectively as a DEA due to its high permittivity and ability to achieve a large strain at break, and our future efforts will evaluate strategies for decreasing the dielectric loss while maintaining (or improving) the dielectric permittivity.

**Table 3.3**: Summary of dielectric properties for the segmented polyureas at a frequency of 1 kHz.

| Hard Segment Content (wt%) | ε' (1 kHz) | ε'' (1 kHz) | Tan δ |
|---|---|---|---|
| 0 | 8.09 | 7.36 | 1.12 |
| 5 | 2.81 | 1.41 | 0.50 |
| 10 | 5.47 | 9.26 | 1.69 |
| 20 | 10.6 | 3.20 | 0.30 |
| 30 | 4.80 | 3.31 | 0.69 |
| 100 | 3.27 | 0.13 | $4.00 \times 10^{-3}$ |

## 3.5 Conclusions

The melt polycondensation of a commercially available, PTMO-based diamine with urea and a chain extender yielded a series of melt processible polyureas synthesized in the absence of toxic isocyanates, catalysts, and solvents. Polyureas with varying hard segment contents formed free-standing creasable films upon melt compression. DSC analysis revealed multiple endothermic transitions in the segmented copolyureas correlating to the soft segment and hard segment melting points. DMA further suggested microphase separation and provided evidence for phase mixing between the hard and soft segments. Tensile analysis revealed high strain at break in the segmented polyureas between 340 to 770% strain, comparable to literature examples of isocyanate-based polyureas. Young's modulus and ultimate stress increased significantly with increasing hard segment incorporation indicating the variability of attainable mechanical properties using this method. Five-cycle hysteresis measurements revealed increasing first-cycle hysteresis with increasing DEOEU incorporation due to increasing hard segment domains. Correspondingly, the instantaneous set also increased with the DEOEU content. Broadband dielectric spectroscopy revealed that the polyurea containing 20 wt.% DEOEU displayed the highest dielectric permittivity

(10.6) of the segmented copolymers measured at 1 kHz and 300K. This data coupled with the tensile properties suggests that this polyurea composition may prove suitable as a candidate for DEA applications provided that the dielectric loss is lowered upon further modification.

## 3.6 Acknowledgements

The authors would like to acknowledge the Huntsman Corporation for generously providing the Jeffamine® utilized in this study. The authors also thank Christina Orsino in the Robert B. Moore group for carrying out variable temperature FTIR experiments. Emmanuel U. Mapesa and Joshua Sangoro acknowledge financial support from the National Science Foundation, Division of Materials Research, Polymers Program, through DMR-1905597.

## 3.7 References

1. S. Corneillie, P. N. Lan, E. Schacht, M. Davies, A. Shard, R. Green, S. Denyer, M. Wassall, H. Whitfield and S. Choong, Polym. Int., 1998, 46, 251-259.
2. A. Sánchez-Ferrer, D. Rogez and P. Martinoty, Macromol. Chem. Phys., 2010, 211, 1712-1721.
3. S. Das, I. Yilgor, E. Yilgor, B. Inci, O. Tezgel, F. L. Beyer and G. L. Wilkes, Polymer, 2007, 48, 290-301.
4. J. P. Sheth, D. B. Klinedinst, G. L. Wilkes, I. Yilgor and E. Yilgor, Polymer, 2005, 46, 7317-7322.
5. R. M. Versteegen, R. P. Sijbesma and E. Meijer, Macromolecules, 2005, 38, 3176-3184.
6. E. Yilgor, G. Ekin Atilla, A. Ekin, P. Kurt and I. Yilgor, Polymer, 2003, 44, 7787-7793.
7. I. Yilgor, T. Eynur, S. Bilgin, E. Yilgor and G. L. Wilkes, Polymer, 2011, 52, 266-274.
8. F. S. Bates, Science, 1991, 251, 898-905.
9. I. Yilgör, E. Yilgör and G. L. Wilkes, Polymer, 2015, 58, A1-A36.
10. I. Yilgor, T. Eynur, E. Yilgor and G. L. Wilkes, Polymer, 2009, 50, 4432-4437.
11. P. Wang, X. Ma, Q. Li, B. Yang, J. Shang and Y. Deng, RSC Advances, 2016, 6, 54013-54019.
12. D. Tang, D.-J. Mulder, B. A. J. Noordover and C. E. Koning, Macromol. Rapid Commun., 2011, 32, 1379-1385.

13. D. Montarnal, P. Cordier, C. Soulié-Ziakovic, F. Tournilhac and L. Leibler, J. Polym. Sci., Part A: Polym. Chem., 2008, 46, 7925-7936.

14. P. Cordier, F. Tournilhac, C. Soulié-Ziakovic and L. Leibler, Nature, 2008, 451, 977.

15. J. M. Dennis, L. I. Steinberg, A. M. Pekkanen, J. Maiz, M. Hegde, A. J. Müller and T. E. Long, Green chemistry, 2018, 20, 243-249.

16. J. M. Sirrine, S. A. Schexnayder, J. M. Dennis and T. E. Long, Polymer, 2018, 154, 225-232

17. Y. Wang, X. Zhou, Q. Chen, B. Chu and Q. Zhang, *IEEE Transactions on Dielectrics and Electrical Insulation*, 2010, **17**, 1036-1042.

18. B. T. White and T. E. Long, Macromol. Rapid Commun., 2019, 40, 1800521.

19. H. S. Nalwa, *Handbook of low and high dielectric constant materials and their applications, two-volume set*, Elsevier, 1999.

20. J. Biggs, K. Danielmeier, J. Hitzbleck, J. Krause, T. Kridl, S. Nowak, E. Orselli, X. Quan, D. Schapeler, W. Sutherland and J. Wagner, Angew. Chem. Int. Ed., 2013, 52, 9409-9421.

21. R. Lorenzini, W. Kline, C. Wang, R. Ramprasad and G. Sotzing, Polymer, 2013, 54, 3529-3533.

22. J. G. Erickson, J. Am. Chem. Soc., 1954, 76, 3977-3978.

23. Z. S. Petrović, Z. Zavargo, J. H. Flyn and W. J. Macknight, J. Appl. Polym. Sci., 1994, 51, 1087-1095.

24. A. H. Willbourn, Journal of Polymer Science, 1959, 34, 569-597.

25. T. Choi, K. A. Masser, E. Moore, J. Weksler, A. Padsalgikar and J. Runt, J. Polym. Sci., Part B: Polym. Phys., 2011, 49, 865-872.

26. L. T. J. Korley, B. D. Pate, E. L. Thomas and P. T. Hammond, Polymer, 2006, 47, 3073-3082.

27. S. K. Jewrajka, J. Kang, G. Erdodi, J. P. Kennedy, E. Yilgor and I. Yilgor, J. Polym. Sci., Part A: Polym. Chem., 2009, 47, 2787-2797.

28. S. Das, D. F. Cox, G. L. Wilkes, D. B. Klinedinst, I. Yilgor, E. Yilgor and F. L. Beyer, Journal of Macromolecular Science, Part B: Physics, 2007, 46, 853-875.

29. G. Erdodi, J. Kang, J. P. Kennedy, E. Yilgor and I. Yilgor, J. Polym. Sci., Part A: Polym. Chem., 2009, 47, 5278-5290

30. L. Zhu, *The journal of physical chemistry letters*, 2014, **5**, 3677-3687.

## 3.8 Supplemental Information

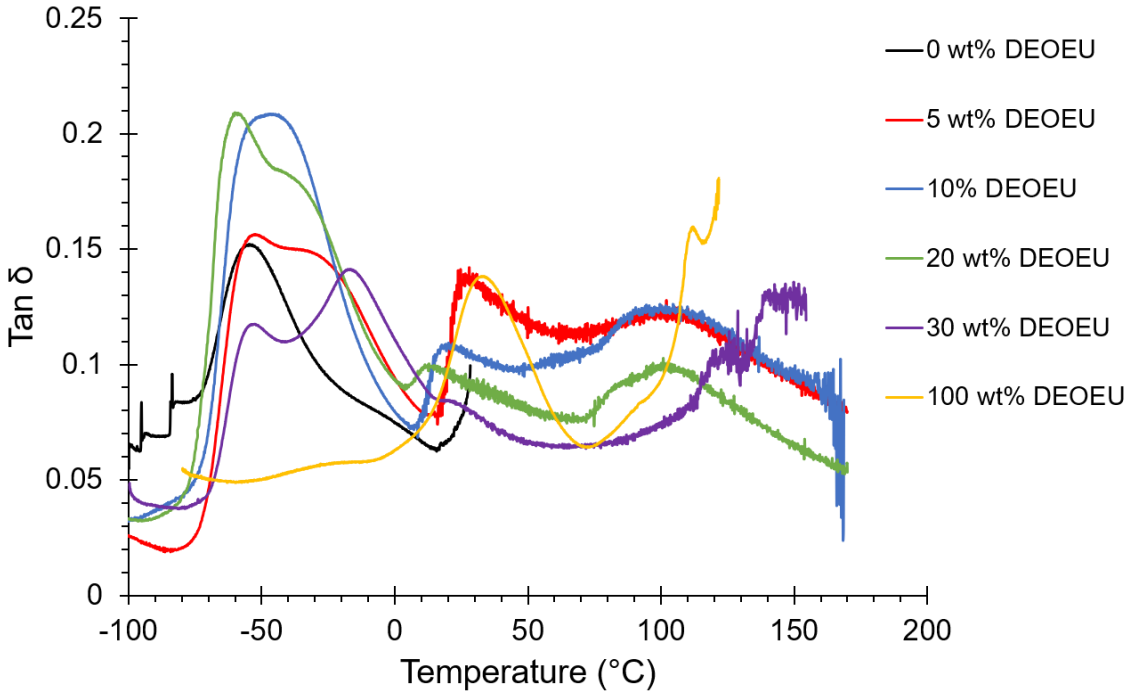


**Figure S3.1**: Corresponding DMA tan δ behavior for polyurea homopolymers and copolymers.

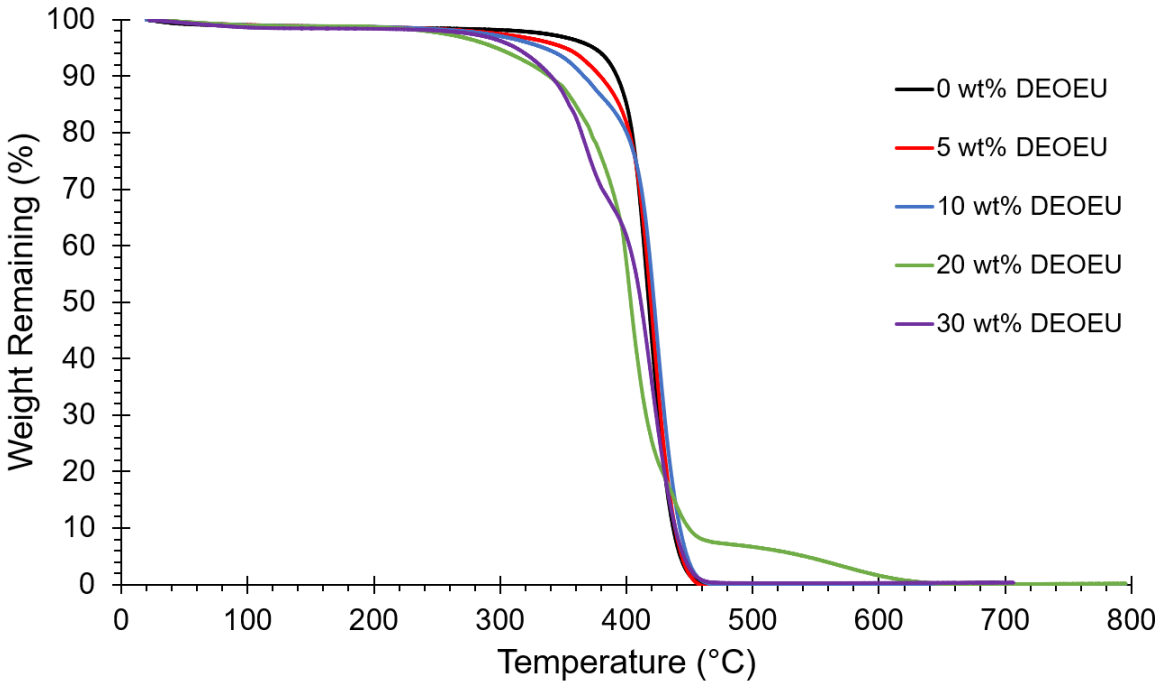


**Figure S3.2**: Thermogravimetric analysis utilizing a 10 °C $min^{-1}$ temperature ramp to 800 °C for the series of polyureas.

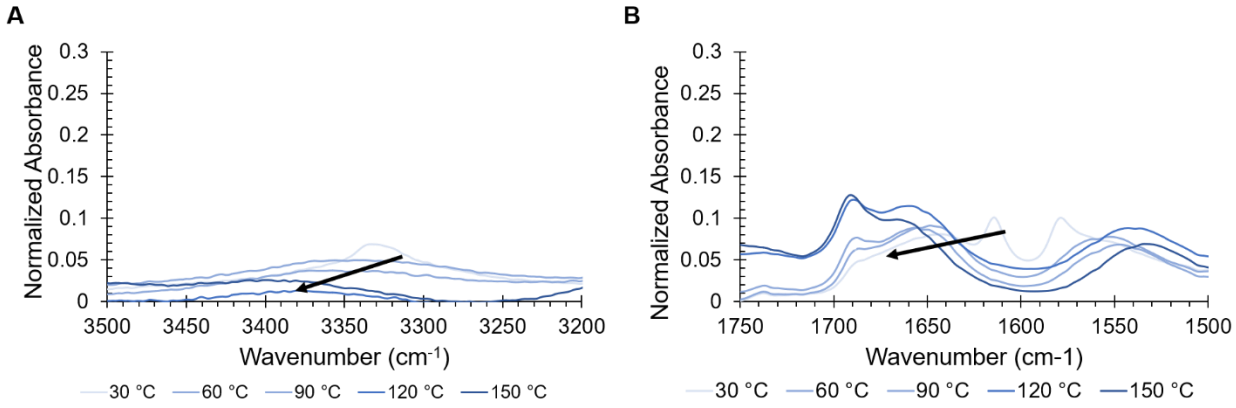


**Figure S3.3**: Variable temperature FTIR of the 0 wt% DEOEU polyurea showing (A) the N-H stretching band shifting from ~3325 $cm^{-1}$ for strongly hydrogen bonded ureas to ~3350 $cm^{-1}$ for weakly hydrogen bonded with increasing temperature (B) the amide band shifting from ~1650 $cm^{-1}$ for strong hydrogen bonding to ~1690 $cm^{-1}$ for weak hydrogen bonding with increasing temperature

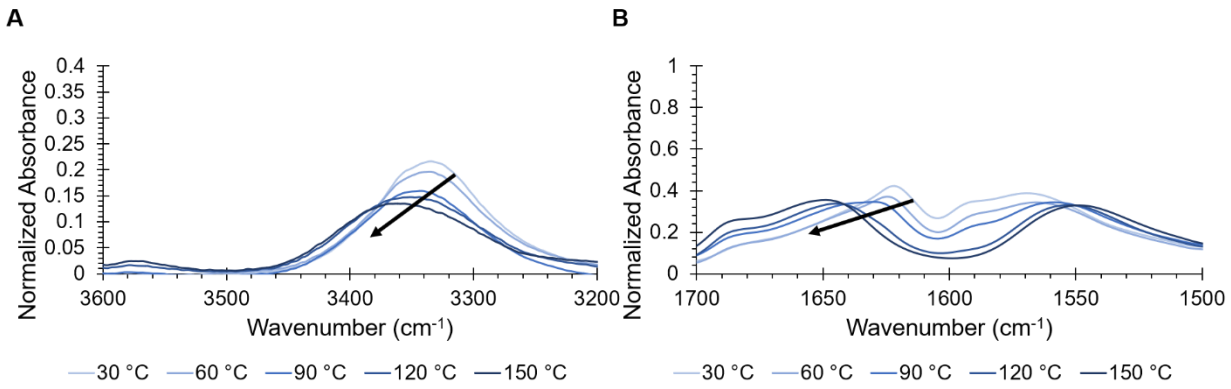


**Figure S3.4**: Variable temperature FTIR of the 30 wt% DEOEU polyurea showing (A) the N-H stretching band shifting from ~3325 $cm^{-1}$ for strongly hydrogen bonded ureas to ~3350 $cm^{-1}$ for weakly hydrogen bonded with increasing temperature (B) the amide band shifting from ~1650 $cm^{-1}$ for strong hydrogen bonding to ~1690 $cm^{-1}$ for weak hydrogen bonding with increasing temperature

# Chapter 4: **Water-soluble poly(ether urea)s for low-temperature extrusion 3D printing**

B. Tyler White[1], Callie Zawaski[2], Christopher B. Williams[2], Timothy E. Long[3*]

[1]Department of Chemistry, Macromolecules Innovation Institute (MII), Virginia Tech, Blacksburg, VA 24061

[2]Department of Mechanical Engineering, Macromolecules Innovation Institute (MII), Virginia Tech, Blacksburg, VA 24061

[3]Biodesign Center for Sustainable Macromolecular Materials and Manufacturing, School for Molecular Sciences, Arizona State University, Tempe, AZ 85287

*To whom correspondence should be addressed: E-mail: Timothy.E.Long@asu.edu.

## 4.1 Abstract

Material extrusion 3D printing shows promise for producing personalized pharmaceutical dosage tablets from water-soluble polymer filaments. However, many water-soluble filaments require temperatures above 100 °C to extrude, which exceeds the degradation temperatures of many active pharmaceutical ingredients. Herein, we describe the synthesis and characterization of a series of water-soluble poly(ether urea)s (PEU) with low melting temperatures for use in material extrusion 3D printing. A series of commercial polyether diamines of varying molecular weights reacted with urea in a melt polycondensation reaction to produce isocyanate-free poly(ether urea)s. The PEU synthesized from the lowest molecular weight polyether (PEU 600) displayed a $T_g$ of -48 °C and no melting transition. The melting temperature increased with increasing molecular weight of the polyether from 13 °C for the median molecular weight (PEU 900) to 35 °C for the highest molecular weight (PEU 2000). PEU 2000 formed a free-standing film after melt processing at 80 °C and displayed mechanical properties comparable to isocyanate-based thermoplastic

polyureas. The low melting temperature of this PEU composition allowed for extrusion 3D printing at 80 °C. Cooling the build stage with dry ice assisted in the solidification of the printed part after extrusion to form a hollow cube. This study demonstrates the ability to 3D print a water-soluble poly(ether urea) at a temperature suitable for incorporating active pharmaceutical ingredients.

## 4.2 Introduction

Additive manufacturing (AM) provides a platform for personalized pharmaceutical dosages due to the ability to print customized tablets with complex geometries. These printed pharmaceuticals provide tunable dissolution rates, dosages, release times, and drug combinations dependent on the patient's needs. Several types of 3D printing technologies have been studied for the printing of oral dosage pharmaceuticals, such as binder jetting, material jetting, and material extrusion.[1-5] Of these technologies, material extrusion shows the greatest ability to print strong parts for oral dose pills with limited or no friability.[6, 7] Extrusion 3D printing of pharmaceutical requires loading the active ingredient into a thermoplastic, water-soluble filament such as poly(vinyl alcohol),[8] hydroxypropyl cellulose,[9] methacrylic copolymers,[9, 10] and polyurethanes.[11] However, these materials all require temperatures between 120 – 200 °C to print, which precludes the use of many active ingredients that degrade at or below those temperatures.[8] Pekkanen and Long et al. reported the synthesis of a semi-crystalline, sulfonated poly(ethylene glycol) (PEG)-based polymer, which extruded at 70 °C and dissolved entirely in water.[12] This polymer demonstrated the ability to print at temperatures low enough for potential active pharmaceuticals to survive.[13, 14]

Polyureas represent another class of polymers commonly used for drug delivery applications.[15-18] Typically, polyurea synthesis involves a multifunctional amine reacting with a

highly reactive diisocyanate. These reactions also utilize toxic organic solvents such as N,N-dimethylformamide (DMF) and require the addition of a metal catalyst to promote urea formation. The potential for these hazardous chemicals to remain in the polymer after processing presents a risk when using these materials for biological applications. Several isocyanate-free routes for synthesizing polyureas exist in the literature to circumvent this issue. These routes primarily include direct $CO_2$ incorporation with a diamine[19, 20] or transureaization between a diamine and biscarbamate.[21] Recently, our group described an isocyanate-, catalyst-, and solvent-free high molecular weight polyurea synthesis utilizing urea as a biologically derived monomer.[22-24] This method has proven effective for synthesizing polyureas with properties comparable to isocyanate-based methods and provides a non-toxic route for synthesizing water-soluble polyureas.

This work details the synthesis and characterization of a series of water-soluble poly(ether urea)s (PEU) for low-temperature extrusion 3D printing utilizing an isocyanate-, catalyst-, and solvent-free synthetic method. We hypothesize that this synthetic process will allow for the synthesis of water soluble polyureas with unique chemical structures. The first goal of this project was to determine the effect of the oligomeric diamine molecular weight on the melting point and mechanical properties of the synthesized polyureas. Next, we aimed to produce filament with a melting temperature below 100 °C for extrusion 3D printing for the potential incorporation of thermally labile additives. The final objective was to print a three-dimensional structure as a proof-of-concept.

## 4.3 Experimental

### 4.3.1 Materials

Three molecular weights ($M_n$ = 1900, 800, and 500 g $mol^{-1}$) of O,O′-Bis(2-aminopropyl) polypropylene glycol-block-polyethylene glycol-block-polypropylene glycol (Jeffamine ED 2003, 900, and 600) were purchased from Sigma Aldrich. Urea (BioReagent, ≥99%) was also purchased from Sigma Aldrich. All chemicals were dried *in vacuo* at 80 °C overnight to remove water before use.

### 4.3.2 Synthesis of Water-Soluble Poly(ether urea)s (PEU)

The synthesis of the poly(ether urea)s from urea was adapted from previously reported procedures.[24-26] As an example, Jeffamine ED 2003 (15 g, 7.89 mmol) was added to a 100-mL, 1-necked, round-bottomed flask with urea (0.474 g, 7.89 mmol). A custom t-necked glass adapter consisting of a nitrogen inlet, spherical ball joint, and spherical socket was inserted into the neck of the round-bottomed flask. A glass condensing tube with a nitrogen outlet and spherical socket joint was connected to the corresponding ball joint from the t-neck. The condensing tube was attached to a 50-mL round-bottomed collection flask, which was cooled in a bath of dry ice and isopropyl alcohol. A metal stir rod was passed through the t-neck to provide overhead mechanical stirring, which was connected by a spherical ball joint attached to Tygon® tubing. The condensing tube's nitrogen outlet was connected to a bubbler of 1M HCl solution with Tygon® tubing to quench the released ammonia that is not condensed. Oxygen was completely removed by carrying out three alternating vacuum and $N_2$ purge cycles in the reaction vessel. Nitrogen was continuously flowed through the reaction vessel at a rate of 10 mL $min^{-1}$ throughout the reaction. Stirring the reaction at 170 °C for 1 h provided a homogeneous melt and initiated the reaction as apparent by the evolution of ammonia gas. The reaction proceeded by ramping the temperature to 200 °C for 1 h followed by 30 min at 220 °C. In the last step, vacuum was applied at 220 °C for 2 h to fully

remove ammonia and drive the reaction to completion. The resultant poly(ether urea)s wrapped the stir rod due to their high viscosity and were used without further purification.

### 4.3.3 Extrusion 3D Printing of PEU 2000

The extrusion 3D printing was performed on a custom 3D printer[13] modified to use a Nordson EFD micro dispensing unit with a nozzle diameter of 1.5 mm for the print head. The ".stl" files were sliced using the open-source engine, Slic3r. The extrusion command was replaced with dispensing from the Nordson system, which was executed by sending a signal from the Arduino on the printer to the dispenser. The printing syringe was set to a temperature of 80 °C, and the dispensing pressure was kept constant at 90 PSI. Printing was done at a single speed of 30 mm $min^{-1}$ to match the material volume output. The print bed was cooled to 0.8 °C by using blocks of dry ice as a coolant. Each layer's height was set at 0.2 mm and there was a one-minute pause between layers to allow for solidification.

### 4.3.4 Analytical Methods

The three PEUs were melt pressed between two Kapton® sheets coated with mold release agent at 80 °C separated by 0.5 mm thick shims. Quench cooling with liquid nitrogen allowed the PEU 2000 film to be removed as a free-standing, creasable film. PEU 600 and PEU 900 did not form free-standing films after melt pressing. Melting temperatures were measured using differential scanning calorimetry (DSC Q2000) equipped with a refrigerated cooling system. The thermal transitions were measured using a heat/cool/heat cycle at a rate of 10 °C $min^{-1}$ under a nitrogen purge. Melting points were determined as the peak of the endothermic transition on the second heat. Dynamic mechanical analysis (DMA) was performed on a TA Instruments Q800 DMA equipped with a liquid nitrogen gas cooling accessory. Oscillatory experiments were carried out at

0.1 strain % and at a frequency of 1 Hz, and the temperature was ramped at 3°C $min^{-1}$. The uniaxial tensile analysis was carried out using an Instron® 5500R. An ASTM D638-V cutting die was used to punch out dogbone shaped testing specimens. Tensile experiments were carried out using a crosshead separation speed of 5 mm $min^{-1}$. Five experiments were performed, and the average results were reported.

## 4.4 Results and Discussion

An isocyanate-, solvent-, and catalyst-free synthetic procedure afforded a series of water-soluble poly(ether urea)s from a commercial polyether diamine and urea as shown in **Figure 4.1**. The Jeffamine ED series consists of three triblock copolymers of varying molecular weights: ED 600 has an $M_n$ of ~ 500 g/mol, ED 900 has an $M_n$ of ~800 g/mol, and ED 2003 has an $M_n$ of ~2,000 g/mol. In each case, the polymer consists primarily of poly(ethylene glycol) (PEG) center blocks capped on either end with lower molecular weight poly(propylene glycol) (PPG) blocks. All three polymers became solids following the polycondensation reaction. The PEU synthesized from

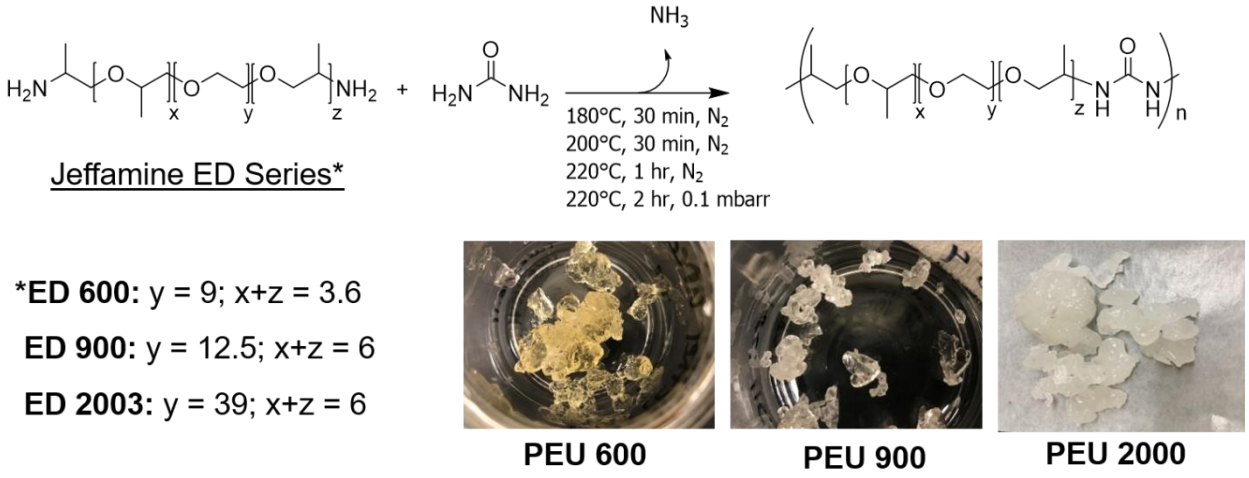


**Figure 4.1**: Synthetic scheme of three water-soluble poly(ether urea)s utilizing urea as a monomer and images revealing their physical properties.

Jeffamine ED 600 (PEU 600) manifested as a yellow, optically clear, flexible solid, as shown in **Figure 4.1**. Similarly, PEU 900 remained optically clear but also appeared colorless likely due to

the absence of color in Jeffamine ED 900 compared to the yellow color of Jeffamine ED 600. The PEU synthesized from Jeffamine ED 2003 (PEU 2000) conversely became a tough, opaque solid during the reaction. All three of these materials successfully dissolved in DI water at a concentration of 1 mg $mL^{-1}$ after approximately 15 minutes of stirring at room temperature.

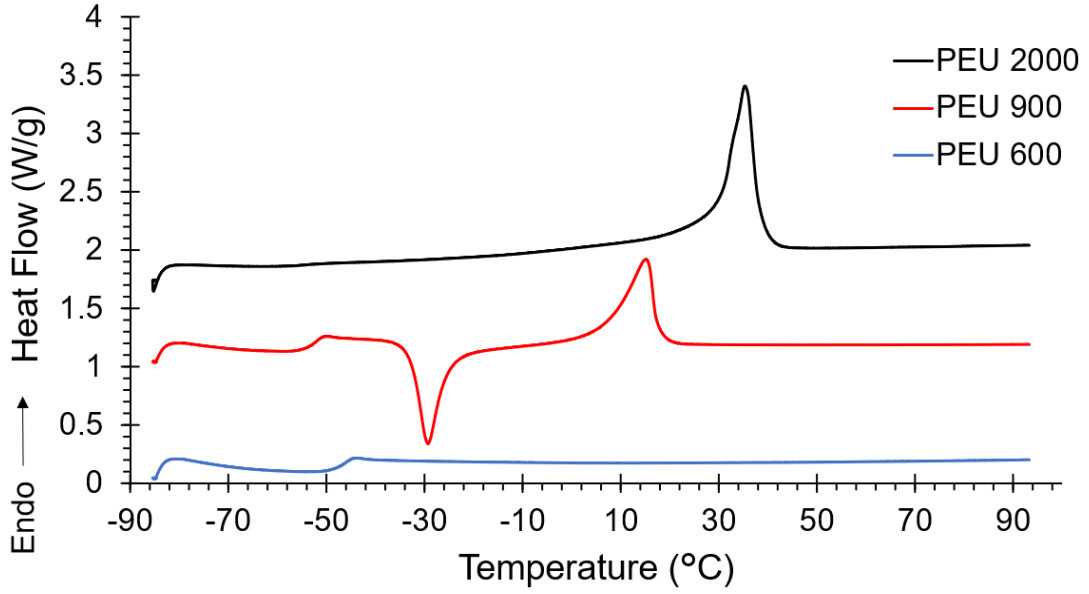


**Figure 4.2**: Second heat DSC thermograms for PEUs synthesized from three Jeffamine precursors.

Differential scanning calorimetry revealed the thermal transitions of each PEU, as shown in **Figure 4.2**. PEU 600 and PEU 900 both displayed prominent $T_g$s at -48 and -53 °C, respectively. PEU 2000, conversely, did not display a defined $T_g$ due to the prominence of the melting endotherm. PEU 2000 exhibited the highest melting point of the three PEUs at 35 °C. This value measured slightly lower than that of the Jeffamine ED2003, which melted at 39 °C. Likewise, the magnitude of the melting enthalpy decreased for PEU 2000 compared to the Jeffamine ED 2003 as summarized in **Table S4.1**. This indicates that the crystallinity of the polymer was somewhat disrupted upon polyurea formation. PEU 900 exhibited a lower melting point, which appeared at

14 °C. Furthermore, a cold crystallization exotherm arose at -30 °C on the second heat following a quench cool. The presence of cold crystallization indicates that the polymer chains lacked sufficient time to fully crystallize during the quench cool, suggesting that the crystallization kinetics are somewhat slower in this sample than in the PEU 2000. The PEU 600 sample showed no observable melting temperature over the whole temperature range tested, likely due to the low molecular weight of the PEG center block preventing crystallization. These DSC results explain the polymers' physical characteristics as well; PEU 2000 appeared opaque due to the crystallinity present in the sample while the other two appeared clear due to their lack of crystallinity at room temperature.

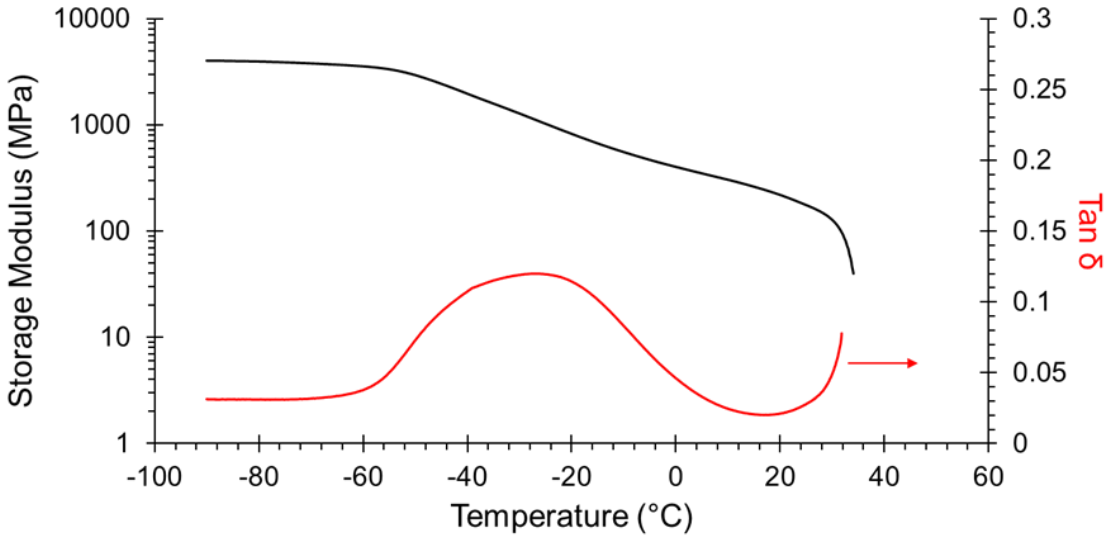


**Figure 4.3**: Storage modulus (black) and tan δ (red) as a function of temperature for PEU 2000.

Compression molding using a melt press at 80 °C allowed for the formation of a creasable, free-standing film of PEU 2000. However, PEU 600 and 900 were unable to produce free-standing films. This likely stems from the lack of crystallinity in these samples at room temperature. The inability of these two PEUs to form films suggests that the bidentate hydrogen bonding in these polymers is spaced too far apart to provide any mechanical integrity. Dynamic mechanical analysis

gave more insight into the thermomechanical properties of PEU 2000, as shown in **Figure 4.3**. The storage modulus remains constant at 3 GPa between -100 and -60 °C before gradually decreasing. A broad tan δ peak that stretches between -60 and 20 °C represents the glass transition temperature of this polymer. This peak's broadness relates to both the crystalline regions of the polymer and the hydrogen bonding, which hinder the mobility of the amorphous phase and broadens the glass transition. Above 20 °C the modulus begins to drop again as the melting point of the polymer approaches. The sample finally exhibits terminal flow ($T_f$) at 34 °C after the polymer reaches its melting point as the sharp drop in modulus indicates.

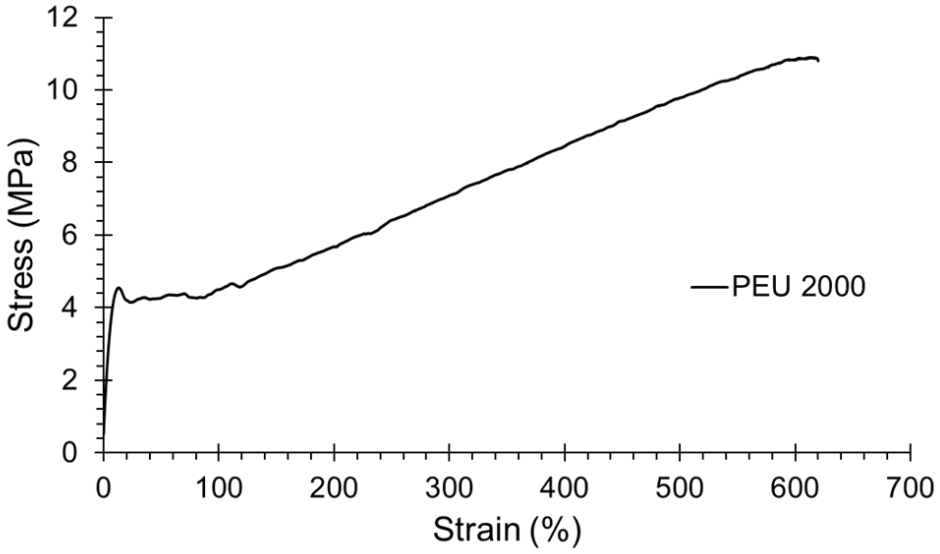


**Figure 4.4**: Tensile properties of a melt pressed PEU 2000 film.

Tensile analysis revealed the mechanical properties of PEU 2000 as shown in **Figure 4.4**. The stress increased rapidly upon the application of strain and reached an average of 5.86 MPa before showing a defined yield point. This material exhibited an average Young's modulus of 30.3 MPa before the yield point. Significant strain hardening occurred beyond the yield point leading to an ultimate strain of 525 %. This polymer's ability to reach high strain-at-break suggests that this

synthetic procedure generated high molecular weight PEUs. The thermal and mechanical properties of PEU 2000 are tabulated in **Table 4.1**.

**Table 4.1**: Thermal, thermomechanical, and tensile properties of PEU 2000.

| | **DSC[a]** | | **DMA[b]** | | **Tensile[c]** | | |
|---|---|---|---|---|---|---|---|
| | $T_m$[d] (°C) | $T_c$[e] (°C) | $T_g$ (°C) | $T_f$ (°C) | Young's Modulus (MPa) | Yield Stress (MPa) | Ultimate Strain (%) |
| **PEU 2000** | 35 | 10 | -27 | 34 | 30 ± 20 | 6 ± 1 | 520 ± 80 |

[a] Heat-quench-heat cycle, 10 °C $min^{-1}$, $N_2$
[b] 3 °C $min^{-1}$, 0.1% amplitude. $T_g$ taken as the peak of the tan δ curve
[c] Cross head displacement of 5 mm $min^{-1}$
[d] Measured during the second heating cycle
[e] Measured from the quench cool cycle

Applying PEU 2000 to an extrusion-based 3D printing process presents several unique challenges. First, making filament from PEU 2000 proved impossible due to the low melting temperature of the polymer. Therefore, the printing required a custom-built 3D printer that utilized a heated reservoir in place of filament, as shown in **Figure 4.5a**. The reservoir maintained a temperature of 80 °C to provide a liquid polymer with sufficient viscosity to extrude from the print nozzle. Following extrusion, each layer must solidify to support the weight of the subsequent layers. However, this poses an issue as the crystallization temperature ($T_C$) of PEU 2000 occurs well below room temperature at 10 °C (**Figure S4.1**). Introducing dry ice to the build stage of the 3D printer allowed for each extruded layer to cool rapidly and crystallize before depositing the next layer (**Figure 4.5a**). As a result, a hollow cube was successfully 3D printed from PEU 2000 (**Figure 4.5b**). This proof of concept demonstrates the ability to 3D print a water-soluble polymer

that extrudes at temperatures low enough to incorporate drugs or other biologically active ingredients.

## 4.5 Conclusions

An isocyanate-, catalyst-, and solvent-free synthetic procedure yielded a series of water-soluble poly(ether urea)s derived from three polymer precursors of varying $M_n$. PEU 2000 exhibited a melting point above room temperature at 35 °C while PEU 900 melted at 13 °C and PEU 600 remained amorphous. All three PEUs dissolved in water within 15 minutes with stirring; however, only PEU 2000 successfully formed a free-standing film upon melt pressing. DMA revealed a broad glass transition in PEU 2000 and revealed a flow temperature of 34 °C. Tensile analysis revealed thermoplastic behavior from PEU 2000 with an average Young's modulus of 30.3 MPa and ultimate strain exceeding 500%. Finally, PEU 2000 was successfully 3D printed at low extrusion temperatures using a custom 3D printer with a dry-ice-cooled build stage.

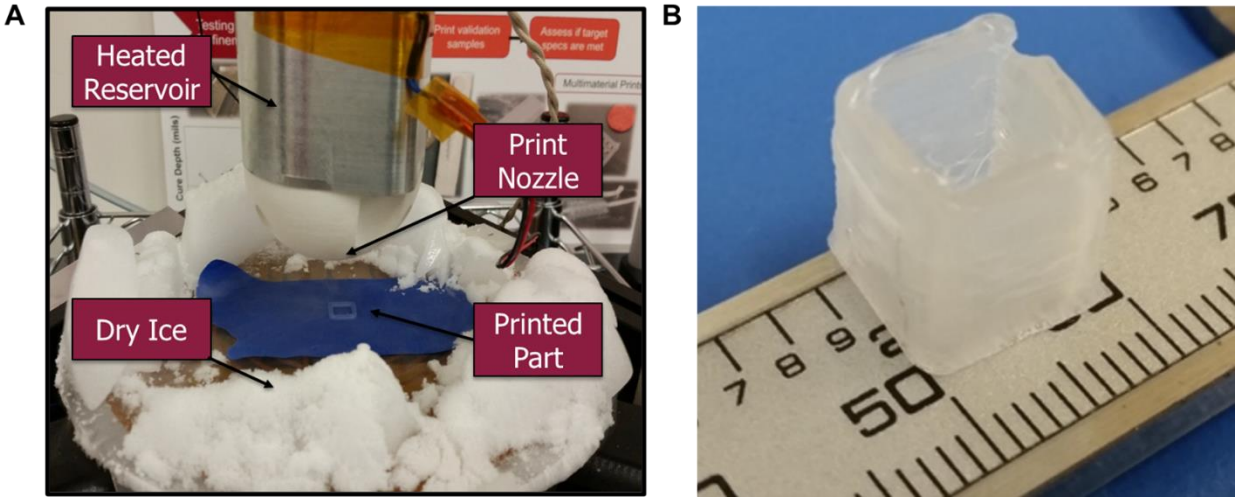


**Figure 4.5**: (A) A custom built, extrusion 3D printer printing onto a build stage cooled by dry ice and (B) a 10 $mm^3$ hollow cube of PEU 2000 3D printed at a low extrusion temperature (80 °C).

## 4.6 Acknowledgements

The authors would like to acknowledge Proctor & Gamble for funding this project.

## 4.7 References


1. Wilts, E. M.; Ma, D.; Bai, Y.; Williams, C. B.; Long, T. E., Comparison of Linear and 4-Arm Star Poly(vinyl pyrrolidone) for Aqueous Binder Jetting Additive Manufacturing of Personalized Dosage Tablets. *ACS Applied Materials & Interfaces* **2019,** *11* (27), 23938-23947.
2. Alhnan, M. A.; Okwuosa, T. C.; Sadia, M.; Wan, K.-W.; Ahmed, W.; Arafat, B., Emergence of 3D Printed Dosage Forms: Opportunities and Challenges. *Pharm. Res.* **2016,** *33* (8), 1817-1832.
3. Goole, J.; Amighi, K., 3D printing in pharmaceutics: A new tool for designing customized drug delivery systems. *Int. J. Pharm.* **2016,** *499* (1), 376-394.
4. Prasad, L. K.; Smyth, H., 3D Printing technologies for drug delivery: a review. *Drug Dev. Ind. Pharm.* **2016,** *42* (7), 1019-1031.
5. Norman, J.; Madurawe, R. D.; Moore, C. M.; Khan, M. A.; Khairuzzaman, A., A new chapter in pharmaceutical manufacturing: 3D-printed drug products. *Adv. Drug Del. Rev.* **2017,** *108*, 39-50.
6. Goyanes, A.; Wang, J.; Buanz, A.; Martínez-Pacheco, R.; Telford, R.; Gaisford, S.; Basit, A. W., 3D Printing of Medicines: Engineering Novel Oral Devices with Unique Design and Drug Release Characteristics. *Mol. Pharm.* **2015,** *12* (11), 4077-4084.
7. Goyanes, A.; Fina, F.; Martorana, A.; Sedough, D.; Gaisford, S.; Basit, A. W., Development of modified release 3D printed tablets (printlets) with pharmaceutical excipients using additive manufacturing. *Int. J. Pharm.* **2017,** *527* (1), 21-30.
8. Goyanes, A.; Buanz, A. B. M.; Hatton, G. B.; Gaisford, S.; Basit, A. W., 3D printing of modified-release aminosalicylate (4-ASA and 5-ASA) tablets. *European Journal of Pharmaceutics and Biopharmaceutics* **2015,** *89*, 157-162.
9. Pietrzak, K.; Isreb, A.; Alhnan, M. A., A flexible-dose dispenser for immediate and extended release 3D printed tablets. *European Journal of Pharmaceutics and Biopharmaceutics* **2015,** *96*, 380-387.
10. Korte, C.; Quodbach, J., Formulation development and process analysis of drug-loaded filaments manufactured via hot-melt extrusion for 3D-printing of medicines. *Pharm. Dev. Technol.* **2018,** *23* (10), 1117-1127.
11. Verstraete, G.; Samaro, A.; Grymonpré, W.; Vanhoorne, V.; Van Snick, B.; Boone, M.; Hellemans, T.; Van Hoorebeke, L.; Remon, J. P.; Vervaet, C., 3D printing of high drug loaded dosage forms using thermoplastic polyurethanes. *Int. J. Pharm.* **2018,** *536* (1), 318-325.
12. Pekkanen, A. M.; Zawaski, C.; Stevenson Jr, A. T.; Dickerman, R.; Whittington, A. R.; Williams, C. B.; Long, T. E., Poly (ether ester) Ionomers as Water-Soluble Polymers for Material Extrusion Additive Manufacturing Processes. *ACS Applied Materials & Interfaces* **2017,** *9* (14), 12324-12331.
13. Zawaski, C. E.; Wilts, E. M.; Chatham, C. A.; Stevenson, A. T.; Pekkanen, A. M.; Li, C.; Tian, Z.; Whittington, A. R.; Long, T. E.; Williams, C. B., Tuning the material properties of a water-soluble ionic polymer using different counterions for material extrusion additive manufacturing. *Polymer* **2019,** *176*, 283-292.
14. Zawaski, C. E.; Chatham, C. A.; Wilts, E. M.; Long, T. E.; Williams, C. B., Using Fillers to Tune Material Properties of an Ion-containing Semi-crystalline Poly(ethylene glycol) for Fused Filament Fabrication Additive Manufacturing. *Additive Manufacturing* **2021**, 101844.
15. Chen, M.; Feng, X.; Xu, W.; Wang, Y.; Yang, Y.; Jiang, Z.; Ding, J., PEGylated polyurea bearing hindered urea bond for drug delivery. *Molecules* **2019,** *24* (8), 1538.

16. Flórez-Grau, G.; Rocas, P.; Cabezón, R.; España, C.; Panés, J.; Rocas, J.; Albericio, F.; Benítez-Ribas, D., Nanoencapsulated budesonide in self-stratified polyurethane-polyurea nanoparticles is highly effective in inducing human tolerogenic dendritic cells. *Int. J. Pharm.* **2016,** *511* (2), 785-793.
17. John, J. V.; Seo, E. J.; Augustine, R.; Jang, I. H.; Kim, D. K.; Kwon, Y. W.; Kim, J. H.; Kim, I., Phospholipid end-capped bioreducible polyurea micelles as a potential platform for intracellular drug delivery of doxorubicin in tumor cells. *ACS Biomaterials Science & Engineering* **2016,** *2* (11), 1883-1893.
18. Valério, A.; Feuser, P. E.; Bubniak, L. D. S.; Santos-Silva, M. C. D.; Araújo, P. H. H. d.; Sayer, C., In vitro biocompatibility and macrophage uptake assays of poly (urea-urethane) nanoparticles obtained by miniemulsion polymerization. *Journal of Nanoscience and Nanotechnology* **2017,** *17* (7), 4955-4960.
19. Wu, C.; Wang, J.; Chang, P.; Cheng, H.; Yu, Y.; Wu, Z.; Dong, D.; Zhao, F., Polyureas from diamines and carbon dioxide: synthesis, structures and properties. *Phys. Chem. Chem. Phys.* **2012,** *14* (2), 464-468.
20. Wang, P.; Ma, X.; Li, Q.; Yang, B.; Shang, J.; Deng, Y., Green synthesis of polyureas from CO 2 and diamines with a functional ionic liquid as the catalyst. *RSC advances* **2016,** *6* (59), 54013-54019.
21. Tang, D.; Mulder, D.-J.; Noordover, B. A. J.; Koning, C. E., Well-defined Biobased Segmented Polyureas Synthesis via a TBD-catalyzed Isocyanate-free Route. *Macromol. Rapid Commun.* **2011,** *32* (17), 1379-1385.
22. Dennis, J. M.; Steinberg, L. I.; Pekkanen, A. M.; Maiz, J.; Hegde, M.; Müller, A. J.; Long, T. E., Synthesis and characterization of isocyanate-free polyureas. *Green chemistry* **2018,** *20* (1), 243-249.
23. Sirrine, J. M.; Schexnayder, S. A.; Dennis, J. M.; Long, T. E., Urea as a monomer for isocyanate-free synthesis of segmented poly (dimethyl siloxane) polyureas. *Polymer* **2018,** *154*, 225-232.
24. White, B. T.; Migliore, J. M.; Mapesa, E. U.; Wolfgang, J. D.; Sangoro, J.; Long, T. E., Isocyanate-and solvent-free synthesis of melt processible polyurea elastomers derived from urea as a monomer. *RSC Advances* **2020,** *10* (32), 18760-18768.
25. Dennis, J. M.; Steinberg, L. I.; Pekkanen, A. M.; Maiz, J.; Hegde, M.; Müller, A. J.; Long, T. E., Synthesis and characterization of isocyanate-free polyureas. *Green Chemistry* **2018**.
26. Sirrine, J. M.; Schexnayder, S. A.; Dennis, J. M.; Long, T. E., Urea as a monomer for isocyanate-free synthesis of segmented poly (dimethyl siloxane) polyureas. *Polymer* **2018**.

## 4.8 Supplemental Information

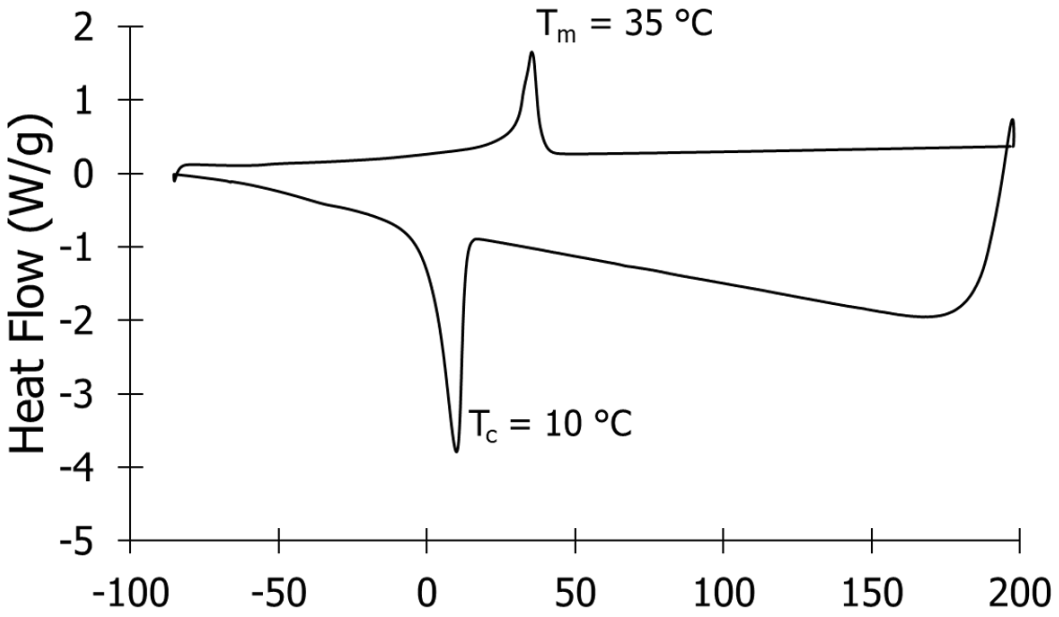


**Figure S4.1**: Quench cool and second heat of PEU 2000 from DSC.

**Table S4.1**: Melting transitions of Jeffamines and their corresponding PEUs.

| | **$T_m$ (°C)**[a] | **$\Delta H_m$ (J/g)**[b] |
|---|---|---|
| **Jeffamine ED 2003** | 39 | 117.0 |
| **PEU 2000** | 35 | 60.58 |
| **Jeffamine ED 900** | 23 | 89.50 |
| **PEU 900** | 14 | 33.07 |

[a] Measured during the second heating cycle

[b] Taken as the area under the exothermic peak on the second heating cycle

# Chapter 5: **Tailoring Charged Block Copolymer Architecture for Tuning Performance**

Invited Book Chapter for *Macromolecular Engineering, 2nd edition*

B. Tyler White, Boer Liu, Kevin J. Drummey, Xi Chen, and Timothy E. Long

## 5.1 Introduction

Block copolymers (BCPs) consist of multiple chemically dissimilar homopolymer subunits covalently attached together. The ability to control the phase behavior and overall properties of these materials through monomer selection and polymer architecture has been studied extensively.[1-3] The past couple of decades has seen an increase in research centered around BCPs containing charged motifs, also known as ionomers. Ionomers became a vital part of the chemical industry since the 1950s with the commercialization of Surlyn™, impacting and creating new markets such as membranes, adhesives, elastomers, coatings, water treatment, and biomedical materials.[4-9] Introducing ionic interactions advantageously impacts polymer structure and enhances mechanical properties and viscoelastic behavior of ionomers.[10] At the molecular level, ionic interactions drive the formation of ionic aggregates, or multiplets, surrounded by a neutral polymer matrix, which effectively restricts polymer chain mobility to form a hard ionic phase depicted in **Figure 5.1** with an increased $T_g$.[11] Varying ionic content and polymer architecture affords materials with tailorable properties,[5, 12] which have been widely used for polymer electrolytes, drug delivery vehicles, water treatment, and fuel cell membranes due to the formation of microphase-separated ion-rich domains.

The properties of charged BCPs depend in part on the architecture of the polymer as well as the chemical identity and placement of the desired charged units. This chapter aims to examine the

structure-property relationships of charged BCPs targeted for a variety of different applications and to compare their properties across different polymer architectures. Four categories of charged BCP architectures are discussed herein including: linear, branched, segmented, and multiply charged BCPs. The section on linear BCPs includes diblocks, triblocks, and multiblocks. Branched BCPs cover a wide variety of topologies including polymer brushes, stars, graft copolymers, and crosslinked networks. Although segmented BCPs describe a class of linear, multiblock copolymers, their unique synthesis and properties warrant a dedicated section of their own. This section will focus primarily on segmented ionenes, polyurethanes, and polyesters. The final section provides an overview on the synthesis and properties of multiply charged BCPs, which present their own unique challenges and benefits.

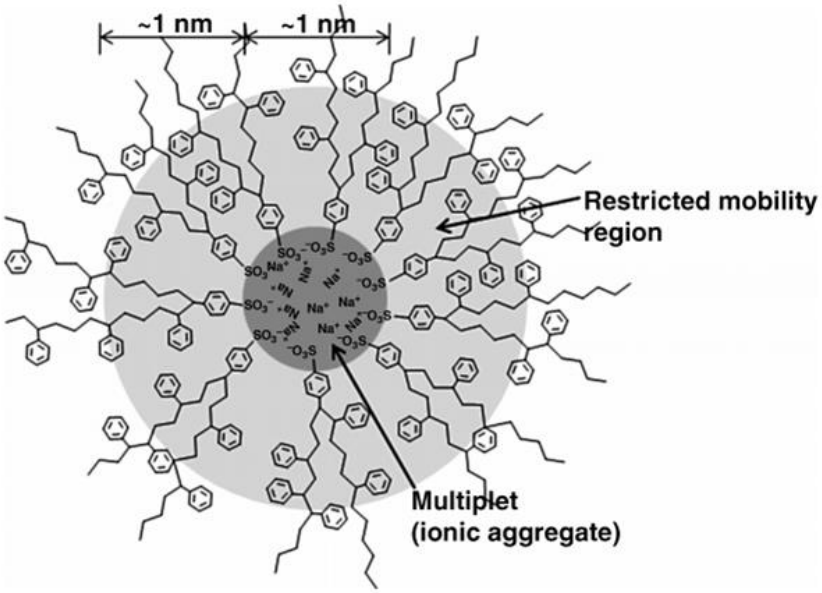


**Figure 5.1**: Representation of ionic aggregates formed by strong electrostatic interactions. Poly(sulfonated styrene) is shown here, but this description is valid for all charged polymers. A region of restricted mobility forms in close proximity to the cluster of charges, forming a higher $T_g$ phase. Adapted from Eisenberg and Moore *et al.* with permission from ACS publications.[4]

## 5.2 Linear Block Copolymers

### 5.2.1 Synthesis

The synthesis of linear, charged block copolymers generally follows one of two routes: direct copolymerization of a charged monomer(s), or post functionalization of a preformed BCP. In either case, the synthesis of the block copolymers most often proceeds through either step-growth[13-27] or chain-growth block copolymerizations. Examples of chain-growth polymerizations used for block copolymer synthesis include reversible addition-fragmentation chain-transfer (RAFT) polymerization,[28-44] cobalt-mediated radical polymerization (CMRP),[45-48] nitroxide-mediated radical polymerization (NMP),[49-53] atom transfer radical polymerization (ATRP),[54-57] ring-opening metathesis polymerization (ROMP),[58, 59] and anionic/cationic polymerization.[60-65] The direct polymerization of charged monomers provides the simplest synthetic pathway and leads to well-defined polymers with charged units in every repeat unit; however, achieving high molecular weight polymers remains challenging for some charged monomers. Alternatively, post-polymerization functionalization allows for the installation of charged moieties into a wide variety of preformed block copolymers.[28, 37, 52, 53, 60, 65-67] However, this approach frequently leads to low conversion and ultimately results in a lower charge density in the ionic block compared to charged monomer polymerization.

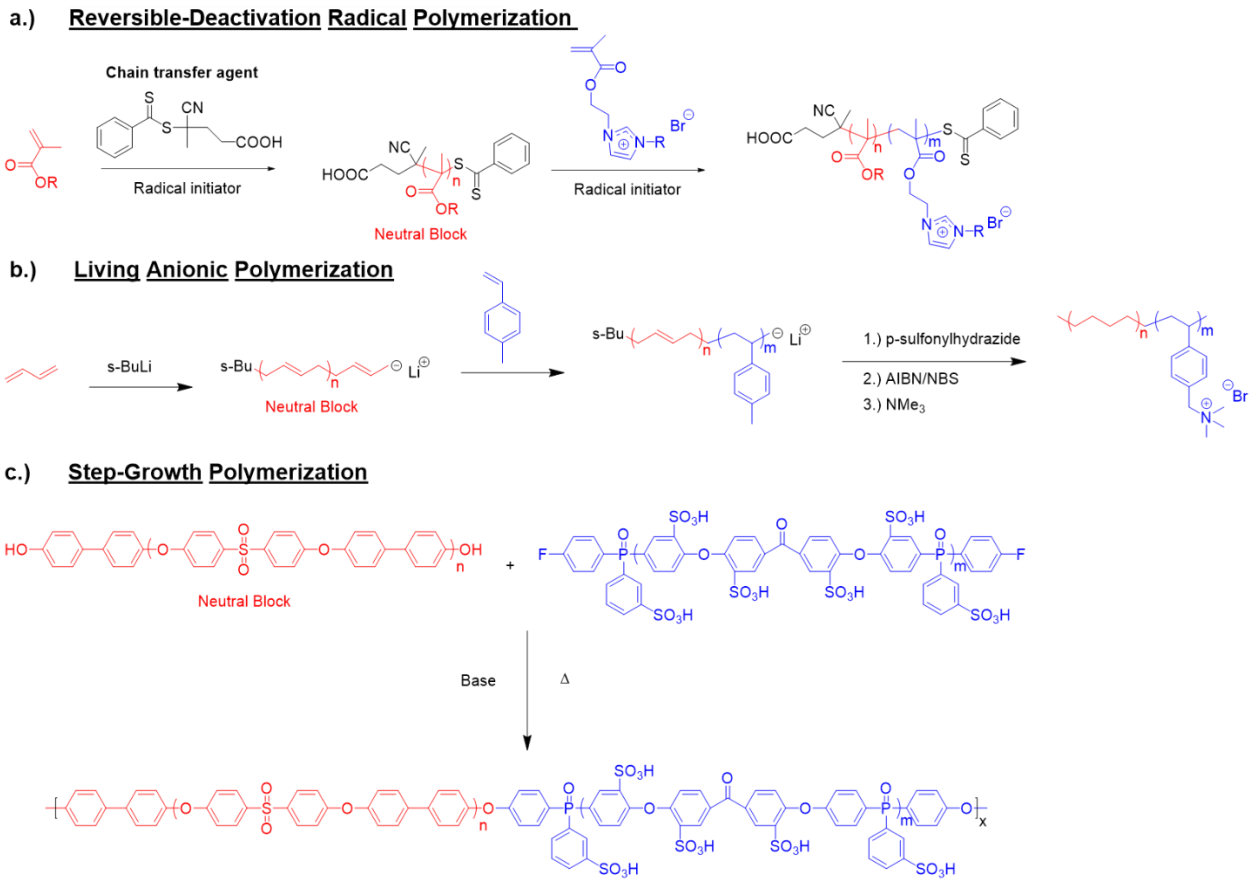


**Figure 5.2**: Representative synthetic methods for block copolymers. (a) sequential RAFT (a form of reversible-deactivation radical polymerization) block copolymerization of a methacrylate and a methacrylated imidazolium ionic liquid,[40] (b) anionic polymerization of butadiene and 4-methylstyrene followed by post polymerization hydrogenation and amine quaternization,[63] (c) polycondensation reaction to form a sulfonated poly(arylene ether phosphine oxide ketone) multiblock copolymer.[18] All figures adapted with permission from ACS Publications.

**Figure 5.2** shows three synthetic methods leading to charged block copolymer formation. **Figure 5.2a** provides an example of the sequential RAFT copolymerization of a neutral acrylic monomer and an imidazolium ionic liquid (IL).[40] The first reaction produces a neutral block with the chain transfer agent covalently attached to one chain end. This allows the imidazolium polymer to grow from the ω-end of the neutral block to yield a diblock copolymer. **Figure 5.2b** demonstrates the sequential anionic polymerization of butadiene and 4-methylstyrene followed by two post-polymerization functionalizations.[63] In this case, the first block consists of polybutadiene which undergoes hydrogenation to form polyethylene. A post-polymerization

bromination of the poly(4-methylstyrene) affords poly(vinylbenzyl bromide) and a subsequent Menshutkin reaction with a substituted amine yields a diblock copolymer containing an ammonium functionalized block. **Figure 5.2c** provides an example of a polycondensation reaction to afford a charged multiblock copolymer.[18] In this example, a post-polymerization sulfonation reaction of a precursor oligomer provides the charged block that is then coupled with a neutral block in a subsequent polycondensation reaction.

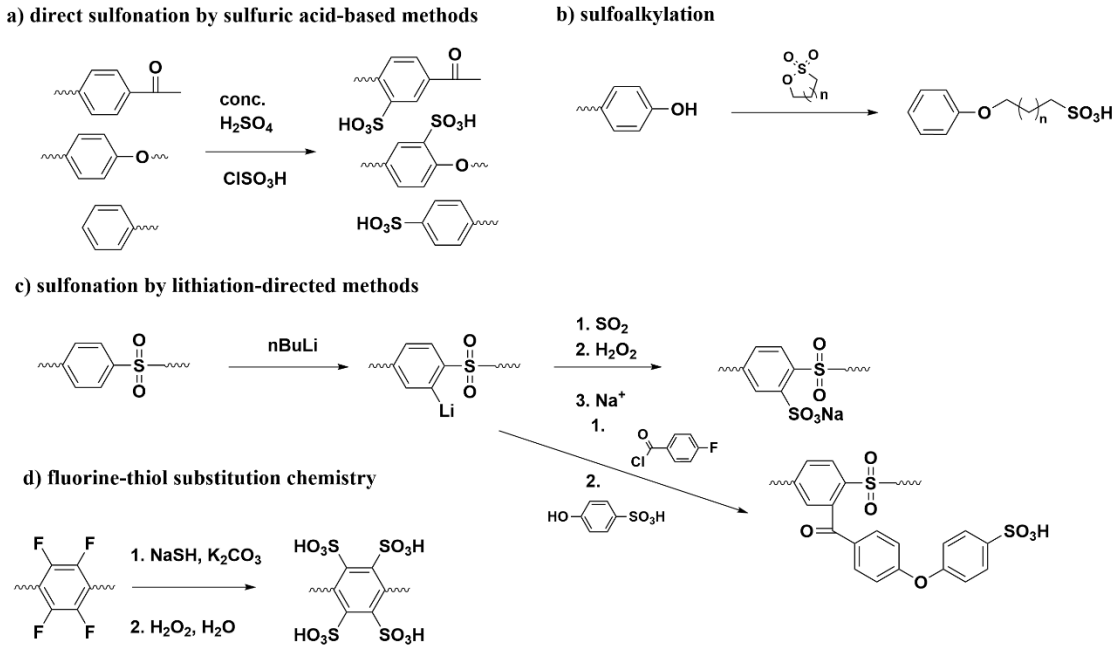


**Figure 5.3**: General methods used to sulfonate monomers or polymers.[13, 14, 68, 69-71]

Apart from nucleophilic substitution reactions, such as the Menshutkin reaction, sulfonation of aromatic polymers remains one of the most common post-polymerization functionalization techniques to incorporate charge into block copolymers. The simplest approach involves the direct sulfonation of an electron-rich phenyl ring using a sulfonation agent such as sulfuric acid or chlorosulfonic acid as shown in **Figure 5.3a**.[13, 14, 68] This method works well for installing a single sulfonate group on an aromatic substituent in the polymer backbone; however, the addition of a sulfonate deactivates the ring towards further sulfonation, which limits the attainable charge

density of the polymer. Sulfoalkylation provides a route towards incorporating multiple sulfonate groups on the same ring.[69] As shown in **Figure 5.3b**, the ring opening reaction between a phenol and a sultone produces a terminal sulfonic acid substituent.[69] This reaction proves especially useful for functionalizing aromatic multiblock copolymers such as poly(arylene ether sulfone). Alternatively, a directed-lithiation approach allows for the attachment of a sulfonate group ortho to the sulfone linkage in aromatic polysulfones (**Figure 5.3c**).[70] Furthermore, a series of nucleophilic aromatic substitution ($S_NAr$) reactions off the lithiation site allows for the attachment of sulfonated side groups to the polymer backbone. Finally, **Figure 5.3d** demonstrates a method of sulfonating highly fluorinated polysulfones once again utilizing $S_NAr$ reactions to displace the fluorine atoms and producing a highly sulfonated polymer.[71]

## 5.2.2 Diblock Copolymers

Linear diblock copolymers represent the simplest architecture for charged BCPs. These BCPs generally consist of a charged polymer block covalently bound to a neutral polymer with a sufficiently different $\chi$ parameter as to promote phase separation. As such, these BCPs self-assemble to form nano-scale phases of ion-rich domains. Similarly, diblocks comprised of hydrophilic and hydrophobic segments will self-assemble in solution to form micelles of controlled size and shape. A near limitless combination of charged polymers, neutral blocks, and counterions exist for exploration, which has garnered significant interest in the scientific community. This section will explore the morphology and structure-property relationships of diblock copolymers and describe their uses as micelles and ion exchange membranes.

### 5.2.2.1 Bulk Morphology

The bulk morphology of charged BCPs, as in any phase separated system, plays perhaps the most important role in determining the structure-property relationships of these materials. Despite

the prominence of charged BCPs in recent literature, understanding of their morphological phase behaviors remains nascent compared to neutral BCPs. Charged BCPs undergo self-assembly and exhibit the same range of morphologies as their neutral counterparts.[45, 59, 72] However, the introduction of charged motifs sometimes leads to enhanced phase separation and unique morphologies. Shim, Bates, and Lodge explored the morphologies of a series of symmetrical BCPs consisting of polystyrene (PS) and poly[(oligo(ethylene glycol) methyl ether methacrylate–*co*–oligo(ethylene glycol) propyl sodium sulfonate methacrylate)] (POEGMA), a precisely sulfonated random copolymer.[67] Small-angle x-ray scattering (SAXS) experiments revealed that BCPs containing less than 3 mol% of sulfonate groups existed in a disordered state, while increasing the ion concentration to 36 mol% resulted in a lamellar morphology. These results concurred with SAXS patterns commonly found for symmetric, neutral BCPs. However, the authors discovered that BCPs containing intermediate ion concentrations of 7 and 23 mol% displayed sets of reflections indicative of long-range order, which the authors attributed to a superlattice structure. In order to prove that the tethered sulfonate groups were responsible for this interesting intermediate morphology, they also examined the effect of doping the neutral BCP with a sodium salt. The SAXS results gave no indication that the superlattice structure formed at any doped salt concentration. The authors speculate that the formation of the lattice structure stems from the competition of packing frustration with the strong electrostatic interactions between charged groups among other factors. The effect of this morphology on thermal, mechanical, and transport properties of the BCP remains unstudied; however, this result indicates a new approach to the design of charged BCPs with unique morphologies.

As mentioned, the incorporation of charged units into a BCP improves phase separation between the neutral and charged blocks compared to fully neutral BCPs.[73, 74] Luo and Hawker *et*

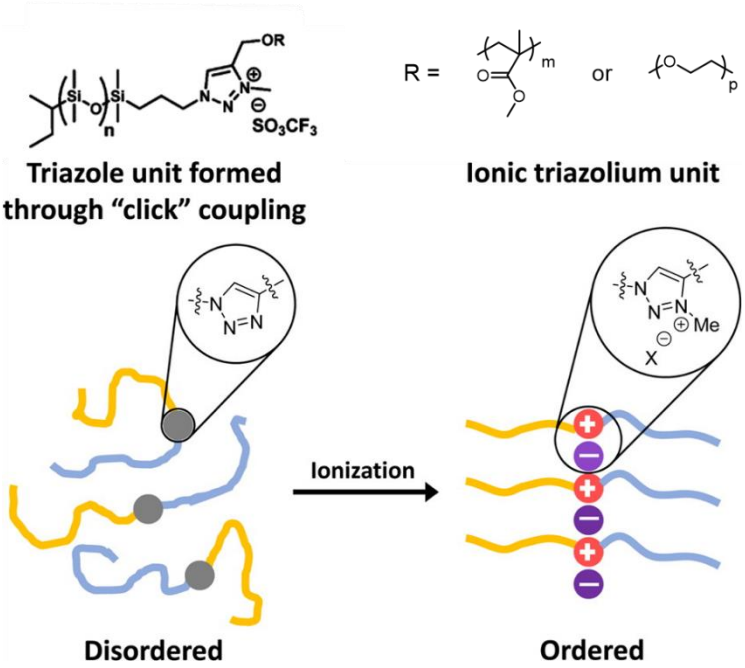


**Figure 5.4**: The incorporation of an ionic unit at the junction between two polymers increase phase separation. Adapted from Luo and Hawker *et al.* with permission from ACS Publications.[64]

*al.* further expanded on this concept demonstrating that incorporating a single ionic group at the junction between two polymer blocks enhances phase separation (**Figure 5.4**).[64] The authors first synthesized homopolymers of poly(dimethyl siloxane) (PDMS), poly(ethylene oxide) (PEO), and poly(methyl methacrylate) (PMMA) using anionic polymerization to generate homopolymers first. Subsequently, an azide-alkyne click reaction coupled the PDMS with either PEO or PMMA to form BCPs with a triazole linking unit. Upon ionization of the triazole unit, the charged block copolymers exhibited larger domain sizes and longer-range ordering than the neutral BCPs as measured using small-angle x-ray scattering (SAXS). Furthermore, the order-disorder transition temperature increased significantly for the charged system indicating the improved stability of the ordered state in the charged BCP. This study further emphasized the ability to use ionic functionality in conjunction with high $\chi$ parameter polymers to tune phase separation in BCPs.

Sudre and Balsara *et al.* explored the effect of the bound ion type on the morphology and conductivity of positively charged BCPs.[52] In this study, the authors examined ammonium and imidazolium-containing BCPs synthesized from the same neutral BCP precursor. SAXS analysis revealed that both sets of BCPs formed lamellar morphologies regardless of ion type, chain length,

or volume fraction of charged units. Although the domain size of the imidazolium-containing BCPs remained smaller than its ammonium counterpart over the entire range of molecular weights, the ionic conductivities and water uptake measured practically identical between the two systems. The authors concluded that the chemical identity of the bound ion has little effect on the morphology and conductivity of the polymer. Prior work from Hemp and Long *et al.* supports the finding that the chemical identity of the bound cation does not significantly change the morphology; however, they found that a larger cation (*i.e.*, phosphonium) did enhance the ionic conductivity and thermal stability compared to ammonium counterparts.[75]

### 5.2.2.2 Solution Morphology

Amphiphilic diblock copolymers exhibit the ability to form nanoscale objects in solution during polymerization in a process of polymerization-induced self-assembly (PISA).[76] Recent literature has explored the effect of incorporating charged units on the PISA of BCPs.[45, 77-80] An example of PISA of poly(ionic liquid) (PIL)-based block copolymer was reported by Yang and Sun *et al*. (**Figure 5.5a**).[77] This block copolymer was composed of poly(vinylbenzyl imidazolium

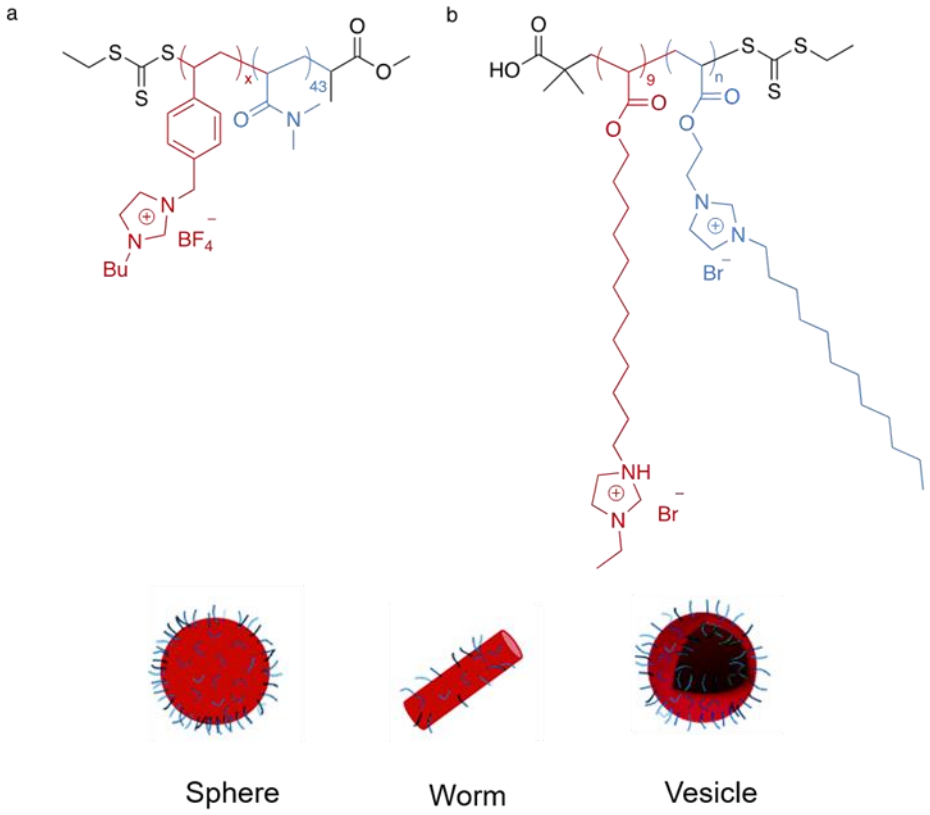


**Figure 5.5**: Poly(ionic-liquid)-based nano-objects. Reproduced from Yang and Sun *et al.* and Depoorter and Bernard e*t al*. with permission from the Centre National de la Recherche Scientifique (CNRS) and The Royal Society of Chemistry.[78]

tetrafluoroborate) and poly(*N*,*N*-dimethylacrylamide). By varying the length of poly(vinylbenzyl imidazolium tetrafluoroborate), the authors obtained a full morphological transition, i.e., sphere, worms, and vesicles. The PISA of sulfonated block copolymers reported by Armes and Smith *et al*. also exhibited this structure-directing morphological transition.[80] The same team evidenced PISA of trimethylammonium-based diblock copolymer into nanoparticles. The morphology of the nanoobject can be further modified into spheres, worms, and vesicles via tuning the length of the uncharged block.[79] The majority examples of PISA of polymer(ionic liquid)-containing block copolymers composed of one PIL block and one neutral block. Depoorter and Bernard et al. presented an all PIL block copolymer nanoparticles that formed controlled morphologies including spheres, rods, and vesicles (**Figure 5.5b**).[78]

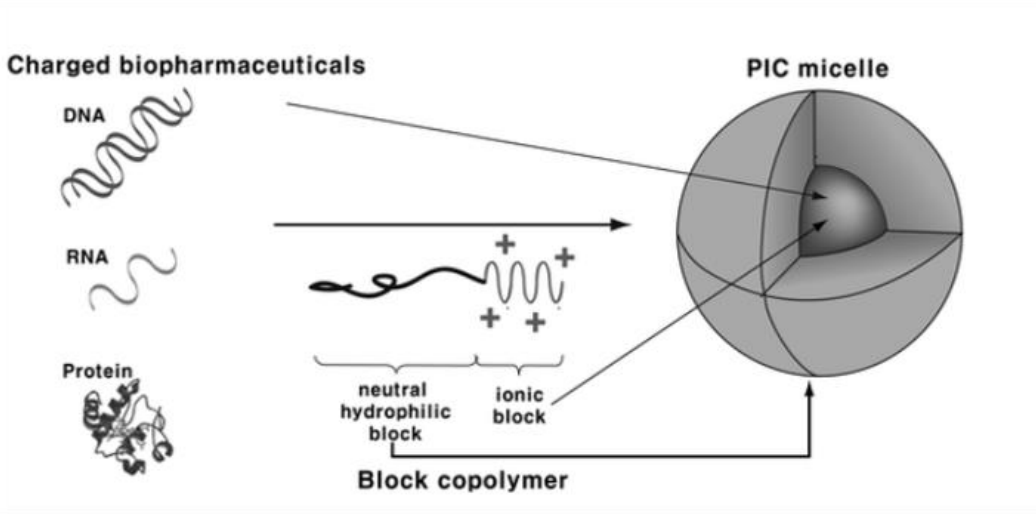


**Figure 5.6**: Schematic diagram of a polyion complex micelle formation from a charged diblock copolymer. Reproduced with permission from Lee and Kataoka with permission from the Royal Society of Chemistry.[83]

The self-assembly of charged BCPs in solution renders them amenable to micelle formation. Indeed, one of the most common applications of charged BCPs involves the formation of micelles for biopharmaceutical delivery applications.[30, 33, 34, 54, 55, 81-85] As demonstrated in **Figure 5.6**, charged amphiphilic BCPs can spontaneously bind with oppositely charged proteins or nucleic acids in aqueous media to form polyion complexes (PIC), or polyplexes.[83] The charged complex forms the core of the micelle, while the neutral hydrophilic block comprises the shell. These polyplex micelles promote efficient delivery of drugs and/or nucleic acids to cells. The design of the BCP remains crucial for tuning the properties of the micelles as well as their efficacy as drug delivery vehicles.

Lodge and Reineke *et al.* have presented detailed studies on polyplex formation between DNA and cationic BCPs providing insight into the effect of hydrophilic block structure and length, DNA architecture, and protonation state on complexation.[33, 34, 39, 81] The length of the DNA chain was shown to influence the size and stability of the formed micelles.[33] The authors demonstrated that longer DNA chains led to the formation of larger polyplex aggregates while shorter chains led to

smaller complexes when the concentration of micelles exceeded that of DNA. Conversely, shorter DNA chains led to larger complexes that precipitated out of solution with an excess of DNA. In terms of polymer structure, both the length and chemical identity of the hydrophilic block appear to have a significant effect on the polyplex size and stability. Utilizing longer hydrophilic blocks relative to the cationic block tends to improve the colloidal stability and results in smaller micelles with a narrow size distribution.[33, 55] However, shorter cationic blocks lead to loosely structured polyplexes while increasing the block length relative to the hydrophilic block decreases the colloidal stability.[33] The incorporation of bulky hydrophilic blocks, such as poly(oligo(ethylene glycol) methyl ether methacrylate) (P(OEGMA)), increased the size of the micelles compared to poly(ethylene glycol) blocks in a solution containing excess DNA. However, the micelle size stabilizes and depends more on the overall hydrophilicity of the polymer when the polymer is in excess relative to DNA.[34] These studies emphasize the structure-property relationships in the cationic BCP polyplexes and provide insight into the future design of micelles for drug delivery applications.

Most research on polyplexes, including the previous examples, rely on ammonium-based cationic blocks for complexation with DNA or other biopharmaceuticals. However, other charged macromolecules also suffice for complexing biopharmaceuticals. For example, Hemp and Long *et al.* synthesized BCPs comprised of a phosphonium-functionalized cationic block and a hydrophilic block (P(OEGMA) or 2-methacryloyloxyethyl phosphorylcholine (MPC)) aimed at nonviral nucleic acid delivery.[30] They found that all BCP compositions efficiently bound DNA and demonstrated excellent colloidal stability. The BCPs all successfully delivered DNA to HepaRG but did not demonstrate a trend in transfection capability with changing phosphonium block lengths or hydrophilic block composition. However, increasing the length of the phosphonium-

containing block did result in increased cell viability for P(OEGMA)-based BCPs. In another study, Jiang and Stenzel *et al.* replaced the synthetic charged BCP with P(OEGMA)-functionalized albumin protein to form polyplexes as a delivery system for Spry1 (a positively charged cancer drug).[82] This BCP effectively complexed with the drug to form stable nanoparticles while maintaining the activity of the pharmaceutical. In fact, the albumin BCP polyplex enhanced the cytotoxicity of Spry1 against breast cancer cells compared to the drug alone. This study indicates the ability to replace synthetic, charged polymers with proteins to form polyplexes for biopharmaceutical delivery.

### 5.2.2.3 Ion Transport Properties

Charged diblock copolymers frequently find use as ion exchange membranes for electrolytes and fuel cells where the charged block (often a flexible, low $T_g$ polymer) promotes ion transport through the material while the neutral block imparts mechanical stability. As mentioned previously, the phase separated morphology of these charged BCPs is key to controlling their properties.[86] Weber and Mahanthappa *et al.* demonstrated the effect of nanoscale morphology on the ionic conductivity of a series of charged BCP derived from imidazolium polymerized ionic liquids (PIL).[53] The authors varied both the PIL volume fraction and the length of the imidazolium alkyl tail independently to determine their effects on the morphology and resultant ionic conductivity of the BCPs. The authors found that neither the morphology nor the ionic conductivity changed significantly as the length of the imidazolium alkyl chain changed. Conversely, changing the volume fraction of the PIL block significantly affected the morphology and, resultantly, the ionic conductivity. The volume fraction of the PILs in the BCPs ranged from 0.19 – 0.5. As such, the morphologies ranged from cylindrical at low volume fractions (0.19-0.29) to lamellae at the highest volume fraction (0.5) with the intermediate volume fraction (0.34) showing a mixture of

cylinders and lamellae. As summarized in **Figure 5.7**, the nanoscale morphology substantially affects the ionic conductivity.[53] PIL homopolymers exhibit the highest conductivity due to the lack of phase separation while BCPs displaying a lamellar morphology experience a five-fold decrease in ionic conductivity. Furthermore, BCPs of cylindrical morphologies (where the PIL comprises the minor fraction) experience a ten-fold decrease in ionic conductivity compared to the lamellar morphology. The authors attribute this decrease in conductivity to a lack of long-range order in the cylindrical morphology as shown through SAXS analysis, which results in grain boundaries, or dead ends, for the ions during conduction. In fact, long-range order appears critical in providing high degrees of connectivity between ion conducting phases. The authors compared solution cast films with good long-range ordering to poorly ordered melt pressed films of identical block composition and found

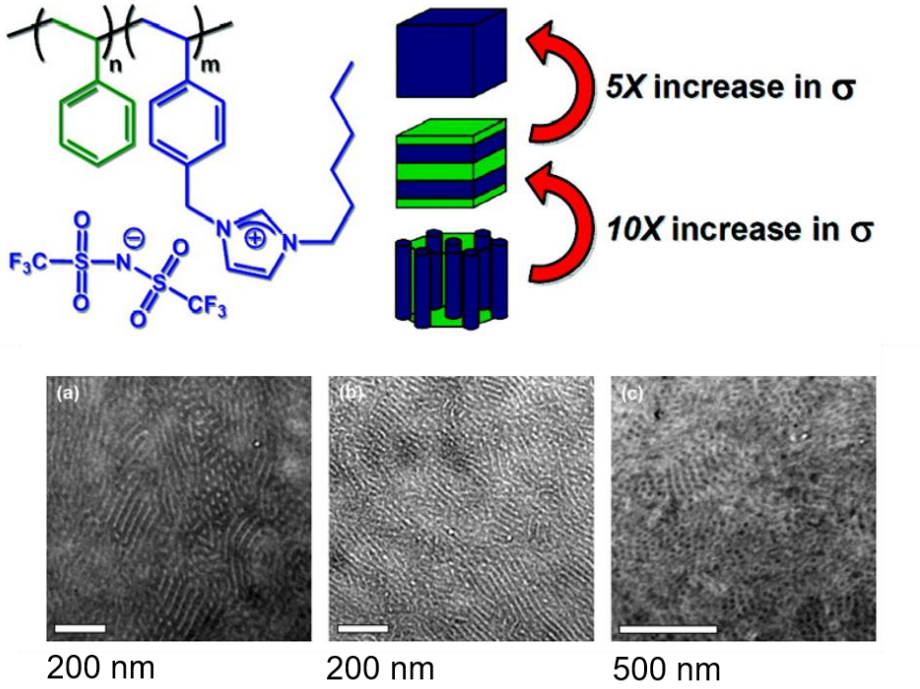


**Figure 5.7**: Ionic conductivity depends heavily on the block morphology copolymer as demonstrated by the diblock copolymer pictured here. TEM images show (a) cylindrical + lamellar morphology of solution cast block copolymer containing 8.6 mol% of the PIL, (b) cylindrical + lamellar morphology of melt pressed block copolymer containing 8.6 mol% of the PIL, and (c) hexagonally packed cylinders in melt pressed block copolymer containing 7.1 mol% of the PIL. Reproduced from Weber and Mahanthappa *et al.* with permission from ACS Publications.[53]

that the solution cast film demonstrated conductivities one order of magnitude higher than those of the melt pressed film.

Winey and Elabd *et al.* further corroborated and expanded on these results.[42, 87] In one study, the authors compared the morphologies of acrylate- and methacrylate-based PIL BCPs.[87] Similar to the aforementioned study, varying the PIL volume fraction led to a series of morphologies including cylinders and lamellae; however, in this case, a coexisting lamellae and three-dimensional network structure arose for the BCP with the highest PIL content. Ionic conductivity measurements revealed that the network morphology led to the highest conductivity due to the highly interconnected ion-conducting phases. Additionally, acrylate-based PILs exhibited a 1.5 – 2 order of magnitude increase in conductivity over methacrylate-based PILs due to the stronger phase separation of the polyacrylate with polystyrene. Winey and Elabd *et al.* also proved that even weak phase separation enhances ion transport over a random copolymer of a single phase.[42] SAXS and TEM images of a methacrylate-based PIL BCPs revealed phase separation with no long-range ordering while the analogous random copolymers exhibited a single phase. The phase separated morphologies enjoyed a two order of magnitude increase in ionic conductivity compared to the random copolymer indicating that local connectivity of ionic domains also contributes significantly to ion transport in charged BCPs.

Various other polymer parameters also affect ion transport in charged diblock copolymers such as the chemical identity of both the charged block and neutral block, the chosen counter ions, and the overall ionic content of the polymer. Unsurprisingly, incorporating a higher mole fraction of ionic groups into a BCP improves ionic conductivity; however, shorter ionic blocks tend to have less of a temperature dependence on conductivity and can intersect or overtake the conductivity curves of longer charged blocks at certain temperatures.[29] Utilizing long alkyl spacers between the

polymer backbone and the charged group lowers the $T_g$ of the polymer allowing for improved ionic conductivity.[37] Likewise, incorporating large counterions with delocalized charge (e.g. triflates, aluminates, and sulfates) serves to both decrease the $T_g$ of the conducting block and provide a weaker ionic interaction with the bound ion, which helps to promote ion transport.[88, 89]

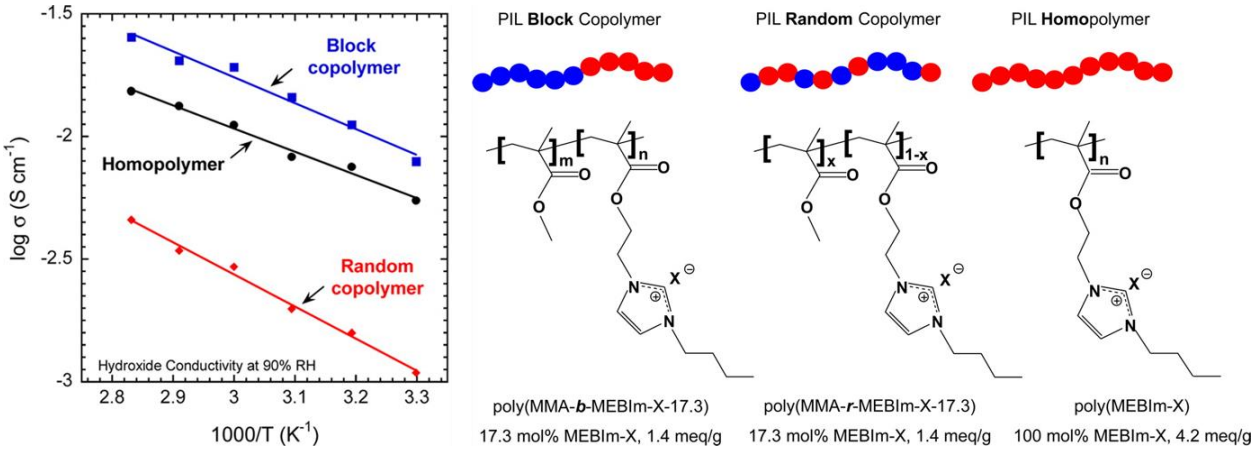


**Figure 5.8**: Effect of block copolymer architecture on hydroxide conductivity in an anion exchange membrane. Block copolymers exhibit higher hydroxide conductivities than either the random copolymer or homopolymer. Adapted from Ye and Elabd *et al.* with permission from ACS Publications.[90]

Charged BCPs that efficiently conduct hydroxide anions find use in solid-state alkaline fuel cells. Ye and Elabd *et al.* studied the effect of morphology on hydroxide conductivity in imidazolium containing diblock copolymers as summarized in **Figure 5.8**.[90] Once again, they demonstrated that the conductivity of the phase separated BCP measured significantly higher than that of the random copolymer at the same PIL content. However, in this case, the BCP hydroxide conductivity measured higher than even the PIL homopolymer at 90% relative humidity despite a similar normalized water content between two polymers. This interesting result led the authors to suggest that the ion-water confinement in the BCP nanochannels accelerates ion-transport and enhances conductivity. Copious amounts of research have focused on charged BCPs for fuel cell membranes, and the following sections on triblock and multiblock copolymers will further cover this application.

### 5.2.3 Triblock Copolymers

Triblock copolymers contain three blocks in the polymer chain as the name implies. Triblock copolymers most frequently take on one of three architectures: ABA, ABC, or A-BC-A. ABA triblock copolymers describe a symmetrical sequence of blocks with two identical A blocks end capping a chemically dissimilar B block. Conversely, three unique polymer blocks comprise ABC type triblocks, which increases the complexity of the system. A-BC-A type triblock copolymers leverage a random copolymer (BC) as the central block as a method of further refining the properties of the BCP. The ability to incorporate thermoplastic elastomer behavior into the polymer represents one of the major advantages of triblock copolymers over diblocks. Utilizing high $T_g$ polymer blocks as end cappers provides mechanical stability to the BCP while a low $T_g$ central block imparts flexibility. As demonstrated in this section, charged groups may be inserted into either the high $T_g$ or low $T_g$ phase of the BCP to improve properties for applications ranging from ion exchange membranes to electromechanical transducers. The morphological and ion transport behaviors of triblock and diblock copolymers are largely similar; however, this section will expand on the previous section and present applications for charged BCPs that require greater mechanical stability that diblocks.

#### 5.2.3.1 Ion Exchange Membranes

The ability of an ion exchange membrane to promote ion transport depends heavily on the water uptake and ion exchange capacity [91] of the polymer. Successful exchange membranes, such as the sulfonated fluoropolymer Nafion™, leverage hydrated nanochannels of ionic domains to efficiently transport ions across the membrane.[92] Although Nafion™ remains the benchmark material for anion exchange membranes, this material does experience drawbacks such as high cost, processing difficulties, and low conductivity at high temperatures and low humidity.[93] With

this knowledge in hand, researchers have investigated BCPs with similar morphologies that circumvent these shortcomings. Early literature examined triblock copolymers bearing sulfonated polystyrene end blocks as a low-cost alternative.[61, 62, 66, 94] Increasing the degree of sulfonation in the styrene blocks increases the water uptake of the polymer and therefore the conductivity to a level comparable to that of Nafion™. However, sulfonation of the polystyrene blocks decreases the thermal stability of the polymer on the order of 100 °C.[94] Additionally, these triblock copolymers exhibit high methanol uptake as well as water, which hinders their use for direct methanol fuel cell membranes.

Effective anion exchange membranes require alkaline stability over long periods of time to prevent degradation during use. Miyatake and coworkers have extensively studied the effect of incorporating ammonium pendent ammonium groups in aromatic and/or partially fluorinated copolymers.[95-99] Mahmoud and Miyatak *et al.* studied a series of quaternaized aromatic/perfluoroaklyl copolymers (QPAF) with attached ammonium groups of varying alkyl lengths as shown in **Figure 5.9**.[99] The ammonium groups containing butyl (QPAF-DMBA) and hexyl aliphatic chains exhibited larger interconnected ionic domains, and therefore enjoy higher hydroxide conductivities compared to the methyl (QPAF-TMA) and imidazole counterparts. Accelerated testing revealed no change in the conductivity of the QPAF-DMBA membrane over 500 h at 80 °C. Likewise, this material showed the highest alkaline stability and managed to retain 58% of its ionic conductivity over 1000 h in 1 M KOH at 60 °C. Finally, the authors demonstrated the ability to use QPAF-DBMA as a membrane in an alkaline fuel cell and obtained maximum power densities of 167 mW $cm^{-2}$. This study clearly demonstrates that the chemical structure of

the charged unit in triblock copolymers has a significant effect on the material's conductivity and fuel cell performance.

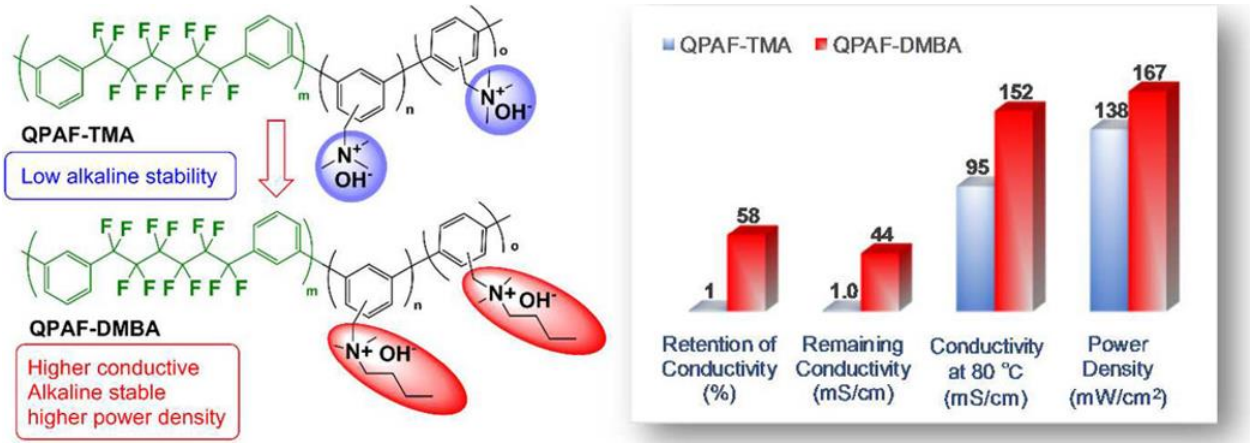


**Figure 5.9**: Quaternized aromatic/perfluoroakyl triblock copolymers and the effect of ammonium group type on fuel cell performance. Reproduced from Mahmoud and Miyatake *et al.* with permission from ACS Publications.[99]

Zhang and Coughlin *et al.* presented a study on the comparison of diblock and triblock copolymers containing phosphonium-derived charged blocks for anion exchange membranes.[44] The bulky phosphonium group afforded solubility in common organic solvents and drastically influenced the morphology of the solution cast membranes. Remarkably, the phosphonium block phase separated from the polyisoprene blocks to constitute the continuous phase even at low volume fractions. The triblock copolymers formed lamellae at phosphonium volume fractions as low as 22 vol.% and the morphology transitioned to hexagonal packing, where the phosphonium blocks made up the continuous matrix, at 30 vol.%. The diblock copolymers exhibited similar behavior but transition to the hexagonally packed morphology at an even lower volume fraction (22 vol.%). The authors contributed this interesting morphological phenomenon to a conformational in the BCPs derived from the bulky size of the phosphonium groups as well as electrostatic forces between the charged groups. Ionic conductivity measurements revealed high chloride conductivities in the lamellar triblock copolymers reaching values up to $6.9 \times 10^{-3}$ S $cm^{-1}$

at 90 °C and 95% humidity. The hexagonally packed diblock copolymer exhibited even higher conductivities reaching a maximum of 2.0 x $10^{-2}$ S $cm^{-1}$ at the same conditions despite containing a similar volume fraction of phosphonium blocks as the triblock. The authors concluded from this that the hexagonally packed morphology provides a more continuous pathway for ion transport than the lamellar morphology. It should be noted, however, that the mechanical properties of these polymers were not tested as part of this study. Although the diblock copolymer demonstrated higher ionic conductivity, the triblock copolymers likely benefited from superior mechanical properties. This tradeoff between conductivity and mechanical stability will become more apparent when discussing electromechanical transducers in the next section.

### 5.2.3.2 Electromechanical Transducers

Electromechanical transducers are a type of device that reversibly converts electrical signals into a mechanical force (actuators) or vice versa (sensors). The desire to produce lightweight and relatively inexpensive transducers has led researchers to explore polymeric materials for use in this application. Ionic polymer-metal composites (IPMC) represent one class of electromechanical transducer that relies heavily on charged BCPs to provide actuation. The devices consist of a charged, electrically insulative BCP sandwiched between two conductive electrodes. Applying a voltage across the device results in a polarization of the electrodes, which produces an electric field that causes the mobile ions in the polymer to migrate towards the oppositely charged electrode.[100] These mobile ions typically transport water with them across the membrane, which results in one side of the polymer swelling and bending the tip of the transducer (actuation). Nafion™ has served as a benchmark material for these applications, as it has for fuel cells, due to its excellent conductivity and mechanical properties while in a hydrated state. However, due to the previously mentioned limitations of Nafion™, the past three decades have seen researchers attempt

to design charged BCPs with sufficient ionic conductivity and modulus to serve as membranes for IPMCs.[101, 102]

Long and coworkers have studied several charged triblock copolymer systems for use as IPMC actuators.[31, 32, 35, 50, 51, 103] Green and Long *et al.* synthesized a triblock copolymer containing a benzyl imidazolium central block with external polystyrene blocks.[50] They found that exchanging the counterion from bromide to bis(trifluoromethane sulfonyl)imide ($Tf_2N$) drastically decreased the $T_g$ of the ionic block and increased the thermal stability of the BCP overall. Ionic conductivities for this BCP ranged from $10^{-7}$ S cm$^{-1}$ to $10^{-4}$ S cm$^{-1}$ over a temperature range of approximately 40 – 140 °C, respectively. The authors plotted the ionic conductivity with respect to the storage modulus of the material as determined from dynamic mechanical analysis. They demonstrated that a two order of magnitude decrease in the storage modulus corresponded with a two and a half order of magnitude increase in ionic conductivity, which neatly revealed the tradeoff between conductivity and modulus in charged BCPs. At room temperature, this BCP displayed a conductivity of 5.0 x $10^{-7}$ S cm$^{-1}$ and a storage modulus of 100 MPa. Though these properties seem inferior to Nafion™ in its hydrated state at room temperature (1.0 x $10^{-1}$ S cm$^{-1}$ and 120 MPa), the authors still successfully fabricated IPMCs that experienced curvatures up to 2.5 times higher than that of Nafion™-based IPMCs under ambient conditions.

Jangu and Long *et al.* expanded on this triblock composition as they replaced the center block with a random copolymer of di(ethylene glycol) methyl ether methacrylate (DEGMEMA) and the same benzyl imidazolium as the previous study to form a series of A-BC-A type triblock copolymers with varying degrees of ion content (**Figure 5.10**).[32] The authors hypothesized that the incorporation of DEGMEMA into the ionic phase would optimize the ionic conductivity due to lowering the $T_g$, increasing the dielectric constant, and incorporating ether units that would assist

in coordinating and transporting ions. AFM showed a lamellar morphology in the triblock copolymer containing 18 mol% ion content; however, increasing the ion content led to less ordered morphologies (**Figure 5.10c-e**). Despite this, the BCPs with the highest ion content demonstrated the highest ionic conductivity approaching $10^{-3}$ S $cm^{-1}$ at ~ 100 °C (**Figure 5.10a**). This BCP served as a membrane for an IPMC after swelling in a commercial IL. The triblock copolymer exhibited a maximum curvature that was approximately two times higher than that of a Nafion™-based actuator swollen with a similar amount of IL (**Figure 5.10b**).

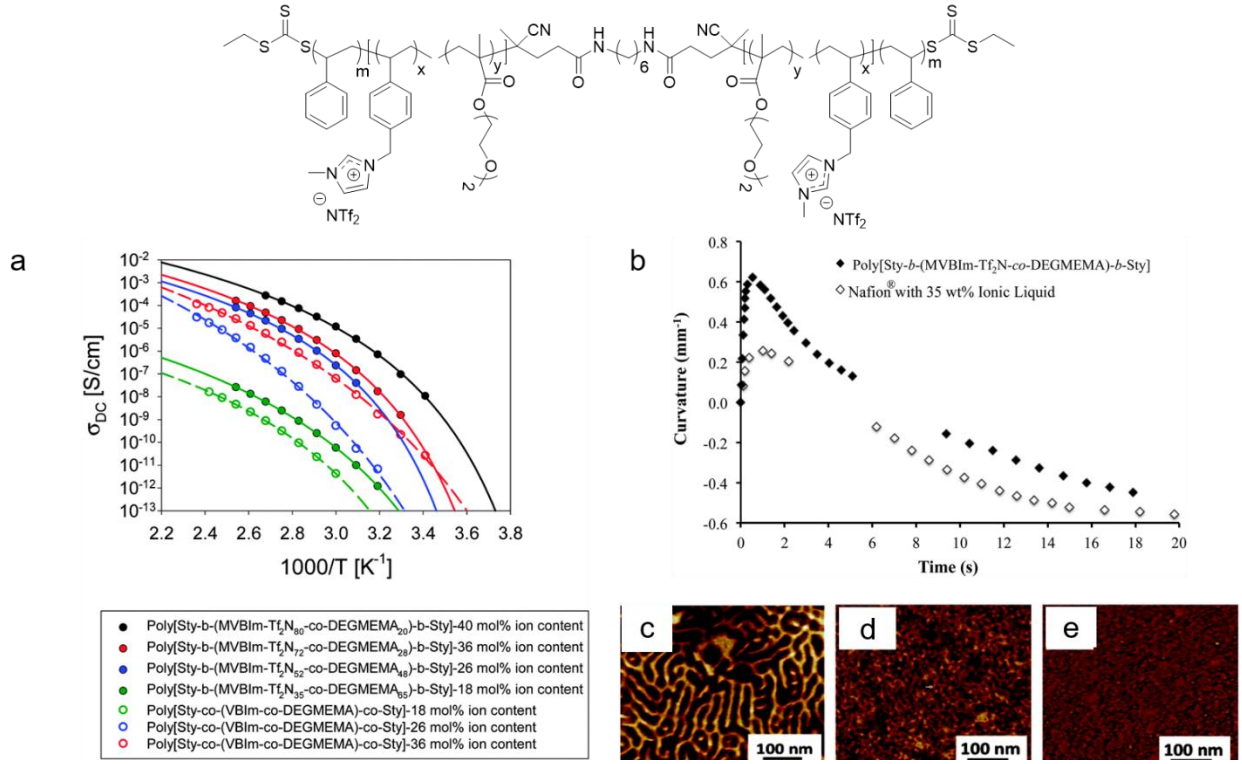


**Figure 5.10**: Triblock copolymer containing an imidazolium center block. (a) Arrhenius plot of ionic conductivity as a function of temperature for block copolymers and random copolymers. (b) Curvature vs. time for an electromechanical transducer of the triblock copolymer compared to Nafion®. AFM images of triblock copolymers containing (c) 18 mol% (d) 26 mol% and (e) 36 mol% ion content. Reproduced from Jangu and Long *et al.* with permission from the Royal Society of Chemistry.[32]

Kim and Park *et al.* presented a systematic study on the factors that affect the electromechanical properties of diblock and triblock copolymers comprised of a poly(methylbutylene) middle block and sulfonated polystyrene (sPS) end blocks.[104] They varied the molecular weight of the sPS

blocks while maintaining a constant degree of sulfonation, and also measured the effect of changing the anion of the IL used to swell the BCPs. Tensile analysis on the BCPs revealed that the triblock copolymers exhibited higher Young's moduli than the diblock, and that increasing the molecular weight of the sPS blocks led to an increase in Young's modulus. All the diblock and triblock copolymers studied exhibited hexagonal cylindrical morphologies with a major sPS phase as determined through SAXS analysis. The BCP films were all swollen with imidazolium ILs before fabricating actuators, and the diblock copolymer swollen with 30 wt.% IL was chosen as an example to study the counterion effect. Interestingly the identity of the imidazolium counter anion drastically affected the properties and actuation performance of the BCPs. Increasing the volume of the anion led to an increase in the sPS domain size, and the largest anion (i.e., $Tf_2N$) produced BCPs with the highest room temperature ionic conductivity. The incorporation of IL also drastically decreased the Young's modulus of the material as expected; however, the $Tf_2N$ counterion led to the smallest change in modulus (75% decrease), while smaller counterions such as hexafluorophosphate ($PF_6$) and tetrafluoroborate ($BF_4$) led to even larger decreases of 89% and 98%, respectively. Despite this, the membranes still maintained sufficiently high moduli for electromechanical testing. As expected, the diblock and triblock copolymers containing the imidazolium IL with the $Tf_2N$ exhibited the largest bending strain compared to the other two anion types.

The authors continued to explore the effect of the BCP architecture and molecular weight on the actuation performance of the diblock and triblock copolymers swollen with 20 to 70 wt.% IL containing the $Tf_2N$ anion.[104] The diblock copolymer actually exhibited the largest domain sizes while the triblock copolymers showed decreasing domain sizes with an increase in the sPS molecular weight. The swollen BCPs experience the same trend in Young's modulus as their dry

counterparts with the triblock copolymer containing the highest molecular weight sPS blocks displaying a modulus over 1 GPa even when swollen with 60 wt.% of IL. Between 20- 60 wt.% IL incorporation, the diblock copolymer maintained the largest bending strain under an applied voltage with the two triblock copolymers decreasing in bending strain as the sPS molecular weight, and Young's modulus, increased. This result apparently indicates that an excessively high modulus may actually hinder the ability of the polymer to actuate. However, the high modulus did allow for the triblock copolymers to maintain actuation potential up to 70 wt.% of IL loading, whereas the diblock failed to actuate above 60 wt.%. Overall, this study demonstrates the necessity to carefully design BCP architecture, molecular weight, and ion content for optimized actuator performance.

### 5.2.4 Multiblock Copolymers

Multiblock copolymers describe a class of BCPs that consist of four or more covalently bound polymer blocks. These BCPs may contain four or more unique polymer blocks, but multiblock copolymers rarely ever exceed five unique blocks (pentablocks). Multiblock copolymers are most often of the type $(A\text{-}B)_n$ where a step-growth polymerization leads to a random distribution of polymer blocks throughout the polymer chain. For charged multiblock copolymers, most approaches utilize a charged, hydrophilic polymer and a hydrophobic neutral block. Ideally, the two chemically dissimilar polymers will microphase separate to give rise to BCPs with useful thermal, electrical, and mechanical properties. Much like triblocks, charged multiblock copolymers find many uses in ion exchange membranes and electromechanical transducers due to their propensity to exhibit high thermal stability and transport properties.

#### 5.2.4.1 Ion Exchange Membranes

Similar to the triblock copolymers from the previous section, charged multiblock copolymers find use as anion exchange membranes for fuel cells due to their thermal and mechanical

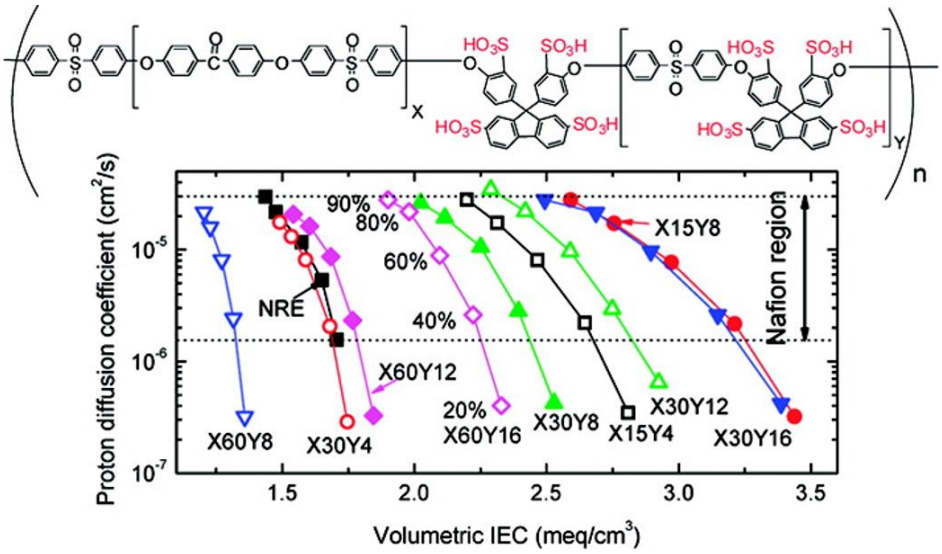


**Figure 5.11**: Proton diffusion coefficients as a function of volumetric ion exchange capacity for a highly sulfonated poly(arylene ether sulfone ketone). The number proceeding X and Y represents the degree of polymerization for each block. Reproduced from Bae and Watanabe *et al.* with permission from ACS Publications.[13]

stabilities.[13, 14, 18, 21, 22] As mentioned previously, successful candidates for fuel cell membranes should ideally maintain high ionic conductivity at low humidity and sustain high temperatures (> 80 °C) for long periods of time. Fluorinated or partially fluorinated BCPs are most frequently employed for these applications; however, the high cost of these polymers limits their practical application in fuel cell membranes. Bae and Watanabe *et al.* designed novel, densely-sulfonated poly(arylene ether sulfone ketones)s (SPESK) BCPs containing microphase separated hydrophilic and hydrophobic segments as shown in **Figure 5.11**.[13, 14] This polymer contains multiple sulfonate groups in the hydrophilic segment, which enhanced the IEC of the BCP. The authors synthesized a series of BCPs of varying block lengths to determine the effect of molecular weight on thermal, mechanical, and electrical properties. Increasing the molecular weight of the charged block correlated with an increase in IEC, which resulted in higher water uptake and ultimately higher proton conductivity across the membrane. In this case, increasing the block length of the hydrophobic block decreased the Young's modulus compared to shorter BCPs with similar ion exchange capacities. Regardless, several membranes exhibited both high mechanical properties and proton conductivities that met

or exceeded those of Nafion™ even at low relative humidity. Furthermore, many of these membranes exhibited excellent hydrolytic stability in boiling water over 24 h. However, like most sulfonated aromatic membranes for fuel cell applications, these materials suffered from poor to moderate oxidative stability with most membranes losing > 50 wt.% of their initial mass after oxidative stability testing.

Miyake and Miyatake *et al.* aimed to improve the oxidative stability of SPESK through the incorporation of phosphine oxide ketone (POK) units in the hydrophilic segment of the multiblock copolymer.[18] Increasing the block length of the densely sulfonated POK block resulted in increased ion exchange capacities as in the previous example. Although the proton conductivity at low humidities failed to reach the level of Nafion™, the highest IEC membrane did exceed the conductivity of Nafion™ by a factor of 1.3. Moreover, the BCPs exhibit higher storage moduli than Nafion™ over the entire range of relative humidities tested indicating that these membranes exhibit superior mechanical properties to Nafion™ even when fully hydrated. Finally, these multiblock copolymer membranes experienced negligible weight loss after thermal and oxidative stability tests, which represents a remarkable improvement over the previous material, and suggests its future use as a fuel cell membrane.

Membranes for alkaline fuel cells require excellent base stability in addition to high hydroxide conductivity. In addition to ammonium, phosphonium, and imidazolium cations, spirocyclic ammonium groups provide improved base stability when incorporated into aromatic multiblock copolymers.[21, 105] For example, Strasser and Knauss *et al.* synthesized a series of polysulfones with increasing wt.% of poly(diallylpiperidinium hydroxide) (PDApipOH) hydrophilic segments for use as base stable fuel cell membranes.[21] All multiblock copolymers exhibited microphase separation according to AFM images, but did not display long-range ordering. Increasing the wt.%

of the charged phase increased the IEC and water uptake as expected. The hydroxide conductivity of these materials never quite reached the value of Nafion™ despite still exhibiting a maximum value on the order of $10^{-1}$ S $cm^{-1}$. Most importantly though, the BCPs showed little to no degradation after 1,000 h in an 80 °C solution of 1 M KOH for membranes containing up to 29 wt.% of PDApipOH. These materials show promise for alkaline fuel cell applications; however, the synthesis of the spirocyclic ammonium polymer still presents significant challenges.

### 5.2.4.2 Electromechanical Transducers

Several studies have begun to explore the structure-property relationships as well as the actuator potential of the commercially-available, sulfonated pentablock copolymer Nexar™.[60, 65, 106] In this pentablock copolymer the sulfonated PS center block serves as a matrix for ion transport, the hydrogenated polyisoprene blocks impart flexibility, and the poly(tert-butyl styrene) end blocks act as physical crosslinking sites. The morphology of this BCP depends significantly on the solution used to cast the membrane. Casting the membrane from a high cyclohexane: THF ratio resulted in a random, poorly ordered morphology, whereas increasing the THF content to 60 vol.% or greater results in lamella or lamella/hexagonal morphologies.[106] Unsurprisingly, the well-ordered morphologies experienced more water uptake and higher ionic conductivities. This resulted in the lamellar/hexagonal membrane demonstrating the highest actuation displacement under an applied 3V. Choi and Winey *et al.* measure the structure property relationships of a series of Nexar™ BCPs with varying volume fractions of sPS.[60] The BCPs take on micellar morphologies in nonpolar solvents and form membranes with discrete microdomains at low volume fractions of sPS (0.378-0.416). Increasing the volume fraction of sPS (0.426 – 0.434) increases the micelle core diameter and produces membranes with interconnected bicontinuous ionic domains. The rate of water vapor transport measured substantially higher for the interconnected morphologies than

the discrete nanodomains as expected. Gao and Long *et al.* reported Nexar™/IL composites as membranes for electromechanical transducers. The authors carried out a metathesis reaction to install imidazolium counterions on the sulfonates allowing for the eventual uptake of free ionic liquid into the membrane. The Nexar™ BCP containing imidazolium counterions displayed higher thermal stability than the sulfonic acid, and films cast from cyclohexane formed uniformly dispersed nanoscale spherical domains. Soaking the membrane in a commercial imidazolium ionic liquid resulted in the uptake of 35 wt.% of ionic liquid into the membrane. The swollen membrane functioned as part of an IPMC that actuated upon the application of a relatively low voltage (4V). Although this system necessitates more morphological and electromechanical characterization, this study clearly demonstrates the promise of utilizing Nexar™/IL composites for electromechanical transducers.

Many sulfonated engineering multiblock copolymers serve as electromechanical transducers including polyimides,[107-109] polyetherimides,[19, 20] polysulfones,[110] and poly(arylene ether ketone)s.[111] In one interesting example, Song and Park *et al.* fabricated sulfonated polyimide transducers in situ self-metallization.[107] A sulfonated poly(amic acid) (SPAA) containing lithium counter ions underwent a metathesis reaction to incorporate $Ag^+$ ions at each carboxylic acid unit as illustrated in **Figure 5.12**. During thermal imidization of the SPAA the $Ag^+$ ions were reduced to form layers of silver nanoparticles on the surfaces of the membrane. TEM images revealed that

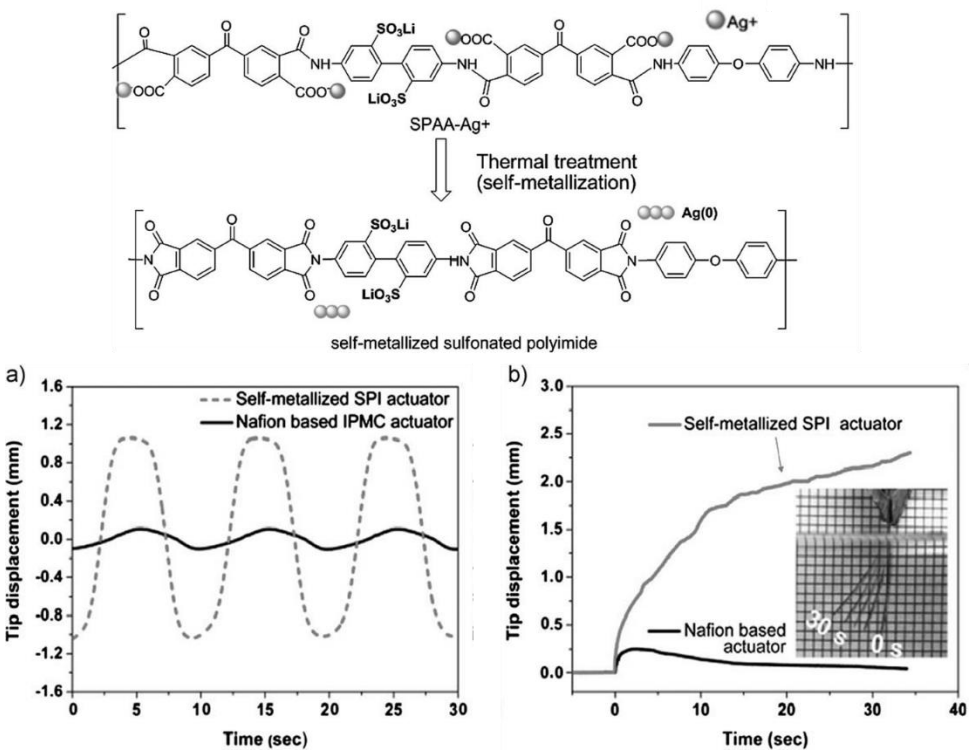


**Figure 5.12**: Sulfonated poly(amic acid) (SPAA) containing silver counterions undergo a thermal treatment to self-metalize and form electromechanical transducers. Plots show tip displacement of the sulfonated polyimide (SPI) compared to Nafion® under (a) an applied AC voltage and (b) an applied DC voltage. Adapted from Song and Park *et al.* with permission from Wiley.[107]

many nanoparticles settled at the polymer-metal interface and served to improve the adhesion of the electrodes to the polymer surface. Actuation testing under very low applied voltages (0.5 V) revealed the electromechanical performance of this material compared to Nafion™. As shown in **Figure 5.12a**, the tip displacement under an applied AC voltage reached 1.12 mm, which was approximately six times higher than that of Nafion™-based actuators. Furthermore, the sulfonated polyimide exhibited much higher tip displacement than Nafion™ under DC voltage and did not experience back relaxation (**Figure 5.12b**), which is characteristic of Nafion™. This study demonstrates a facile approach to fabricating transducers by leveraging the architecture of the charged BCP, and similar approaches may find use in other multiblock copolymers.

## 5.3 Branched Ionic Block Copolymers

### 5.3.1 Ionic Block Copolymer Brush

### 5.3.1.1 Synthesis and Structure-Property Relationships

The preparation of BCP brushes generally involves two methods: physisorption and covalent attachment. For polymer physisorption, BCPs anchor onto a modified substrate mostly through ionic or H-bonding interactions ("grafting to" method), representing a more convenient and reversible strategy. One example is shown in **Figure 5.13**; the polyelectrolyte brush adsorbs the diblock copolymer brush through electrostatic interaction where the diblock copolymer consists of one oppositely charged block and one neutral block.[112] In a following work, the authors prepared a poly(acrylic acid) (PAA) brush and poly(N-methyl-2-vinyl pyridinium)-*b*-poly(ethylene oxide) (P2MVP-*b*-PEO) for antifouling applications.[113] The brush exhibited low adsorption of P2MVP-*b*-PEO at low pH while PAA was unchanged at this condition. Increasing the pH deprotonated PAA resulting in electrostatic interactions forming between PAA and P2MVP-*b*-PEO, which resulted in adsorption. The ionic BCP brush showed excellent antifouling properties in proteins such as lysozyme, fibrinogen, bovine serum albumin, and *b*-lactoglobuline due to the formation of weak interactions between PEO and these proteins. Similar applications are also achieved in micelle systems.[114]

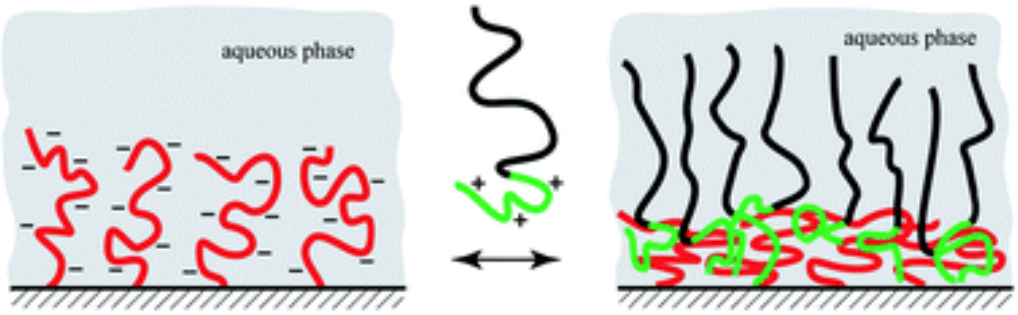


**Figure 5.13**: Charge-driven and reversible assembly of ionic BCP brush. Adapted from de Vos and Stuart *et al.* with permission from the Royal Society of Chemistry.[112]

The area of ionic BCP brushes has extended to zwitterions as such systems improve thermal, thermomechanical, and static dielectric properties of the polymer.[115] In a representative work, the grafting-to method enabled fundamental studies on brush density, polymer composition,

chain length, and polydispersity of zwitterion BCP brushes (**Figure 5.**).[116] Tuning the molecular weight and brush density led to control over antifouling properties of BCP brushes. Using ATRP, the same group prepared PPO-*b*-poly(sulfobetaine methacrylate) (PPO-*b*-poly(SBMA)) with varying lengths of the zwitterionic block tethering onto a substrate via self-assembled monolayers (electrostatic interaction).[117]

As another option, chemically "grafting to" represents an irreversible method of tethering polymer chains on the surface, eliminating the use of solvent.[118] "Grafting to" through chemical bonding also imparts stability under conditions where high shear forces are applied.[119] The previously-discussed BCP brushes contain an ionic bottom layer and a neutral upper layer. Alternatively, a scenario in which the ionic block serves as the top layer is potentially worth investigating. In this case, counterion effects are vital as presented by Liu and Zhou *et al*. As shown in their work, the friction coefficient of polyelectrolyte brushes was tuned from ~$10^{-3}$ to ~100 according to the counterions series $Cl^-$ < $ClO4^-$ < $PF6^-$ < $TFSI^-$.[120]

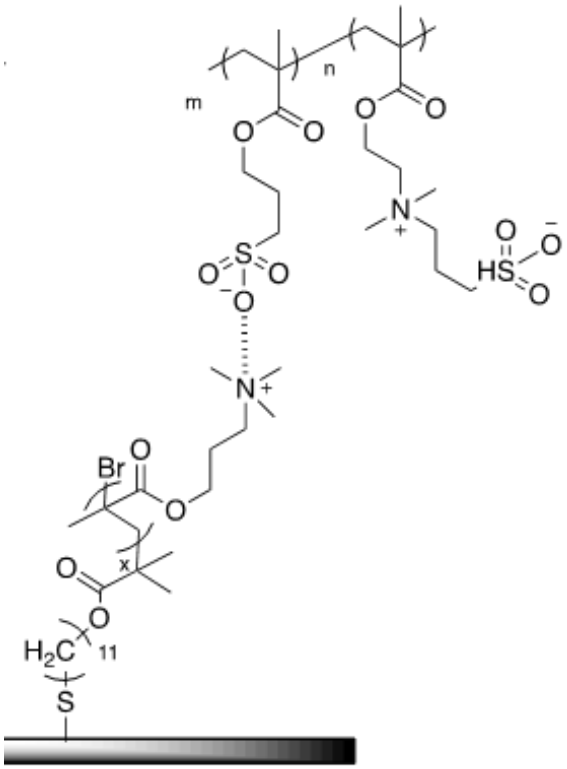


**Figure 5.14**: Ion-pair anchoring of zwitterionic copolymer brushes.[116]

The "grafting to" method is generally experimentally convenient and offers control over the brush. However, there are some limitations, such as relatively low grafting density compared to the "grating from" method.[119] Thus, the "grating from" method via surface-initiated polymerizations" provides an alternative strategy to achieve control over brush density, thickness, and functionality.[119]

First , a monolayer carrying the functionality is formed on the substrate, for example, thiols on gold, silanes on glass ($Si/SiO_2$) and plasma oxidized polymers.[119] Then, chain-growth polymerization, typically controlled radical polymerization, enables the grating of brushes. The Brittain group reported a library of AB and ABA types of polystyrene and poly(methyl methacrylate) BCP brushes through surface-initiated ATRP.[121, 122] Osborne and Huck *et al*. presented the synthesis of BCP brushes using aqueous ATRP.[123] These literature laid a solid foundation for the synthesis of ionic BCP brushes for applications such as the extracellular matrix.[124] Dong and Ober *et al.* prepared well-defined BCP brushes of poly(acrylamide)-*b*-poly(acrylic acid) (PAAm-*b*-PAA) and poly(oligo(ethylene glycol)methylether methacrylate)-*b*-PAA (POEGMA-*b*-PAA), then surface-functionalized the BCP brushes with a peptide for cell adhesion surfaces. Due to the potential interaction of the carboxylic acid group with the ATRP catalyst,[125] the second block, PAA, was prepared via chain extension of sodium acrylate (NaA) and further protonation.[126] Ionic BCP brushes are not limited to surface brush applications. Using RAFT polymerization, Qiao and Ran *et al*. designed a polycarboxylate-b- polyoxyethylene brush for graphene oxide (GO) aqueous suspension preventing aggregation of GO sheets.[127] The presented ionic BCP brush exhibited a more effective dispersing ability for the GO sheet than the commercial random copolymer counterpart. A comb-shaped ionic multiblock copolymer brush is described by Norsten and Ding *et al.* (**Figure 5.15**).[128] The comb-shaped copolymers were prepared through the copolymerization of BPA, 6F-bisphenol A, and poly(α-methyl)styrene substituted BPA, which was synthesized via anionic polymerization. The poly(α-methyl)styrene was subsequently subjected to sulfonation to yield the ionic comb. The "extreme" amphiphilic nature of the comb enabled high proton conductivities with dimensional stability compared to Nafion™ owing to the fluorinated segment.

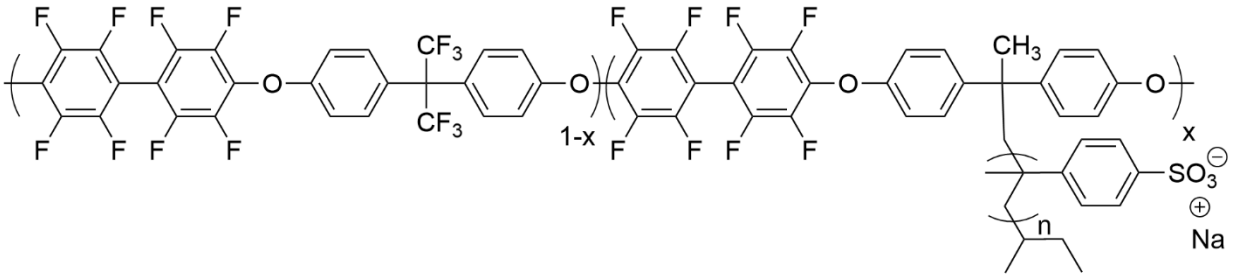


**Figure 5.15**: Synthesis of sulfonated comb-shaped copolymers.[128]

### 5.3.1.2 Biological Applications

Charged polymers tend to bind proteins and cells via electrostatic interaction. Researchers are leveraging these properties of charged polymer brushes for developing surfaces that adsorb proteins for analytical devices and protein purification.[129] One specific effort is to improve specific recognition between ionic polymers and proteins.[130] The following example illustrates the utilization of the electrical nature of ionic polymers, i.e., cationic, anionic, and zwitterionic polymer.[131] Here, the adsorption of albumin proteins was higher than 50 ng/cm$^2$ for the cationic and anionic brushes, while the adsorption of protein on the zwitterionic brush was not detectable. Though electrostatic interactions enable the modulation of protein adsorption, these processes sometimes induce damage to protein structures when the desorption process is involved.[129] Utilizing hydrophobicity of the neutral polymer provides an alternative way for adsorbing/desorbing proteins freely.[132] However, hydrophobic interactions between proteins and polymers are generally weak and less selective.[132] Therefore, combining electrostatic and hydrophobic interactions offers a selective and relatively mild system for protein adsorption/desorption.[133, 134] Of all the neutral polymers, poly(N-isopropylacrylamide) (PIPAAm) is special due to its thermally-responsive property, *i.e.*, the PIPAAm block contracts as the temperature increases to the lower critical solution temperature (LCST) (32 ºC). The LCST

transition of PIPAAm blocks induces a switch from an extended to a collapsed structure, thus enabling the tuning of overall surface hydrophobicity and charge density.[135]

In recent work, the Okano group designed a BCP brush containing poly(3-acrylamidopropyl trimethylammonium chloride)-*b*-poly(N-isopropylacrylamide) (PAPTAC-*b*-PIPAAm) via ATRP, where the PAPTAC block provided electrostatic interaction and PIPAAm block imparted thermal-responsiveness and hydrophobic interactions (**Figure 5.16A**). As shown in **Figure 5.16C**, at high temperature, a shrunken polymer brush exposed the ionic block to proteins, which enabled the adsorption. Decreasing temperature swelled the brush and therefore released proteins due to the weak hydrophobic interaction between PIPAAm and proteins. In their work of investigated milk proteins, the BCP brush indicated better desorption of acidic and relatively small proteins via temperature stimuli, where the adsorption can be tuned via varying the length of the PAPTAC segment. Compared to the random copolymer brush analog (**Figure 5.16b)**, the BCP yielded densely packed ionic groups, therefore, exhibited stronger cationic properties, as demonstrated using packed-column elution of adenosine nucleotides.

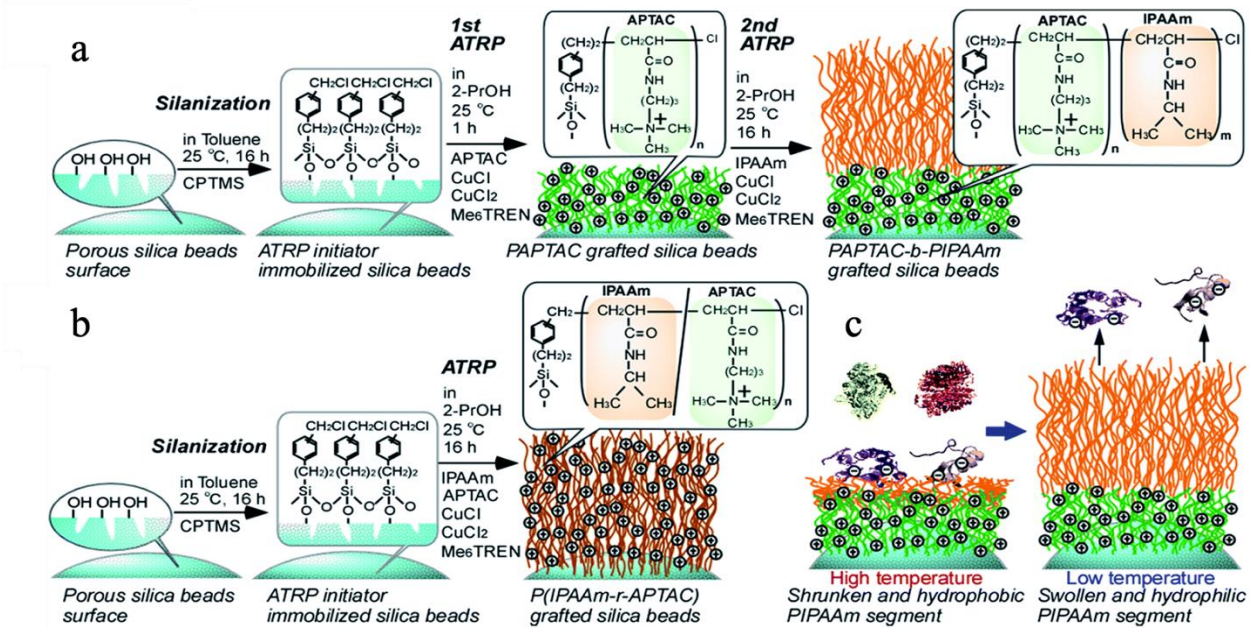


**Figure 5.16**: Cationic (a) block and (b) random copolymer brush. (c) Thermally modulated interactions between proteins and BCP brush. Adapted from Nagase and Okano *et al.* with permission from The Royal Society of Chemistry.[134]

In the following work, Nagase and Kanazawa *et al*. utilized ionic BCP brushes for the purification of cells.[136] Here, the authors synthesized poly(*N*,*N*-dimethylaminopropylacrylamide) PDMAPAAm and PIPAAm BCP brushes using activator regenerated by electron transfer-ATRP (ARGET-ATRP), where PDMAPAAm imparted adhesion and detachment ability to bone-marrow-derived stem cells.[137] The BCP brushes exhibited adsorption of bone stem cells exclusively, enabling their purification from contaminant cells. Similar to the previous report, the BCP brush offered thermoresponsive adsorption/detachment due to the PIPAAm block occurring at 20 °C. Alternatively, anionic BCP brush, poly(2-acrylamido-2-methylpropanesulfonic acid) (AMPS)-*b*-PIPAAm (PAMPS-*b*-PIPAAm) showed the effectiveness of interacting with basic proteins over modulated temperatures. Additionally, the anionic BCP brush displayed stronger interactions compared to the random copolymer brush analog.

### 5.3.2 Star and Micelle-like Ionic Block Copolymer

The design and synthesis of novel star and micelle-like ionic BCPs have attracted significant attention because of their unique chemical structures and derived properties.[138-141] Incorporating ionic blocks into star and micelle polymers affords self-assembled supramolecular structures and stimuli-responsive properties. As shown in **Figure 5.17a**, a four-arm star composed of a PIL block, poly(N-vinylimidazolium salt), and a thermoresponsive block, poly(NIPAAm). A tetrafunctional chain transfer agent (CTA) afforded the synthesis of the water-soluble PIL star. The dithiocarbamate-type CTA exhibited superior control of polydispersities compared to the xanthate-type CTA due to a higher transfer constant in the dithiocarbamate-type CTA.[142] The position of PIL in the star BCP played a vital role in the self-assembly of polymers. As shown in **Figure 5.17a**, the authors compared two star-shaped BCPs having poly(N-vinylimidazolium salt) and poly(NIPAAm) as the core, respectively. The star BCP with poly(N-vinylimidazolium salt) core exhibited a one-step transition of a star to large micellar clusters. In contrast, the star BCP with poly(NIPAAm) core displayed two-step transitions, involving the formation of small micelles at ~ 33 °C that  then aggregated into dehydrated clusters.

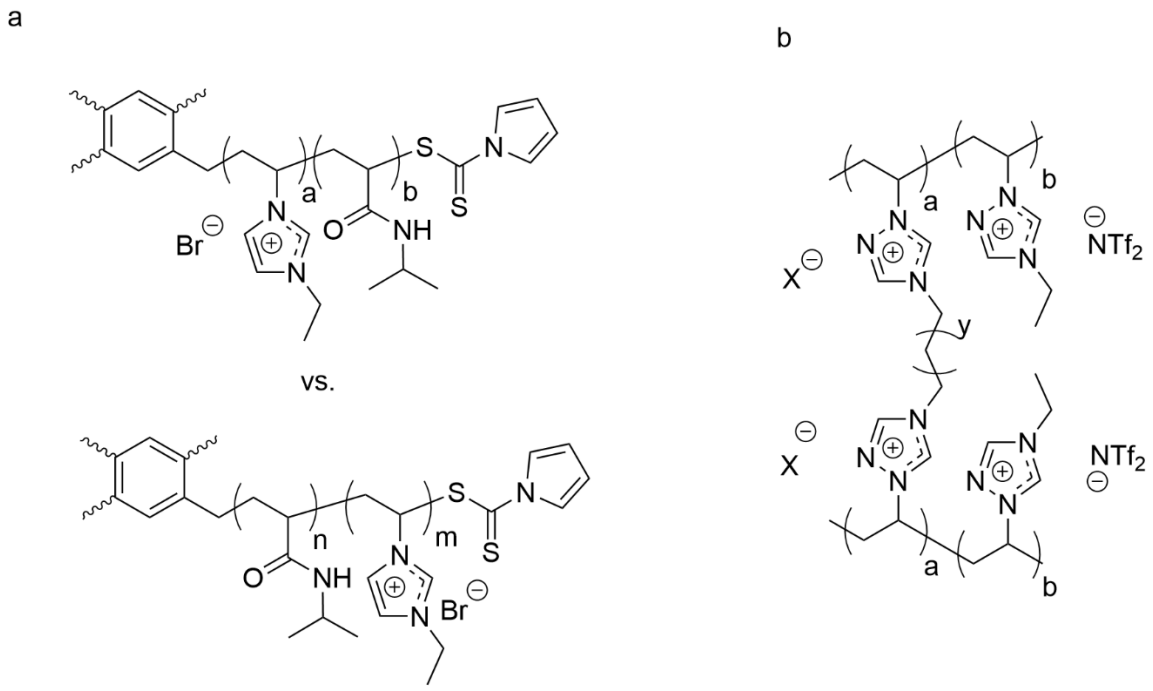


**Figure 5.17:** (a) Ionic BCP star polymer.[143] (b) Crosslinked ionic BCP forming core-shell nanoparticles.[144]

The synthesis of star BCPs using two-step living radical polymerization enabled control of the block lengths. However, this strategy often involved complicated steps and purifications, limiting large-scale production and applications. Zhang and Yuan *et al*. presented a facile synthesis of core-shell ionic BCP nanoparticles via the crosslinking of the diblock copolymer, which realized the control over nanostructures through tuning crosslinker length.[145] This method afforded stable microstructures through chemical crosslinking compared to the self-assembly of the linear BCP. In a later study, Mori and Nakabayashi *et al*. prepared poly(triazole)-*b*-poly(triazolium) copolymers via RAFT polymerization.[146] Then, quaternization of poly(triazole) block afforded the core-shell nanoparticle through interchain crosslinking (**Figure 5.17b**). The authors discovered that the ionic conductivity of nanoparticles was largely related to the counter ion $X^-$, where $Br^-$ as the counterion displayed a three-times-higher ionic conductivity than the case of $Cl^-$ as the counterion. Combining "grafting to" and "grating from" strategies, Cao and Saito *et al*. attached

carboxylic acid terminated PEO (blue lines in **Figure 5.18**) and poly(potassium (styrene-4-sulfonyltrifluoromethyl-sulfonyl)imide) poly(STF-K+) (purple dots in **Figure 5.18**) to the polyhedral oligomeric silsesquioxane (POSS) nanoparticle (the orange ball in **Figure 5.18**).[147] Early work demonstrated applications of Poly(STF-Li+) containing BCPs as conducting membranes.[31] For most of the ionic BCPs, tuning the relative length of hydrophobic and ionic blocks enables the modulation of ionic conductivity. In this work, the conductivity of nanoparticles can be tuned via varying the grafting ratio of the PEO and poly(STF-Li+) without manipulating the chain length. Thus, their work opened a gate to the design of ion conducting polymer nanoparticles.

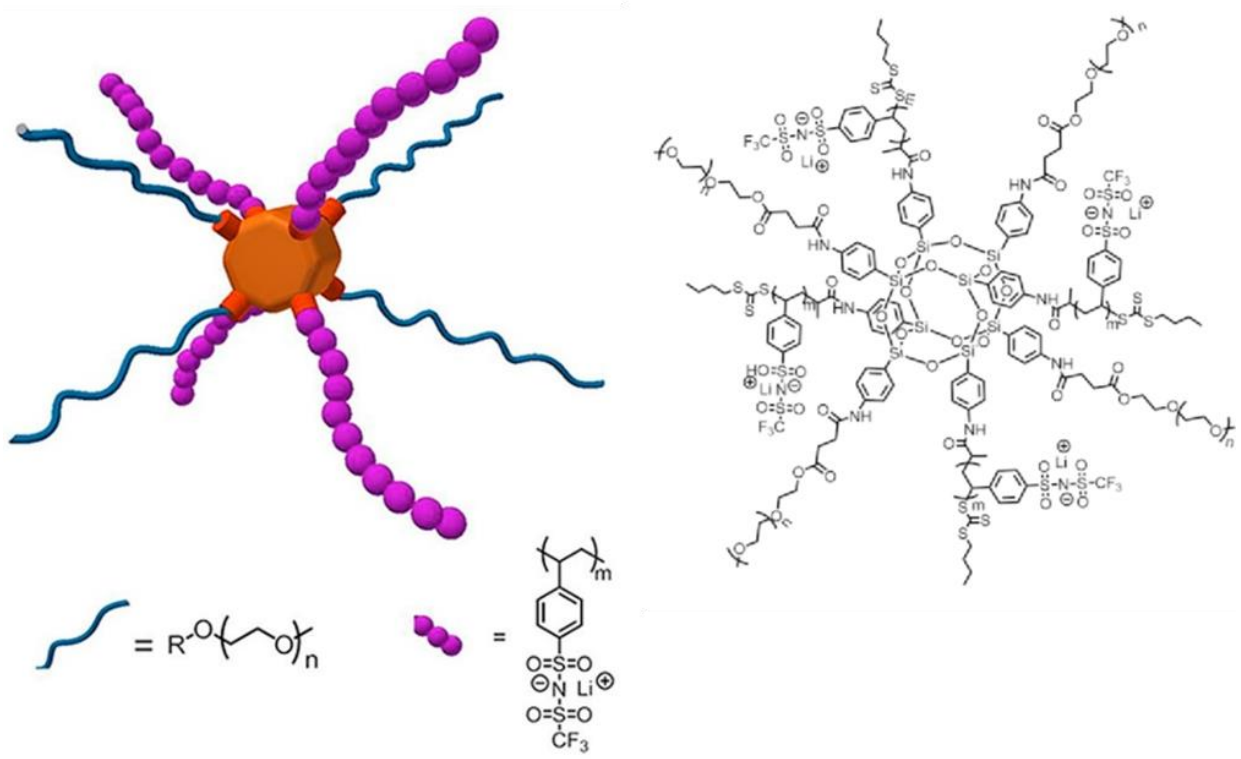

**Figure 5.18**: Star-shaped ionic block copolymer. Adapted from Cao and Saito *et al.* with permission from Elsevier.[147]

## 5.3.3 Crosslinked Ionic Block Copolymers and Block Copolymer Ionic Gels

Polymer structure has significant effects on conductivity, dimensional durability, and chemical stability of the conductive membrane.[148] As demonstrated above, ionic micelles formed through self-assembly suffer from low dimensional durability and chemical stability due to non-covalent binding between assembled polymer chains. In order to achieve high performance and stability, ionic polymers containing rigid backbones such as polysulfones,[149] poly(styrene)s,[103], poly(phenylene oxide)s,[150] have been widely investigated. Besides manipulating the chemistry, incorporation of covalent crosslinks into ionic polymers is an emerging strategy for high-performance conductive membranes, including quaternization via diamines,[151-153] metathesis of pendant side-chain double bonds, [154] and click chemistry.[148] A representative example is shown in **Figure 5.19**. Here, quaternary ammonium containing poly(2,6-dimethyl-1,4-phenylene oxide) (black line and red dot) was functionalized with alkylene side chain (wavy blue line).[148] The authors employed dithiols under UV illumination to afford crosslinked ionic BCP via thiol-ene chemistry. The designed network achieved higher dimensional stability compared to the uncrosslinked ionic copolymer. Among all crosslinked membranes, the hydroxide conductivity of the best trial was three times greater than that of the uncrosslinked membrane under the same conditions. In another example, quaternized DABCO enabled the crosslinking of poly(phenylene oxide) and cellulose for fabricating the multiblock copolymer. The designed copolymer network displayed improved tensile properties, alkaline stability, and ionic conductivity compared to the uncrosslinked DABCO quaternized poly(phenylene oxide).[155]

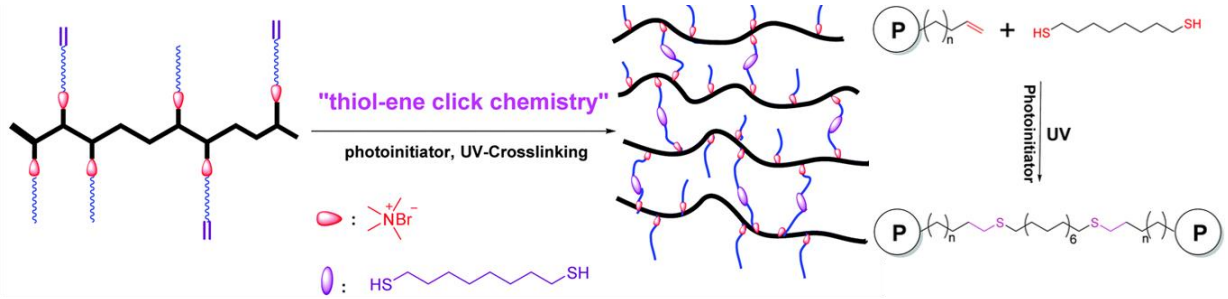


**Figure 5.19**: Cross-linked comb-shaped ionic BCP. Adapted from Zhu and Hickner *et al.* with permission from The Royal Society of Chemistry [148]

Explorations on the sol-gel transition of ionic liquid (IL) gel have drawn attention for potential applications in additive manufacturing[156, 157] and biomedical materials.[158, 159] Combination of ILs and BCPs enabled the development of free-standing objects for application as solid electrolytes.[160] One example was presented by Imaizumi and Watanabe *et al*., where a blend of a polystyrene-*b*-poly(methyl methacrylate)-*b*-polystyrene (SMS) triblock copolymer and 1-ethyl-3-methylimidazolium bis(trifluoromethanesulfonyl)amide ([$C_2$mim][$NTf_2$]) afforded ion gels owing to the physical crosslinking of the outer polystyrene block.[161] The ionic gel exhibited an ionic conductivity exceeding $10^{-3}$ S $cm^{-1}$ at room temperature, which enabled applications as electrolytes for anionic polymer actuators. The sol-gel transition of this ionic gel was $T_g$-dependent and related to the molecular weight of the polystyrene block. Besides $T_g$, lower critical solution temperature (LCST) is another option for thermoresponsive sol-gel transitions when incorporating polymer blocks such as PNIPAm by itself (32 °C),[162] poly(benzyl methacrylate) (PBnMA) in [$C_2$mim][$NTf_2$] IL (105 °C),[163] and poly(2-phenylethyl methacrylate) (PPhEtMA) also in

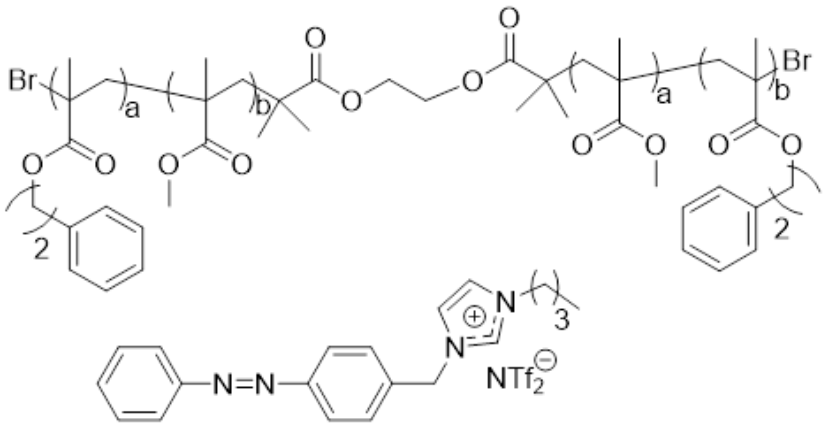


**Figure 5.20**: Triblock copolymer and ionic liquid network gel.[165]

[$C_2$mim][$NTf_2$] IL (42 °C).[164] Later on, Wang and Watanabe *et al*. utilized azobenzene IL ([Azo][$NTf_2$)]) for light-controlled sol-gel transitions (chemical structures are shown in **Figure 5.**).[165] Previous work demonstrated that *trans*-[Azo][$NTf_2$)] displayed a higher affinity for the PPhEtMA block than for *cis*-[Azo][$NTf_2$)].[166] Therefore, when the light was irradiated, the *trans*-[Azo][$NTf_2$)] crosslinked the outer PPhEtMA block and formed an ionic gel and returned to the solution state when the light was off. **Figure 5.** illustrates the reversible photoinduced sol-gel transitions of triblock copolymer and IL complex, where storage modulus exhibited reversible increasing/decreasing upon switching the UV light on/off, respectively. In the following work, the authors compared the viscoelastic property change of PPhEtMA and [Azo][$NTf_2$)] IL complex with poly(benzyl methacrylate) and [Azo][$NTf_2$)] IL complex, where the benzyl group was directly attached to the ester. In contrast, poly(benzyl methacrylate) and [Azo][$NTf_2$)] IL complex exhibited a sharp decrease in G', indicating a softening of the gel state. Thus, structure modification achieved versatile photoresponsive ionic gels with varied rheological transitions.[167]

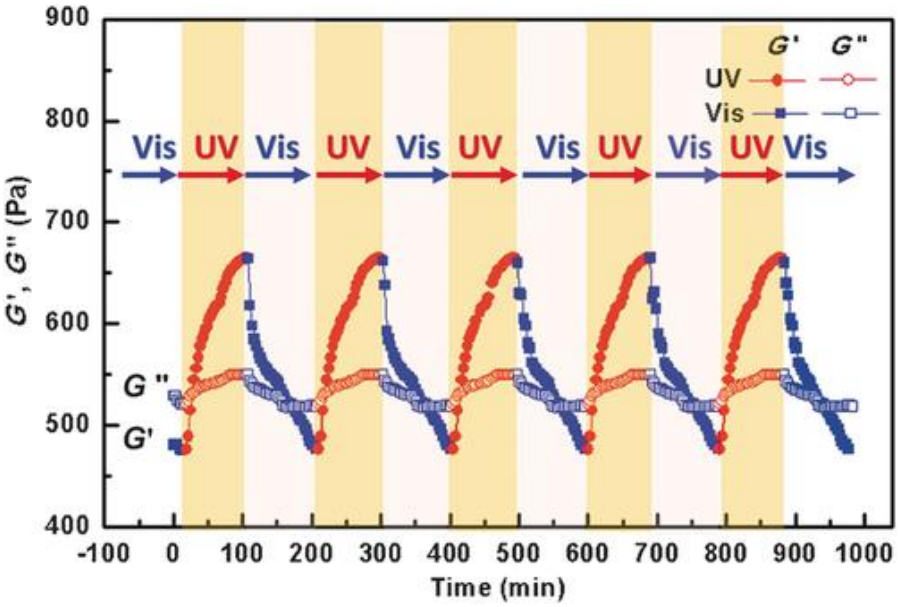


**Figure 5.21**: Storage modulus (G') and loss modulus (G") for the triblock copolymer and IL complex under sequential irradiation of UV and visible light at a bistable temperature (57 °C). Adapted with permission from Wang and Watanabe *et al*. with permission from Wiley.[165]

## 5.4 Segmented Block Copolymers

Segmented BCPs are a special type of multiblock copolymer consist of two microphase separated segments referred to as the soft segment (SS) and the hard segment (HS). The soft segment most often consists of a low $T_g$ oligomer while the hard segment exhibits a much higher $T_g$ and often includes physical crosslinks stemming from intermolecular interactions and/or crystalline domains. The SS here provides flexibility and elasticity to the polymer while the HS provides mechanical reinforcement. As with other multiblock copolymers mentioned earlier, segmented BCPs are most often synthesized through step-growth reactions between A-A and B-B type monomers. Common segmented BCPs include polyurethane [54] and polyester thermoplastic elastomers, and this section will discuss the charged analogs of these materials. Recent literature has also focused on ionenes as a relatively new class of segmented BCP, and their structure-property relationships are discussed herein. Non-segmented ionenes fall under the category of multiply charged BCPs for the purposes of this review and are discussed in the corresponding section.

### 5.4.1 Ionenes

The field of ionenes, or polymers containing quaternary heteroatoms in the polymer backbone, has grown rapidly in recent decades. Ionenes are highly charged polymers with two charges per repeat unit and are most frequently synthesized through the stoichiometric polymerization of a dihalide and a ditertiary amine or phosphine. Recent reviews covering the general synthesis and material properties of these polymers negates the need to describe the rich chemistry of ionenes herein.[168, 169] However, the structure-property relationships of segmented ionenes warrants attention due to their unique properties. Long *et al*. developed a facile synthesis of bis-imidazolium-containing segmented copolymers (**Figure 5.22**).[170] $S_N2$ reactions enabled the

coupling of dibromides and *bis*-imidazoles, affording a segmented BCP through step-growth polymerization. Varying the molecular weight of poly(tetramethylene oxide) (PTMO) further tuned thermal mechanical properties and morphological structures of the copolymers. Further investigations revealed an increased stress at break owing to the strain-induced crystallization property of PTMO.[171] Molecular weight of PTMO also played a vital role in applications as electrospinning, where increasing molecular weight offered an increase of fiber diameter.

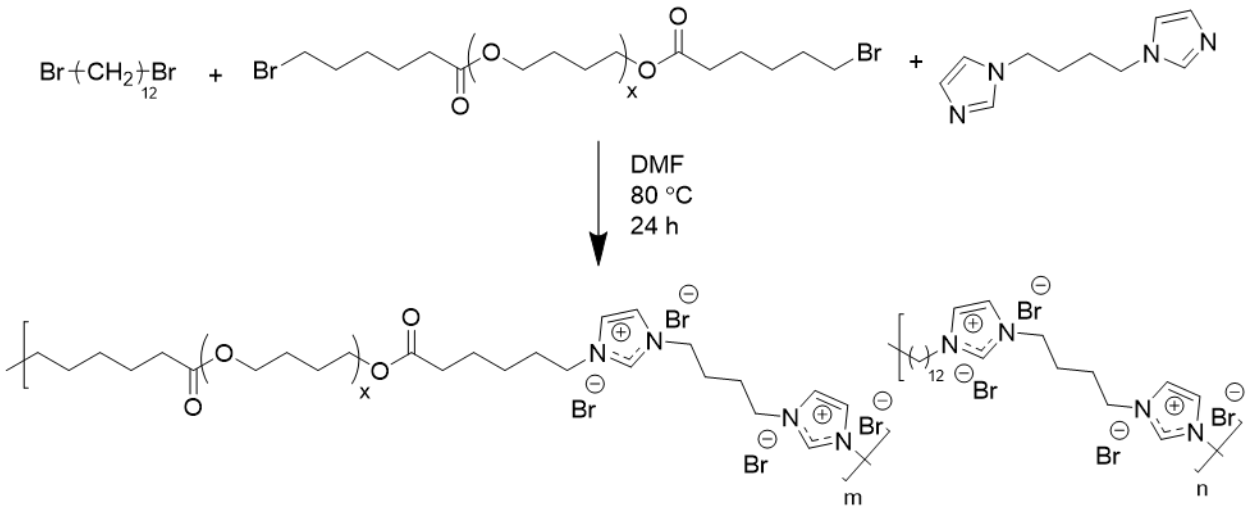


**Figure 5.22**: Synthesis of imidazolium ionene segmented BCPs containing 1,12-dibromododecane and bromine-terminated PTMO. Reproduced from Williams and Long *et al.* with permission from Elsevier.[170]

Several studies have incorporated ionenes into classical step-growth polymers such as polyurethanes [17, 25, 54, 172] and polyesters.[15, 23, 24] For example, Gao and Long *et al.* synthesized segmented PUs utilizing an imidazolium diol chain extender for the HS as shown in **Figure 5.23**.[17] The SS consisted of a PTMO oligomer and the imidazolium unit resided solely in the HS. As with all segmented BCPS, this PU exhibited two $T_g$s indicative of phase separation between the low $T_g$ SS (-60 °C) and the higher $T_g$ HS (132 °C). AFM and SAXS confirmed phase separation in the PUs and revealed that the ionene PU displayed more percolated HS domains compared to the neutral control. This in turn enhanced the modulus of the ionene. The ionic conductivity of the

ionene measured exceptionally low at room temperature ($10^{-12}$ S cm$^{-1}$) likely due to the high $T_g$ of the conductive phase. The authors incorporated varying levels of free IL into the ionene PU to determine the effect on the polymers' thermomechanical and transport properties. As shown in **Figure 5.23a**, the $T_g$ of the HS decreased from 132 to 37 ° C upon IL incorporation while the SS $T_g$ remained unchanged. This suggests that the IL resides solely in the HS owing to the intermolecular ionic interactions with the ionene. The presence of free IL significantly enhanced the conductivity of the ionene (**Figure 5.23b**); however, the conductivity remained moderately low even with 30 wt% IL incorporation (~$10^{-5}$ S cm$^{-1}$ at 100 °C).

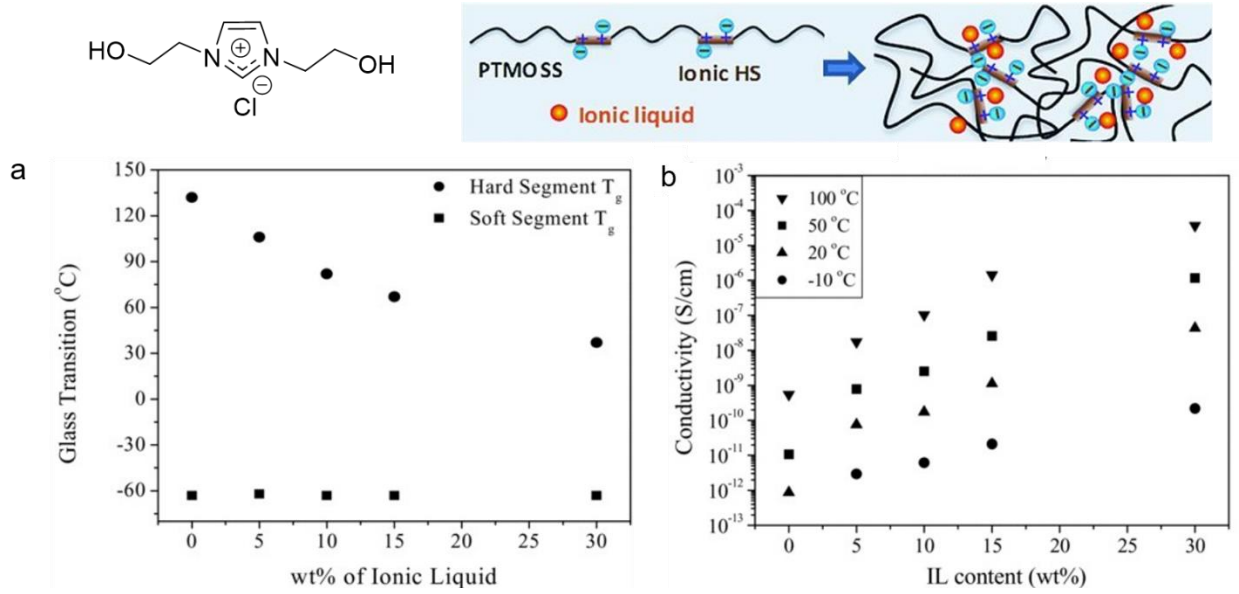


**Figure 5.23**: An imidazolium diol forms the hard segment of a PU. (a) Glass transition temperatures of the hard and soft segment of an imidazolium-containing PU as a function of added ionic liquid content. (b) Effect of ionic liquid content on ionic conductivity over a range of temperatures. Reproduced from Gao and Long *et al.* with permission from Wiley.[17]

Choi and Lee *et al*. synthesized a series of segmented ionene copolyesters containing an imidazolium HS and PEG SS.[15] The authors varied the counterion, PEG molecular weight, and HS spacer length to study the structure-property relationships in these ionenes. The length of the alkyl spacer and the size of the counterion affected the ability of PEG to crystallize and therefore the conductivity of the ionenes. Large $Tf_2N$ anions prevented the PEG segments from crystallizing

when the alky spacers were short (C6 vs C11) due to the interaction of the PEG chains with the ions. For the polymers that crystallized, the conductivity dropped sharply upon reaching the crystallization temperature due to decreased ion mobility from the formation of crystalline phases. Ionenes derived from 1 kg $mol^{-1}$ PEG displayed higher ionic conductivity below the melting temperature than those synthesized from 2 kg $mol^{-1}$ PEG due to the presence of a larger amorphous phase. The $Tf_2N$ ions unsurprisingly provided the highest conductivity and ionenes bearing these counterions exhibited conductivities on the order of $10^{-5}$ S $cm^{-1}$.

### 5.4.2 Polyurethane- and polyester-based ionomers

Step-growth polymers such as PUs and polyesters containing pendent charged moieties represent another class of segmented BCPs. The Long group has reported several examples of charged segmented PU BCPs and their recent review details the structure-property relationships and applications of ion-containing PUs.[16, 26, 173] The presence of a pendent sulfonate group in a segmented PU affects the thermomechanical and transport properties of the material dependent on the location of the charge placement (HS vs. SS).[16] Incorporating the sulfonate into the PEG-based SS inhibited crystallization and raised the $T_g$ from -52 °C to -26 °C. Installing the sulfonate group in the hard segment led to a larger increase in the soft segment $T_g$ (-5 °C) and prevented the crystallization of both phases due to significant phase mixing. The extent of phase mixing had a deleterious effect on the mechanical properties resulting in a Young's modulus less than that of both the sulfonated SS PU (SSSPU) and the uncharged control PU. The SSSPU facilitated the uptake of a commercial imidazolium IL to form composite membranes for enhanced ionic conductivity.[174] The $T_g$ of the SS decreased with increasing IL while the HS $T_g$ remained the same indicating that the IL only resides in the charged SS phase. Correspondingly, the ionic conductivity

increased from approximately $10^{-8}$ S $cm^{-1}$ to a maximum of ~5.0 x $10^{-4}$ S $cm^{-1}$ with 25 wt% IL at room temperature.

One of the primary uses for charged segmented PUs is for producing waterborne PU (WPU) dispersions. The incorporation of a charged hydrophilic (e.g., carboxylate, sulfonate, ammonium, phosphonium) unit into the segmented PU facilitates water-dispersibility. The ability to use water as a dispersant allows for the removal of toxic, organic solvents, which renders these materials useful for a variety of biomedical applications from antimicrobial coatings to 3D printing cell scaffolds.[175, 176] Several recent reviews have discussed in detail the general chemistry and applications of WPUs, and as such they will not be discussed again here.[177-180] Hemp and Long *et al.* presented an example of a segmented WPU copolymer bearing a trialkyl phosphonium substituent in the HS with a PEG-based SS. The authors varied the mol% of the HS as well as the length of the phosphonium alkyl groups (ethyl or butyl) to determine their effect on the thermal and mechanical properties of the polymers. Increasing the HS content decreased the SS melting point but demonstrated no discernible effect on the SS $T_g$. For PUs containing the same HS content, the phosphonium alkyl length determined the mechanical properties. Both phosphonium PUs displayed a higher and more extended plateau modulus compared to the uncharged analog. The tributylphosphonium PU achieved a much higher Young's modulus than the control, but also experienced plastic deformation in contrast to the other two PU compositions. Furthermore, the triethylphosphonium PU showed a significantly lower modulus and stress at break due to an increased amount of water absorption. These phosphonium PUs also demonstrated water-dispersibility and the ability to bind DNA, which suggests their use for non-viral gene delivery vehicles.

Though relatively few examples exist in literature, incorporating charged groups into segmented polyesters can also tune the thermomechanical and morphological properties of these materials.[27, 91] Zhang and Long *et al.* studied the effect of incorporating a sulfonate group into either the hard or soft segment of an amorphous polyester.[27] The $T_g$ of the HS increased dramatically from 80 – 140 °C with increasing HS sulfonation from 0-5 mol% due to ionic interactions between sulfonate groups. However, increasing HS sulfonation also led to a decrease in mechanical properties, which may suggest some degree of phase mixing. Conversely, the modulus and tensile strength of the sulfonated SS polyester improved upon the addition of higher degrees of sulfonation. These studies demonstrate the ability to modify the thermal, mechanical, and morphological properties of commercially relevant segmented BCPs.

## 5.5 Multiply Charged Block Copolymers

This section focuses on the synthesis of multiply charged ionomers, whose structures contain more than one pair of anions and cations in each charged unit. In addition, this section summarizes strategies for building BCPs using multiply charged ionomers for novel applications. Attention is given to the challenges and strategies for overcoming the difficult polymerization of highly charged monomers or modifications of polymers. Significant progress towards new chemistries has developed in response to the inherent thermal and base instability of cation-containing polymers. This section focuses on the synthetic pathways to afford monomer structures containing different motifs, including quaternary ammonium, imidazolium, and sulfate groups, as well as the discussion of the influence of charged groups on the structure-property relationships of BCPs and applications. Overall, this section complements other application-based literature on charged BCPs while focusing on how increased monomer charge density plays a role in structure-property relationships. Increasing monomer charge density facilitates the formation of charged

monomer domains, allowing for enhanced polymer chain organization and ion transport. Therefore, it is advantageous to understand the synthetic challenges to create highly charged polymers, and the influence that charge density plays on the structure-property relationships of ion-containing polymers. The extent of this section will focus on the cationic and anionic structures of multiply charged monomers and polymers. Moreover, the main synthetic methods of the multiply charged monomers and polymers will be discussed in detail. Additional details on structure-property relationships and emerging applications of polymers with multiply charged monomers will be discussed. This section aims to present and generalize the fundamental methodologies used in designing highly charged monomers and inspire the novel design of more advanced systems.

### 5.5.1 Recent Synthetic Advances for Highly Charged Monomers

Recently, monomers carrying more than one charge site emerged as a new functional design feature for novel charged polymers. On the molecular level, charged polymers take on a few primary chemicals and structural motifs that instill Coulombic charges along or pendant to the polymer backbone. For positively charged polymers, these motifs are primarily heteroatom-based with common functional units such as quaternary ammonium, phosphonium, imidazolium, triazolium, sulfonium, and a wide variety of others. Negative-charged monomers, on the other hand, typically exist as sulfonate, carboxylate, and phosphates in either their acid or salt forms. The primary multiply charged motifs are listed in **Table 5.1**, featuring the common polymer types found in literature. The added complexity in these charged features arises from differences in charge delocalization, electronegativity, and geometry effects of each ion and counterion that influence their properties. The following sections will introduce the common motifs found in recent literature.

**Table 5.1**: Synthetic motifs used to design multiply charged polymers, separated by charged functionalities.

| | Charged Functionality | Polymer Types | References |
|---|---|---|---|
| A | 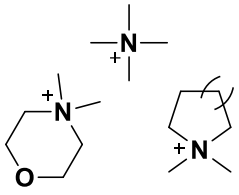 | (Meth)acrylic<br>Styrenic<br>Poly(arylene ether sulfone)<br>Poly(sulfone)<br>Poly(phenylene oxide) | 181 |
| B | 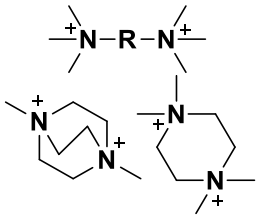 | (Meth)acrylic<br>Styrenic<br>Poly(arylene ether sulfone)<br>Poly(sulfone)<br>Poly(phenylene oxide)<br>Poly Ionene | 5, 12, 182-184 |
| C | 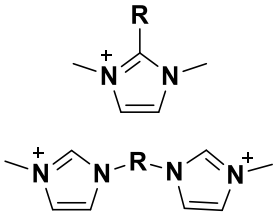 | (Meth)acrylic<br>Styrenic<br>Poly(arylene ether sulfone)<br>Poly(sulfone)<br>Poly(phenylene oxide) | 185-188 |
| D | 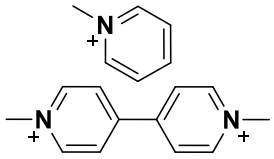 | (Meth)acrylic<br>Styrenic<br>Poly(arylene ether sulfone)<br>Poly(sulfone)<br>Poly(phenylene oxide) | 189-193 |
| E | 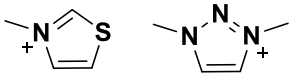 | (Meth)acrylic<br>Poly(ether) | 194, 195 |
| F | 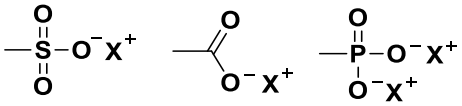 | (Meth)acrylic<br>Vinyl<br>Poly(arylene ether)<br>Poly(phenylene)<br>Polyimide | 71, 196, 197 |

As previously mentioned for linear BCPs, the synthesis of multiply charged polymers follows one of two primary methods: 1) direct polymerization of charged monomers or 2) post-polymerization modification of a polymer backbone to introduce charges or quaternizable groups.

Direct polymerization results in the desired repeating unit when polymerized. However, it is often challenging due to monomer solubility, monomer stability, or changes in polymerization kinetics, etc. Post-polymerization modifications are disadvantageous due to incomplete functionalization of a polymer backbone, resulting in a polymer structure with varying charge distribution along the polymer backbone. The formation of a specific charged feature may have multiple synthetic strategies, yet the resultant polymer structure may yield nuanced differences in charge placement or degree of substitution, leading to inconsistent properties.[198, 199] Current literature on multiply-charged cations primarily focus on nitrogen-containing groups, with a large body of literature dedicated to quaternary ammonium charges. Although phosphonium cations are noted for potential advantages, particularly enhanced thermal properties and electronegativity considerations for ion-pair strength,[200-202] little to no literature incorporates multiple phosphonium or sulfonium groups as multiply charged polymer features.

## 5.5.2 Multiple Cationic Charged Monomers and Corresponding Block Copolymers

### 5.5.2.1 Monomers Containing Multiple Cationic Charges

Facile synthesis of cationic groups arises from the straightforward Menschutkin substitution reaction, which combines an electrophilic alkyl halide and a tertiary heteroatom-based compound resulting in the quaternary, positively charged salt product.[203] This reaction takes many forms, ranging from the quaternization of a simple trialkylamine to a more recent 1,2,3-triazine. The Menschutkin reaction rate changes with temperature and leaving group selection, but Hoffmann elimination and the reverse substitution reactions occur readily at elevated temperatures above 160 $^{o}$C due to counterion nucleophilicity.[5, 168, 200, 204] Some of the first dicationic polymerizable groups entered the field in the late 1960s following the prominence of singly-

charged (meth)acrylic, styrenic, diallylic, and ionene polyelectrolytes used in water purification.[205, 206] These doubly-charged monomers consisted of bis-quaternary functionalities as either di(meth)acrylate-, diallyl-, and even tetraallyl-ammonium chlorides and showed promise as ion-exchange resins.[207, 208]

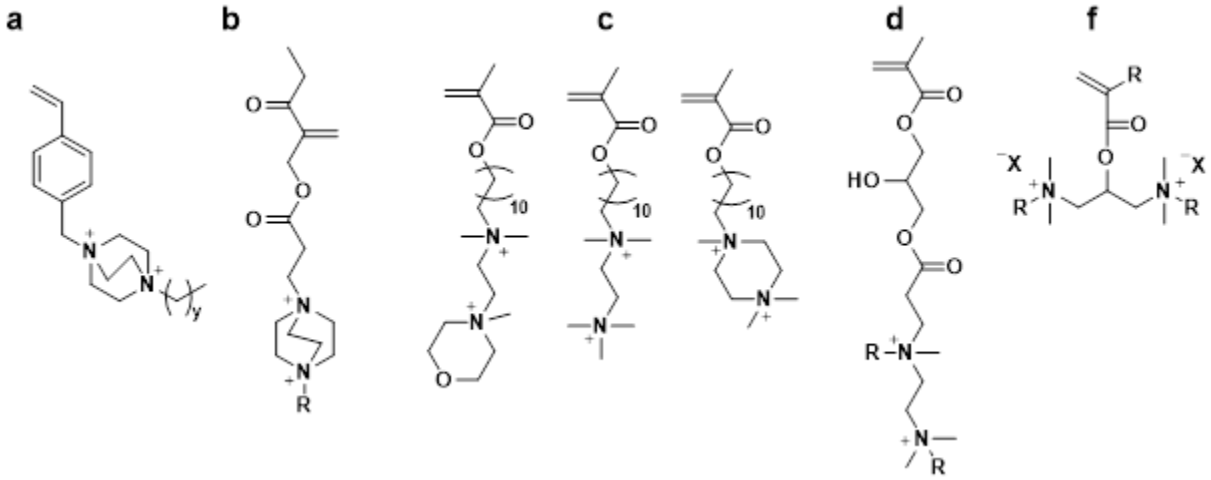


**Figure 5.24**: Examples of some common multiply charged quaternary ammonium motifs found in the literature.[181-183, 209, 210]

The Long group recently published a library of styrenic monomers containing 1,4-diazabicyclo[2.2.2]octane (DABCO) with tailorable pendant alkyl groups (**Figure 5.24a)**.[182] Ideal solvent selection enabled precipitation of each quaternized intermediate, simplifying the purification process. After monoalkylation of DABCO, the remaining tertiary amine in the structure became less reactive due to the electron-withdrawing effect from the first quaternization. Dizman noted a similar reduction in quaternization kinetics of the second tertiary amine, requiring reflux conditions to synthesize their methacrylate-based charged DABCO monomer (**Figure 5.24b)**.[209] Other representative motifs found in literature stem from linear charged ethylene diamine structures or piperazine and morpholine-like structures seen in **Figure 5.24c**.[181] Ayfer and Avci *et al.* utilized amine Michael addition chemistry on a mixed acrylate/methacrylate to develop

novel charged monomers by reacting various amines with quaternizable tertiary amine groups with a tethered acrylate (**Figure 5.24d).**[183]

Apart from direct quaternization methods with alkyl bromides, Kim and Ikeda *et al.* devised a novel method to prepare *bis*-quaternary ammonium salts by varying reaction conditions with epichlorohydrin.[210] By closely monitoring the reaction kinetics, they found that epichlorohydrin reacts quantitatively with two equivalents of trialkyl amine in the presence of the trialkylamine hydrochloride due to neighboring group effects (**Figure 5.24f**). Another functionality showing up in charged polymer literature is quaternized heteroatom-based polymers (**Table 5.C**). One of the primary differences between the conventional quaternary ammonium and a charged heterocycle is the differences in molecular geometry, which could prove advantageous for various properties involving counterion association like ion transport. These charged heteroatoms include imidazolium, pyridinium, triazolium, and thiazolium, to name the motifs found commonly in literature. Imidazolium or methylimidazolium functionalities recently gained attention for their potential biological and engineering applications.[202, 211-216] Vinyl-type *bis*-imidazolium monomers with varying alkyl spacers are most prevalent due to the ease of using multiple Menschutkin substitution reactions in parallel. Zheng and Yan *et al.* modified vinylimidazolium with numerous alkyl spacers ranging from 2 to 12 carbons on the N3 position.[212] Simple alkylation with alkyl bromide-functionalized imidazolium facilitated the synthesis of *bis*-imidazolium vinyl monomers shown in **Figure 5.25a**. These monomers and polymers show promising antibacterial properties due to the quaternary charges and long alkyl chains.[217] In terms of the building block for segmented copolymer and ionenes, diol- and diamine-functionalized bisimidazoliums resulted in polyesters and polyimides containing ionic liquid imidazolium groups (**Figure 5.25b**). Post-polymerization modifying polymers such as poly(arylene ether sulfones) and

poly(esters) with imidazolium and other quaternizable groups provide strategies for multiply charged segmented copolymers and ionenes, as shown in **Figure 5.25c**. A few highly charged pyridinium-type monomers exist in literature as bipyridinium motifs, or viologens, having interesting optoelectronic properties (**Table 5.1D**).[218] Readily quaternizable nitrogens within the bipyridine structure enable tailoring of the monomer or polymer structure to styrenic,[189, 219, 220] methacrylates,[221] vinyl pyridine,[190] and other monomers.[191, 218] Ogoshi and Nakamoto *et al.* utilized a styrenic bipyridinium monomer in the synthesis of thermo-responsive host-guest polymers with heteromacrocyclic structures like cyclodextrins and curcubit[7].[189]

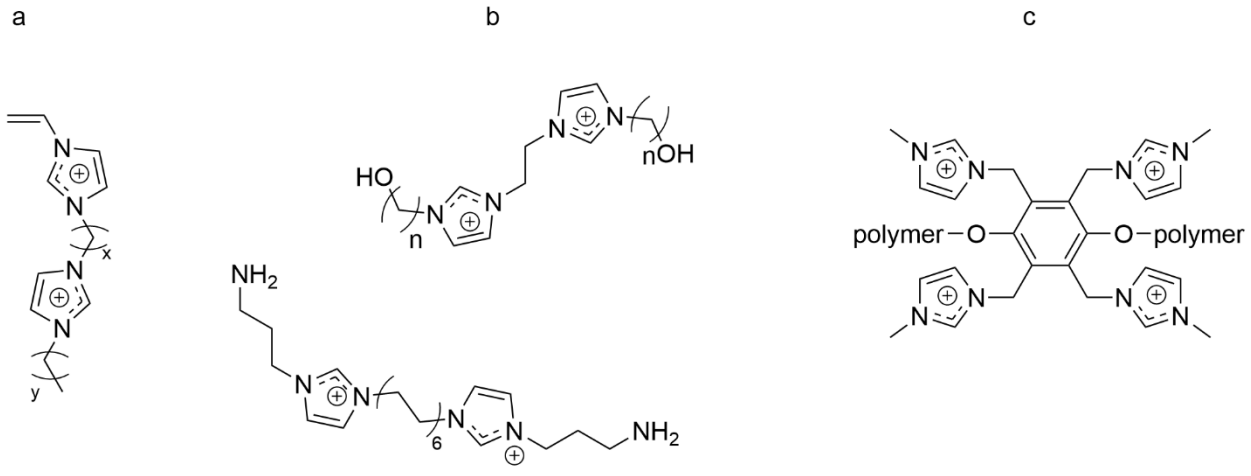


**Figure 5.25**: Typical methods for designing vinylimidazolium monomers and multiply charged building blocks for segmented copolymer and ionenes.[187, 188, 198]

Post-polymerization modifications are also an important synthetic method to incorporate multiple positive charges on the quaternizable functionalities in the pendent group. Unlike direct polymerization of charged monomers, post-polymerization modification generally lacks quantitative conversion methods due to steric interactions of reagents and the polymer backbone. These methods primarily include chloromethylation,[222] bromination,[223, 224] and lithiation.[225] An example of chloromethylation involved multifunctional tertiary amines like DABCO, which took advantage of the mono-chloromethylated establishing di- and tri-quaternized pendant groups.[226]

Recently, the Jannasch group led the way methodically choosing and synthesizing new monomers to post-polymerization brominate and different motifs to quaternize those monomers.[198] One such example utilizes hydroquinone monomers that are di-, tri- and tetra-methylated in the synthesis of PAES with a bisphenol A comonomer allowing for systemic variation of ion distribution and charge density along the polymer backbone (**Figure 5.26**).[198]

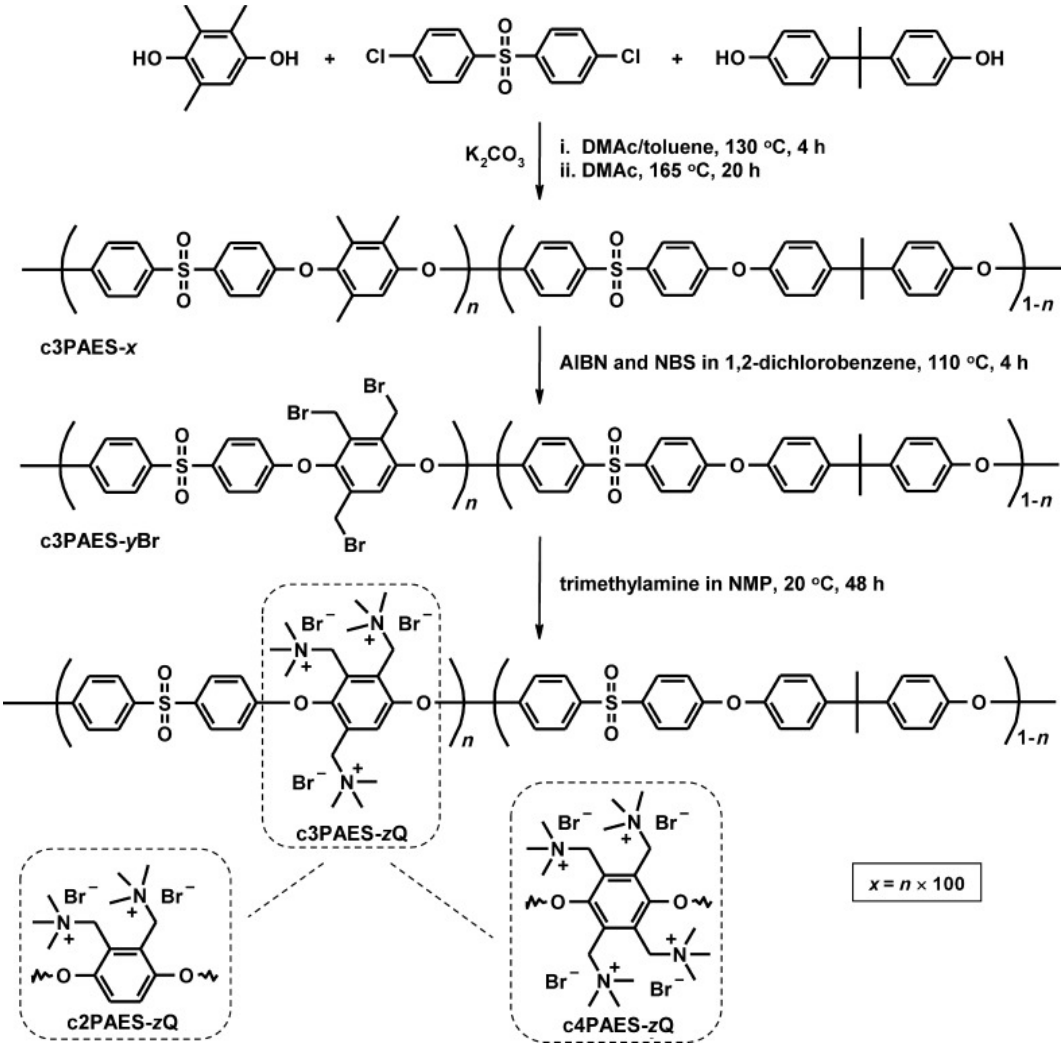


**Figure 5.26**: Synthetic pathway to multiply charged segmented copolymers through polycondensation, benzylic bromination, and quaternization. Reproduced from Weiber and Jannasch *et al.* with permission from European Chmical Societies Publishing.[198]

### 5.5.2.2 Multiply Charged Cationic Block Copolymers

#### 5.5.2.2.1 Chain-growth Method

As illustrated above, one of the main methods for building charged polymers includes the direct polymerization of charged monomers. Long's group recently developed a styrenic DABCO-based monomer with two quaternary ammonium charges.[5, 12, 182] Utilizing the styrenic DABCO-based monomer, the authors designed ABA triblock copolymers for enhanced microphase separation compared to copolymers with the randomly polymerized analog[5] and monoionic-based styrenic monomer.[12] Small angle X-ray scattering (SAXS) analysis demonstrated a hierarchical microstructure in which BCP self-assembled into highly ordered lamellar morphologies (**Figure 5.27**).[12] In addition, the long octadecane chain and DABCO moiety formed amphiphilic pendant groups and induced the formation of secondary structure. This work also highlighted superior thermomechanical properties of the DABCO-containing BCP over their random copolymer analog. The BCP displayed a robust physical crosslinked network retaining the mechanical integrity below the degradation temperature.

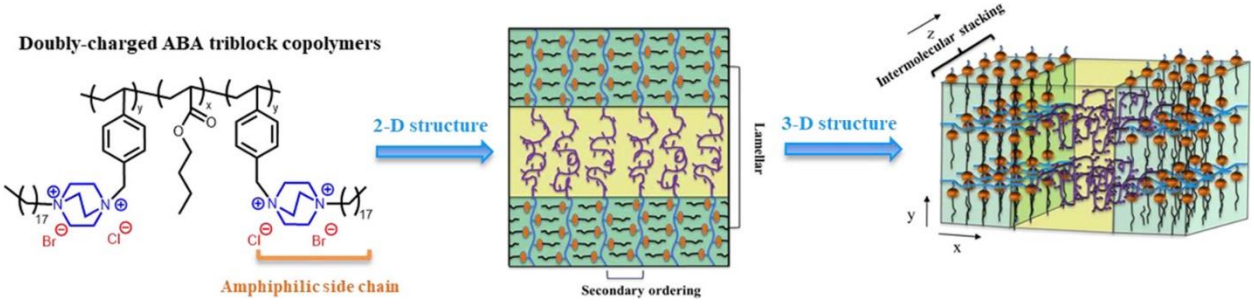


**Figure 5.27**: Doubly charged DABCO containing ABA triblock copolymer. Reproduced from Chen and Long *et al.* with permission from the ACS Publications.[12]

Mountrichas and Pispas *et al*. synthesized a series of double hydrophilic BCPs (DHBCs) consisting of a doubly-charged styrenic polyelectrolyte block and a poly(ethylene oxide) block via anionic polymerization.[227] Subsequent phenol deprotection, formaldehyde condensation, and

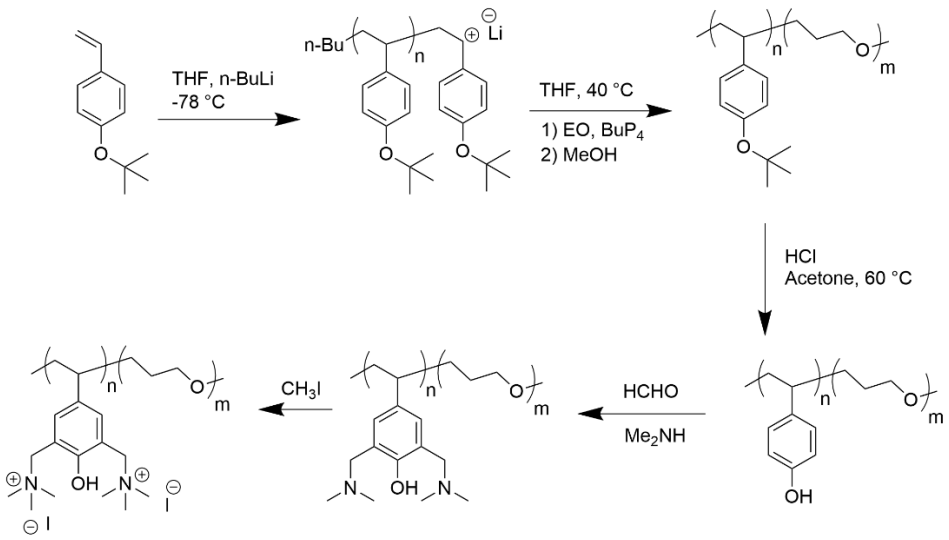


**Figure 5.28**: Synthetic scheme for the preparation of the functional DHBCs. Reproduced from Mountrichas and Pispas *et al.* with the permission from Wiley.[227]

quaternization enabled the placement of two cationic sites per repeat unit, as shown in **Figure 5.**. Štěpánek and Pispas *et al*. discovered evidence of the formation of spherical aggregates when complexing such DHBCs with sodium dodecyl sulfate (SDS). This was unique compared to other DHBCs and surfactant complexes as the formation of core-shell particles are normally observed in such complexes. The authors attributed this to two reasons: the rigidity of the styrenic block and the high positively charge density of the polycationic block, both of which prevented the complex from rearrangement.[228] Further studies on this system in acidic solution elucidated that the size of aggregates was independent of the ratio of DHBCs and SDS. In addition, SAXS indicated that the binding of SDS to both DHBC and poly(ethylene oxide) blocks.[229] In the same vein, Kayaianni and Pispas *et al*. investigated complexes of DHBC with different proteins, including globular bovine serum albumin (BSA) or rod-like bovine fibrinogen (FBG). DHBC exhibits excellent properties for stabilization of colloids, crystal growth modification, micelle formation, and drug delivery systems etc. In this work, the authors did not observe protein denaturation upon complexation with DHBC, which opens the gate for investigations of protein-

polyelectrolyte complexation.[230] Later on, the same team demonstrated the formation of core/corona nanostructures via complexation of DHBS and PMMA.[231]

### 5.5.2.2.2 Through Step-growth Method

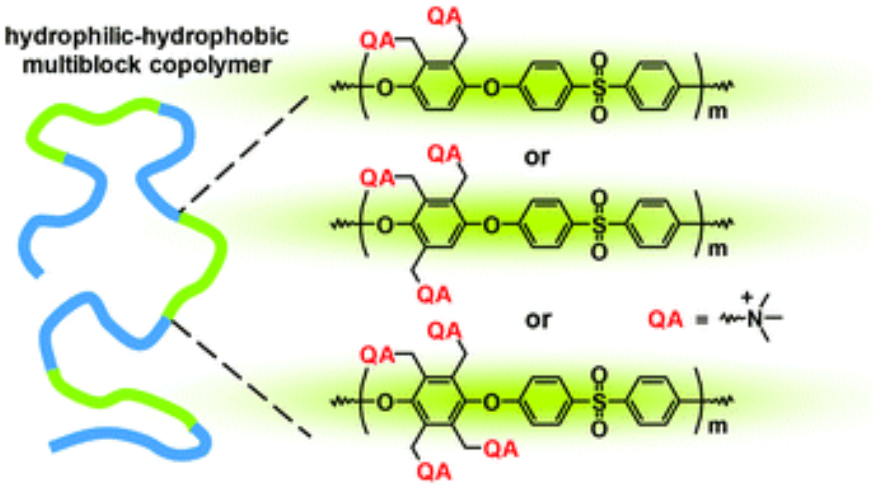


**Figure 5.29**: Anion conducting multiblock poly(arylene ether sulfone)s functionalized with quaternary ammonium groups. Reproduced from Weiber and Jannasch *et al.* with permission from the Royal Society of Chemistry.[224]

Random, statistical, and multiblock copolymerization of multiply charged building block and a non-charged monomer elucidated the influence of ion conductivity on the controlled distribution of charges (**Figure 5.**).[224] In these systems, charged groups are exclusively concentrated to one polymeric block, leading to microphase separated domains. The concentrated ionic phase maintained the proton conductivity, and the non-charged block ensured the mechanical properties for applications as membranes. The Jannasch group prepared randomly copolymerized ionenes functionalized to contain two, three, and four quaternary ammonium groups.[198] Later on, the group improved the ion conductivity and phase separation using a statistically copolymerized system incorporating up to six quaternary charges onto a single repeating unit using a hexamethyl dihydroxybiphenyl.[223] This work elucidated the structure-property relationships of alternating copolymer systems on morphology and ion conductivity.[223] The alternating copolymer system with two or three quaternary ammonium groups offered a 1.6 times higher conductivity compared with the statistical copolymer system. In contrast, the conductivity displayed a similar value for

the alternating and statistical copolymers carrying four quaternary ammonium groups, emphasizing the importance of polymer structure and ionic concentration.[223] In a different study, Pham and Jannasch *et al.* used the tetramethyl hydroquinone PAES and, instead of quaternizing with conventional imidazole or trimethylamine motifs, quaternized with cyclic secondary amines forming bis-*N*-spirocyclic quaternary groups.[232] Wu and Xu *et al.* recently published an extensive review looking into the nuances behind sulfonated chemistry in relation to advancing proton exchange fuel cell membranes.[233] Similarly, Li and Coleman *et al.* sought to create a diamine containing two imidazolium functionalities. Trends in thermal properties of the resulting polymers with both monomers in **Figure 5.25b** showed a decrease in $T_g$ as a function of increasing ionic liquid monomers incorporation.[185]

### 5.5.3 Incorporating Multiple Anions or Acid Groups into Block Copolymers

Monomers bearing negatively charged functionalities like sulfonates, carboxylates, and phosphates found increasing prominence and attention for their applications in materials for water treatment, electroactive materials, fuel cells, and other emerging areas.[4, 115, 234-241] The discovery of sulfonated polystyrene and the subsequent commercialization of Nafion™ (a perfluorinated sulfonated polyethylene copolymer) spurred interests in the synthesis of more advanced, tailored polymers. Moreover, it is important to develop a fundamental understanding of the effect of charge density on structure-property-morphology relationships of the polymer. This section will review the synthetic efforts designed to incorporate multiple negative charges onto a polymer chain to exploit the advantages negatively charged groups may have on polymer properties.

#### 5.5.3.1 Sulfonated Systems

Fitzgerald and Weiss *et al.* reviewed the major bodies of literature introducing sulfonate charges onto BCPs ionomers in 1988, in which most of the methods are still used today.[242] Many

of the sulfonated strategies involved either a pre- or post-polymerization sulfonation step. For example, many common sulfonated monomers were afforded through direct sulfonation utilizing electrophilic aromatic substitution [71] reaction with fuming sulfuric acid (**Figure 5.a**).[243] At the same time, using the same reaction conditions, poly(arylene ether sulfones) post-polymerization sulfonation is possible. One drawback of using fuming sulfuric acid as a sulfonating agent stems from possible crosslinking side reactions of chain scission.[244] Similarly, chlorosulfonic acid suffers from the same chain scission and crosslinking reactions to the polymer backbone under extremely harsh conditions such as high temperature.[243, 245] Post-sulfonation reactions using the previous methods are inhomogeneous due to resultant hydrophilic ionomer insolubility in chlorinated solvents.[243] An alternative method using trimethylsilyl chlorosulfonate (TMSCS) circumvents the drastic hydrophobic to hydrophilic switch upon sulfonation due to the trimethylsilyl sufonic ester. It is reported that the TMSCS also decreases side reactions seen with the previous methods.[244, 246]

Interest in highly sulfonated monomers for step-growth polymerizations began with work performed by the McGrath group introducing the disodium 3,3-disulfonate-4,4-dichlorodiphenylsulfone (SDCDPS) monomer into poly(arylene ether sulfone) copolymer systems (**Figure 5.30a**).[247] This direct polymerization method avoided any unwanted side reactions while obtaining highly sulfonated polymers. This pioneering effort transformed the area of sulfonated polymers by initializing some design parameters for sulfonated polymers. SDCDPS is used extensively on its own in poly(arylene ether sulfones), but the modification to form various diamines for polyamine and polyimide structures is also common.[248, 249] In general, the main design parameters include: 1) taking advantage of the directing power of EAS, 2) potential for enhanced thermal stability and sulfonate acidity on deactivated rings (sulfone, ketone, phosphine oxide, etc.),[250, 251] 3) balance between hydrophilic and hydrophobic domains. The most important

parameter is the directing power of the sulfonation reaction. Many types of structures are possible from the sulfonation of deactivated rings at the 2 and 2' positions, sulfonation of activated rings at the 3 and 3' positions, and the sulfonation of phenyl substituents at their four or para position. Phosphine oxide- and ketone-based monomers are sulfonated meta to the electron-withdrawing substituents, generally at the 3 and 3' positions.[250, 252]

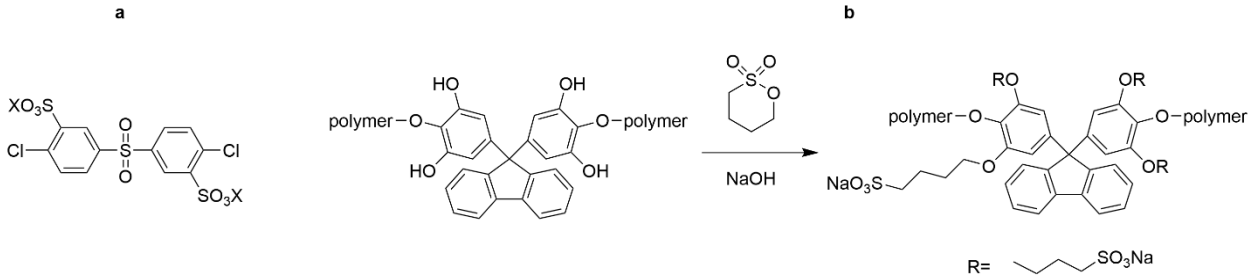


**Figure 5.30**: Multiply functionalized sulfonated building blocks.[69, 247]

Sulfoalkylation represents another method for placing sulfonated groups away from the polymer backbone. Instead of relying on the directed sulfonation using EAS, sulfoalkylation utilizes a ring-opening reaction of sultones and acidification to tether sulfuric acid groups to the polymer main chain by an alkyl linkage. Most commonly, amino and hydroxyl groups attack the sultone ring forming the sulfoalkylated product (**Figure 5.30b**). This is the primary synthetic route to sulfobetaines especially pronounced in the polyzwitterion literature.[115] Moreover, the design of monomers with several nucleophilic sites for ring-opening presents a facile strategy for multi-sulfoalkylated monomers. Polymerization of monomers with multiple hydroxyls would end up crosslinking, so most monomers have aromatic methyl ethers that are converted to the hydroxyl form using $BBr_3$ *O*-demethylation.[69]

For membrane and fuel cell applications, BCPs offered a higher degree of proton conductivity as these structures provided higher separation between the hydrophilic ionic block and the hydrophobic block compared to statistical copolymers. Most of the multiple sulfonated

BCPs are obtained by step growth methods which generally proceed via electrophilic aromatic substitution reactions [71]. Given this chemistry, sulfonated derivatives of poly(arylene ether)s, poly(arylene ether sulfone)s (SPAES), poly(arylene ether ketone)s (SPAEK), poly(arylene sulfide sulfone)s, polyimides, and polyphenylenes received attention widely owing to their uses in membrane applications.[253, 254] Takamuku and Jannasch introduced the sulfonated ionic group exclusively to the ortho position to impede desulfonation reactions; EAS, lithiation-sulfonation-oxidation, and another EAS procedures have also facilitated synthesis of the ortho-substituted sulfonated polysulfones BCP.[255] These studies measured efficient proton transport across the membranes owing to the microphase-separated structure. Particularly, a longer ionic block (n = 2 in **Figure 5.31**) led to restricted water uptake, and higher $T_g$ as the highly sulfonated block offered improved chain stiffness and concentrated ionic interaction.[255] Others in the Jannasch group studied the influence of sulfonated charge density along the polymer backbone and segmented block lengths on microphase separation.[256-258]

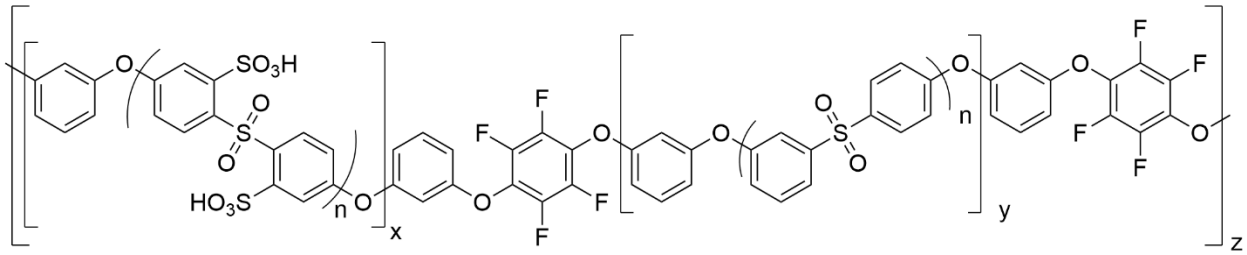


**Figure 5.31**: Synthetic pathway to multiblock sulfonated polysulfones. Reproduced from Takakumu and Jannasch with permission from Wiley.[255]

### 5.5.3.2 Phosphonated, Carboxylated, and Other Acidic Systems

Sulfonated polymers comprise most of the highly negatively charged polymer literature while relatively few highly charged BCPs possess carboxylated or phosphorylated features. This section will briefly discuss multiply functionalized phosphonated and carboxylated building blocks aiming to provide a route for the development of such multiply charged BCPs. To start,

phosphonic acid-containing polymers effectively contain two acid groups, but the two groups differ greatly in their pKa values. Lafitte and Jannasch recently published an extensive review looking into the nuances behind phosphorus chemistry in relation to advancing proton exchange fuel cell membranes.[259] Synthetically, phosphonation requires different pathways to create polymerizable monomers or to modify existing polymers compared to the EAS mechanism for sulfonation. For example, Michaelis-Arbuzov rearrangement of a trialkyl phosphite to phosphonate constitutes one of the main mechanisms to phosphonate polymers, which was then converted to phosphonic acid groups through Acid hydrolysis. One common phosphonic-acid containing monomer is vinylphosphonic acid. Vinylphosphonic acid is radically polymerizable and finds uses as a comonomer in block and grafted copolymers.[260, 261] Phosphonic acid-containing polymers show enhanced hydrogen bonding and amphoteric properties due to the carbonyl and diacid groups. Compared to other acids like sulfonates and carboxylates, phosphonic acid-modified polymers have a more complicated solubility behavior. Most commonly, polymers must be functionalized with phosphonate esters to achieve higher conversions, which were then hydrolyzed into acid groups.

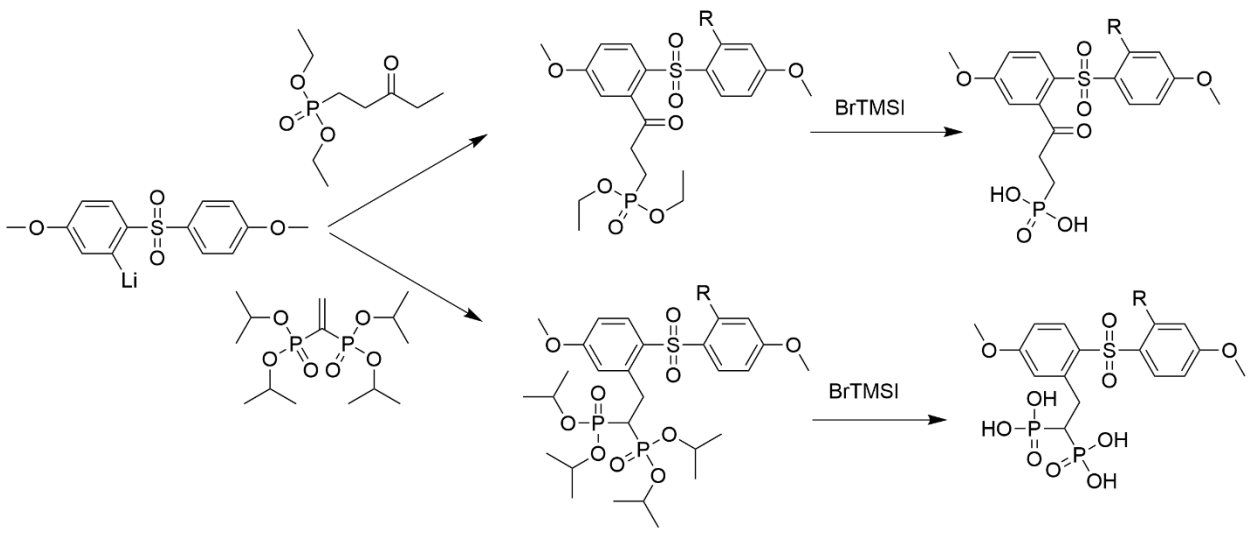


**Figure 5.32**: Schematic showing the synthesis of mono- and bisphosphonated polysulfones using lithiation chemistry. The degree of substitutions varied, noting unsubstituted, monosubstituted, and disubstituted sulfone groups.[197]

Parvole and Jannasch *et al.* published recent work using lithiation chemistry to modify PAES with mono- and bis(phosphonic acid) functionalities.[197] Reactivity of the lithiated sites with various phosphonated esters works best when introducing a γ-ketophosphonated side chain (**Figure 5.32**). Other reactions introducing α- and β-ketophosphonated side chains resulted in labile C-P bonds due to proximity to methylene protons. The same lithiation chemistry yielded a higher charge density of the carbonyl and reaction inefficiency due to acidic phosphonated side chains using tetraalkyl ethenylidene-bisphosphonates. Abouzari-Lotf and Schiraldi *et al.* directly polymerized bisphosphonated bisphenol following a phosphate-phosphonate rearrangement.[262] This phosphonation deactivated the bisphenol groups to nucleophilic substitution, requiring an activated decafluorobiphenyl monomer to polymerize the bisphenol. Masked bisphenols with carbamate substituents tend to enhance nucleophilic substitution, but the strongly deactivating bisphosphonates made polymerizations unsuccessful through typical nucleophilic substitution. Most other charged polymer literature containing phosphonates only uses monophosphonation techniques to modify polymers.[263, 264] As synthetic strategies develop even more, highly

phosphonated polymers may compete with sulfonated polymers due to the enhanced hydrolytic stability of C-P bonds.

Carboxylates have pKa higher than sulfonate and phosphonate counterparts, making their use in technologies such as proton exchange membranes. So far, several main strategies found to incorporate multiple carboxylates onto a polymer chain. One of the first methods used by Penelle *et al.* relied on the ring opening polymerization of cyclcopropane-1,1-dicarboxylate esters.[265] Alternating polymerization of stilbene or styrene with maleic anhydride and subsequent hydrolysis under aqueous alkali hydroxide solution enabled anionic polyelectrolytes with highly tunable charge densities, ranging from one carboxylate to 4 carboxylates per repeating unit.[239, 266, 267] The strategically placed monomers along the backbone allow for tailored polyion complexation, such as binding to biological proteins to inhibit certain biochemical pathways.[239] Chain extension of the alternating copolymer of stilbene and maleic anhydride and subsequent acid hydrolysis yielded a double hydrophilic polyampholyte block copolymer.[268] The block copolymer formed polyion complexation and the size of the complexation is pH dependent.[269]

## 5.6 Conclusions

Linear BCPs comprise a majority of the charged BCP literature and find applications in micelles for pharmaceutical delivery, ion exchange membranes for fuel cells and energy storage, and electromechanical transducers to name just a few. Diblock copolymers represent the simplest charged BCP system, and as such their morphologies and properties are the most studied. PISA of diblock copolymers allow for the formation of well-defined nanostructures in solution. Micelles formed from charged diblock copolymers complex with oppositely charged biopharmaceuticals to efficiently aid in drug delivery. The incorporation of charged units can also enhance phase separation in bulk BCP films over their neutral counterparts, especially when the charged groups

are inserted at the interface of the two blocks. The bulk morphology significantly impacts ion transport in linear charged BCPs. Morphologies exhibiting long-range order of interconnected ionic domains allow for easier ion transport than less well-ordered phases. The chemical identity of the bound ion plays a relatively small part in tuning the properties of the BCP; however, the size of the counterion has a significant influence on the thermal, morphological, and electrical properties of the material. Meanwhile, increasing the volume fraction of the ionic block generally improves ionic conductivity and increases water uptake.

Although triblock and multiblock copolymers tend to have more mechanical stability than diblock copolymers, the modulus and ionic conductivity typically exhibit an inverse relationship. Therefore, charged BCPs for applications such as fuel cells and electromechanical transducers require careful synthetic design to optimize performance. Multiblock copolymers most often consist of microphase separated engineering thermoplastics with greater than five blocks per polymer chain. These BCPs tend to have higher thermal stability than diblock or triblock copolymer, but rarely exhibit long-range morphological order as diblocks and triblocks do, which potentially negatively impacts the ionic conductivity. As a result, multiblock copolymers often require a high degree of water uptake for efficient operation as fuel cells. Swelling linear charged BCPs with IL also helps to improve the conductivity at the expense of modulus.

Ion-containing BCP systems with branching features employ a wide variety of architectures including brush, grafting, star, micelle, and networks. “Grafting to” and “grating from” are two main strategies to realize branching. “Grafting to” method afforded facile chemistries and reversible features for application such as protein/cell adsorption/desorption, whereas the “grafting from” procedure imparts controls over chemistry, molecular weight, dispersity, and density of branching, which influence the structure-property relationships and self-assembly properties. BCP

ionic gels exhibit sol-gel transitions and enabled advanced technologies such as additive manufacturing and biological applications, where thermal and light-induced sol-gel transition play the leading role. The future development of ionic BCP with unique topologies and architectures holds the key for the progress of fields ranging from ion-exchange membranes, fuel cell membranes, antifouling surfaces, and protein/cell purification to electrochemical energy conversion and storage to biological applications.

Segmented BCPs combine a flexible, low $T_g$ SS with a high $T_g$ HS to create microphase separated materials with elastomeric properties. Combining ionenes with classical step-growth polymers such as polyesters and PUs allows for the synthesis of industrially relevant polymers with controlled charge densities. Segmented BCPs display lower conductivities than most well-ordered diblocks and triblocks; however, the incorporation of IL into the membrane enhances the conductivity to competitive levels. Installing the charged unit into the HS or SS determines where the free IL is directed upon swelling. PUs with charged SS swollen with IL allows for enhanced conductivity without sacrificing mechanical properties. Conversely, PUs with charged HS leads to substantial phase mixing, which diminishes the properties of the material. Most significantly, charged PUs allow for water dispersibility, which eliminates the need for toxic organic solvents when utilizing PU solutions.

The design of multiply charged polymers remains a critical area of research and challenges researchers to develop new ways to create novel monomers and revitalize old ones with high charge density. Fundamental polymer chemistry demonstrates two main methods to develop highly charged polymer systems, direct polymerization of charged monomers, and post-polymerization modification of neutral polymers. The richness in multiply charged polymers stems from the variety of structural motifs possible like quaternary ammonium, imidazolium, triazolium,

sulfonate, phosphorylate, and carboxylate groups. Overcoming the design of BCP building blocks is the key to advanced multiply charged BCPs even further for emerging applications in the future. Impressive developments in chemical design led to advances in structure-property relationships in many application areas. Unique combinations of tailorable properties apply to fields such as gas separation, biotechnology, membranes, and others in polymer science. Further development of structure-property relationships will stimulate new applications for ionic BCPs in the future.

## 5.7 References


1. Bates, F. S.; Fredrickson, G. H., Block copolymer thermodynamics: theory and experiment. *Annual review of physical chemistry* **1990,** *41* (1), 525-557.
2. Hamley, I. W., *Developments in block copolymer science and technology*. John Wiley & Sons: 2004.
3. Smart, T.; Lomas, H.; Massignani, M.; Flores-Merino, M. V.; Perez, L. R.; Battaglia, G., Block copolymer nanostructures. *Nano Today* **2008,** *3* (3-4), 38-46.
4. Hickner, M. A., Ion-containing polymers: new energy & clean water. *Mater. Today* **2010,** *13*, 34-41.
5. Zhang, K.; Fahs, G. B.; Drummey, K. J.; Moore, R. B.; Long, T. E., Doubly-Charged Ionomers with Enhanced Microphase-Separation. *Macromolecules* **2016,** *49* (18), 6965-6972.
6. Bolto, B.; Gregory, J., Organic polyelectrolytes in water treatment. *Water Res.* **2007,** *41*, 2301-2324.
7. Yarusso, D. J., Quantifying the Relationship Between Peel and Rheology for Pressure Sensitive Adhesives. *The Journal of Adhesion* **1999,** *70*, 299-320.
8. Couture, G.; Alaaeddine, A.; Boschet, F.; Ameduri, B., Polymeric materials as anion-exchange membranes for alkaline fuel cells. *Progress in Polymer Science (Oxford)* **2011,** *36*, 1521-1557.
9. Lawrence, P. G.; Lapitsky, Y., Ionically Cross-Linked Poly(allylamine) as a Stimulus-Responsive Underwater Adhesive: Ionic Strength and pH Effects. *Langmuir* **2015,** *31*, 1564-1574.
10. Eisenberg, A. A.; King, M., Ion-containing polymers : physical properties and structure. **1977**, 287.
11. Eisenberg, A.; Hird, B.; Moore, R., A new multiplet-cluster model for the morphology of random ionomers. *Macromolecules* **1990,** *23* (18), 4098-4107.
12. Chen, X.; Talley, S. J.; Haag, J. V.; Spiering, G. A.; Liu, B.; Drummey, K. J.; Murayama, M.; Moore, R. B.; Long, T. E., Doubly Charged ABA Triblock Copolymers: Thermomechanically Robust Physical Network and Hierarchical Microstructures. *Macromolecules* **2019,** *52* (23), 9168-9176.
13. Bae, B.; Miyatake, K.; Watanabe, M., Sulfonated Poly(arylene ether sulfone ketone) Multiblock Copolymers with Highly Sulfonated Block. Synthesis and Properties. *Macromolecules* **2010,** *43* (6), 2684-2691.

14. Bae, B.; Yoda, T.; Miyatake, K.; Uchida, H.; Watanabe, M., Proton-Conductive Aromatic Ionomers Containing Highly Sulfonated Blocks for High-Temperature-Operable Fuel Cells. *Angewandte Chemie International Edition* **2010,** *49* (2), 317-320.
15. Choi, U. H.; Kwon, Y. K.; Lee, M., Correlating morphology to thermal and electrical properties in imidazolium-poly(ethylene glycol) copolyesters. *Polymer* **2018,** *146*, 420-428.
16. Gao, R.; Zhang, M.; Dixit, N.; Moore, R. B.; Long, T. E., Influence of ionic charge placement on performance of poly (ethylene glycol)-based sulfonated polyurethanes. *Polymer* **2012,** *53* (6), 1203-1211.
17. Gao, R.; Zhang, M.; Wang, S. W.; Moore, R. B.; Colby, R. H.; Long, T. E., Polyurethanes Containing an Imidazolium Diol‐Based Ionic‐Liquid Chain Extender for Incorporation of Ionic‐Liquid Electrolytes. *Macromolecular Chemistry and Physics* **2013,** *214* (9), 1027-1036.
18. Miyake, J.; Watanabe, M.; Miyatake, K., Sulfonated poly (arylene ether phosphine oxide ketone) block copolymers as oxidatively stable proton conductive membranes. *ACS applied materials & interfaces* **2013,** *5* (13), 5903-5907.
19. Rajagopalan, M.; Jeon, J.-H.; Oh, I.-K., Electric-stimuli-responsive bending actuator based on sulfonated polyetherimide. *Sensors and Actuators B: Chemical* **2010,** *151* (1), 198-204.
20. Rajagopalan, M.; Oh, I.-K., Fullerenol-Based Electroactive Artificial Muscles Utilizing Biocompatible Polyetherimide. *ACS Nano* **2011,** *5* (3), 2248-2256.
21. Strasser, D. J.; Graziano, B. J.; Knauss, D. M., Base stable poly (diallylpiperidinium hydroxide) multiblock copolymers for anion exchange membranes. *Journal of Materials Chemistry A* **2017,** *5* (20), 9627-9640.
22. Takamuku, S.; Jannasch, P., Fully aromatic block copolymers for fuel cell membranes with densely sulfonated nanophase domains. *Macromolecular rapid communications* **2011,** *32* (5), 474-480.
23. Tamami, M.; Hemp, S. T.; Zhang, K.; Zhang, M.; Moore, R. B.; Long, T. E., Poly(ethylene glycol)-based ammonium ionenes containing nucleobases. *Polymer* **2013,** *54* (6), 1588-1595.
24. Tamami, M.; Williams, S. R.; Park, J. K.; Moore, R. B.; Long, T. E., Poly(propylene glycol)-based ammonium ionenes as segmented ion-containing block copolymers. *Journal of Polymer Science Part A: Polymer Chemistry* **2010,** *48* (19), 4159-4167.
25. Wu, F.; Huang, C.-L.; Zeng, J.-B.; Li, S.-L.; Wang, Y.-Z., Synthesis and characterization of segmented poly (butylene succinate) urethane ionenes containing secondary amine cation. *Polymer* **2014,** *55* (16), 4358-4368.
26. Zhang, M.; Hemp, S. T.; Zhang, M.; Allen, M. H.; Carmean, R. N.; Moore, R. B.; Long, T. E., Water-dispersible cationic polyurethanes containing pendant trialkylphosphoniums. *Polymer Chemistry* **2014,** *5* (12), 3795-3803.
27. Zhang, M.; Zhang, M.; Moore, R. B.; Long, T. E., Influence of charge placement on the thermal and morphological properties of sulfonated segmented copolyesters. *Polymer* **2013,** *54* (14), 3521-3528.
28. Choi, J.-H.; Xie, W.; Gu, Y.; Frisbie, C. D.; Lodge, T. P., Single ion conducting, polymerized ionic liquid triblock copolymer films: High capacitance electrolyte gates for n-type transistors. *ACS applied materials & interfaces* **2015,** *7* (13), 7294-7302.
29. Evans, C. M.; Sanoja, G. E.; Popere, B. C.; Segalrnan, R. A., Anhydrous Proton Transport in Polymerized Ionic Liquid Block Copolymers: Roles of Block Length, Ionic Content, and Confinement. *Macromolecules* **2016,** *49* (1), 395-404.

30. Hemp, S. T.; Smith, A. E.; Bryson, J. M.; Allen, M. H.; Long, T. E., Phosphonium-Containing Diblock Copolymers for Enhanced Colloidal Stability and Efficient Nucleic Acid Delivery. *Biomacromolecules* **2012,** *13* (8), 2439-2445.
31. Jangu, C.; Savage, A. M.; Zhang, Z.; Schultz, A. R.; Madsen, L. A.; Beyer, F. L.; Long, T. E., Sulfonimide-containing triblock copolymers for improved conductivity and mechanical performance. *Macromolecules* **2015,** *48* (13), 4520-4528.
32. Jangu, C.; Wang, J.-H. H.; Wang, D.; Fahs, G.; Heflin, J. R.; Moore, R. B.; Colby, R. H.; Long, T. E., Imidazole-containing triblock copolymers with a synergy of ether and imidazolium sites. *Journal of Materials Chemistry C* **2015,** *3* (16), 3891-3901.
33. Jung, S.; Lodge, T. P.; Reineke, T. M., Complexation between DNA and Hydrophilic-Cationic Diblock Copolymers. *The Journal of Physical Chemistry B* **2017,** *121* (10), 2230-2243.
34. Jung, S.; Lodge, T. P.; Reineke, T. M., Structures and Protonation States of Hydrophilic–Cationic Diblock Copolymers and Their Binding with Plasmid DNA. *The Journal of Physical Chemistry B* **2018,** *122* (9), 2449-2461.
35. Margaretta, E.; Fahs, G. B.; Inglefield Jr, D. L.; Jangu, C.; Wang, D.; Heflin, J. R.; Moore, R. B.; Long, T. E., Imidazolium-containing ABA triblock copolymers as electroactive devices. *ACS applied materials & interfaces* **2016,** *8* (2), 1280-1288.
36. Mori, H.; Yahagi, M.; Endo, T., RAFT polymerization of N-vinylimidazolium salts and synthesis of thermoresponsive ionic liquid block copolymers. *Macromolecules* **2009,** *42* (21), 8082-8092.
37. Nykaza, J. R.; Ye, Y.; Elabd, Y. A., Polymerized ionic liquid diblock copolymers with long alkyl side-chain length. *Polymer* **2014,** *55* (16), 3360-3369.
38. Porcarelli, L.; Shaplov, A. S.; Salsamendi, M.; Nair, J. R.; Vygodskii, Y. S.; Mecerreyes, D.; Gerbaldi, C., Single-ion block copoly (ionic liquid) s as electrolytes for all-solid state lithium batteries. *ACS applied materials & interfaces* **2016,** *8* (16), 10350-10359.
39. Sprouse, D.; Jiang, Y.; Laaser, J. E.; Lodge, T. P.; Reineke, T. M., Tuning Cationic Block Copolymer Micelle Size by pH and Ionic Strength. *Biomacromolecules* **2016,** *17* (9), 2849-2859.
40. Vijayakrishna, K.; Jewrajka, S. K.; Ruiz, A.; Marcilla, R.; Pomposo, J. A.; Mecerreyes, D.; Taton, D.; Gnanou, Y., Synthesis by RAFT and ionic responsiveness of double hydrophilic block copolymers based on ionic liquid monomer units. *Macromolecules* **2008,** *41* (17), 6299-6308.
41. Yang, Y.; Zheng, J.; Man, S.; Sun, X.; An, Z., Synthesis of poly (ionic liquid)-based nano-objects with morphological transitions via RAFT polymerization-induced self-assembly in ethanol. *Polymer Chemistry* **2018,** *9* (7), 824-827.
42. Ye, Y.; Choi, J.-H.; Winey, K. I.; Elabd, Y. A., Polymerized Ionic Liquid Block and Random Copolymers: Effect of Weak Microphase Separation on Ion Transport. *Macromolecules* **2012,** *45* (17), 7027-7035.
43. Yuan, J.; Schlaad, H.; Giordano, C.; Antonietti, M., Double hydrophilic diblock copolymers containing a poly (ionic liquid) segment: Controlled synthesis, solution property, and application as carbon precursor. *European polymer journal* **2011,** *47* (4), 772-781.
44. Zhang, W.; Liu, Y.; Jackson, A. C.; Savage, A. M.; Ertem, S. P.; Tsai, T.-H.; Seifert, S.; Beyer, F. L.; Liberatore, M. W.; Herring, A. M.; Coughlin, E. B., Achieving Continuous Anion Transport Domains Using Block Copolymers Containing Phosphonium Cations. *Macromolecules* **2016,** *49* (13), 4714-4722.

45. Cordella, D.; Debuigne, A.; Jerome, C.; Kochovski, Z.; Taton, D.; Detrembleur, C., One-Pot Synthesis of Double Poly(Ionic Liquid) Block Copolymers by Cobalt-Mediated Radical Polymerization-Induced Self-Assembly (CMRPISA) in Water. *Macromolecular Rapid Communications* **2016,** *37* (14), 1181-1187.
46. Cordella, D.; Kermagoret, A.; Debuigne, A.; Jérôme, C.; Mecerreyes, D.; Isik, M.; Taton, D.; Detrembleur, C., All poly (ionic liquid)-based block copolymers by sequential controlled radical copolymerization of vinylimidazolium monomers. *Macromolecules* **2015,** *48* (15), 5230-5243.
47. Coupillaud, P.; Fèvre, M.; Wirotius, A. L.; Aissou, K.; Fleury, G.; Debuigne, A.; Detrembleur, C.; Mecerreyes, D.; Vignolle, J.; Taton, D., Precision Synthesis of Poly (Ionic Liquid) ‐ Based Block Copolymers by Cobalt ‐ Mediated Radical Polymerization and Preliminary Study of Their Self ‐ Assembling Properties. *Macromolecular rapid communications* **2014,** *35* (4), 422-430.
48. Detrembleur, C.; Debuigne, A.; Hurtgen, M.; Jérôme, C.; Pinaud, J.; Fèvre, M.; Coupillaud, P.; Vignolle, J.; Taton, D., Synthesis of 1-vinyl-3-ethylimidazolium-based ionic liquid (co) polymers by cobalt-mediated radical polymerization. *Macromolecules* **2011,** *44* (16), 6397-6404.
49. Cheng, S.; Beyer, F. L.; Mather, B. D.; Moore, R. B.; Long, T. E., Phosphonium-containing ABA triblock copolymers: controlled free radical polymerization of phosphonium ionic liquids. *Macromolecules* **2011,** *44* (16), 6509-6517.
50. Green, M. D.; Wang, D.; Hemp, S. T.; Choi, J.-H.; Winey, K. I.; Heflin, J. R.; Long, T. E., Synthesis of imidazolium ABA triblock copolymers for electromechanical transducers. *Polymer* **2012,** *53* (17), 3677-3686.
51. Jangu, C.; Wang, J.-H. H.; Wang, D.; Sharick, S.; Heflin, J. R.; Winey, K. I.; Colby, R. H.; Long, T. E., Well-Defined Imidazolium ABA Triblock Copolymers as Ionic-Liquid-Containing Electroactive Membranes. *Macromolecular Chemistry and Physics* **2014,** *215* (13), 1319-1331.
52. Sudre, G.; Inceoglu, S.; Cotanda, P.; Balsara, N. P., Influence of bound ion on the morphology and conductivity of anion-conducting block copolymers. *Macromolecules* **2013,** *46* (4), 1519-1527.
53. Weber, R. L.; Ye, Y.; Schmitt, A. L.; Banik, S. M.; Elabd, Y. A.; Mahanthappa, M. K., Effect of Nanoscale Morphology on the Conductivity of Polymerized Ionic Liquid Block Copolymers. *Macromolecules* **2011,** *44* (14), 5727-5735.
54. Bayó-Puxan, N.; Dufresne, M.-H.; Felber, A. E.; Castagner, B.; Leroux, J.-C., Preparation of polyion complex micelles from poly (ethylene glycol)-block-polyions. *Journal of controlled release* **2011,** *156* (2), 118-127.
55. Dufresne, M.-H.; Elsabahy, M.; Leroux, J.-C., Characterization of Polyion Complex Micelles Designed to Address the Challenges of Oligonucleotide Delivery. *Pharmaceutical Research* **2008,** *25* (9), 2083-2093.
56. Schneider, Y.; Modestino, M. A.; McCulloch, B. L.; Hoarfrost, M. L.; Hess, R. W.; Segalman, R. A., Ionic conduction in nanostructured membranes based on polymerized protic ionic liquids. *Macromolecules* **2013,** *46* (4), 1543-1548.
57. Texter, J.; Vasantha, V. A.; Crombez, R.; Maniglia, R.; Slater, L.; Mourey, T., Triblock Copolymer Based on Poly (propylene oxide) and Poly (1 ‐ [11 ‐ acryloylundecyl] ‐ 3 ‐ methyl ‐ imidazolium bromide). *Macromolecular rapid communications* **2012,** *33* (1), 69-74.

58. Scalfani, V. F.; Wiesenauer, E. F.; Ekblad, J. R.; Edwards, J. P.; Gin, D. L.; Bailey, T. S., Morphological phase behavior of poly (RTIL)-containing diblock copolymer melts. *Macromolecules* **2012,** *45* (10), 4262-4276.
59. Wiesenauer, E. F.; Edwards, J. P.; Scalfani, V. F.; Bailey, T. S.; Gin, D. L., Synthesis and ordered phase separation of imidazolium-based alkyl–ionic diblock copolymers made via ROMP. *Macromolecules* **2011,** *44* (13), 5075-5078.
60. Choi, J.-H.; Willis, C. L.; Winey, K. I., Structure–property relationship in sulfonated pentablock copolymers. *Journal of membrane science* **2012,** *394*, 169-174.
61. Elabd, Y. A.; Napadensky, E., Sulfonation and characterization of poly (styrene-isobutylene-styrene) triblock copolymers at high ion-exchange capacities. *Polymer* **2004,** *45* (9), 3037-3043.
62. Elabd, Y. A.; Walker, C. W.; Beyer, F. L., Triblock copolymer ionomer membranes Part II. Structure characterization and its effects on transport properties and direct methanol fuel cell performance. *Journal of Membrane Science* **2004,** *231* (1-2), 181-188.
63. Li, Y.; Liu, Y.; Savage, A. M.; Beyer, F. L.; Seifert, S.; Herring, A. M.; Knauss, D. M., Polyethylene-based block copolymers for anion exchange membranes. *Macromolecules* **2015,** *48* (18), 6523-6533.
64. Luo, Y. D.; Montarnal, D.; Treat, N. J.; Hustad, P. D.; Christianson, M. D.; Kramer, E. J.; Fredrickson, G. H.; Hawker, C. J., Enhanced Block Copolymer Phase Separation Using Click Chemistry and Ionic Junctions. *ACS Macro Lett.* **2015,** *4* (12), 1332-1336.
65. Gao, R.; Wang, D.; Heflin, J. R.; Long, T. E., Imidazolium sulfonate-containing pentablock copolymer–ionic liquid membranes for electroactive actuators. *Journal of Materials Chemistry* **2012,** *22* (27), 13473-13476.
66. Kim, J.; Kim, B.; Jung, B., Proton conductivities and methanol permeabilities of membranes made from partially sulfonated polystyrene-block-poly(ethylene-ran-butylene)-block-polystyrene copolymers. *Journal of Membrane Science* **2002,** *207* (1), 129-137.
67. Shim, J.; Bates, F. S.; Lodge, T. P., Superlattice by charged block copolymer self-assembly. *Nature Communications* **2019,** *10* (1), 2108.
68. Matsumoto, K.; Nakagawa, T.; Higashihara, T.; Ueda, M., Sulfonated poly(ether sulfone)s with binaphthyl units as proton exchange membranes for fuel cell application. *Journal of Polymer Science Part A: Polymer Chemistry* **2009,** *47* (21), 5827-5834.
69. Wang, C.; Li, N.; Shin, D. W.; Lee, S. Y.; Kang, N. R.; Lee, Y. M.; Guiver, M. D., Fluorene-based poly(arylene ether sulfone)s containing clustered flexible pendant sulfonic acids as proton exchange membranes. *Macromolecules* **2011,** *44*, 7296-7306.
70. Lafitte, B.; Jannasch, P., Proton-Conducting Aromatic Polymers Carrying Hypersulfonated Side Chains for Fuel Cell Applications. *Adv. Funct. Mater.* **2007,** *17* (15), 2823-2834.
71. Takamuku, S.; Wohlfarth, A.; Manhart, A.; Räder, P.; Jannasch, P., Hypersulfonated polyelectrolytes: preparation, stability and conductivity. *Polymer Chemistry* **2015,** *6* (8), 1267-1274.
72. Scalfani, V. F.; Wiesenauer, E. F.; Ekblad, J. R.; Edwards, J. P.; Gin, D. L.; Bailey, T. S., Morphological Phase Behavior of Poly(RTIL)-Containing Diblock Copolymer Melts. *Macromolecules* **2012,** *45* (10), 4262-4276.
73. Zare, P.; Stojanovic, A.; Herbst, F.; Akbarzadeh, J.; Peterlik, H.; Binder, W. H., Hierarchically nanostructured polyisobutylene-based ionic liquids. *Macromolecules* **2012,** *45* (4), 2074-2084.

74. Feng, X.; Tousley, M. E.; Cowan, M. G.; Wiesenauer, B. R.; Nejati, S.; Choo, Y.; Noble, R. D.; Elimelech, M.; Gin, D. L.; Osuji, C. O., Scalable fabrication of polymer membranes with vertically aligned 1 nm pores by magnetic field directed self-assembly. *Acs Nano* **2014,** *8* (12), 11977-11986.
75. Hemp, S. T.; Zhang, M.; Allen Jr., M. H.; Cheng, S.; Moore, R. B.; Long, T. E., Comparing Ammonium and Phosphonium Polymerized Ionic Liquids: Thermal Analysis, Conductivity, and Morphology. *Macromolecular Chemistry and Physics* **2013,** *214* (18), 2099-2107.
76. Charleux, B.; Delaittre, G.; Rieger, J.; D'Agosto, F., Polymerization-Induced Self-Assembly: From Soluble Macromolecules to Block Copolymer Nano-Objects in One Step. *Macromolecules* **2012,** *45* (17), 6753-6765.
77. Yang, Y.; Zheng, J.; Man, S.; Sun, X.; An, Z., Synthesis of poly(ionic liquid)-based nano-objects with morphological transitions: Via RAFT polymerization-induced self-assembly in ethanol. *Polymer Chemistry* **2018,** *9*, 824-827.
78. Depoorter, J.; Yan, X.; Zhang, B.; Sudre, G.; Charlot, A.; Fleury, E.; Bernard, J., All poly(ionic liquid) block copolymer nanoparticles from antagonistic isomeric macromolecular blocks: Via aqueous RAFT polymerization-induced self-assembly. *Polymer Chemistry* **2021,** *12*, 82-91.
79. Smith, G. N.; Canning, S. L.; Derry, M. J.; Jones, E. R.; Neal, T. J.; Smith, A. J., Ionic and Nonspherical Polymer Nanoparticles in Nonpolar Solvents. *Macromolecules* **2020**.
80. Smith, G. N.; Canning, S. L.; Derry, M. J.; Mykhaylyk, O. O.; Norman, S. E.; Armes, S. P., Influence of an ionic comonomer on polymerization-induced self-assembly of diblock copolymers in non-polar media. *Polymer Chemistry* **2020,** *11*, 2605-2614.
81. Jiang, Y.; Reineke, T. M.; Lodge, T. P., Complexation of DNA with Cationic Copolymer Micelles: Effects of DNA Length and Topology. *Macromolecules* **2018,** *51* (3), 1150-1160.
82. Jiang, Y. Y.; Lu, H. X.; Chen, F.; Callari, M.; Pourgholami, M.; Morris, D. L.; Stenzel, M. H., PEGylated Albumin-Based Polyion Complex Micelles for Protein Delivery. *Biomacromolecules* **2016,** *17* (3), 808-817.
83. Lee, Y.; Kataoka, K., Biosignal-sensitive polyion complex micelles for the delivery of biopharmaceuticals. *Soft Matter* **2009,** *5* (20), 3810-3817.
84. Hu, X.; Zhang, Y.; Xie, Z.; Jing, X.; Bellotti, A.; Gu, Z., Stimuli-responsive polymersomes for biomedical applications. *Biomacromolecules* **2017,** *18* (3), 649-673.
85. Miyata, K.; Christie, R. J.; Kataoka, K., Polymeric micelles for nano-scale drug delivery. *Reactive and Functional Polymers* **2011,** *71* (3), 227-234.
86. Wang, X.; Goswami, M.; Kumar, R.; Sumpter, B. G.; Mays, J., Morphologies of block copolymers composed of charged and neutral blocks. *Soft Matter* **2012,** *8* (11), 3036-3052.
87. Choi, J.-H.; Ye, Y.; Elabd, Y. A.; Winey, K. I., Network Structure and Strong Microphase Separation for High Ion Conductivity in Polymerized Ionic Liquid Block Copolymers. *Macromolecules* **2013,** *46* (13), 5290-5300.
88. Nakabayashi, K.; Umeda, A.; Sato, Y.; Mori, H., Synthesis of 1,2,4-triazolium salt-based polymers and block copolymers by RAFT polymerization: Ion conductivity and assembled structures. *Polymer* **2016,** *96*, 81-93.
89. Keith, J. R.; Rebello, N. J.; Cowen, B. J.; Ganesan, V., Influence of Counterion Structure on Conductivity of Polymerized Ionic Liquids. *ACS Macro Lett.* **2019,** *8* (4), 387-392.
90. Ye, Y. S.; Sharick, S.; Davis, E. M.; Winey, K. I.; Elabd, Y. A., High Hydroxide Conductivity in Polymerized Ionic Liquid Block Copolymers. *ACS Macro Lett.* **2013,** *2* (7), 575-580.

91. Szymczyk, A.; Ezquerra, T.; Roslaniec, Z., Poly (ether-block-sulfonated ester) copolymers. I. Phase structure and physical properties. *Journal of Macromolecular Science, Part B* **2001,** *40* (5), 669-684.
92. Mauritz, K. A.; Moore, R. B., State of understanding of Nafion. *Chemical reviews* **2004,** *104* (10), 4535-4586.
93. Pan, M.; Pan, C.; Li, C.; Zhao, J., A review of membranes in proton exchange membrane fuel cells: Transport phenomena, performance and durability. *Renewable and Sustainable Energy Reviews* **2021,** *141*, 110771.
94. Sangeetha, D., Conductivity and solvent uptake of proton exchange membrane based on polystyrene(ethylene-butylene) polystyrene triblock polymer. *European Polymer Journal* **2005,** *41* (11), 2644-2652.
95. Akiyama, R.; Yokota, N.; Nishino, E.; Asazawa, K.; Miyatake, K., Anion conductive aromatic copolymers from dimethylaminomethylated monomers: synthesis, properties, and applications in alkaline fuel cells. *Macromolecules* **2016,** *49* (12), 4480-4489.
96. Mahmoud, A. M. A.; Elsaghier, A. M. M.; Miyatake, K., Effect of ammonium groups on the properties of anion conductive membranes based on partially fluorinated aromatic polymers. *RSC advances* **2016,** *6* (33), 27862-27870.
97. Ono, H.; Miyake, J.; Shimada, S.; Uchida, M.; Miyatake, K., Anion exchange membranes composed of perfluoroalkylene chains and ammonium-functionalized oligophenylenes. *Journal of Materials Chemistry A* **2015,** *3* (43), 21779-21788.
98. Yokota, N.; Shimada, M.; Ono, H.; Akiyama, R.; Nishino, E.; Asazawa, K.; Miyake, J.; Watanabe, M.; Miyatake, K., Aromatic copolymers containing ammonium-functionalized oligophenylene moieties as highly anion conductive membranes. *Macromolecules* **2014,** *47* (23), 8238-8246.
99. Mahmoud, A. M. A.; Elsaghier, A. M. M.; Otsuji, K.; Miyatake, K., High Hydroxide Ion Conductivity with Enhanced Alkaline Stability of Partially Fluorinated and Quaternized Aromatic Copolymers as Anion Exchange Membranes. *Macromolecules* **2017,** *50* (11), 4256-4266.
100. Graziani, S., Ionic Polymer Metal Composites as Post-silicon Transducers for the Realisation of Smart Systems. ROYAL SOC CHEMISTRY: 2016; pp 158-214.
101. Duncan, A. J.; Leo, D. J.; Long, T. E., Beyond Nafion: Charged Macromolecules Tailored for Performance as Ionic Polymer Transducers. *Macromolecules* **2008,** *41* (21), 7765-7775.
102. White, B. T.; Long, T. E., Advances in Polymeric Materials for Electromechanical Devices. *Macromolecular Rapid Communications* **2019,** *40* (1), 1800521.
103. Green, M. D.; Choi, J.-H.; Winey, K. I.; Long, T. E., Synthesis of Imidazolium-Containing ABA Triblock Copolymers: Role of Charge Placement, Charge Density, and Ionic Liquid Incorporation. *Macromolecules* **2012,** *45* (11), 4749-4757.
104. Kim, O.; Kim, S. Y.; Park, B.; Hwang, W.; Park, M. J., Factors Affecting Electromechanical Properties of Ionic Polymer Actuators Based on Ionic Liquid-Containing Sulfonated Block Copolymers. *Macromolecules* **2014,** *47* (13), 4357-4368.
105. Pham, T. H.; Jannasch, P., Aromatic Polymers Incorporating Bis-N-spirocyclic Quaternary Ammonium Moieties for Anion-Exchange Membranes. *ACS Macro Lett.* **2015,** *4* (12), 1370-1375.
106. Zheng, W.; Cornelius, C. J., Solvent tunable multi-block ionomer morphology and its relationship to modulus, water swelling, directionally dependent ion transport, and actuator performance. *Polymer* **2016,** *103*, 104-111.

107. Song, J.; Jeon, J. H.; Oh, I. K.; Park, K. C., Electro-active Polymer Actuator Based on Sulfonated Polyimide with Highly Conductive Silver Electrodes Via Self-metallization. *Macromolecular Rapid Communications* **2011,** *32* (19), 1583-1587.
108. Imaizumi, S.; Ohtsuki, Y.; Yasuda, T.; Kokubo, H.; Watanabe, M., Printable Polymer Actuators from Ionic Liquid, Soluble Polyimide, and Ubiquitous Carbon Materials. *ACS Applied Materials & Interfaces* **2013,** *5* (13), 6307-6315.
109. Vallejo, E.; Pourcelly, G.; Gavach, C.; Mercier, R.; Pineri, M., Sulfonated polyimides as proton conductor exchange membranes. Physicochemical properties and separation H+/Mz+ by electrodialysis comparison with a perfluorosulfonic membrane. *Journal of Membrane Science* **1999,** *160* (1), 127-137.
110. Tang, Y.; Chen, C.; Ye, Y. S.; Xue, Z.; Zhou, X.; Xie, X., The enhanced actuation response of an ionic polymer–metal composite actuator based on sulfonated polyphenylsulfone. *Polymer Chemistry* **2014,** *5* (20), 6097-6107.
111. Tas, S.; Zoetebier, B.; Sukas, O. S.; Bayraktar, M.; Hempenius, M.; Vancso, G. J.; Nijmeijer, K., Ion-Selective Ionic Polymer Metal Composite (IPMC) Actuator Based on Crown Ether Containing Sulfonated Poly(Arylene Ether Ketone). *Macromol. Mater. Eng.* **2017,** *302* (4), 6.
112. de Vos, W. M.; Kleijn, J. M.; de Keizer, A.; Cohen Stuart, M. A., Ultradense Polymer Brushes by Adsorption. *Angew. Chem. Int. Ed.* **2009,** *48* (29), 5369-5371.
113. de Vos, W. M.; Meijer, G.; de Keizer, A.; Cohen Stuart, M. A.; Kleijn, J. M., Charge-driven and reversible assembly of ultra-dense polymer brushes: formation and antifouling properties of a zipper brush. *Soft Matter* **2010,** *6* (11), 2499-2507.
114. Brzozowska, A. M.; Hofs, B.; de Keizer, A.; Fokkink, R.; Cohen Stuart, M. A.; Norde, W., Reduction of protein adsorption on silica and polystyrene surfaces due to coating with Complex Coacervate Core Micelles. *Colloids and Surfaces A: Physicochemical and Engineering Aspects* **2009,** *347* (1), 146-155.
115. Scott, P. J.; Spiering, G. A.; Wang, Y.; Seibers, Z. D.; Moore, R. B.; Kumar, R.; Lokitz, B. S.; Long, T. E., Phosphonium-Based Polyzwitterions: Influence of Ionic Structure and Association on Mechanical Properties. *Macromolecules* **2020,** *53* (24), 11009-11018.
116. Chang, Y.; Shih, Y.-J.; Lai, C.-J.; Kung, H.-H.; Jiang, S., Blood-Inert Surfaces via Ion-Pair Anchoring of Zwitterionic Copolymer Brushes in Human Whole Blood. *Adv. Funct. Mater.* **2013,** *23*, 1100-1110.
117. Chang, Y.; Chen, S.; Zhang, Z.; Jiang, S., Highly Protein-Resistant Coatings from Well-Defined Diblock Copolymers Containing Sulfobetaines. *Langmuir* **2006,** *22* (5), 2222-2226.
118. Chou, Y.-N.; Venault, A.; Cho, C.-H.; Sin, M.-C.; Yeh, L.-C.; Jhong, J.-F.; Chinnathambi, A.; Chang, Y.; Chang, Y., Epoxylated Zwitterionic Triblock Copolymers Grafted onto Metallic Surfaces for General Biofouling Mitigation. *Langmuir* **2017,** *33* (38), 9822-9835.
119. Edmondson, S.; Osborne, V. L.; Huck, W. T. S., Polymer brushes via surface-initiated polymerizations. *Chem. Soc. Rev.* **2004,** *33* (1), 14-22.
120. Wei, Q.; Cai, M.; Zhou, F.; Liu, W., Dramatically Tuning Friction Using Responsive Polyelectrolyte Brushes. *Macromolecules* **2013,** *46* (23), 9368-9379.
121. Sedjo, R. A.; Mirous, B. K.; Brittain, W. J., Synthesis of Polystyrene-block-poly(methyl methacrylate) Brushes by Reverse Atom Transfer Radical Polymerization. *Macromolecules* **2000,** *33* (5), 1492-1493.

122. Granville, A. M.; Boyes, S. G.; Akgun, B.; Foster, M. D.; Brittain, W. J., Synthesis and Characterization of Stimuli-Responsive Semifluorinated Polymer Brushes Prepared by Atom Transfer Radical Polymerization. *Macromolecules* **2004,** *37* (8), 2790-2796.
123. Osborne, V. L.; Jones, D. M.; Huck, W. T. S., Controlled growth of triblock polyelectrolyte brushes. *Chem. Commun.* **2002,** (17), 1838-1839.
124. Lilge, I.; Schönherr, H., Synthesis and characterization of well-defined ligand-terminated block copolymer brushes for multifunctional biointerfaces. *Polymer* **2016,** *98*, 409-420.
125. Coessens, V.; Pintauer, T.; Matyjaszewski, K., Functional polymers by atom transfer radical polymerization. *Prog. Polym. Sci.* **2001,** *26* (3), 337-377.
126. Dong, R.; Krishnan, S.; Baird, B. A.; Lindau, M.; Ober, C. K., Patterned Biofunctional Poly(acrylic acid) Brushes on Silicon Surfaces. *Biomacromolecules* **2007,** *8* (10), 3082-3092.
127. Qiao, M.; Wu, S.; Wang, Y.; Ran, Q., Brush-like block copolymer synthesized via RAFT polymerization for graphene oxide aqueous suspensions. *RSC Advances* **2017,** *7* (8), 4776-4782.
128. Norsten, T. B.; Guiver, M. D.; Murphy, J.; Astill, T.; Navessin, T.; Holdcroft, S.; Frankamp, B. L.; Rotello, V. M.; Ding, J., Highly Fluorinated Comb-Shaped Copolymers as Proton Exchange Membranes (PEMs): Improving PEM Properties Through Rational Design. *Adv. Funct. Mater.* **2006,** *16* (14), 1814-1822.
129. Nagase, K.; Kobayashi, J.; Kikuchi, A.; Akiyama, Y.; Kanazawa, H.; Okano, T., Thermally-modulated on/off-adsorption materials for pharmaceutical protein purification. *Biomaterials* **2011,** *32* (2), 619-627.
130. Xu, Y.; Takai, M.; Ishihara, K., Protein adsorption and cell adhesion on cationic, neutral, and anionic 2-methacryloyloxyethyl phosphorylcholine copolymer surfaces. *Biomaterials* **2009,** *30* (28), 4930-4938.
131. Sakata, S.; Inoue, Y.; Ishihara, K., Molecular Interaction Forces Generated during Protein Adsorption to Well-Defined Polymer Brush Surfaces. *Langmuir* **2015,** *31* (10), 3108-3114.
132. Kanazawa, H.; Kashiwase, Y.; Yamamoto, K.; Matsushima, Y.; Kikuchi, A.; Sakurai, Y.; Okano, T., Temperature-responsive liquid chromatography. 2. Effects of hydrophobic groups in N-isopropylacrylamide copolymer-modified silica. *Anal. Chem.* **1997,** *69* (5), 823-830.
133. Nagase, K.; Geven, M.; Kimura, S.; Kobayashi, J.; Kikuchi, A.; Akiyama, Y.; Grijpma, D. W.; Kanazawa, H.; Okano, T., Thermoresponsive Copolymer Brushes Possessing Quaternary Amine Groups for Strong Anion-Exchange Chromatographic Matrices. *Biomacromolecules* **2014,** *15* (3), 1031-1043.
134. Nagase, K.; Kobayashi, J.; Kikuchi, A.; Akiyama, Y.; Kanazawa, H.; Okano, T., Protein separations via thermally responsive ionic block copolymer brush layers. *RSC Advances* **2016,** *6* (31), 26254-26263.
135. Heskins, M.; Guillet, J. E., Solution properties of poly (N-isopropylacrylamide). *Journal of Macromolecular Science—Chemistry* **1968,** *2* (8), 1441-1455.
136. Nagase, K.; Ota, A.; Hirotani, T.; Yamada, S.; Akimoto, A. M.; Kanazawa, H., Thermoresponsive Cationic Block Copolymer Brushes for Temperature-Modulated Stem Cell Separation. *Macromol. Rapid Commun.* **2020,** *41* (19), 2000308.
137. Nagase, K.; Hatakeyama, Y.; Shimizu, T.; Matsuura, K.; Yamato, M.; Takeda, N.; Okano, T., Thermoresponsive Cationic Copolymer Brushes for Mesenchymal Stem Cell Separation. *Biomacromolecules* **2015,** *16* (2), 532-540.
138. Riess, G., Micellization of block copolymers. *Prog. Polym. Sci.* **2003,** *28* (7), 1107-1170.

139. Hadjichristidis, N.; Iatrou, H.; Pitsikalis, M.; Pispas, S.; Avgeropoulos, A., Linear and non-linear triblock terpolymers. Synthesis, self-assembly in selective solvents and in bulk. *Prog. Polym. Sci.* **2005,** *30* (7), 725-782.
140. Hadjichristidis, N., Synthesis of miktoarm star ( μ - star) polymers. *J. Polym. Sci., Part A: Polym. Chem.* **1999,** *37* (7), 857-871.
141. Xiao, J.; He, Q.; Yang, M.; Li, H.; Qiu, X.; Wang, B.; Zhang, B.; Bu, W., Hierarchical self-assembly of miktoarm star copolymers with pathway complexity. *Polymer Chemistry* **2021**.
142. Moad, G.; Chiefari, J.; Chong, Y. K.; Krstina, J.; Mayadunne, R. T. A.; Postma, A.; Rizzardo, E.; Thang, S. H., Living free radical polymerization with reversible addition – fragmentation chain transfer (the life of RAFT). *Polym. Int.* **2000,** *49* (9), 993-1001.
143. Mori, H.; Ebina, Y.; Kambara, R.; Nakabayashi, K., Temperature-responsive self-assembly of star block copolymers with poly (ionic liquid) segments. *Polymer journal* **2012,** *44* (6), 550-560.
144. Lo, C.-T.; Isawa, Y.; Nakabayashi, K.; Mori, H., Design of ion-conductive core-shell nanoparticles via site-selective quaternization of triazole–triazolium salt block copolymers. *European Polymer Journal* **2018,** *105*, 339-347.
145. Zhang, W.; Kochovski, Z.; Schmidt, B. V. K. J.; Antonietti, M.; Yuan, J., Crosslinked 1,2,4-triazolium-type poly(ionic liquid) nanoparticles. *Polymer* **2016,** *107*, 509-516.
146. Mori, H.; Ebina, Y.; Kambara, R.; Nakabayashi, K., Temperature-responsive self-assembly of star block copolymers with poly(ionic liquid) segments. *Polym. J.* **2012,** *44* (6), 550-560.
147. Cao, P.-F.; Wojnarowska, Z.; Hong, T.; Carroll, B.; Li, B.; Feng, H.; Parsons, L.; Wang, W.; Lokitz, B. S.; Cheng, S.; Bocharova, V.; Sokolov, A. P.; Saito, T., A star-shaped single lithium-ion conducting copolymer by grafting a POSS nanoparticle. *Polymer* **2017,** *124*, 117-127.
148. Zhu, L.; Zimudzi, T. J.; Li, N.; Pan, J.; Lin, B.; Hickner, M. A., Crosslinking of comb-shaped polymer anion exchange membranes via thiol–ene click chemistry. *Polymer Chemistry* **2016,** *7* (14), 2464-2475.
149. Suga, T.; Wi, S.; Long, T. E., Synthesis of Diazocine-Containing Poly(arylene ether sulfone)s for Tailored Mechanical and Electrochemical Performance. *Macromolecules* **2009,** *42* (5), 1526-1532.
150. Mohanty, A. D.; Lee, Y.-B.; Zhu, L.; Hickner, M. A.; Bae, C., Anion Exchange Fuel Cell Membranes Prepared from C–H Borylation and Suzuki Coupling Reactions. *Macromolecules* **2014,** *47* (6), 1973-1980.
151. Park, J.-S.; Park, S.-H.; Yim, S.-D.; Yoon, Y.-G.; Lee, W.-Y.; Kim, C.-S., Performance of solid alkaline fuel cells employing anion-exchange membranes. *J. Power Sources* **2008,** *178* (2), 620-626.
152. Srour, H.; Leocmach, M.; Maffeis, V.; Ghogia, A. C.; Denis-Quanquin, S.; Taberlet, N.; Manneville, S.; Andraud, C.; Bucher, C.; Monnereau, C., Poly(ionic liquid)s with controlled architectures and their use in the making of ionogels with high conductivity and tunable rheological properties. *Polymer Chemistry* **2016,** *7* (43), 6608-6616.
153. Teresa Pérez-Prior, M.; Ureña, N.; Tannenberg, M.; del Río, C.; Levenfeld, B., DABCO-functionalized polysulfones as anion-exchange membranes for fuel cell applications: Effect of crosslinking. *J. Polym. Sci., Part B: Polym. Phys.* **2017,** *55* (17), 1326-1336.
154. Zha, Y.; Disabb-Miller, M. L.; Johnson, Z. D.; Hickner, M. A.; Tew, G. N., Metal-Cation-Based Anion Exchange Membranes. *J. Am. Chem. Soc.* **2012,** *134* (10), 4493-4496.

155. Kang, D. H.; Das, G.; Yoon, H. H.; Kim, I. T., A Composite Anion Conducting Membrane Based on Quaternized Cellulose and Poly(Phenylene Oxide) for Alkaline Fuel Cell Applications. *Polymers* **2020,** *12* (11), 2676.
156. Chimene, D.; Lennox, K. K.; Kaunas, R. R.; Gaharwar, A. K., Advanced Bioinks for 3D Printing: A Materials Science Perspective. *Annals of Biomedical Engineering* **2016,** *44* (6), 2090-2102.
157. Lee, K. H.; Zhang, S.; Gu, Y.; Lodge, T. P.; Frisbie, C. D., Transfer Printing of Thermoreversible Ion Gels for Flexible Electronics. *ACS Applied Materials & Interfaces* **2013,** *5* (19), 9522-9527.
158. Klouda, L., Thermoresponsive hydrogels in biomedical applications: A seven-year update. *European Journal of Pharmaceutics and Biopharmaceutics* **2015,** *97*, 338-349.
159. O'Lenick, T. G.; Jiang, X.; Zhao, B., Thermosensitive Aqueous Gels with Tunable Sol−Gel Transition Temperatures from Thermo- and pH-Responsive Hydrophilic ABA Triblock Copolymer. *Langmuir* **2010,** *26* (11), 8787-8796.
160. Ueki, T.; Nakamura, Y.; Usui, R.; Kitazawa, Y.; So, S.; Lodge, T. P.; Watanabe, M., Photoreversible gelation of a triblock copolymer in an ionic liquid. *Angew. Chem.* **2015,** *127* (10), 3061-3065.
161. Imaizumi, S.; Kokubo, H.; Watanabe, M., Polymer Actuators Using Ion-Gel Electrolytes Prepared by Self-Assembly of ABA-Triblock Copolymers. *Macromolecules* **2012,** *45* (1), 401-409.
162. Li, C.; Tang, Y.; Armes, S. P.; Morris, C. J.; Rose, S. F.; Lloyd, A. W.; Lewis, A. L., Synthesis and Characterization of Biocompatible Thermo-Responsive Gelators Based on ABA Triblock Copolymers. *Biomacromolecules* **2005,** *6* (2), 994-999.
163. Ueki, T.; Watanabe, M., Macromolecules in Ionic Liquids: Progress, Challenges, and Opportunities. *Macromolecules* **2008,** *41* (11), 3739-3749.
164. Kitazawa, Y.; Ueki, T.; McIntosh, L. D.; Tamura, S.; Niitsuma, K.; Imaizumi, S.; Lodge, T. P.; Watanabe, M., Hierarchical Sol–Gel Transition Induced by Thermosensitive Self-Assembly of an ABC Triblock Polymer in an Ionic Liquid. *Macromolecules* **2016,** *49* (4), 1414-1423.
165. Wang, C.; Hashimoto, K.; Tamate, R.; Kokubo, H.; Watanabe, M., Controlled Sol–Gel Transitions of a Thermoresponsive Polymer in a Photoswitchable Azobenzene Ionic Liquid as a Molecular Trigger. *Angew. Chem. Int. Ed.* **2018,** *57* (1), 227-230.
166. Wang, C.; Ma, X.; Kitazawa, Y.; Kobayashi, Y.; Zhang, S.; Kokubo, H.; Watanabe, M., From Macromolecular to Small-Molecular Triggers: Facile Method toward Photoinduced LCST Phase Behavior of Thermoresponsive Polymers in Mixed Ionic Liquids Containing an Azobenzene Moiety. *Macromol. Rapid Commun.* **2016,** *37* (23), 1960-1965.
167. Wang, C.; Hashimoto, K.; Tamate, R.; Kokubo, H.; Morishima, K.; Li, X.; Shibayama, M.; Lu, F.; Nakanishi, T.; Watanabe, M., Viscoelastic change of block copolymer ion gels in a photo-switchable azobenzene ionic liquid triggered by light. *Chem. Commun.* **2019,** *55*, 1710-1713.
168. Williams, S. R.; Long, T. E., Recent advances in the synthesis and structure-property relationships of ammonium ionenes. *Progress in Polymer Science (Oxford)* **2009,** *34*, 762-782.
169. Bara, J. E.; O'Harra, K. E., Recent Advances in the Design of Ionenes: Toward Convergence with High-Performance Polymers. *Macromolecular Chemistry and Physics* **2019,** *220* (13), 1900078.

170. Williams, S. R.; Salas-de la Cruz, D.; Winey, K. I.; Long, T. E., Ionene segmented block copolymers containing imidazolium cations: Structure–property relationships as a function of hard segment content. *Polymer* **2010,** *51* (6), 1252-1257.
171. Schreiner, C.; Bridge, A. T.; Hunley, M. T.; Long, T. E.; Green, M. D., Segmented imidazolium ionenes: Solution rheology, thermomechanical properties, and electrospinning. *Polymer* **2017,** *114*, 257-265.
172. Williams, S. R.; Wang, W.; Winey, K. I.; Long, T. E., Synthesis and morphology of segmented poly (tetramethylene oxide)-based polyurethanes containing phosphonium salts. *Macromolecules* **2008,** *41* (23), 9072-9079.
173. Gao, R.; Ramirez, S. M.; Inglefield, D. L.; Bodnar, R. J.; Long, T. E., The preparation of cation-functionalized multi-wall carbon nanotube/sulfonated polyurethane composites. *Carbon* **2013,** *54*, 133-142.
174. Gao, R. Synthesis and Properties of Ion-Containing Block and Segmented Copolymers and Their Composites. Virginia Tech, 2012.
175. Hung, K.-C.; Tseng, C.-S.; Dai, L.-G.; Hsu, S.-h., Water-based polyurethane 3D printed scaffolds with controlled release function for customized cartilage tissue engineering. *Biomaterials* **2016,** *83*, 156-168.
176. Udabe, E.; Isik, M.; Sardon, H.; Irusta, L.; Salsamendi, M.; Sun, Z.; Zheng, Z.; Yan, F.; Mecerreyes, D., Antimicrobial polyurethane foams having cationic ammonium groups. *Journal of Applied Polymer Science* **2017,** *134* (45), 45473.
177. Nelson, A. M.; Long, T. E., Synthesis, Properties, and Applications of Ion-Containing Polyurethane Segmented Copolymers. *Macromolecular Chemistry and Physics* **2014,** *215* (22), 2161-2174.
178. Mucci, V. L.; Hormaiztegui, M. V.; Aranguren, M. I., Plant oil-based waterborne polyurethanes: a brief review. *Journal of Renewable Materials, 8 (6)* **2020**, 579-601.
179. Santamaria-Echart, A.; Fernandes, I.; Barreiro, F.; Corcuera, M. A.; Eceiza, A., Advances in Waterborne Polyurethane and Polyurethane-Urea Dispersions and Their Eco-friendly Derivatives: A Review. *Polymers* **2021,** *13* (3), 409.
180. Zhou, X.; Li, Y.; Fang, C.; Li, S.; Cheng, Y.; Lei, W.; Meng, X., Recent advances in synthesis of waterborne polyurethane and their application in water-based ink: a review. *Journal of Materials Science & Technology* **2015,** *31* (7), 708-722.
181. Joynes, D.; Sherrington, D., Novel polymerizable mono-and divalent quaternary ammonium cationic surfactants: I. Synthesis, structural characterization and homopolymerization. *Polymer* **1996,** *37* (8), 1453-1462.
182. Zhang, K.; Drummey, K. J.; Moon, N. G.; Chiang, W. D.; Long, T. E., Styrenic DABCO salt-containing monomers for the synthesis of novel charged polymers. *Polymer Chemistry* **2016,** *7* (20), 3370-3374.
183. Ayfer, B.; Dizman, B.; Elasri, M. O.; Mathias, L. J.; Avci, D., Synthesis and antibacterial activities of new quaternary ammonium monomers. *Designed monomers and polymers* **2005,** *8* (5), 437-451.
184. Mountrichas, G.; Mantzaridis, C.; Pispas, S., Well‐Defined Flexible Polyelectrolytes with Two Cationic Sites per Monomeric Unit. *Macromol. Rapid Commun.* **2006,** *27* (4), 289-294.
185. Li, P.; Zhao, Q.; Anderson, J. L.; Varanasi, S.; Coleman, M. R., Synthesis of copolyimides based on room temperature ionic liquid diamines. *J. Polym. Sci., Part A: Polym. Chem.* **2010,** *48* (18), 4036-4046.

186. Lee, M.; Choi, U. H.; Colby, R. H.; Gibson, H. W., Ion conduction in imidazolium acrylate ionic liquids and their polymers. *Chemistry of Materials* **2010,** *22* (21), 5814-5822.
187. Lee, M.; Choi, U. H.; Salas‐de la Cruz, D.; Mittal, A.; Winey, K. I.; Colby, R. H.; Gibson, H. W., Imidazolium polyesters: structure–property relationships in thermal behavior, ionic conductivity, and morphology. *Adv. Funct. Mater.* **2011,** *21* (4), 708-717.
188. Muñoz-Bonilla, A.; Fernández-García, M., Polymeric materials with antimicrobial activity. *Prog. Polym. Sci.* **2012,** *37* (2), 281-339.
189. Ogoshi, T.; Masuda, K.; Yamagishi, T.-a.; Nakamoto, Y., Side-chain polypseudorotaxanes with heteromacrocyclic receptors of cyclodextrins (CDs) and Cucurbit [7] uril (CB7): their contrast lower critical solution temperature behavior with α-CD, γ-CD, and CB7. *Macromolecules* **2009,** *42* (21), 8003-8005.
190. Izumrudov, V. A.; Zhiryakova, M. V.; Melik-Nubarov, N. S., Supercharged pyridinium polycations and polyelectrolyte complexes. *Eur. Polym. J.* **2015,** *69*, 121-131.
191. Xuehui, S.; Yu-kun, Y.; Fengcai, L., Novel polyimide ionene: Synthesis and characterization of polyimides containing aromatic bipyridinium salt. *Polymer* **1997,** *38* (18), 4737-4741.
192. Luo, J.; Zhang, L.; Lu, J.; Bai, L.; He, X.; Meng, F., Polymerised ionic liquid crystals bearing imidazolium and bipyridinium groups. *Liq. Cryst.* **2017,** *44* (8), 1293-1305.
193. Kijima, M.; Setoh, K.; Shirakawa, H., Self-doped polyphenylenes containing electron-accepting viologen sde group. *Chem. Lett* **2000,** *29*, 936.
194. Obadia, M. M.; Jourdain, A.; Serghei, A.; Ikeda, T.; Drockenmuller, E., Cationic and dicationic 1, 2, 3-triazolium-based poly (ethylene glycol ionic liquid) s. *Polymer Chemistry* **2017,** *8* (5), 910-917.
195. Tejero, R.; Arbe, A.; Fernández-García, M.; López, D., Nanostructuration by self-assembly in N-alkyl thiazolium and triazolium side-chain polymethacrylates. *Macromolecules* **2015,** *48* (19), 7180-7193.
196. Matsumoto, A.; Odani, T.; Sada, K.; Miyata, M.; Tashiro, K., Intercalation of alkylamines into an organic polymer crystal. *Nature* **2000,** *405* (6784), 328-330.
197. Parvole, J.; Jannasch, P., Poly(arylene ether sulfone)s with phosphonic acid and bis(phosphonic acid) on short alkyl side chains for proton-exchange membranes. *J. Mater. Chem.* **2008,** *18* (45), 5547-5556.
198. Weiber, E. A.; Jannasch, P., Ion Distribution in Quaternary-Ammonium-Functionalized Aromatic Polymers: Effects on the Ionic Clustering and Conductivity of Anion-Exchange Membranes. *ChemSusChem* **2014,** *7*, 2621-2630.
199. Weiber, E. A.; Jannasch, P., Polysulfones with highly localized imidazolium groups for anion exchange membranes. *J. Membr. Sci.* **2015,** *481*, 164-171.
200. Hemp, S. T.; Zhang, M.; Allen, M. H.; Cheng, S.; Moore, R. B.; Long, T. E., Comparing ammonium and phosphonium polymerized ionic liquids: Thermal analysis, conductivity, and morphology. *Macromol. Chem. Phys.* **2013,** *214*, 2099-2107.
201. Anderson, E. B.; Long, T. E., Imidazole- and imidazolium-containing polymers for biology and material science applications. *Polymer* **2010,** *51*, 2447-2454.
202. Green, M. D.; Long, T. E., Designing Imidazole-Based Ionic Liquids and Ionic Liquid Monomers for Emerging Technologies. *Polymer Reviews* **2009,** *49*, 291-314.
203. Wang, Z., Menschutkin Reaction. In *Comprehensive Organic Name Reactions and Reagents*, John Wiley & Sons, Inc.: Hoboken, 2010; pp 1897-1900.

204. Hemp, S. T.; Zhang, M.; Tamami, M.; Long, T. E., Phosphonium ionenes from well-defined step-growth polymerization: thermal and melt rheological properties. *Polymer Chemistry* **2013,** *4*, 3582.
205. Bolto, B. A., Soluble polymers in water purification. *Prog. Polym. Sci.* **1995,** *20*, 987-1041.
206. Ottenbrite, R. M.; Ryan, W. S., Cyclopolymerization of N,N-Dialkyldiallylammonium Halides. A Review and Use Analysis. *Industrial & Engineering Chemistry Product Research and Development* **1980,** *19*, 528-532.
207. Rembaum, A.; Singer, S.; Keyzer, H., Ionene polymers. III. Dicationic crosslinking agents. *Journal of Polymer Science Part B: Polymer Letters* **1969,** *7*, 395-402.
208. Asrof Ali, S.; Zaka Ahmed, S.; Hamad, E. Z. Z.; Ali, S. A.; Ahmed, S. Z.; Hamad, E. Z. Z.; Asrof Ali, S.; Zaka Ahmed, S.; Hamad, E. Z. Z., Cyclopolymerization studies of diallyl- and tetraallylpiperazinium salts. *J. Appl. Polym. Sci.* **1996,** *61*, 1077-1085.
209. Dizman, B.; Elasri, M. O.; Mathias, L. J., Synthesis and antimicrobial activities of new water-soluble bis-quaternary ammonium methacrylate polymers. *J. Appl. Polym. Sci.* **2004,** *94*, 635-642.
210. Kim, T.-S.; Hirao, T.; Ikeda, I., Preparation of bis-quaternary ammonium salts from epichlorohydrin. *Journal of the American Oil Chemists' Society* **1996,** *73*, 943-943.
211. Lin, B.; Qiu, L.; Qiu, B.; Peng, Y.; Yan, F., A soluble and conductive polyfluorene ionomer with pendant imidazolium groups for alkaline fuel cell applications. *Macromolecules* **2011,** *44*, 9642-9649.
212. Zheng, Z.; Xu, Q.; Guo, J.; Qin, J.; Mao, H.; Wang, B.; Yan, F., Structure-Antibacterial Activity Relationships of Imidazolium-Type Ionic Liquid Monomers, Poly(ionic liquids) and Poly(ionic liquid) Membranes: Effect of Alkyl Chain Length and Cations. *ACS Applied Materials and Interfaces* **2016,** *8*, 12684-12692.
213. Zohreh, N.; Tavakolizadeh, M.; Hosseini, S. H.; Pourjavadi, A.; Bennett, C., Tungstate-loaded triazine-based magnetic poly(Bis-imidazolium ionic liquid): An effective bi-functional catalyst for tandem selective oxidation/Knoevenagel condensation in water. *Polymer (United Kingdom)* **2017,** *112*, 342-350.
214. Jheng, L. c.; Hsu, S. L. c.; Lin, B. y.; Hsu, Y. l., Quaternized polybenzimidazoles with imidazolium cation moieties for anion exchange membrane fuel cells. *J. Membr. Sci.* **2014,** *460*, 160-170.
215. Allen, M. H.; Green, M. D.; Getaneh, H. K.; Miller, K. M.; Long, T. E., Tailoring charge density and hydrogen bonding of imidazolium copolymers for efficient gene delivery. *Biomacromolecules* **2011,** *12*, 2243-50.
216. Chen, X.; Zhao, J.; Zhang, J.; Qiu, L.; Xu, D.; Zhang, H.; Han, X.; Sun, B.; Fu, G.; Zhang, Y.; Yan, F., Bis-imidazolium based poly(ionic liquid) electrolytes for quasi-solid-state dye-sensitized solar cells. *J. Mater. Chem.* **2012,** *22*, 18018.
217. Muñoz-Bonilla, A.; Fernández-García, M., Polymeric materials with antimicrobial activity. *Prog. Polym. Sci.* **2012,** *37*, 281-339.
218. Kijima, M.; Setoh, K.; Shirakawa, H., Synthesis of a novel ionic liquid crystalline polythiophene having viologen side chain. *Chem. Lett.* **2000,** *20*, 936-937.
219. Yang, X.; Liu, L.; Yang, W., Direct preparation of monodisperse core-shell microspheres with surface antibacterial property by using bicationic viologen surfmer. *Polymer* **2012,** *53*, 2190-2196.
220. Yang, H.; Tan, Y.; Hao, J.; Yang, H.; Liu, F., Side-chain polypseudorotaxanes by threading cucurbit[7]uril onto poly-N-n-butyl-N′-(4-vinylbenzyl)-4,4′-bipyridinium bromide

chloride: Synthesis, characterization, and properties. *Journal of Polymer Science, Part A: Polymer Chemistry* **2010,** *48*, 2135-2142.
221. Wang, Z.; Tsarevsky, N. V., Well-defined polymers containing high density of pendant viologen groups. *Journal of Polymer Science, Part A: Polymer Chemistry* **2017,** *55*, 1173-1182.
222. Li, X.; Liu, Q.; Yu, Y.; Meng, Y., Synthesis and properties of multiblock ionomers containing densely functionalized hydrophilic blocks for anion exchange membranes. *J. Membr. Sci.* **2014,** *467*, 1-12.
223. Weiber, E. A.; Jannasch, P., Anion-conducting polysulfone membranes containing hexa-imidazolium functionalized biphenyl units. *J. Membr. Sci.* **2016,** *520*, 425-433.
224. Weiber, E. A.; Meis, D.; Jannasch, P., Anion conducting multiblock poly(arylene ether sulfone)s containing hydrophilic segments densely functionalized with quaternary ammonium groups. *Polym. Chem.* **2015,** *6*, 1986-1996.
225. Li, N.; Zhang, Q.; Wang, C.; Lee, Y. M.; Guiver, M. D., Phenyltrimethylammonium functionalized polysulfone anion exchange membranes. *Macromolecules* **2012,** *45*, 2411-2419.
226. Wu, X.; Chen, W.; Yan, X.; He, G.; Wang, J.; Zhang, Y.; Zhu, X., Enhancement of hydroxide conductivity by the di-quaternization strategy for poly(ether ether ketone) based anion exchange membranes. *Journal of Materials Chemistry A* **2014,** *2*, 12222.
227. Mountrichas, G.; Pispas, S., Novel double hydrophilic block copolymers based on poly(p-hydroxystyrene) derivatives and poly(ethylene oxide). *J. Polym. Sci., Part A: Polym. Chem.* **2007,** *45* (24), 5790-5799.
228. Štěpánek, M.; Matějíček, P.; Procházka, K.; Filippov, S. K.; Angelov, B.; Šlouf, M.; Mountrichas, G.; Pispas, S., Polyelectrolyte−Surfactant Complexes Formed by Poly[3,5-bis(trimethylammoniummethyl)4-hydroxystyrene iodide]-block-poly(ethylene oxide) and Sodium Dodecyl Sulfate in Aqueous Solutions. *Langmuir* **2011,** *27* (9), 5275-5281.
229. Hajduová, J.; Procházka, K.; Šlouf, M.; Angelov, B.; Mountrichas, G.; Pispas, S.; Štěpánek, M., Polyelectrolyte–Surfactant Complexes of Poly[3,5-bis(dimethylaminomethyl)-4-hydroxystyrene]-block-poly(ethylene oxide) and Sodium Dodecyl Sulfate: Anomalous Self-Assembly Behavior. *Langmuir* **2013,** *29* (18), 5443-5449.
230. Karayianni, M.; Radeva, R.; Koseva, N.; Pispas, S., Electrostatic complexation of a double hydrophilic block polyelectrolyte and proteins of different molecular shape. *J. Polym. Sci., Part B: Polym. Phys.* **2016,** *54* (15), 1515-1529.
231. Murmiliuk, A.; Matějíček, P.; Filippov, S. K.; Janata, M.; Šlouf, M.; Pispas, S.; Štěpánek, M., Formation of core/corona nanoparticles with interpolyelectrolyte complex cores in aqueous solution: insight into chain dynamics in the complex from fluorescence quenching. *Soft Matter* **2018,** *14* (37), 7578-7585.
232. Pham, T. H.; Jannasch, P., Aromatic Polymers Incorporating Bis-N-spirocyclic Quaternary Ammonium Moieties for Anion-Exchange Membranes. *ACS Macro Letters* **2015,** *4*, 1370-1375.
233. Wu, L.; Zhang, Z.; Ran, J.; Zhou, D.; Li, C.; Xu, T., Advances in proton-exchange membranes for fuel cells: an overview on proton conductive channels (PCCs). *PCCP* **2013,** *15* (14), 4870-4887.
234. Freyer, J. L.; Brucks, S. D.; Campos, L. M., Fully charged: Maximizing the potential of cationic polyelectrolytes in applications ranging from membranes to gene delivery through rational design. *J. Polym. Sci., Part A: Polym. Chem.* **2017,** *55*, 3167-3174.

235. Choi, J. H.; Willis, C. L.; Winey, K. I., Structure-property relationship in sulfonated pentablock copolymers. *J. Membr. Sci.* **2012,** *394-395*, 169-174.
236. Filice, S.; D'Angelo, D.; Scarangella, A.; Iannazzo, D.; Compagnini, G.; Scalese, S., Highly effective and reusable sulfonated pentablock copolymer nanocomposites for water purification applications. *RSC Adv.* **2017,** *7*, 45521-45534.
237. Margaretta, E.; Fahs, G. B.; Inglefield, D. L.; Jangu, C.; Wang, D.; Heflin, J. R.; Moore, R. B.; Long, T. E., Imidazolium-Containing ABA Triblock Copolymers as Electroactive Devices. *Acs Applied Materials & Interfaces* **2016,** *8* (2), 1280-1288.
238. Watson, B. M.; Kasper, F. K.; Mikos, A. G., Phosphorous-containing polymers for regenerative medicine. *Biomedical Materials* **2014,** *9*, 025014.
239. Savage, A. M.; Li, Y.; Matolyak, L. E.; Doncel, G. F.; Turner, S. R.; Gandour, R. D., Anti-HIV activities of precisely defined, semirigid, carboxylated alternating copolymers. *J. Med. Chem.* **2014,** *57*, 6354-6363.
240. Ju, L.; Mondschein, R. J.; Vandenbrande, J. A.; Arrington, C. B.; Long, T. E.; Moore, R. B., Phosphonated Poly(ethylene terephthalate) ionomers as compatibilizers in extruded Poly(ethylene terephthalate)/Poly(m-xylylene adipamide) blends and oriented films. *Polymer* **2020,** *205*, 122891.
241. Cao, K.; Serrano, J. M.; Liu, T.; Stovall, B. J.; Xu, Z.; Arrington, C. B.; Long, T. E.; Odle, R. R.; Liu, G., Impact of metal cations on the thermal, mechanical, and rheological properties of telechelic sulfonated polyetherimides. *Polymer Chemistry* **2020,** *11* (2), 393-400.
242. Fitzgerald, J. J.; Weiss, R. A., Synthesis, Properties, and Structure of Sulfonate Ionomers. *Journal of Macromolecular Science, Part C: Polymer Reviews* **1988,** *28*, 99-185.
243. Iojoiu, C.; Maréchal, M.; Chabert, F.; Sanchez, J.-Y., Mastering Sulfonation of Aromatic Polysulfones: Crucial for Membranes for Fuel Cell Application. *Fuel Cells* **2005,** *5* (3), 344-354.
244. Takamuku, S.; Jannasch, P., Properties and degradation of hydrocarbon fuel cell membranes: a comparative study of sulfonated poly(arylene ether sulfone)s with different positions of the acid groups. *Polymer Chemistry* **2012,** *3*, 1202.
245. Unveren, E. E.; Erdogan, T.; Çelebi, S. S.; Inan, T. Y., Role of post-sulfonation of poly(ether ether sulfone) in proton conductivity and chemical stability of its proton exchange membranes for fuel cell. *Int. J. Hydrogen Energy* **2010,** *35*, 3736-3744.
246. Skalski, T. J. G.; Britton, B.; Peckham, T. J.; Holdcroft, S., Structurally-Defined, Sulfo-Phenylated, Oligophenylenes and Polyphenylenes. *J. Am. Chem. Soc.* **2015,** *137*, 12223-12226.
247. Wang, F.; Hickner, M.; Kim, Y. S.; Zawodzinski, T. A.; McGrath, J. E., Direct polymerization of sulfonated poly(arylene ether sulfone) random (statistical) copolymers: Candidates for new proton exchange membranes. *J. Membr. Sci.* **2002,** *197*, 231-242.
248. Lee, K. H.; Lee, S. Y.; Shin, D. W.; Wang, C.; Ahn, S. H.; Lee, K. J.; Guiver, M. D.; Lee, Y. M., Structural influence of hydrophobic diamine in sulfonated poly(sulfide sulfone imide) copolymers on medium temperqture PEM fuel cell. *Polymer (United Kingdom)* **2014,** *55*, 1317-1326.
249. Xie, W.; Geise, G. M.; Freeman, B. D.; Lee, H. S.; Byun, G.; McGrath, J. E., Polyamide interfacial composite membranes prepared from m-phenylene diamine, trimesoyl chloride and a new disulfonated diamine. *J. Membr. Sci.* **2012,** *403-404*, 152-161.

250. Miyake, J.; Watanabe, M.; Miyatake, K., Sulfonated Poly(arylene ether phosphine oxide ketone) Block Copolymers as Oxidatively Stable Proton Conductive Membranes. *ACS Applied Materials & Interfaces* **2013,** *5*, 5903-5907.
251. Liao, H.; Zhang, K.; Tong, G.; Xiao, G.; Yan, D., Sulfonated poly(arylene ether phosphine oxide)s with various distributions and contents of pendant sulfonic acid groups synthesized by direct polycondensation. *Polym. Chem.* **2014,** *5*, 412-422.
252. Liu, C.; Li, L.; Liu, Z.; Guo, M.; Jing, L.; Liu, B.; Jiang, Z.; Matsumoto, T.; Guiver, M. D., Sulfonated naphthalenic polyimides containing ether and ketone linkages as polymer electrolyte membranes. *J. Membr. Sci.* **2011,** *366*, 73-81.
253. Park, C. H.; Lee, C. H.; Guiver, M. D.; Lee, Y. M., Sulfonated hydrocarbon membranes for medium-temperature and low-humidity proton exchange membrane fuel cells (PEMFCs). *Prog. Polym. Sci.* **2011,** *36* (11), 1443-1498.
254. Maier, G.; Meier-Haack, J., Sulfonated Aromatic Polymers for Fuel Cell Membranes. In *Fuel Cells II*, Scherer, G. G., Ed. Springer Berlin Heidelberg: Berlin, Heidelberg, 2008; pp 1-62.
255. Takamuku, S.; Jannasch, P., Multiblock Copolymers with Highly Sulfonated Blocks Containing Di- and Tetrasulfonated Arylene Sulfone Segments for Proton Exchange Membrane Fuel Cell Applications. *Advanced Energy Materials* **2012,** *2* (1), 129-140.
256. Takamuku, S.; Jannasch, P., Multiblock copolymers containing highly sulfonated poly(arylene sulfone) blocks for proton conducting electrolyte membranes. *Macromolecules* **2012,** *45*, 6538-6546.
257. Jutemar, E. P.; Takamuku, S.; Jannasch, P., Sulfonated poly(arylene ether sulfone) ionomers containing di- and tetrasulfonated arylene sulfone segments. *Polym. Chem.* **2011,** *2*, 181-191.
258. Weiber, E. A.; Takamuku, S.; Jannasch, P., Highly proton conducting electrolyte membranes based on poly(arylene sulfone)s with tetrasulfonated segments. *Macromolecules* **2013,** *46*, 3476-3485.
259. Bingöl, B.; Jannasch, P., CHAPTER 13. Proton Conducting Phosphonated Polymers and Membranes for Fuel Cells. 2014; pp 271-293.
260. Parvole, J.; Jannasch, P., Polysulfones Grafted with Poly(vinylphosphonic acid) for Highly Proton Conducting Fuel Cell Membranes in the Hydrated and Nominally Dry State. *Macromolecules* **2008,** *41*, 3893-3903.
261. Perrin, R.; Elomaa, M.; Jannasch, P., Nanostructured proton conducting polystyrene-poly(vinylphosphonic acid) block copolymers prepared via sequential anionic polymerizations. *Macromolecules* **2009,** *42*, 5146-5154.
262. Abouzari-Lotf, E.; Ghassemi, H.; Shockravi, A.; Zawodzinski, T.; Schiraldi, D., Phosphonated poly(arylene ether)s as potential high temperature proton conducting materials. *Polymer* **2011,** *52*, 4709-4717.
263. Higashihara, T.; Fukuzaki, N.; Tamura, Y.; Rho, Y.; Nakabayashi, K.; Nakazawa, S.; Murata, S.; Ree, M.; Ueda, M., Polymer electrolyte membrane based on polyacrylate with phosphonic acidvia long alkyl side chains. *J. Mater. Chem. A* **2013,** *1*, 1457-1464.
264. Liu, B.; Robertson, G. P.; Guiver, M. D.; Shi, Z.; Navessin, T.; Holdcroft, S., Fluorinated poly(aryl ether) containing a 4-bromophenyl pendant group and its phosphonated derivative. *Macromol. Rapid Commun.* **2006,** *27*, 1411-1417.
265. Penelle, J.; Xie, T., Synthesis, characterization, and thermal properties of poly(trimethylene-1,1-dicarboxylate) polyelectrolytes. *Macromolecules* **2001,** *34*, 5083-5089.

266. Li, Y.; Zhang, M.; Mao, M.; Turner, S. R.; Moore, R. B.; Mourey, T. H.; Slater, L. A.; Hauenstein, J. R., Chain stiffness of stilbene containing alternating copolymers by SAXS and SEC. *Macromolecules* **2012,** *45*, 1595-1601.
267. Li, Y.; Mao, M.; Matolyak, L. E.; Turner, S. R., Sterically crowded anionic polyelectrolytes with tunable charge densities based on stilbene-containing copolymers. *ACS Macro Letters* **2012,** *1*, 257-260.
268. Savage, A. M.; Ullrich, E.; Chin, S. M.; Kiernan, Z.; Kost, C.; Turner, S. R., Synthesis and characterization of double hydrophilic block copolymers containing semi-rigid and flexible segments. *J. Polym. Sci., Part A: Polym. Chem.* **2015,** *53* (2), 219-227.
269. Savage, A. M.; Ullrich, E.; Kost, C.; Turner, S. R., Salt- and pH-Responsive Semirigid/Flexible Double-Hydrophilic Block Copolymers. *Macromol. Chem. Phys.* **2016,** *217* (15), 1737-1744.

# Chapter 6: **Vat photopolymerization of unsaturated polyesters utilizing a polymerizable ionic liquid as a non-volatile reactive diluent**

Published in *Polymer* **2021,** *223*, 123727.

B. Tyler White,[a] Viswanath Meenakshisundaram,[b] Keyton D. Feller,[b] Christopher B. Williams,[b] Timothy E. Long [c*]

[a]Department of Chemistry, Macromolecules Innovation Institute (MII), Virginia Tech, Blacksburg, VA 24061, USA
[b]Department of Mechanical Engineering, Macromolecules Innovation Institute (MII), Virginia Tech, Blacksburg, VA 24061, USA
[c]Biodesign Center for Sustainable Macromolecular Materials and Manufacturing, School for Molecular Sciences, Arizona State University, Tempe, AZ 85287, USA

*To whom correspondence should be addressed: E-mail: Timothy.E.Long@asu.edu.

**Keywords**: unsaturated polyesters, additive manufacturing, vat photopolymerization, ionic liquid

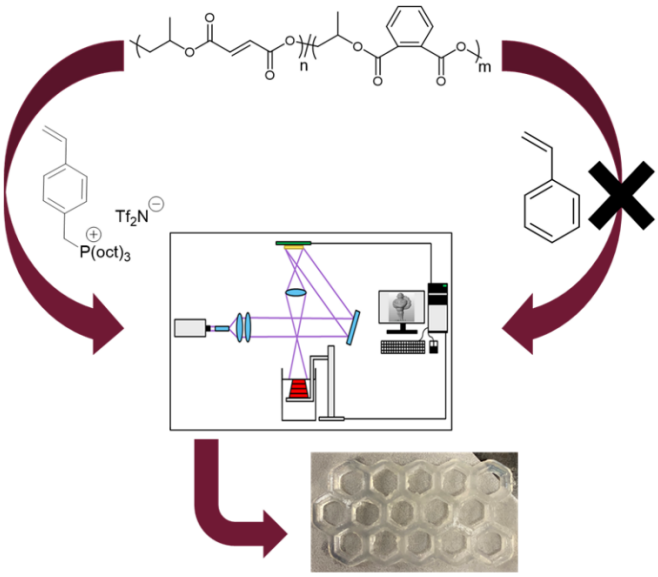


## 6.1 Abstract

Unsaturated polyester resins (UPRs) enjoy numerous applications as structural adhesives in glass fiber laminates, concrete flooring, and masonry repair. Typically, UPRs consist of unsaturated polyester (UPE) oligomers with up to 50 wt.% of a reactive diluent such as styrene.

The ability of these resins to cure rapidly upon UV irradiation, in conjunction with a photoinitiator, enables vat photopolymerization (VP) 3D printing. However, the volatility and toxicity of styrene limits the use of traditional UPRs for VP. This report describes a nonvolatile ionic liquid reactive diluent for UPRs, which, in combination with the unreactive diluent dimethoxyethane, produce resins suitable for VP. Photorheological experiments help guide resin design for VP based on a series of synthesized UPEs and PIL concentrations. Photocured networks exhibit increasing degradation temperatures with increasing PIL incorporation from 215 to 279 °C. VP of a selected UPR composition demonstrated the ability to form self-supporting, geometrically complex 3D printed structures, suggesting the opportunity to utilize a common industrial feedstock as a component of a novel VP resin system. Dried and unextracted 3D printed test specimens exhibit ionic conductivities spanning from $10^{-8}$ to $10^{-5}$ S $cm^{-1}$ between 60 and 150 °C, which indicate a potential additional attribute for 3D printed UPE parts.

## 6.2 Introduction

Unsaturated polyester resins (UPR) find extensive use in fiber-reinforced composites due to their ease of processability, low cost, and synthetic versatility.[1, 2] Glass-fiber-reinforced (GFR) resins consist of an unsaturated polyester (UPE) oligomer dissolved in a reactive diluent (typically styrene), which are then mixed with chopped glass fibers, compression molded, and thermally cured to produce a final part. The synthesis of UPEs usually proceeds with the reaction of a diol with an unsaturated anhydride or acid and often requires the presence of a catalyst to promote esterification. Propylene glycol and maleic anhydride are the most common monomers for UPE synthesis; however, a variety of different diols and anhydrides are suitable to produce UPEs with a wide range of physical properties.[3-5] Moreover, the incorporation of a small amount of a saturated anhydride, such as phthalic anhydride, improves the solubility of UPEs in styrene and provides

control over the crosslinking density of the final UPR.[6] In a typical industrial process, UPE synthesis involves the melt polycondensation of propylene glycol, maleic anhydride (MA), and phthalic anhydride (PA).[3, 7-9] Conducting the reaction at temperatures in excess of 200 °C ensures that a majority of the maleic acid isomerizes to the more reactive fumaric acid during the process. Additionally, *p*-xylene acts as an azeotroping agent in conjunction with a nitrogen purge to drive the reaction to completion through continuous removal of the condensate, i.e., water, from the reactor.

A reactive diluent, such as styrene, serves to reduce the viscosity of the UPE and provide an efficient environment for radical crosslinking to occur. However, due to the volatility and carcinogenicity of styrene, slightly less dangerous vinyl and acrylic monomers often serve as alternate reactive diluents. Examples of these alternative reactive diluents include divinylbenzene, divinyl ethers, N-vinylpyrrolidone, and methyl acrylates.[4, 10-12] Although these monomers are also toxic and volatile, they tend to produce less of an odor than styrene, which makes them more appealing for industrial applications. Polymerizable ionic liquids (PILs) represent another interesting, albeit unexplored, class of reactive diluents for crosslinking UPEs. Ionic liquids (ILs) have exhibited promise as green polymerization solvents due to their low volatility and chemical stabilities. Furthermore, many examples of ILs containing polymerizable moieties exist commercially and within the literature.[13-15] Utilizing PILs as a reactive diluent in UPRs will provide a less volatile replacement to styrene as well as impart additional functionality (e.g. ionic conductivity, hydrophobicity, thermal stability) into cured UPR networks.[16] Currently, only one example of ionically conductive UPRs exists in literature to the best of our knowledge.[17] Sassman and Weichold synthesized poly(ethylene glycol) based UPEs doped with lithium salt and crosslinked with styrene. They demonstrated the ability to use these resins as resistivity sensors in

concrete on construction sites. This result suggests that UPRs formulated with PILs may also prove interesting for electronic applications.

Vat photopolymerization (VP, also referred to as "stereolithography") additive manufacturing (AM) produces 3D structures in a layer-by-layer process using light to selectively cure a vat of liquid photopolymer.[18-21] The toxicity of styrene becomes especially pertinent when considering the use of UPRs as a resin for VP. Most VP printers operate with an open vat outside of a fume hood, which can lead to inhalation of the dangerous monomer. Recent examples form literature include several examples of AM of UPRs for cell scaffolds.[22-26] Gonçalves and Coelho *et al.* synthesized UPEs from bio-based acids and 3D printed cell scaffolds using microstereo-thermal lithography.[23] Although this technique produced cell scaffolds with high resolution and good cell adhesion and proliferation, the resin still required the use of styrene, which is not ideal for use in an open vat. One common approach to avoid the use of styrene involves utilizing diethyl fumarate (DEF) as a reactive diluent.[22, 24, 25] For example, Luo and Becker *et al.* use this method to VP biodegradable cell scaffolds from UPRs containing poly(propylene fumarate) and DEF.[22] Although their synthetic method produces UPEs with precise molecular weights and narrow distributions, the procedure requires an additional step for catalytic isomerization to obtain the *trans* fumarate isomer. In this study, we present a low-volatility UPR using industrially relevant processes for the UPE synthesis and leveraging a PIL reactive diluent to allow for VP processing. We explore the structure-property-processing relationships of the photocured UPRs and demonstrate the ability to print high-resolution 3D structures.

## 6.3 Experimental Section

### 6.3.1 Materials

Maleic anhydride (MA, ≥ 99%), 4-vinylbenzyl chloride (VBC, ≥ 90%), and 0.1 M KOH solution were purchased from Fluka Analytical. Phthalic anhydride (PA, ≥ 99%), 1,2-propanediol (PG, ≥ 99.5%), trioctylphosphine (TOP, 90%), diphenyl(2,4,6-trimethylbenzoyl)phosphine oxide (TPO, 97%), 2,6-di-tert-butyl-4-methylphenol (BHT, ≥ 99%), phenolphthalein (reagent grade), p-xylene (≥ 99%), and diethylene glycol dimethyl ether (dimethoxyethane, 99%) were all purchased from Sigma Aldrich. Acetonitrile and toluene (HPLC grade) were purchased from Fisher Chemical and ethanol (200 proof) was purchased from Deacon Laboratories. Lithium bis(trifluoromethanesulfonyl) imide ($LiTf_2N$, >98%) and 2,5-bis(5-tert-butyl-benzoxazol-2-yl) thiophene (BBOT, >98%) were purchased from Tokyo Chemical Industry. All reagents were used as received unless otherwise indicated. Ultra-high purity Ar gas (99.999%) was purchased from Praxair.

## 6.3.2 Synthesis of UPE oligomers

The synthesis of the UPE oligomers was derived and modified from previous literature examples.[3, 7-9] In a typical reaction, 1,2-propanediol (20.000 g, 0.263 mol), MA (11.714 g, 0.119 mol), and PA (17.696 g, 0.119 mol) were added to a 250-mL, 3-necked, round-bottomed flask equipped with a rubber septum, a custom glass adapter with a spherical socket joint, and a Dean-Stark apparatus with a condenser. The ratio of MA to PA was varied dependent on the targeted PA content in the polyester backbone. A steel mechanical stir rod was passed through the glass adapter to provide overhead mechanical stirring, and the spherical socket was connected to a spherical ball joint attached to Tygon® tubing to create a seal around the stir rod. Argon was continuously flowed through the system via an inlet inserted into the rubber septum and an outlet from the condenser leading to a bubbler. The reaction mixture became a homogeneous liquid upon stirring at 130 °C. The reaction progress was monitored periodically by titrating aliquots with 0.1 M KOH to obtain

the acid number (ASTM D4662). Once the acid number dropped to 200 mg KOH $g^{-1}$, the reaction temperature was increased to 165 °C and 6 wt.% of p-xylene was added as an azeotroping agent to facilitate water removal during the polycondensation. After the acid number fell to 130 mg KOH $g^{-1}$ the temperature was increased to 210 °C for the remainder of the reaction. The reaction was terminated upon cooling to room temperature once the acid number decreased to between 30 – 40 mg KOH $g^{-1}$.

### 6.3.3 Synthesis of 4-vinylbenzyltrioctylphosphonium chloride (VBTOP Cl)

TOP (55.19 g, 0.149 mol), VBC (25 g, 0.164 mol), and acetonitrile (400 mL) were added to a single-necked round-bottomed flask equipped with a magnetic stir bar. A small amount of BHT (<1 wt.%) was added as a radical inhibitor to the solution in order to prevent premature polymerization of the styrenic monomers. The reaction solution was sparged with argon and allowed to react at 70 °C for 24 h. Acetonitrile was removed by rotary evaporation and the product remained as a white powder. The powder was recrystallized from hexanes, filtered, and washed 3 times with cold hexanes (~400 mL). The final product was dried overnight at 40 °C under reduced pressure (~0.1 in Hg) to give a yield of > 90%. $^{1}$H NMR (400 MHz, $CDCl_3$, 25 °C) (δ, ppm): 0.87 (9H, m, -$CH_3$), 1.17 – 1.50 (36 H, broad, -$(CH_2)_6$-), 2.39 (6H, m, P-$CH_2$-), 4.30 (2H, d, phenyl-$CH_2$-P-), 5.28 (1H, dt, =CH-), 5.74 (1H, dt, =$CH_2$ cis), (1H, q, =$CH_2$ trans), 7.39 (4H, m, phenyl). $^{31}$P NMR (400 MHz, $CDCl_3$, 25 °C) (δ, ppm): 31.5 (1P, s) (**Figure S6.2**).

### 6.3.4 Ion exchange to 4-vinylbenzyltrioctylphosphonium bis(trifluoromethanesulfonyl)imide (VBTOP Tf2N)

VBTOP Cl (25 g, 0.048 mol) was added to a 250 mL beaker equipped with a magnetic stir bar and dissolved in acetone (100 mL). In a separate 1-L beaker, an excess of $LiTf_2N$ (75.5 g, 0.263

mol) was also dissolved in acetone (300 mL) under magnetic stirring. The two solutions were combined and allowed to stir for 24 h to facilitate the ion exchange. Acetone was removed by rotary evaporation to afford a mixture of a viscous liquid and LiCl. The product was dissolved in dichloromethane and washed 3 times with DI water to remove the LiCl salt. Subsequent rotary evaporation and drying under reduced pressure produced a viscous, room temperature PIL (yield > 95%). A small aliquot of VBTOP $Tf_2N$ was dissolved in acetone and 1-3 drops of $AgNO_3$ solution was added to confirm that the ion exchange was complete; if any chloride anions remained, an ion exchange would occur to form AgCl as a white precipitate. Quantitative ion exchange was further confirmed by chemical shifts in the $^1H$ NMR spectrum compared to the VBTOP Cl. $^1H$ NMR (400 MHz, $CDCl_3$, 25 °C) (δ, ppm): 0.87 (9H, m, $-CH_3$), 1.17 – 1.50 (36 H, broad, $-(CH_2)_6-$), 2.08 (6H, m, P-$CH_2$-), 3.60 (2H, d, phenyl-$CH_2$-P-), 5.28 (1H, dt, =CH-), 5.74 (1H, dt, $=CH_2$ cis), (1H, q, $=CH_2$ trans), ), 7.19 (2H, dd, phenyl) 7.39 (2H, d, phenyl). $^{31}P$ NMR (400 MHz, $CDCl_3$, 25 °C) (δ, ppm): 31.5 (1P, s).

### 6.3.5 VP 3D Printing

Liquid photopolymer resins were produced containing 60 wt.% of UPE-23 and 40 wt.% VBTOP $TF_2N$ diluted with 30 wt.% (relative to total UPE and VBTOP) dimethoxyethane. In a typical procedure, UPE-23 (63 g) and VBTOP $TF_2N$ (42 g, 0.0542 mol) were added to a 250-mL jar with a stir bar. Next, 45 mL of dimethoxyethane was added and the solution was stirred until the solution became homogeneous. TPO (1.57 g, 0.0045 mol) and BBOT (0.105 g, 2.44 mmol) were dissolved in the remaining 3 mL of dimethoxyethane and added to the UPE solution to bring the final concentration to 70 wt.% solids. A custom VP printer was used to fabricate 3D objects with the prepared resin. The printer comprised of a LED projector (405 nm) as the light source. A UV projector (PRO4710:Wintech Digital), with a projected pixel size of 35.5 microns and a projection

area of 68x38 mm, was used to project patterned UV light on the resin surface with an intensity of 30 mw/cm$^2$. A custom vat and recoating system were built to contain and recoat the resin during the layer-by-layer manufacturing process. A glass build stage was mounted to a z-elevator, and the layer thickness was controlled using a combination of dipping in the resin and recoating blade-mediated smoothening. Each 100 μm thick layer was cured for 13 s at an intensity of 30 mW/cm$^2$ using a 405 nm wavelength of light.

### 6.3.6 Analytical methods

Nuclear magnetic resonance spectroscopy (NMR) was performed on an Agilent U4-DD2 spectrometer at 23 °C and 400 MHz. Polyester oligomers and PIL were dissolved in deuterated chloroform ($CDCl_3$) to obtain $^1$H NMR and $^{31}$P NMR spectra. A TA Instruments Q500 facilitated thermogravimetric analysis (TGA) experiments at a heating rate of 10 °C min$^{-1}$ from 23 °C to 800 °C under nitrogen flow. Subsequently, differential scanning calorimetry (DSC) was performed on vacuum-dried samples in a TA Instruments DSC Q2000. Glass transition temperatures ($T_g$) were determined at the half-height midpoint of the endothermic step transitions. Photorheological experiments utilized a TA instruments Discovery HR2 rheometer equipped with a photo attachment containing a 20 mm quartz bottom geometry to allow for penetration of UV light into the sample. The photocurable solutions were oscillated at 1 Hz and 0.1% strain at room temperature and allowed to equilibrate for 30 s before being irradiated with UV light at 250 mW/cm$^2$ for 5 minutes. The storage and loss moduli (G' and G") were measured throughout, and the crossover point was evaluated at the first point in which the storage modulus exceeded the loss modulus.

Electrochemical impedance spectroscopy (EIS) was performed on a Metrohm Autolab PGSTAT302N operating in two-electrode mode. In-plane impedance measurements were carried

out by sandwiching 3D printed films in a Teflon® supported conductivity cell and measuring the impedance across the film as a function of frequency from 0.1 – 100,000 Hz at an amplitude of 0.3 V. All experiments were carried out in an Espec BTL-433 benchtop environmental chamber. Samples were equilibrated at each temperature for 10 min before measuring the impedance in triplicate. Ionic conductivities were calculated using the following equation:

$$\sigma = \frac{L}{AR}$$

where σ is the ionic conductivity, L is the length between the two electrodes, A is the cross-sectional area, and R is the resistance. The resistance was taken as the Z value extrapolated to 0 Hz from the plateau in the Bode plot (**Figure S6.4B**). The three-parameter Vogel-Fulcher-Tammann (VFT) equation is as follows:

$$\sigma\,(T) = \sigma_0\, exp\, \frac{-B}{T - T_0}$$

where σ (T) is the ionic conductivity at a given temperature, B is a constant related to the activation energy, and $T_0$ is the Vogel temperature where the motion of ions stops. To determine the VFT parameters, the VFT equation was fit to the conductivity data using the Excel Solver tool.

Scanning electron microscopy (SEM) was performed using a JEOL JSM IT500HR scanning electron microscope. A Cressington sputter coater 208HR provided a 10 nm Au/Pd conductive coating on 3D printed structures. This coating allowed for high resolution images at 500x, 100x, 25x, and 10x magnification. The secondary electron detector maintained 15.0 kV for all images.

## 6.4 Results and Discussion

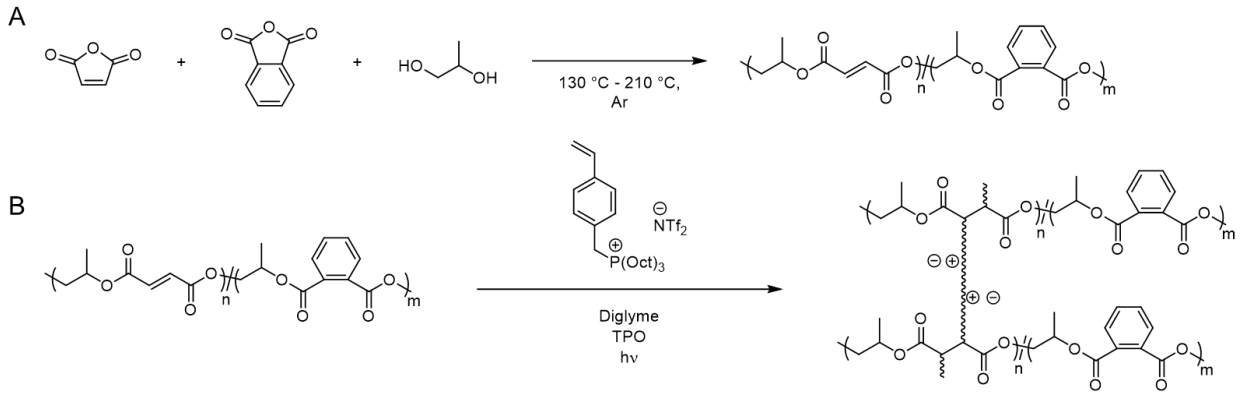


**Scheme 6.1**: (A) Synthesis of UPE oligomers and (B) Subsequent photocuring of UPE oligomers with a phosphonium PIL reactive diluent.

The synthesis of UPEs containing propylene glycol (PG) proceeded as shown in **Scheme 6.1A**. Monitoring the acid-number with titrations throughout the reaction allowed for the synthesis of oligomers with targeted number-average molecular weights between approximately 1.5 - 2.0 kg/mol. Targeting this number-average molecular weight ensured that the polymer would not crosslink prematurely and improved the solubility of the UPE in the diluent.[3] Two temperature regimes facilitated the synthesis of UPE oligomers. First, monoester formation occurred at 130 °C between the diol and the ring-opened diacids.[7, 9] Second, polycondensation occurred above 160 °C with the addition of p-xylene, which acted as an azeotropic agent to facilitate water removal and drive the equilibrium forward. Performing the temperature ramp in stages helped to minimize loss of the PG due to volatilization. Upon completion of the reaction and subsequent cooling, PG-based UPEs all behaved as brittle solids with a colorless to pale yellow appearance.

$^{1}$H NMR spectroscopy allowed for the calculation of the phthalic anhydride (PA) incorporation (**Figure S6.1**) as well as the percentage of fumarate (*trans*) and maleate (*cis*) isomers present in the backbone. Compositional information for each UPE is tabulated in **Table 6.1**, and the copolymer nomenclature follows the convention of "UPE-x" where "x" represents the calculated

mol% of PA in the final product. Heating the reaction to a final temperature above 200 °C facilitated isomerization of the maleate to fumarate,[1, 27] which resulted in the UPEs containing between 94-97 mol% of fumarate isomers. Obtaining high degrees of isomerization in the UPE leads to fast curing times due to the increased reactivity of the trans isomer (fumarate) compared to the cis (maleate).[3, 28] Differential scanning calorimetry revealed predictable trends in $T_g$s for both UPE series. As shown in **Figure 6.1**, UPE-0 displayed a $T_g$ of 18 °C. The $T_g$ increased with addition of the rigid PA monomer from 24 °C for UPE-23, to 38 °C for UPE-37.

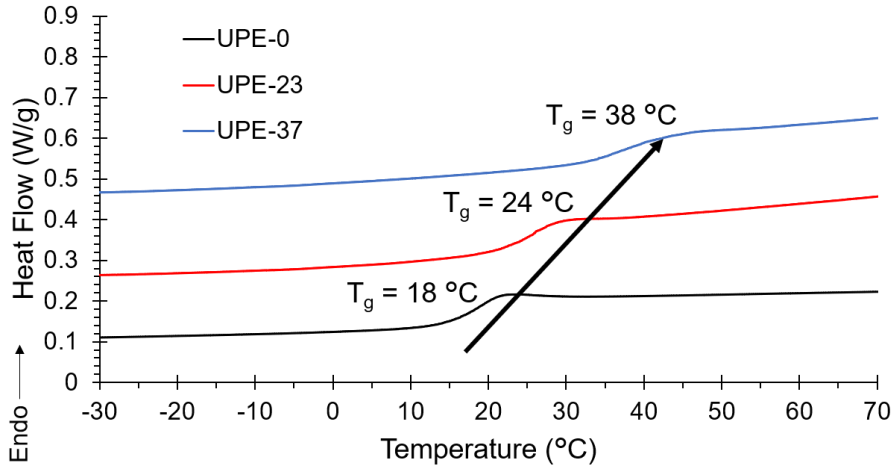


**Figure 6.1**: DSC thermograms of UPEs containing 0, 23, and 37 mol% of PA in the backbone.

The synthesis and subsequent ion exchange of VBTOP Cl afforded a room temperature PIL to serve as an effectively non-volatile reactive diluent for the photocurable UPE oligomers. This styrenic-based PIL maintains similar reactivity to styrene, which is a commonly used co-monomer for UPRs, and a previous report describes its ability to be printed via VP.[29] Moreover, the use of long octyl groups on the phosphonium substituent decreases the $T_g$ and promotes higher ionic conductivities than shorter alkyl groups.[15] Unfortunately, all UPEs proved insoluble in the VBTOP PIL regardless of PA content; however, employing dimethoxyethane as a low-volatility diluent mitigated this issue. Dimethoxyethane exhibits a boiling point of 162 °C as well as a relatively low vapor pressure, rendering this solvent suitable as a diluent for VP resins.

All UPE compositions dissolved in conjunction with 40 wt.% VBTOP $Tf_2N$ at a concentration of 50 wt.% solids in dimethoxyethane. However, the UPE-0/VBTOP $Tf_2N$ mixture exhibited only partial solubility at higher concentrations. Increasing the PA content in the UPE backbone appeared to increase its solubility in dimethoxyethane. UPE-25/VBTOP $Tf_2N$ dissolved readily at concentrations as high as 70 wt.% solids, while UPE-40/VBTOP $Tf_2N$ remained soluble even up to 80 wt.% solids.

**Table 6.1**: Unsaturated polyester compositions measured from $^1$H NMR analysis and $T_g$ measured from DSC.

| PG (mmol) | MA (mmol) | PA (mmol) | Target PA Content (mol%) | Actual PA Content (mol%) | Trans fumarate isomer (mol%) | Cis maleate Isomer (mol%) | $T_g$ (°C), DSC [a] |
|---|---|---|---|---|---|---|---|
| 0.263 | 239 | 0 | 0 | 0 | 95 | 5 | 18 |
| 0.263 | 119 | 119 | 25 | 23 | 94 | 6 | 24 |
| 0.263 | 48 | 191 | 40 | 37 | 97 | 3 | 38 |

**a)** Measured during the second heating cycle. Heating rate: 10 °C min$^{-1}$ under $N_2$

Photorheological experiments provided a method of screening viable compositions for VP 3D printing. These experiments elucidated the photocuring kinetics of a resin through the examination of the storage and loss moduli as a function of exposure to UV light. As photocuring occurs, the storage modulus increases until it exceeds the loss modulus; this point is known as the crossover time. The crossover time, although not considered the gel point of the polymer network, indicates the point at which the liquid resin transitions to solid-like properties. Knowledge of the crossover time helped to guide the printing process parameters (*e.g.*, layer exposure time). Two variables

were individually tested to determine their effect on the photocuring properties of the UPR. First, the concentration of the UPR remained constant, while examining the effect of PA content in the UPE backbone (**Figure 6.2A**). The resins for these experiments contained 70 wt.% of solids dissolved in dimethoxyethane where 60 wt.% of the solids consisted of UPE and VBTOP $Tf_2N$, which comprised the remaining 40 wt.%. At this concentration, the crossover time remained low (2 – 5 s) for the UPE-23 and UPE-37 samples (**Figure 6.2C**). The crossover time slowed marginally upon increasing the PA content from 23 to 37 mol% at 70 wt.% solids as expected due to the decrease in unsaturated units in the backbone. The UPE-0 composition appeared to have a slower crossover time at 70 wt.% solids compared to the other two; however, this composition was not fully miscible above 50 wt.% solids as mentioned previously. Therefore, photocuring resulted in heterogeneous films and longer crossover times, which would result in longer exposure times for each layer and thus slower printing. The plateau modulus also increased as expected with decreasing PA content due to the increased density of crosslinkable sites. (**Figure 6.2D**).

In a second set of experiments, the PA content in the UPE backbone remained constant at 37 mol% and the solids content varied between 50, 70, and 80 wt.% solids (**Figure 6.2B**). Again, the solids consisted of 60 wt.% UPE oligomers and 40 wt.% VBTOP $Tf_2N$. The concentration significantly impacted both crossover time and plateau modulus when all other variables remained constant. While the crossover time only increased slightly from 70 to 80 wt.% solids, a significant

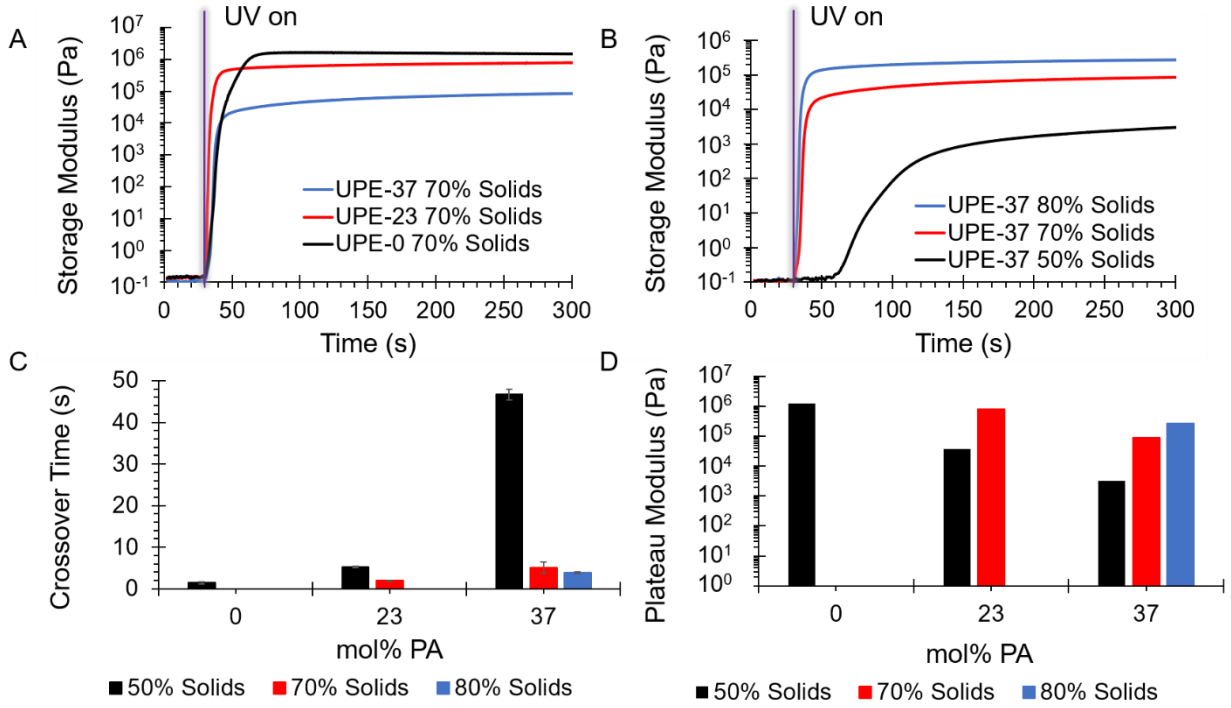


**Figure 6.2**: Photorheology data for selected UPRs probing the effect of A.) phthalic anhydride content and B.) solids content on curing kinetics. C, D.) Summary of modulus crossover times and plateau storage modulus respectively as a function of PA content and solution concentration.

increase in crossover time occurred when decreasing the concentration to 50 wt.% solids. Likewise, the plateau modulus decreased with decreasing solids content due to plasticization of the network with dimethoxyethane. These results informed the decision to utilize UPE-23 for further experiments owing to the fast-crosslinking kinetics ($\leq$ 5 s) and suitable plateau modulus ($G' > 10^5$ Pa) for printing.[20, 21]

Further photorheological experiments elucidated the effect of varying the concentration of VBTOP PIL in a resin containing UPE-23. Interestingly, the amount of PIL in the resin apparently exhibited little effect on the crossover time and plateau modulus as summarized in **Figure 6.3**. The crossover time remained relatively unchanged (between 2-3 s) with decreasing PIL incorporation from 40 wt.% to 0 wt.%. This indicated that the photocuring reaction occurred rapidly even in the absence of a small molecule crosslinker; however, incorporation of the VBTOP PIL remained crucial for modifying the thermal, mechanical, and electrical properties of the printed parts. Similarly, the plateau storage moduli did not change significantly between 0 – 20 wt.% of PIL incorporation. At 30 and 40 wt.% of PIL concentration the modulus dropped substantially due to the decreased amount of UPE-23 in the resin; however, the moduli remained above $10^5$ Pa in both samples.

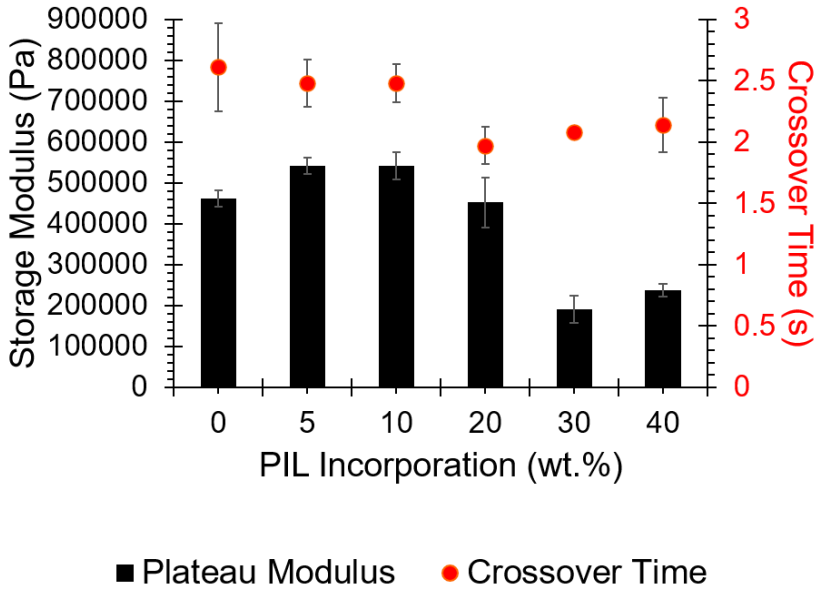


**Figure 6.3**: Summary of plateau moduli and crossover times from photorheological experiments in which the amount of VBTOP PIL varied from 0 to 40 wt.%.

Photocured disks from the rheometer were further heated *in vacuo* at 120 °C to remove as much dimethoxyethane as possible and a subsequent acetone extraction removed any unreacted monomers. The gel fractions for each sample fell between 80-82 wt.%, which indicated that some of the UPE and VBTOP remained unincorporated in the network. Thermogravimetric analysis of the extracted samples verified the incorporation of VBTOP $TF_2N$ into the network. **Figure 6.4** shows the thermal weight loss profiles of photocured disks from resins containing UPE-23 and 0, 5, 10, 20, 30, and 40 wt.% VBTOP PIL. Each sample containing more than 5 wt.% PIL exhibited a two-step degradation process. The wt.% of the second degradation steps increased with increasing PIL resin incorporation, which indicated the integration of a proportional amount of VBTOP PIL into the network. Furthermore, the 5 wt.% degradation temperature ($T_{d,5\%}$) increased with increasing PIL incorporation from 215 to 279 °C for 0 and 40 wt.% PIL respectively (**Figure 6.4** inset). One potential explanation for the increase in $T_{d,5\%}$ with increasing PIL content stems from the hydrolysis of the polyester. For example, at elevated temperatures in the presence of atmospheric water, the polyester will hydrolyze into volatile fumaric acid repeat units. Those repeat units that are crosslinked with VBTOP $Tf_2N$ will

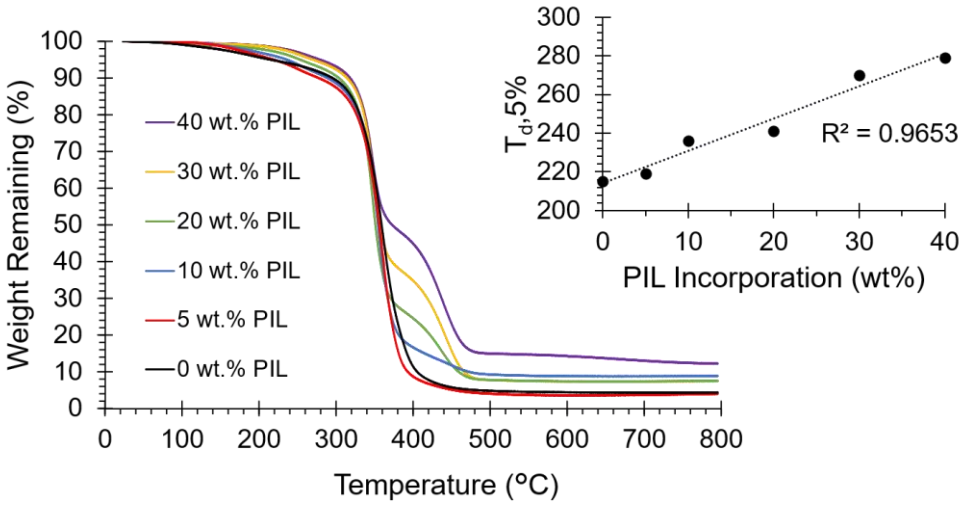


**Figure 6.4:** Thermogravimetric analysis of photocured and solvent extracted UPRs containing varied amounts of PIL. The inset plot reveals the trend in $T_{d,5\%}$ with increasing PIL content.

retain higher molecular weights, which will likely prevent them from volatilizing and subsequently decrease the $T_{d,5\%}$.

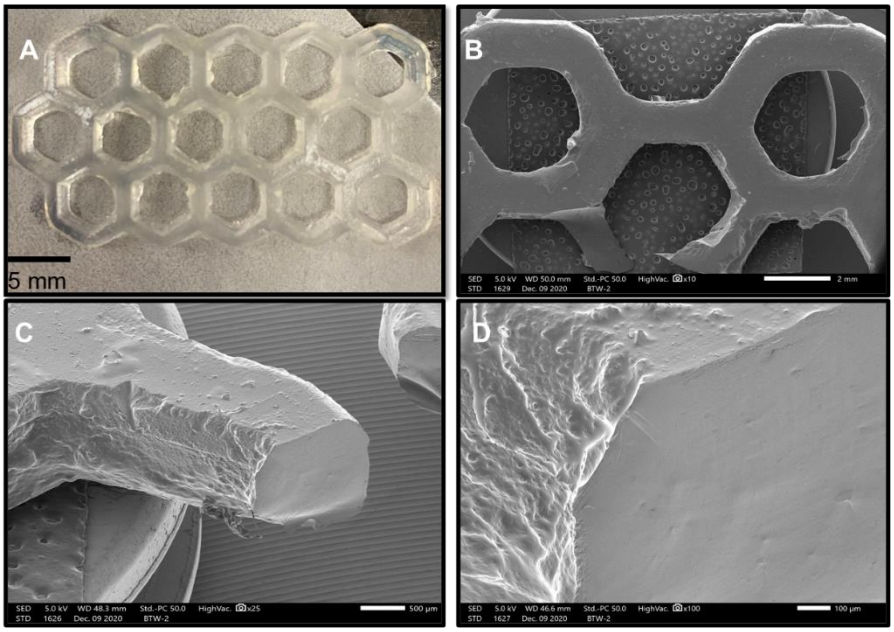


**Figure 6.5**: (A) Three-dimensional architecture of UPR printed through VP (B) SEM image of A at 10x magnification (C) image of a fracture surface at 25x magnification and (D)100x magnification.

As mentioned, resins containing 60 wt.% UPE-23 and 40 wt.% VBTOP $Tf_2N$ at 70 wt.% solids in dimethoxyethane demonstrated prerequisite rheology and reactivity for VP printing. The photopolymer resin successfully enabled production of high-resolution 3D architectures as shown in **Figure 6.5A**. SEM images of the fracture surface revealed a smooth surface without visible layers as shown in **Figure 6.5B-D**. Heating the 3D printed test specimens at 120 °C *in vacuo* until the achieved a constant mass ensured the complete removal of dimethoxyethane from the printed part.

Electrochemical impedance spectroscopy analysis of the printed and heated test specimens elucidated the ionic conductivity of this printed composition. **Figure 6.6** demonstrates the effect of temperature on ionic conductivity in the cured UPR. The printed UPR did not exhibit any measurable ionic conductivity at room temperature presumably due to the relatively high $T_g$ of this network, which measured at 36 °C with DSC (**Figure S6.3**). However, from 60 - 150 °C, the sample exhibited Vogel-Fulcher-Tammann (VFT) behavior as shown from the linear fit, and the

VFT parameters are tabulated in **Table S6.2**. The conductivity experienced strong temperature dependence ranging from $10^{-8}$ S $cm^{-1}$ at 60 °C to $10^{-5}$ S $cm^{-1}$ at 150 °C. While these conductivity values are not considered especially high for a highly charged polymeric system, these data do suggest that the PIL may impart additional functionality to 3D printed UPRs, especially when utilized at higher temperatures. Furthermore, future studies will focus on incorporating PEG-based UPEs into the resin to decrease the $T_g$ of the network and enhance ionic conductivity.

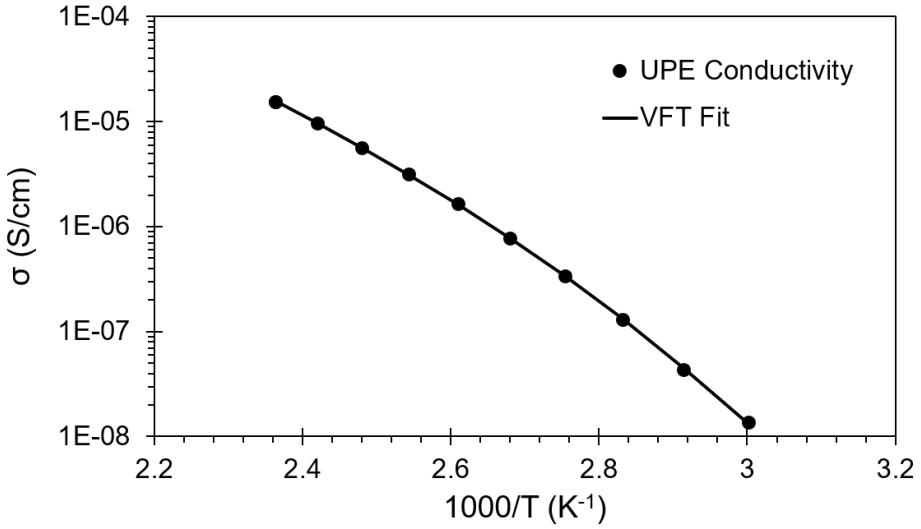


**Figure 6.6**: Ionic conductivity as a function of temperature for a 3D printed UPR specimen comprised of 40 wt.% VBTOP $Tf_2N$.

## 6.5 Conclusions

A phosphonium PIL acts as a nonvolatile, nontoxic replacement to styrene as a reactive diluent in UPRs for VP additive manufacturing processes. Incorporating varying amounts of PA into the UPE backbone allowed for modification of available crosslinking sites and solubility in the low-volatility unreactive diluent. Photorheological experiments screened various compositions and demonstrated that 40 wt.% UPE-23 oligomer with 40 wt.% VBTOP $Tf_2N$ PIL at a concentration of 70 wt.% solids showed the most promise for VP printing. TGA further revealed a linear increase in the $T_{d,5\%}$ of the cured network as the VBTOP PIL content increased from 0

to 40 wt.% The resin containing UPE-23 and 40 wt.% VBTOP $Tf_2N$ PIL at 70 wt.% solids in dimethoxyethane enabled VP of high-resolution 3D parts. Finally, the ionic conductivities of these 3D printed networks exhibited VFT behavior with conductivities reaching $1x10^{-5}$ S $cm^{-1}$ at 150 °C. Overall, this study demonstrates the potential to safely 3D print a highly commercially relevant polymer through VP utilizing low-volatility diluents in place of traditionally used styrene.

## 6.6 Acknowledgements

The authors would like to acknowledge Dr. Phil Scott for contributing his expertise in photopolymer resin design.

## 6.7 References

1. Scheirs, J.; Long, T. E., *Modern polyesters: chemistry and technology of polyesters and copolyesters*. John Wiley & Sons: 2005.
2. Penczek, P.; Czub, P.; Pielichowski, J., Unsaturated polyester resins: chemistry and technology. In *Crosslinking in materials science*, Springer: 2005; pp 1-95.
3. Malik, M.; Choudhary, V.; Varma, I., Current status of unsaturated polyester resins. *Journal of Macromolecular Science, Part C: Polymer Reviews* **2000,** *40* (2-3), 139-165.
4. Trivedi, B., *Maleic anhydride*. Springer Science & Business Media: 2013.
5. Ahamad, A.; Mohan, A.; Safeer, M.; Thachil, E. T., Synthesis of unsaturated polyester resin—effect of anhydride composition. *Designed Monomers and Polymers* **2001,** *4* (3), 260-267.
6. Matynia, T.; Worzakowska, M.; Tarnawski, W., Synthesis of unsaturated polyesters of increased solubility in styrene. *J. Appl. Polym. Sci.* **2006,** *101* (5), 3143-3150.
7. Jedlovčnik, R.; Šebenik, A.; Golob, J.; Korbar, J., Step-growth polymerization of maleic anhydride and 1, 2-propylene glycol. *Polymer Engineering & Science* **1995,** *35* (17), 1413-1417.
8. Jones, F. R., Chapter 26 - Unsaturated Polyester Resins. In *Brydson's Plastics Materials (Eighth Edition)*, Gilbert, M., Ed. Butterworth-Heinemann: 2017; pp 743-772.
9. Yang, Y.; Pascault, J., Modeling of unsaturated polyester prepolymer structures. I. Chain branches and overall chain end numbers. *J. Appl. Polym. Sci.* **1997,** *64* (1), 133-145.
10. Campanella, A.; Scala, J. J. L.; Wool, R., Fatty acid-based comonomers as styrene replacements in soybean and castor oil-based thermosetting polymers. *J. Appl. Polym. Sci.* **2011,** *119* (2), 1000-1010.
11. Kim, H. G.; Oh, D. H.; Lee, H. B.; Min, K. E., Effect of reactive diluents on properties of unsaturated polyester/montmorillonite nanocomposites. *J. Appl. Polym. Sci.* **2004,** *92* (1), 238-242.
12. Liu, W.; Xie, T.; Qiu, R., Styrene-free unsaturated polyesters for hemp fibre composites. *Composites Sci. Technol.* **2015,** *120*, 66-72.

13. Lu, J.; Yan, F.; Texter, J., Advanced applications of ionic liquids in polymer science. *Prog. Polym. Sci.* **2009,** *34* (5), 431-448.
14. Green, M. D.; Long, T. E., Designing imidazole-based ionic liquids and ionic liquid monomers for emerging technologies. *Polymer Reviews* **2009,** *49* (4), 291-314.
15. Chen, M.; White, B. T.; Kasprzak, C. R.; Long, T. E., Advances in phosphonium-based ionic liquids and poly(ionic liquid)s as conductive materials. *Eur. Polym. J.* **2018,** *108*, 28-37.
16. M. S. S. Esperança, J.; Canongia Lopes, J. N.; Tariq, M.; Santos, L. M. N. B. F.; Magee, J. W.; Rebelo, L. P. N., Volatility of Aprotic Ionic Liquids — A Review. *Journal of Chemical & Engineering Data* **2010,** *55* (1), 3-12.
17. Sassmann, P. B.; Weichold, O., Preparation and characterisation of ion-conductive unsaturated polyester resins for the on-site production of resistivity sensors. *Ionics* **2019**, 1-8.
18. Ian Gibson, I. G., Additive Manufacturing Technologies 3D Printing, Rapid Prototyping, and Direct Digital Manufacturing. Springer: 2015.
19. Jacobs, P. F., *Rapid prototyping & manufacturing: fundamentals of stereolithography*. Society of Manufacturing Engineers: 1992.
20. Sirrine, J. M.; Meenakshisundaram, V.; Moon, N. G.; Scott, P. J.; Mondschein, R. J.; Weiseman, T. F.; Williams, C. B.; Long, T. E., Functional siloxanes with photo-activated, simultaneous chain extension and crosslinking for lithography-based 3D printing. *Polymer* **2018**.
21. Scott, P. J.; Meenakshisundaram, V.; Chartrain, N. A.; Sirrine, J. M.; Williams, C. B.; Long, T. E., Additive Manufacturing of Hydrocarbon Elastomers via Simultaneous Chain Extension and Cross-linking of Hydrogenated Polybutadiene. *ACS Applied Polymer Materials* **2019**.
22. Luo, Y.; Dolder, C. K.; Walker, J. M.; Mishra, R.; Dean, D.; Becker, M. L., Synthesis and biological evaluation of well-defined poly (propylene fumarate) oligomers and their use in 3D printed scaffolds. *Biomacromolecules* **2016,** *17* (2), 690-697.
23. Gonçalves, F. A.; Costa, C. S.; Fabela, I. G.; Farinha, D.; Faneca, H.; Simões, P. N.; Serra, A. C.; Bártolo, P. J.; Coelho, J. F., 3D printing of new biobased unsaturated polyesters by microstereo-thermal-lithography. *Biofabrication* **2014,** *6* (3), 035024.
24. Lee, J. W.; Kang, K. S.; Lee, S. H.; Kim, J.-Y.; Lee, B.-K.; Cho, D.-W., Bone regeneration using a microstereolithography-produced customized poly (propylene fumarate)/diethyl fumarate photopolymer 3D scaffold incorporating BMP-2 loaded PLGA microspheres. *Biomaterials* **2011,** *32* (3), 744-752.
25. Beke, S.; Anjum, F.; Tsushima, H.; Ceseracciu, L.; Chieregatti, E.; Diaspro, A.; Athanassiou, A.; Brandi, F., Towards excimer-laser-based stereolithography: a rapid process to fabricate rigid biodegradable photopolymer scaffolds. *Journal of the Royal Society Interface* **2012,** *9* (76), 3017-3026.
26. Gonçalves, F.; Fonseca, A.; Domingos, M.; Gloria, A.; Serra, A.; Coelho, J., The potential of unsaturated polyesters in biomedicine and tissue engineering: Synthesis, structure-properties relationships and additive manufacturing. *Prog. Polym. Sci.* **2017,** *68*, 1-34.
27. Curtis, L.; Edwards, D.; Simons, R.; Trent, P.; Von Bramer, P., Investigation of maleate-fumarate isomerization in unsaturated polyesters by nuclear magnetic resonance. *Industrial & Engineering Chemistry Product Research and Development* **1964,** *3* (3), 218-221.

28. Melville, H.; Burnett, G., Rate constants for polymerization reactions. *Journal of Polymer Science* **1954,** *13* (71), 417-426.
29. Schultz, A. R.; Lambert, P. M.; Chartrain, N. A.; Ruohoniemi, D. M.; Zhang, Z.; Jangu, C.; Zhang, M.; Williams, C. B.; Long, T. E., 3d printing phosphonium ionic liquid networks with mask projection microstereolithography. *ACS Macro Letters* **2014,** *3* (11), 1205-1209.

## 6.8 Supplemental Information

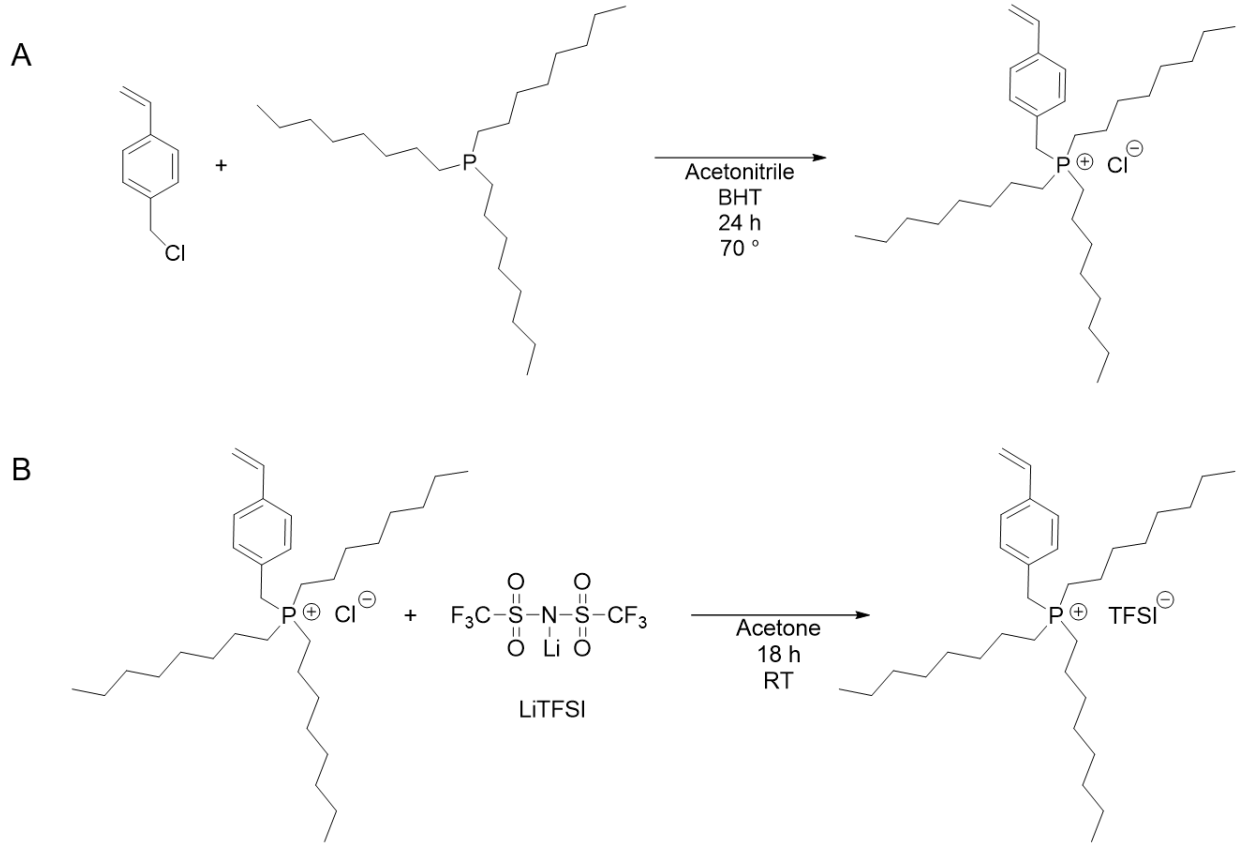


**Scheme S6.1:** A) Synthesis of VBTOP Cl and B) subsequent ion exchange to VBTOP $Tf_2N$.

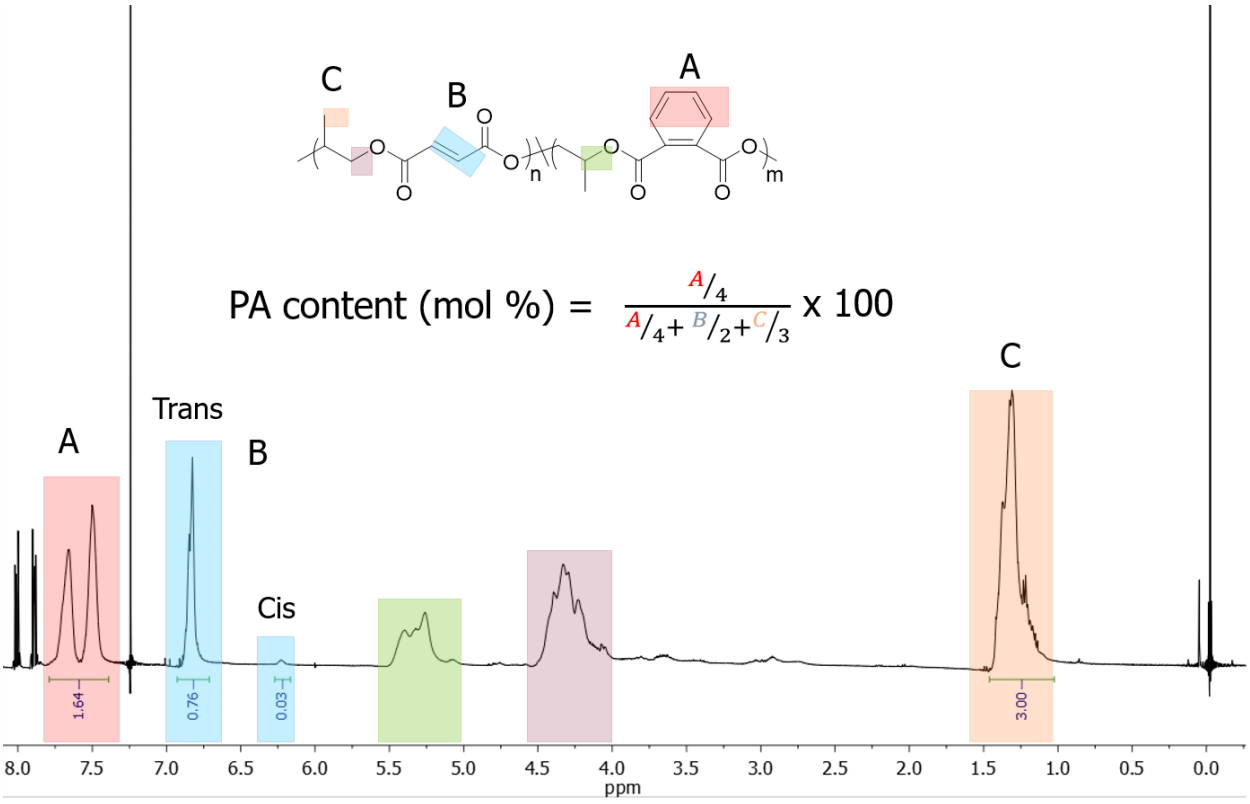


**Figure S6.1:** Representative $^{1}$H NMR spectrum of synthesized UPE.

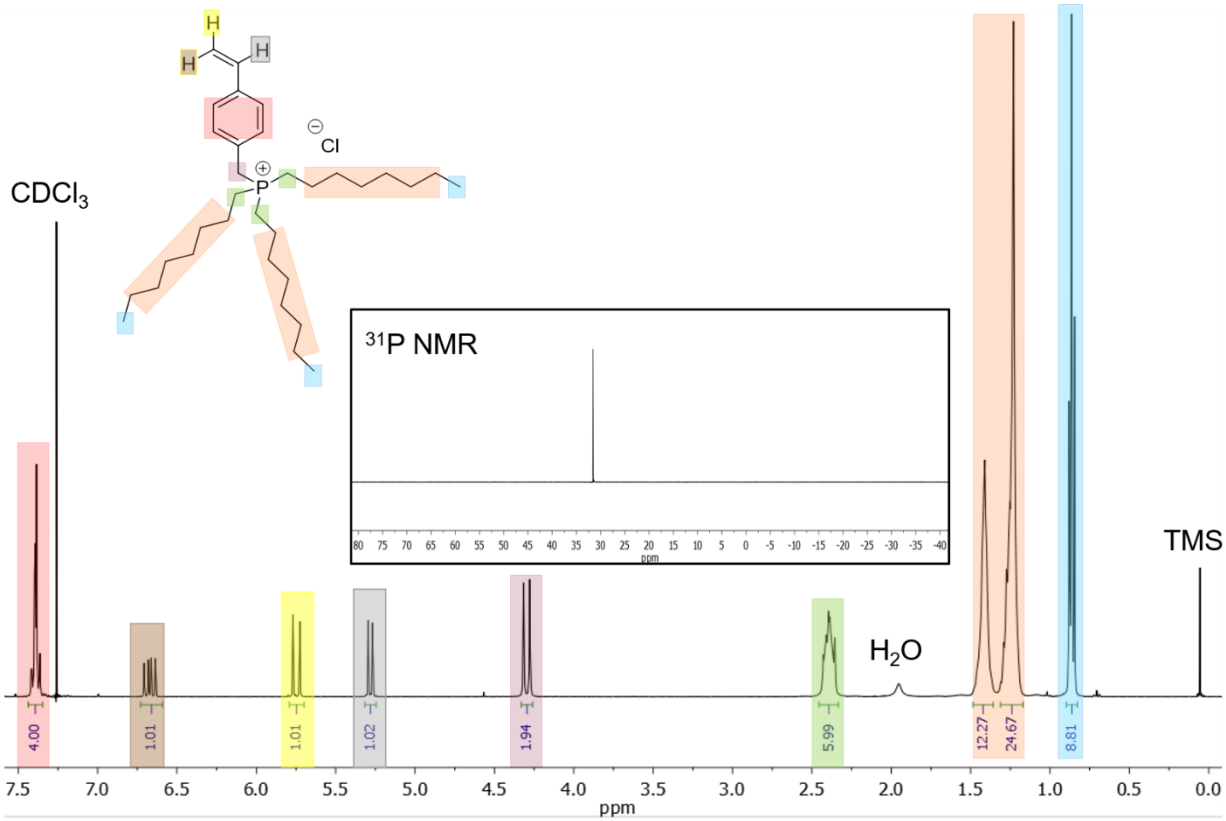


**Figure S6.2**: $^{1}$H NMR spectrum of VBTOP Cl with $^{31}$P NMR inset.

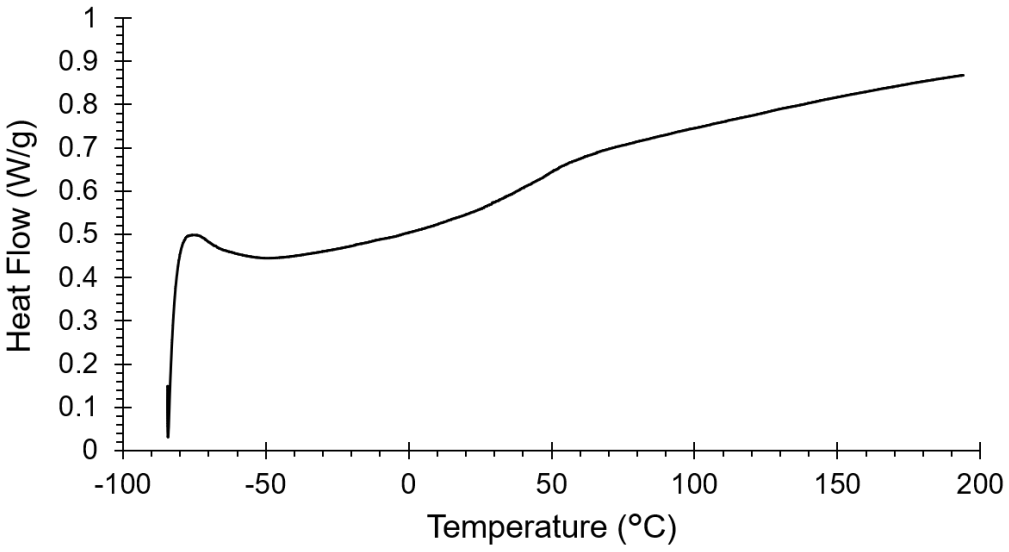


**Figure S6.3**: DSC thermogram of photocured UPE-23 with 40 wt.% VBTOP $Tf_2N$ showing a broad $T_g$ centered around 36 °C.

**Table S6.1**: UPR compositions and photorheology results.

| UPE | [UPE] (wt.%) | [PIL] (wt.%) | [Solids] (wt.%) | Crossover Time (s) | Plateau Modulus (MPa) |
|---|---|---|---|---|---|
| **UPE-0** | **60** | **40** | **50** | **1.47 ± 0.25** | **1.24 ± 0.04** |
| **UPE-23** | **100** | **0** | **70** | **2.61 ± 0.36** | **0.46 ± 0.02** |
| | **95** | **5** | **70** | **2.48 ± 0.19** | **0.54 ± 0.02** |
| | **90** | **10** | **70** | **2.48 ± 0.16** | **0.54 ± 0.03** |
| | **80** | **20** | **70** | **1.96 ± 0.15** | **0.45 ± 0.06** |
| | **70** | **30** | **70** | **2.08 ± 0.03** | **0.19 ± 0.03** |
| | **60** | **40** | **70** | **2.14 ± 0.22** | **0.8 ± 0.01** |
| | **60** | **40** | **50** | **5.24 ± 0.21** | **$0.03 \pm 5.5 \times 10^{-3}$** |
| **UPE-37** | **60** | **40** | **50** | **46.7 ± 1.29** | **$3.37 \times 10^{-3} \pm 0.05 \times 10^{-3}$** |
| | **60** | **40** | **70** | **5.09 ± 1.42** | **0.08 ± 0.01** |
| | **60** | **40** | **80** | **3.91 ± 0.13** | **0.25 ± 0.02** |

**Table S6.2**: Conductivity parameters for dried 3D printed UPRs.

| | $\sigma_0$ (S/cm) | B | $T_0$ (K) |
|---|---|---|---|
| **UPE-23/ VBTOP$_{40}$** | **4.85 x $10^{-1}$** | **2287** | **201.86** |

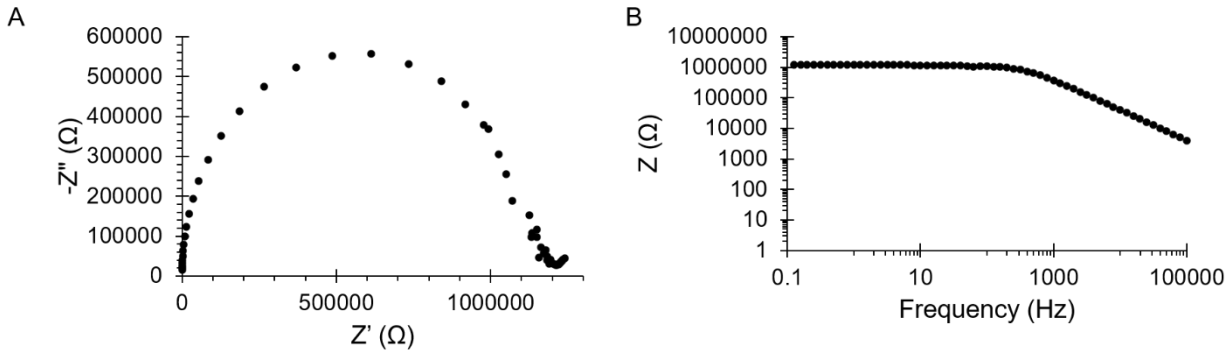


**Figure S6.4**: Representative Nyquist (A) and Bode (B) plots for a dried 3D printed sample of UPE-23/ VBTOP $Tf_2N$ measured at 150 °C.

# Chapter 7: **Segmented Poly(siloxane urethane) Containing a Phosphonium-Functionalized Soft Segment**

B. Tyler White[1] and Timothy E. Long[2*]

[1]Department of Chemistry, Macromolecules Innovation Institute (MII), Virginia Tech, Blacksburg, VA 24061

[2]Biodesign Center for Sustainable Macromolecular Materials and Manufacturing, School for Molecular Sciences, Arizona State University, Tempe, AZ 85287

*To whom correspondence should be addressed: E-mail: Timothy.E.Long@asu.edu.

## 7.1 Abstract

Charged block copolymers find use as ion exchange membranes for ionic-polymer metal composites; however, few studies have leveraged segmented polyurethanes for this application. This work describes the synthesis of a novel poly(siloxane urethane) (PSiU) bearing a pendent phosphonium motif in the soft segment. The synthesis of a novel phosphonium diester ionic liquid allowed for the insertion of the charged group into a poly(dimethyl siloxane) matrix through a transesterification reaction. A PSiU comprised of 70 wt.% of the phosphonium SS formed flexible and optically transparent films upon solution casting. Differential scanning calorimetry revealed a soft segment $T_g$ of -118 °C, which agreed well with a neutral control PSiU. Dynamic mechanical analysis and small angle X-ray scattering confirmed the presence of microphase separation in the phosphonium PSiU. Finally, impedance analysis revealed Arrhenius behavior in the ionic conductivity of the phosphonium PSiU as a function of temperature. The ionic conductivity ranged from $10^{-8}$ S cm$^{-1}$ to $10^{-6}$ S cm$^{-1}$ over a range of temperature from 25 - 85 °C. The room temperature ionic conductivity of this PSiU compared well with that of an imidazolium-containing triblock

copolymer from literature that was utilized for ionic polymer-metal composite actuators, which suggests that this material may prove suitable for that application as well.

## 7.2 Introduction

Segmented polyurethanes (PU) generally consist of a multiblock copolymer that microphase separates into a soft segment (SS) and a hard segment (HS). A low $T_g$ oligomer such as poly(ethylene glycol) (PEG), poly(propylene glycol) (PPG), poly(tetramethylene oxide) (PTMO), or poly(dimethyl siloxane) (PDMS) frequently serves as the SS and provides flexibility and elasticity to the polymer.[1] Conversely, the HS comprises of a small-molecule diisocyante and an optional chain extender, which produces a segment with a much higher $T_g$ due to hydrogen bonding. The microphase separation in segmented PUs proves essential in controlling their thermal, morphological, and (thermo)mechanical properties.[1] Utilizing more non-polar SSs such as PDMS generally leads to better phase separation from the highly polar HS. Conversely, increasing the polarity of the SS may result in phase mixing, which diminishes the properties of the PU.

Ion transport in charged block copolymers depends heavily on obtaining a continuous ionic microphase across the polymer film.[2] For this reason, most studies focus on linear diblock or triblock copolymers with well-defined morphologies containing long-range order for polymer electrolyte applications.[2-6] Regardless, several recent examples from literature have incorporated charged units into segmented PUs.[7-12] For example, Gao and Long *et al*. demonstrated the effect of installing a sulfonate group in both the SS and HS of a segmented, PEG-based PU.[7] Inserting the sulfonate group into the SS increased the $T_g$ from -52 °C to -26 °C owing to the intermolecular ionic interactions between the sulfonates. However, the sulfonate groups also disrupted the crystallinity of the PEG phase and led to an amorphous SS phase. Incorporating the charge into

the hard segment surprisingly affected the $T_g$ of the SS even more, raising it to -5 °C due to a large degree of phase mixing, which also negatively impacted the mechanical properties of the PU. The authors further measured the ionic conductivity of the sulfonated SS PU and demonstrated the ability of the polymer to swell in a commercial ionic liquid (IL).[13] Despite this, very few other examples exist that incorporate charged groups into the SS of a segmented PU.

Ionic polymer-metal composites (IPMCs) leverage charged polymers as membranes for electromechanical transducers. Polymers used for this application primarily consist of charged, linear triblock and multiblock copolymers.[14] Ideally, these polymers will exhibit high ionic conductivities ($> 10^{-6}$ S $cm^{-1}$) for transduction, and a suitable storage modulus ($\geq$ 100 MPa) for actuator fabrication. Unfortunately, the ionic conductivity and modulus of a polymer are generally inversely proportional to each other, meaning that ionic polymers for this application require careful synthetic design.[15] Microphase separated block copolymers serve well for this application due to the ability to segregate the charged unit into a low $T_g$ polymer phase while a higher $T_g$ phase imparts mechanical stability. Many examples exist of imidazolium-, ammonium-, and sulfonate-derived block copolymers for IPMCs; however, to the best of our knowledge no examples exist of phosphonium-containing polymers for IPMCs despite evidence that they provide higher ionic conductivity than their nitrogen-based analogues.[16] Furthermore, very few reports discuss IPMCs based on segmented PU membranes, and those that do typically utilize commercially-available, neutral PUs swollen with IL.[17] This work describes the synthesis of a novel phosphonium IL for the purposes of producing PDMS-based PUs containing a phosphonium-derived SS. We hypothesize that the low $T_g$ PDMS SS will lead to excellent phase separation, which will result in a high ionic conductivity of the phosphonium counterion. Ultimately, the aim of this study is to produce a segmented PU with suitable properties for eventual use in IPMCs.

## 7.3 Experimental

### 7.3.1 Materials

Allyl Bromide (97%), n-tributylphosphine (99%), dimethyl malonate (98%), 1,8-diazabicyclo(5.4.0)undec-7-ene (DBU, 98%), dibutyltin dilaurate (DBTDL, 95%) were purchased from Sigma Aldrich. N,N-dimethylformamide (DMF, extra dry, 99.8%) and tetrahydrofuran (THF, extra dry, 99.9%) were purchased from Acros Organics. Hydroxyl terminated poly(dimethyl siloxane) (PDMS, DMS-C15, ~1.5 kg $mol^{-1}$) was purchased from Gelest. Dichloromethane (DCM), hexanes, and anhydrous diethyl ether were purchased from Fisher chemical. Lithium bis(triflouromethanesulfonyl) imide ($LiTf_2N$, >98%) was purchased from Tokyo Chemical Industry. Ultra-high purity Argon gas (99.999%) was purchased from Praxair. Dicyclohexylmethane-4,4'-Diisocyanate (HMDI, Desmodur W) was generously donated by Covestro.

### 7.3.2 Synthesis of allyltributylphosphonium bromide (ATPB)

The synthesis of ATPB was modified from a previously reported procedure.[18] Tributylphosphine (26.825 g, 132 mmol) was added to a three-neck round bottom flask equipped with an addition funnel and stir bar. Allyl bromide (30 g, 248 mmol) was added to the addition funnel and the reaction vessel was allowed to cool to 0 °C. The allyl bromide was added dropwise to the reaction over 30 minutes. The reaction was allowed to continue overnight, and a precipitate was observed. The mixture was diluted with diethyl ether (~100 mL), filtered, and washed three times with ether before drying *in vacuo* at room temperature overnight. The dried white crystals displayed a melting temperature between 78- 80 °C (1 °C $min^{-1}$). $^1$H NMR (400 MHz, d6-acetone, 25 °C), δ (ppm) 0.96 (t, 9H, -$CH_3$), 1.49 (m, 6H, -$CH_2$-), 1.69 (m, 6H, -$CH_2$-), 2.56 (m, 6H, $CH_2P$),

3.62 (q, 2H, $CH_2$-CH=$CH_2$), 5.38 (dd, 1H, cis H of =$CH_2$), 5.58 (dd, 1H, trans H of =$CH_2$), 5.95 (m, 1H, $CH_2$=). $^{31}$P NMR (400 MHz, d6-acetone, 25 °C), δ (ppm) 31.7 (s).

### 7.3.3 Ion Exchange to allyltributylphosphonium bis(trifluoromethanesulfonyl)imide (ATP $Tf_2N$)

ATPB (20 g, 96.6 mmol) was dissolved in 70 mL of acetone and added to a solution of $LiTf_2N$ (110 g, 531 mmol) in acetone (380 mL). The solution was allowed to stir overnight at room temperature. Acetone was removed using rotary evaporation and the resultant product was dissolved in DCM. The DCM solution was washed 3 times with DI water to remove the LiBr salt side product. ATP $Tf_2N$ was concentrated and dried *in vacuo* to yield a white solid. The solid displayed a melting temperature of 27-29 °C (1 °C $min^{-1}$). The complete ion exchange was confirmed with $^1$H NMR spectroscopy and by testing an aliquot with a solution of silver nitrate to ensure that no silver bromide formed in the solution. $^1$H NMR (400 MHz, d6-acetone, 25 °C), δ (ppm) 0.96 (t, 9H, -$CH_3$), 1.49 (m, 6H, -$CH_2$-), 1.69 (m, 6H, -$CH_2$-), 2.41 (m, 6H, $CH_2$P), 3.36 (q, 2H, $CH_2$-CH=$CH_2$), 5.46 (dd, 1H, cis H of =$CH_2$), 5.55 (dd, 1H, trans H of =$CH_2$), 5.95 (m, 1H, $CH_2$=). $^{31}$P NMR (400 MHz, d6-acetone, 25 °C), δ (ppm) 32.3 (s).

### 7.3.4 Synthesis of dimethylmalonatetributylphosphonium bis(trifluoromethanesulfonyl)imide (DMMP $Tf_2N$)

ATP $Tf_2N$ (15 g, 28.6 mmol) and dimethyl malonate (3.785 g, 286 mmol) were charged to a one-necked round-bottomed flask with a catalytic amount of DBU (1 wt.%) and dissolved in THF (85 mL). The solution was sparged with argon and allowed to react at 40 °C for 24 h. THF was removed by rotary evaporation and the product was concentrated *in vacuo* as a viscous yellow liquid. The product was washed with hexanes 3 times to remove residual unreacted dimethyl

malonate. $^{1}$H NMR (400 MHz, d6-acetone, 25 °C), δ (ppm) 0.96 (t, 9H, -$CH_3$), 1.22 (d, 3H, $CH_3$-CH-) 1.49 (m, 6H, -$CH_2$-), 1.69 (m, 6H, -$CH_2$-), 2.49 (m, 7H, $CH_2$P, CH-$CH_3$), 2.63 (t, 1H, COO-CH-COO), 3.74 (s, 6H, COO-$CH_3$). $^{31}$P NMR (400 MHz, d6-acetone, 25 °C), δ (ppm) 34.2 (s)

### 7.3.5 Synthesis of poly(dimethylsiloxane) (PDMS) functionalized DMMP $Tf_2N$

PDMS (14.587 g, 9.15 mmol) and ATP $Tf_2N$ (3.00 g, 4.57 mmol) were charged to a two-necked round-bottomed flask and purged with argon. A catalytic amount of titanium isopropoxide ( 50 ppm) was added to promote esterification. The heterogeneous mixture became homogeneous after reacting for 2 h at 80 °C and the reaction was allowed to continue for an additional 2 h to ensure completion. $^{1}$H NMR confirmed the successful synthesis as evident by the disappearance of the malonate methyl ester peak at 0.96 ppm and the appearance of a peak at 4.2 ppm (4 H) from the methylene group next to the newly formed ester bonds (**Figure S7.3**).

### 7.3.6 Synthesis of poly(siloxane urethane) bearing DMMP $Tf_2N$ soft segments

A poly(siloxane urethane) containing 70 wt.% of a DMMP $Tf_2N$ functionalized SS was targeted. PDMS functionalized DMMP $Tf_2N$ (5.17 g, 1.4 mmol) was added to a 250 mL three-necked round-bottomed flask equipped with an addition funnel and a glass mechanical stir rod with a PTFE stir paddle. HMDI (2.133 g, 8.1 mmol) was added dropwise from the addition funnel under argon flow, and the reaction was stirred at 80 °C. The heterogeneous mixture became homogeneous upon the addition of the DBTDL catalyst (50 ppm). The reaction proceeded for 4 h and the viscosity increased substantially as the prepolymer was formed. 1,4-butanediol (0.607 g, 6.7 mmol) was dissolved in anhydrous DMF (10.5 mL) and sparged with argon. The solution was transferred via cannula to the addition funnel and was added dropwise to the prepolymer. The addition funnel was washed with an additional 2 mL of DMF to ensure complete transfer of the

1,4-butanediol to the reaction. The reaction proceeded for 24 h at 80 °C before the solution was precipitated 3 times in diethyl ether to yield a fluffy, yellow solid. The product was dried *in vacuo* at 60 °C overnight to remove the remaining diethyl ether.

### 7.3.7 Synthesis of poly(siloxane urethane) control

A neutral control polyurethane containing 70 wt.% soft segment was synthesized by using the same prepolymer method described for the charged polyurethane. However, in this case the hydroxyl terminated PDMS oligomer was used directly for the soft segment, and a 50/50 v/v mixture of THF and DMF was used as the solvent to maintain miscibility as described by Yilgor and Yilgor *et al*.[19]

### 7.3.8 Analytical methods

NMR spectroscopy was performed on an Agilent MR4 400 MHz spectrometer operating at room temperature. Differential scanning calorimetry (DSC) was performed on a TA Instruments Q200 DSC equipped with a liquid nitrogen cooling system. A heating/cool/ heat cycle was run at a rate of 10 °C $min^{-1}$ from -150 to 200 °C under a constant helium purge. The glass transition temperatures were determined from the second heat cycle and were measured at the half-height of the endothermic step transitions. Dynamic mechanical analysis (DMA) was carried out using a TA Instruments Q800 DMA equipped with a liquid nitrogen gas cooling accessory. The storage and loss moduli were measured under oscillatory tension over a range of temperatures from -150 – 120 °C with a heating/cooling rate of 3 °C $min^{-1}$. The oscillatory frequency was 1 Hz, and the strain was held at 0.1% such that it remained within the linear viscoelastic region. Tensile properties were measured with an Instron® 5500R on dogbone samples punched from solvent cast films using an ASTM D638-V cutting die. The crosshead separation speed for each tensile experiment was

held constant at 5 mm $min^{-1}$. The single depicted stress/strain curve and the corresponding tensile values for each sample were reported as an average of 5 runs.

Small angle X-ray scattering (SAXS) experiments were performed using a Rigaku S-Max 3000 3 pinhole SAXS system, equipped with a rotating anode emitting X-ray with a wavelength of 0.154 nm (Cu Kα). The sample-to-detector distance was 1005 mm, and the q-range was calibrated using a silver behenate standard. Two-dimensional SAXS patterns were obtained using a 2D multiwire, proportional counting, gas-filled detector, with an exposure time of 2 h. The SAXS data were corrected for sample thickness, transmission, and background, and were put on an absolute scale by correction using a glassy carbon standard from the Advanced Photon Source (APS). All the SAXS data were analyzed using the SAXSGUI software package to obtain radially integrated SAXS intensity versus the scattering vector q, where $q = (4\pi/\lambda)\sin(\theta)$, θ is one half of the scattering angle and λ is the X-ray wavelength.

Electrochemical impedance spectroscopy (EIS) was performed on a Metrohm Autolab PGSTAT302N operating in two-electrode mode. Through-plane impedance measurements were taken by sandwiching a solvent-cast film between two aluminum disks in contact with copper leads connected to the electrodes. The impedance across the film was measured at an amplitude of 0.3 V over a range of frequencies from 0.1 – 100,000 Hz. All impedance measurements took place in an Espec BTL-433 benchtop environmental chamber. The sample was equilibrated at each temperature and at 20% relative humidity for at least 2 h before measuring the impedance in triplicate. The following equation allows for the calculation of ionic conductivity from the measured DC impedance:

$$\sigma = \frac{L}{AR}$$

where σ is the ionic conductivity, L is the length between the two electrodes, A is the cross-sectional area, and R is the resistance. The resistance was taken as the Z value extrapolated to 0 Hz from the plateau in the Bode plot (**Figure S7.4**). The three-parameter Vogel-Fulcher-Tammann (VFT) equation is as follows:

$$\sigma\,(T) = \sigma_0\, exp\, \frac{-B}{T-T_0}$$

where σ (T) is the ionic conductivity at a given temperature, B is a constant related to the activation energy, and $T_0$ is the Vogel temperature where the motion of ions stops. The Excel Solver tool provided a fit of the VFT equation to the conductivity data, which allowed for determination of the VFT parameters.

## 7.4 Results and Discussions

The facile synthesis of ATPB and subsequent ion metathesis (**Scheme 7.1a**) afforded an electrophilic phosphonium IL suitable for a nucleophilic addition reaction with dimethyl malonate (**Scheme 7.1b**). Interestingly, $^1$H NMR (**Figure 7.1**) indicates that the carbanion exclusively reacts at the tail position on the vinyl substituent instead of the head position as commonly seen in other

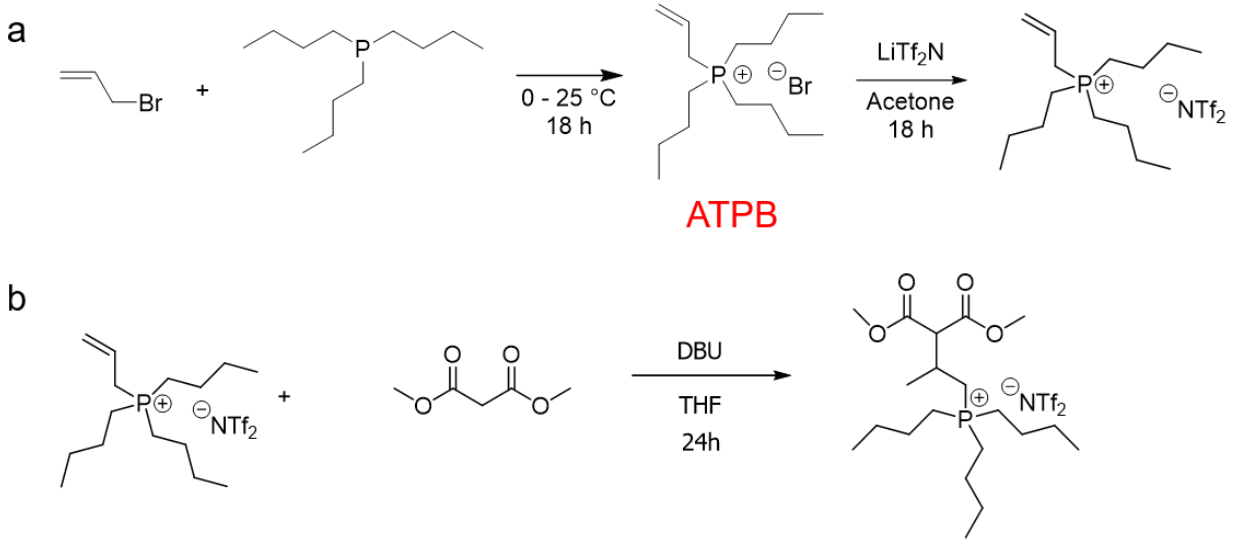


**Scheme 7.1**: (a) Synthesis of ATP Br and subsequent metathesis to ATP $Tf_2N$ and (b) synthesis of DMMP $Tf_2N$

nucleophilic addition reactions such as the Michael addition reaction.[20] However, examination of the transition states for each potential product isomer supports this reaction mechanism (**Scheme S7.1**). Namely, the addition of the carbanion at the head of the vinyl substituent pushes the negative charge onto a secondary carbon, which produces a less stable carbanion than the primary carbanion which potentially forms when the nucleophile reacts at the tail position. The coupling of this phosphonium IL with a diester enables the insertion of the charged unit into a PDMS matrix through transesterification (**Scheme S7.2**). This phosphonium-functionalized PDMS served as the soft segment for a segmented poly(siloxane urethane) (PSiU)

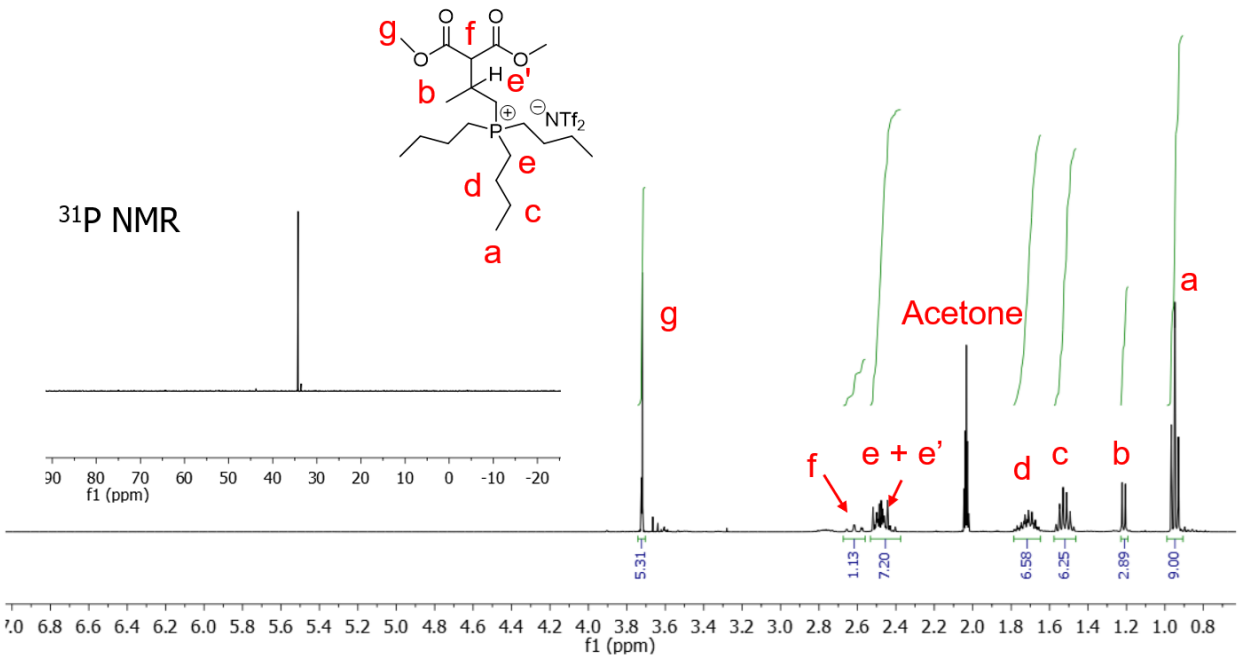


**Figure 7.1:** $^{1}$H NMR spectrum of DMMP $Tf_2N$ with an insert showing the $^{31}$P NMR spectrum.

**Scheme 7.2** shows the synthesis of the phosphonium-functionalized PSiU with a targeted SS composition of 70 wt.%. The reaction employed the two-step prepolymer method in which the SS was preformed and then chain extended with 1,4-butanediol to form the hard segment. The resultant polymer formed a free-standing, flexible, and optically transparent yellow film. This same synthetic method provided a control PSiU synthesized from uncharged PDMS. The synthesis

of the control PSiU required a mixed solvent system of THF/DMF as demonstrated in the work of Yilgor and Yilgor *et al.*[19] due to the immiscibility of the PDMS with DMF before the PSiU formation. Conversely, the PSiU becomes insoluble in THF as molecular weight builds throughout the reaction. Fortunately, phosphonium-functionalized PDMS dissolves readily in DMF, which provides one synthetic advantage over the uncharged system. The control PSiU also formed free-standing, flexible, and optically clear films comparable to the charged PSiU.

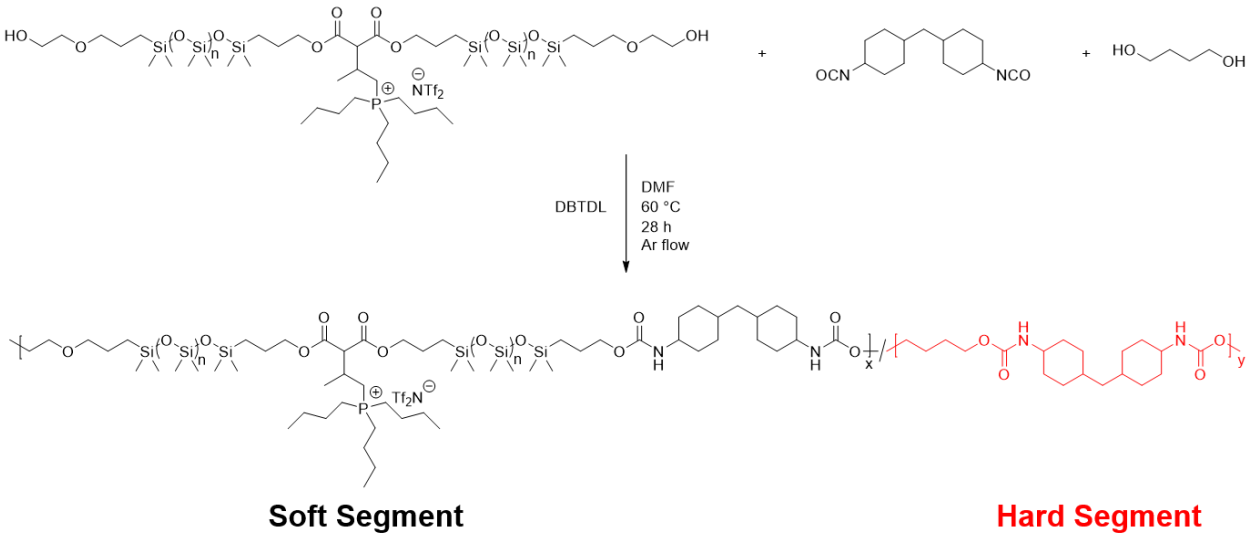


**Scheme 7.2**: Synthetic scheme for the segmented, phosphonium-functionalized PSiU

DSC analysis suggested the presence of microphase separation in the phosphonium PSiU (**Figure 7.2**). The first heat displayed a $T_g$ at -118 °C for the PDMS phase and an endothermic transition centered at 132 °C, which indicated the disruption of the HS phase. Upon quench cooling and subsequent heating, the $T_g$ remained the same; however, the transition at 132 °C disappeared. This phenomenon likely occurs because after the disruption of the hydrogen bonding in the HS and quench cooling, the HS did not have sufficient time to reorganize before the second heat. The $T_g$ of the control sample also sat at -117 °C, which proves that the incorporation of the phosphonium group into the PDMS phase did not increase the $T_g$ through the presence of

intermolecular ionic interactions. Indeed, the bulky phosphonium motif and $Tf_2N$ anion were chosen specifically to weaken the ionic interactions, which promotes higher ionic conductivity and lower $T_g$s. The sharp peak at -25 °C in the phosphonium PSiU curves as well as the noise that occurs between 75 - 100 °C in the control are artifacts that do not occur when measuring these

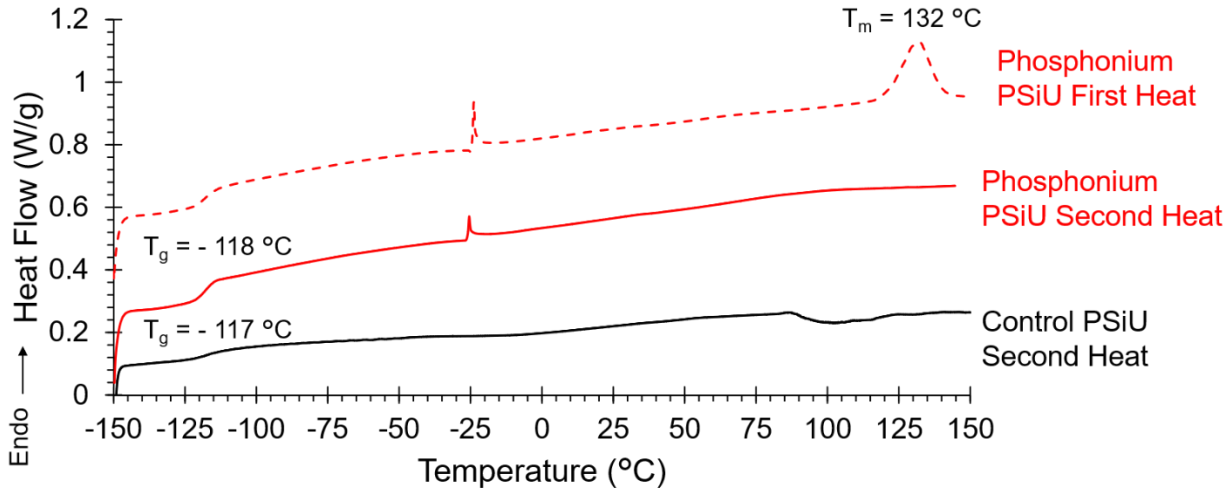


**Figure 7.2**: DSC curves of the first heat (red dashed lines) and second heat (solid red line) for the phosphonium PSiU compared to the control PSiU (black line).

samples on non-cryogenic instruments.

DMA revealed very similar behavior in the $T_g$s of the two PSiU samples as shown in **Figure 7.3**. At -150 °C both PSiU samples exhibited a storage modulus on the order of 2-3 GPa as expected for a glassy polymer. At approximately -100 °C, the storage moduli for both polymers began to decrease indicative of the PDMS $T_g$. The phosphonium PSiU displays a second tan δ peak after the $T_g$ at approximately -50 °C, which indicates the melting point of the PDMS.[19] The control PSiU does not experience this melting transition perhaps due to the overall lower molecular weight of the PDMS segment; the phosphonium PSiU SS consists of two 1,500 g $mol^{-1}$ PDMS oligomers covalently attached to the phosphonium while the control sample only contains one 1,500 g $mol^{-1}$ oligomer in the SS. The storage modulus plateaus for each of the samples at around 100 MPa owing to the presence of a strongly hydrogen bonded HS. The plateau modulus of the charged

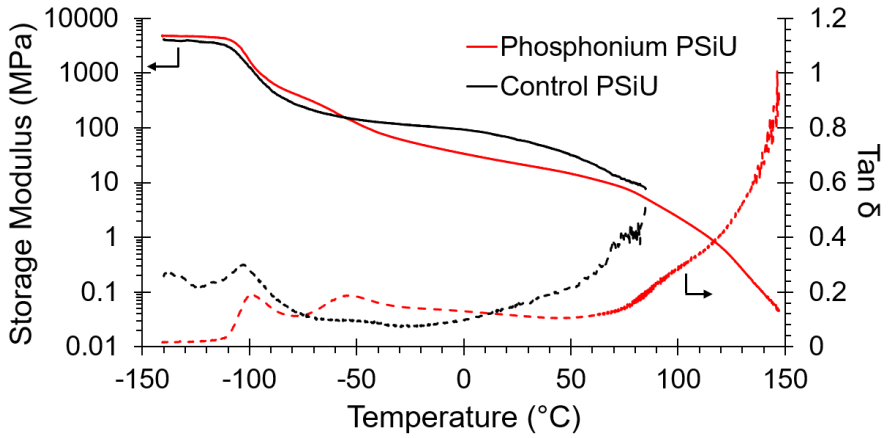


**Figure 7.3**: DMA plots of the phosphonium PSiU (red) and control PSiU (black).

PSiU exhibited more of a temperature dependence than the control as revealed in the downward sloping modulus after $T_g$. The control polymer experienced terminal flow at ~85 °C whereas the plateau of the charged PSiU extended to ~150 °C before flow. This extended plateau likely indicates a higher molecular weight in the phosphonium PSiU compared to the control; an increase in the number of entanglements frequently leads to extended plateau moduli in PUs.[1] However, the DMA curve for the control PSiU correlates well with what is seen in literature for a similar polymer.[19] This data further confirmed that the insertion of phosphonium units in the SS did not affect the $T_g$ of the PDMS phase, and also provided more evidence of strong phase separation between the SS and HS.

SAXS measurements further elucidated the bulk morphology of the two PSiU samples as shown in **Figure 7.4**. Both polymers exhibited microphase separation as indicated from the well-defined scattering peaks at q = 0.48 and 0.72 $nm^{-1}$ for the phosphonium and control PSiU respectively. The domain size of the phosphonium PSiU measured slightly higher (13.09 nm) than that of the control PSiU (8.73 nm). This difference may stem from the increased volume of the phosphonium-functionalized PDMS phase relative to the control. The phosphonium PSiU also exhibited a smaller peak at a higher q value of 1.2 $nm^{-1}$, which correlates to a domain spacing of

2.5 nm. This peak indicates the presence of a secondary ordered structure, which is presumably related to the spacing between ionic groups in the SS.

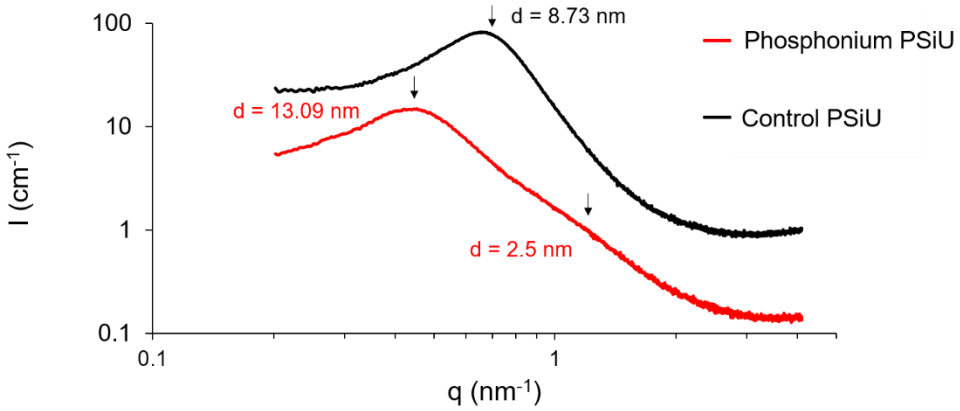


**Figure 7.4**: SAXS measurements for phosphonium PSiU (red) and the neutral, control PSiU (black)

Measuring the ionic conductivity of the charged PSiU provides one of the best metrics to determine the ability of this material to serve as a membrane for IPMCs. **Figure 7.5** reveals the conductivity of the phosphonium PSiU as a function of temperature at 20% relative humidity. At 25 °C (~3.35 1000 $K^{-1}$) the sample exhibited an ionic conductivity of 3.0 x $10^{-8}$ S $cm^{-1}$. As the temperature increased to 85 °C, the ionic conductivity also improved to a maximum value of 1.19 x $10^{-6}$ S $cm^{-1}$. The temperature dependence on conductivity for this polymer appears less severe compared to other charged block copolymers;[13, 15, 18, 21] the conductivity only increases on the scale of 1.5 orders of magnitude over the 60 °C temperature range. This reduced temperature dependence likely stems from the fact that this temperature range begins ~140 °C above the PDMS $T_g$. Therefore, the polymer chains already enjoy sufficient mobility for ion transport and further increases in temperature provide a diminishing return for conductivity. The red line in **Figure 7.5** shows the best-fit line for the VFT equation, which allowed for the determination of the VFT parameters (**Table 7.1**). This PSiU displayed a particularly low Vogel temperature ($T_0$), or the temperature at which all ionic motion ceases, of 75.7 K due to the extremely low $T_g$ of the conductive PDMS

phase. This implies that the polymer will exhibit some degree ionic conductivity at temperatures well below ambient conditions.

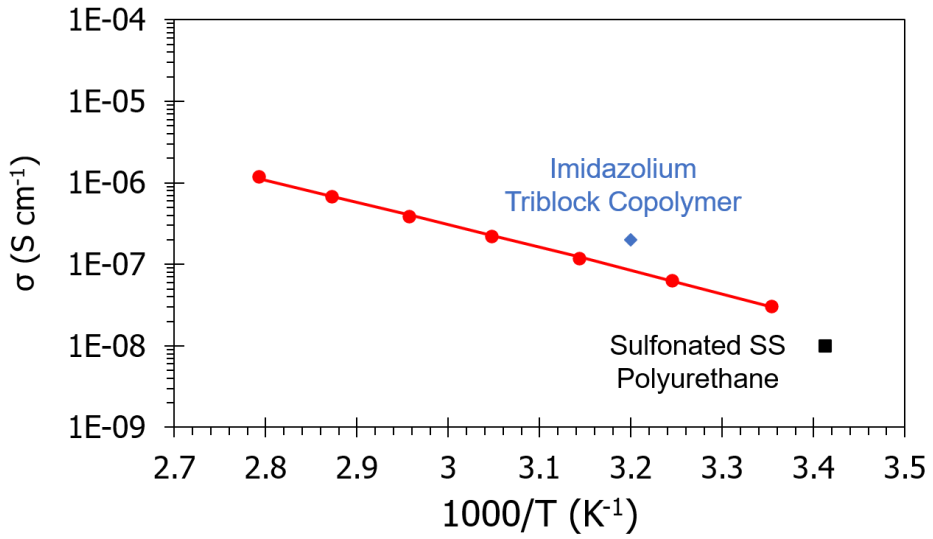


**Figure 7.5**: Ionic conductivity of phosphonium PSiU as a function of temperature (red circles). The red line represents the best fit line from the VFT equation. The black square and blue diamond display comparisons for ionic conductivities of a sulfonated PU[7] and imidazolium triblock copolymer[15] from literature, respectively.

Though the conductivity at room temperature remains low, it does compare well to a similar charged PU. Specifically, Gao and Long *et al.* reported the synthesis and characterization of a segmented PU containing a sulfonate group in the PEG-based SS.[7, 13] The room temperature conductivity of this segmented PU (black square in **Figure 7.5**) measured on the same order of magnitude as the phosphonium PSiU ($10^{-8}$ S $cm^{-1}$) despite the presumed improvement in phase separation of the siloxane-based PU. However, the relative humidity was maintained at 20% when measuring the conductivity of the PSiU, whereas the sulfonated SS PU was likely measured at ambient conditions (~40% relative humidity). Given that sulfonated polymers tend to absorb more atmospheric water at higher humidity and therefore exhibit higher ionic conductivities,[22, 23] it remains likely that the PSiU conductivity may be even higher than the sulfonated PU when controlling for humidity. Despite the disparate humidity conditions, this comparison seems to disprove the hypothesis that utilizing a phosphonium-functionalized PDMS SS would significantly enhance the ionic conductivity over a charged PU with a lesser degree of

phase separation. Green and Long *et al.* provide another comparison of an imidazolium triblock copolymer utilized for IPMCs (blue diamond in **Figure 7.5**).[15] This microphase separated block copolymer exhibited an ionic conductivity on the order of $10^{-7}$ S $cm^{-1}$ at 40 °C, which falls close to the value measured for the phosphonium PSiU at 45°C. The triblock copolymer demonstrated the ability to actuate under an applied voltage at ambient conditions when coated with electrodes. Given the similarities in conductivity and storage moduli between the two polymers, the PSiU presented in this study shows potential for use as a membrane in IPMCs.

**Table 7.1**: VFT parameters for phosphonium PSiU determined from impedance spectroscopy.

| | **$\sigma_0$ (S $cm^{-1}$)** | **B** | **$T_0$ (K)** |
|---|---|---|---|
| **Phosphonium PSiU** | 7.59 x $10^{-1}$ | 3790 | 75.7 |

## 7.5 Conclusions

A novel phosphonium IL monomer allowed for the installation of a charged unit into the PDMS phase of a segmented polyurethane. The synthesis of a PSiU containing 70 wt.% of a phosphonium-functionalized SS afforded a flexible and optically transparent film. Thermal analysis revealed that the introduction of the phosphonium unit in the SS did not affect the $T_g$ as compared with a neutral control SiPU. DMA allowed for the measurement of the thermomechanical properties and suggested that microphase separation occurred between the HS and SS. SAXS analysis further confirmed the presence of microphase separation and revealed that the charged PSiU displayed larger domain sizes than the control. Finally, impedance measurements showed Arrhenius-type behavior in the phosphonium PSiU as a function of temperature. The room temperature conductivity measured relatively low at 3.0 x$10^{-8}$ S $cm^{-1}$; however, comparisons of this material to the conductivity of other charged block copolymers in

literature suggest that this phosphonium PSiU may find use as an ion exchange membrane in IPMCs.

## 7.6 Acknowledgements

The authors would like to acknowledge Glenn Spiering from the Robert B. Moore research group for performing SAXS experiments.

## 7.7 References

1. Yilgör, I.; Yilgör, E.; Wilkes, G. L., Critical parameters in designing segmented polyurethanes and their effect on morphology and properties: A comprehensive review. *Polymer* **2015,** *58*, A1-A36.
2. Weber, R. L.; Ye, Y.; Schmitt, A. L.; Banik, S. M.; Elabd, Y. A.; Mahanthappa, M. K., Effect of Nanoscale Morphology on the Conductivity of Polymerized Ionic Liquid Block Copolymers. *Macromolecules* **2011,** *44* (14), 5727-5735.
3. Evans, C. M.; Sanoja, G. E.; Popere, B. C.; Segalrnan, R. A., Anhydrous Proton Transport in Polymerized Ionic Liquid Block Copolymers: Roles of Block Length, Ionic Content, and Confinement. *Macromolecules* **2016,** *49* (1), 395-404.
4. Choi, J.-H.; Ye, Y.; Elabd, Y. A.; Winey, K. I., Network Structure and Strong Microphase Separation for High Ion Conductivity in Polymerized Ionic Liquid Block Copolymers. *Macromolecules* **2013,** *46* (13), 5290-5300.
5. Ye, Y.; Choi, J.-H.; Winey, K. I.; Elabd, Y. A., Polymerized Ionic Liquid Block and Random Copolymers: Effect of Weak Microphase Separation on Ion Transport. *Macromolecules* **2012,** *45* (17), 7027-7035.
6. Zhang, W.; Liu, Y.; Jackson, A. C.; Savage, A. M.; Ertem, S. P.; Tsai, T.-H.; Seifert, S.; Beyer, F. L.; Liberatore, M. W.; Herring, A. M.; Coughlin, E. B., Achieving Continuous Anion Transport Domains Using Block Copolymers Containing Phosphonium Cations. *Macromolecules* **2016,** *49* (13), 4714-4722.
7. Gao, R.; Zhang, M.; Dixit, N.; Moore, R. B.; Long, T. E., Influence of ionic charge placement on performance of poly (ethylene glycol)-based sulfonated polyurethanes. *Polymer* **2012,** *53* (6), 1203-1211.
8. Gao, R.; Zhang, M.; Wang, S. W.; Moore, R. B.; Colby, R. H.; Long, T. E., Polyurethanes Containing an Imidazolium Diol-Based Ionic-Liquid Chain Extender for Incorporation of Ionic-Liquid Electrolytes. *Macromolecular Chemistry and Physics* **2013,** *214* (9), 1027-1036.
9. Zhang, M.; Hemp, S. T.; Zhang, M.; Allen, M. H.; Carmean, R. N.; Moore, R. B.; Long, T. E., Water-dispersible cationic polyurethanes containing pendant trialkylphosphoniums. *Polym. Chem.* **2014,** *5* (12), 3795-3803.
10. Gao, R.; Ramirez, S. M.; Inglefield, D. L.; Bodnar, R. J.; Long, T. E., The preparation of cation-functionalized multi-wall carbon nanotube/sulfonated polyurethane composites. *Carbon* **2013,** *54*, 133-142.

11. Wu, F.; Huang, C.-L.; Zeng, J.-B.; Li, S.-L.; Wang, Y.-Z., Synthesis and characterization of segmented poly (butylene succinate) urethane ionenes containing secondary amine cation. *Polymer* **2014,** *55* (16), 4358-4368.
12. Williams, S. R.; Wang, W.; Winey, K. I.; Long, T. E., Synthesis and morphology of segmented poly (tetramethylene oxide)-based polyurethanes containing phosphonium salts. *Macromolecules* **2008,** *41* (23), 9072-9079.
13. Gao, R. Synthesis and Properties of Ion-Containing Block and Segmented Copolymers and Their Composites. Virginia Tech, 2012.
14. White, B. T.; Long, T. E., Advances in Polymeric Materials for Electromechanical Devices. *Macromol. Rapid Commun.* **2019,** *40* (1), 1800521.
15. Green, M. D.; Wang, D.; Hemp, S. T.; Choi, J.-H.; Winey, K. I.; Heflin, J. R.; Long, T. E., Synthesis of imidazolium ABA triblock copolymers for electromechanical transducers. *Polymer* **2012,** *53* (17), 3677-3686.
16. Hemp, S. T.; Zhang, M.; Allen Jr, M. H.; Cheng, S.; Moore, R. B.; Long, T. E., Comparing ammonium and phosphonium polymerized ionic liquids: thermal analysis, conductivity, and morphology. *Macromolecular Chemistry and Physics* **2013,** *214* (18), 2099-2107.
17. Okuzaki, H.; Takagi, S.; Hishiki, F.; Tanigawa, R., Ionic liquid/polyurethane/PEDOT: PSS composites for electro-active polymer actuators. *Sensors and Actuators B: Chemical* **2014,** *194*, 59-63.
18. Liang, S.; O'Reilly, M. V.; Choi, U. H.; Shiau, H.-S.; Bartels, J.; Chen, Q.; Runt, J.; Winey, K. I.; Colby, R. H., High Ion Content Siloxane Phosphonium Ionomers with Very Low Tg. *Macromolecules* **2014,** *47* (13), 4428-4437.
19. Yilgör, E.; Tulpar, A.; Kara, Ş.; Yilgör, I., High Strength Silicone-Urethane Copolymers: Synthesis and Properties. In *Silicones and Silicone-Modified Materials*, American Chemical Society: 2000; Vol. 729, pp 395-407.
20. Mather, B. D.; Viswanathan, K.; Miller, K. M.; Long, T. E., Michael addition reactions in macromolecular design for emerging technologies. *Progress in Polymer Science* **2006,** *31* (5), 487-531.
21. Jangu, C.; Wang, J.-H. H.; Wang, D.; Sharick, S.; Heflin, J. R.; Winey, K. I.; Colby, R. H.; Long, T. E., Well-Defined Imidazolium ABA Triblock Copolymers as Ionic-Liquid-Containing Electroactive Membranes. *Macromolecular Chemistry and Physics* **2014,** *215* (13), 1319-1331.
22. Bae, B.; Miyatake, K.; Watanabe, M., Sulfonated Poly(arylene ether sulfone ketone) Multiblock Copolymers with Highly Sulfonated Block. Synthesis and Properties. *Macromolecules* **2010,** *43* (6), 2684-2691.
23. Strasser, D. J.; Graziano, B. J.; Knauss, D. M., Base stable poly (diallylpiperidinium hydroxide) multiblock copolymers for anion exchange membranes. *Journal of Materials Chemistry A* **2017,** *5* (20), 9627-9640.

## 7.8 Supplemental Information

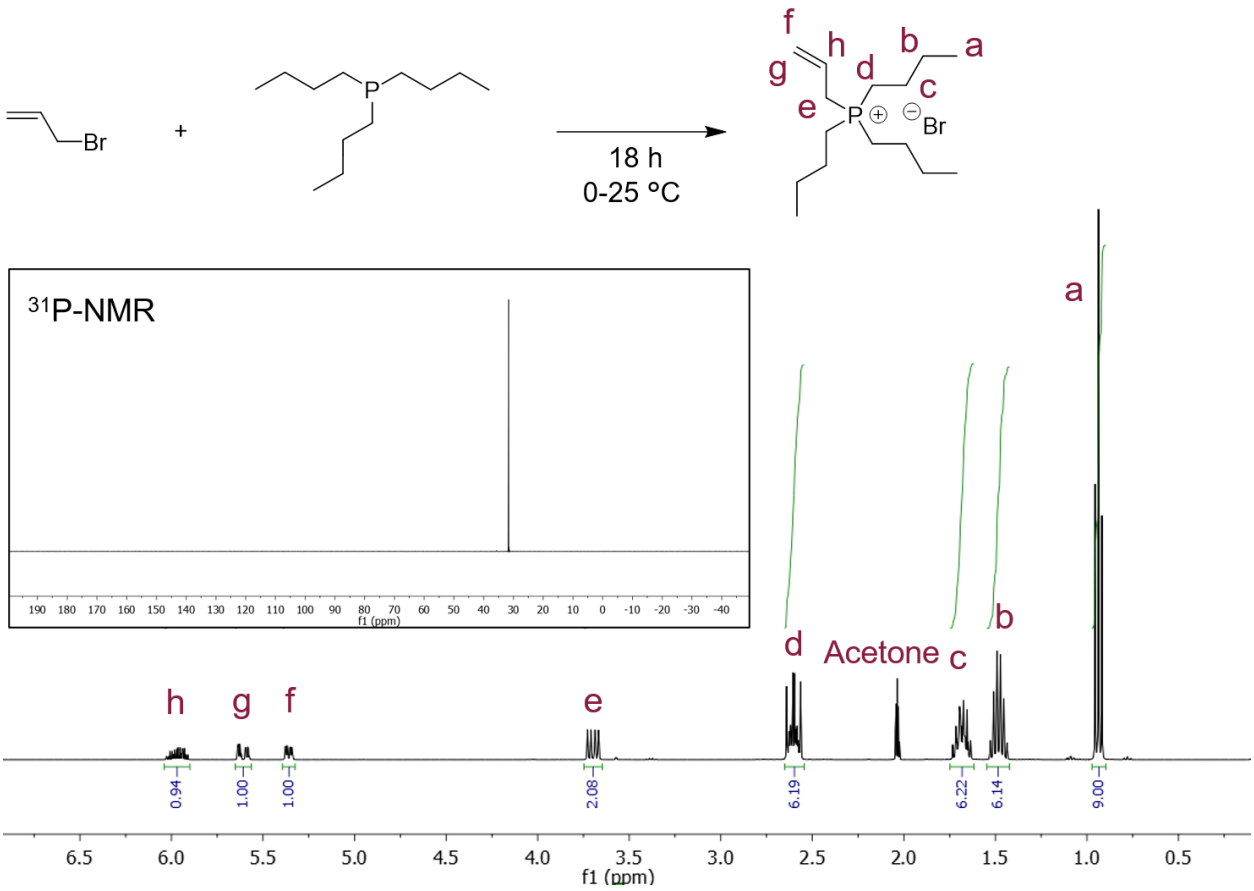


**Figure S7.1:** Synthesis and NMR spectra of ATPB.

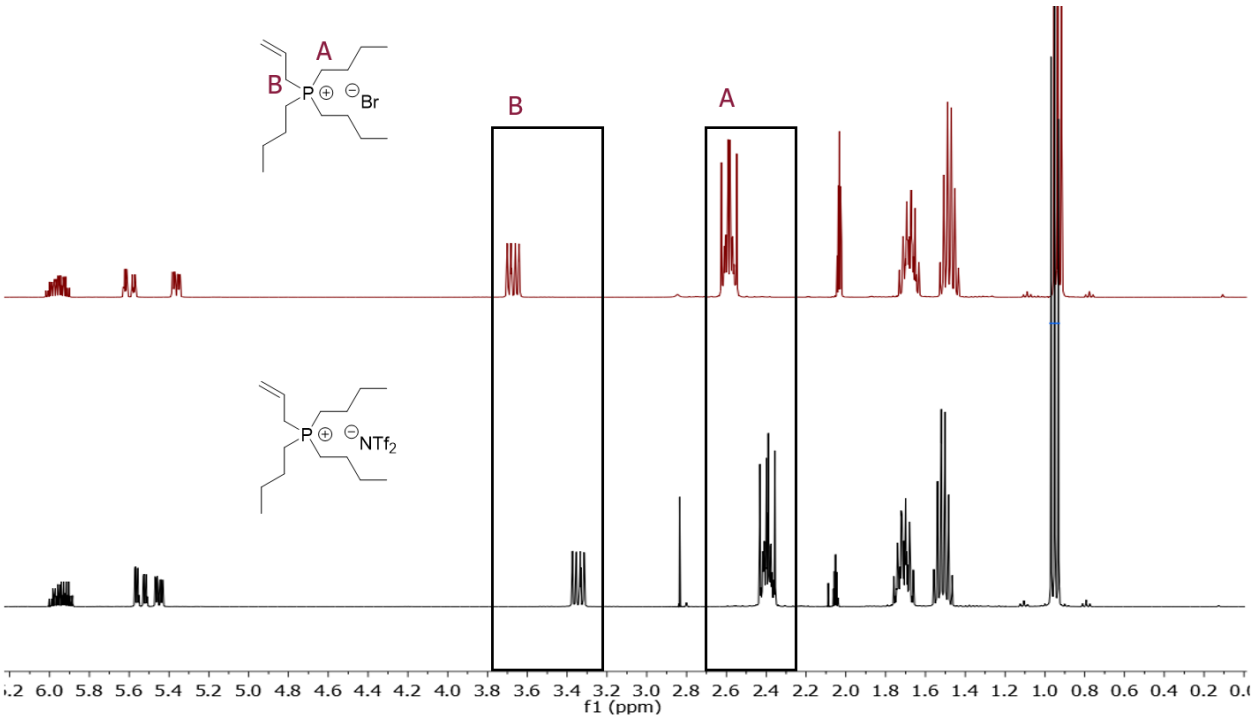


**Figure S7.2**: NMR spectra showing complete ion exchange of ATPB to ATP $Tf_2N$.

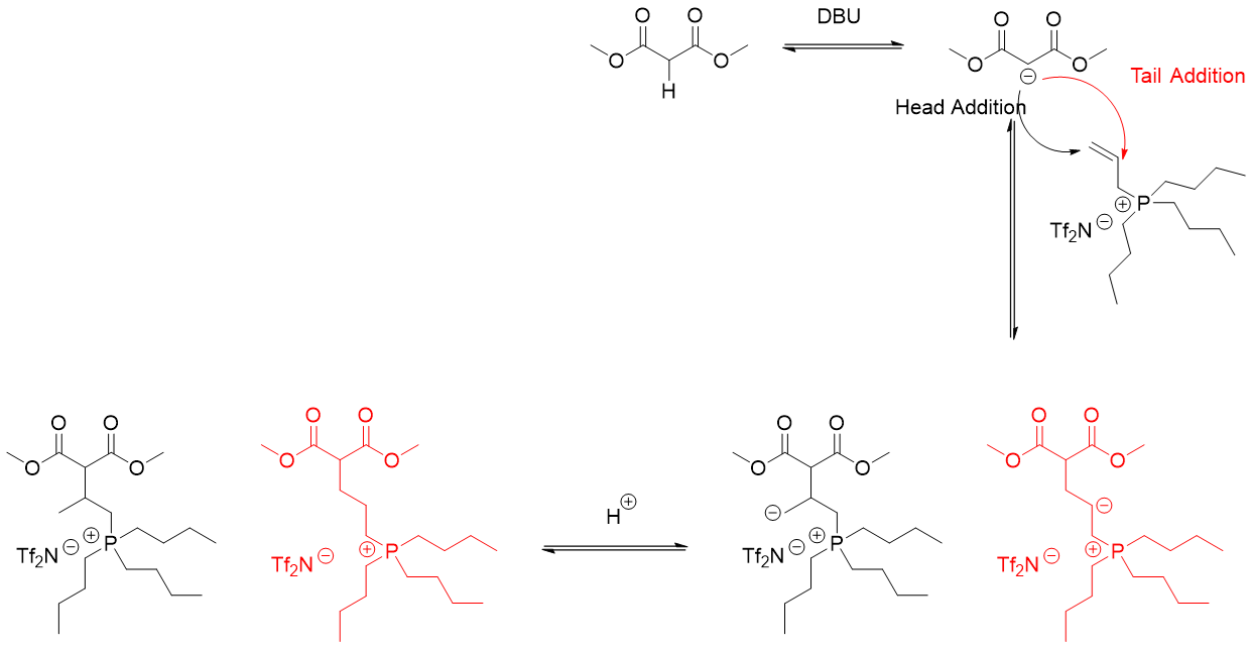


**Scheme S7.1**: Potential transition states of DMMP $Tf_2N$ after undergoing either head addition (black) or tail addition (red).

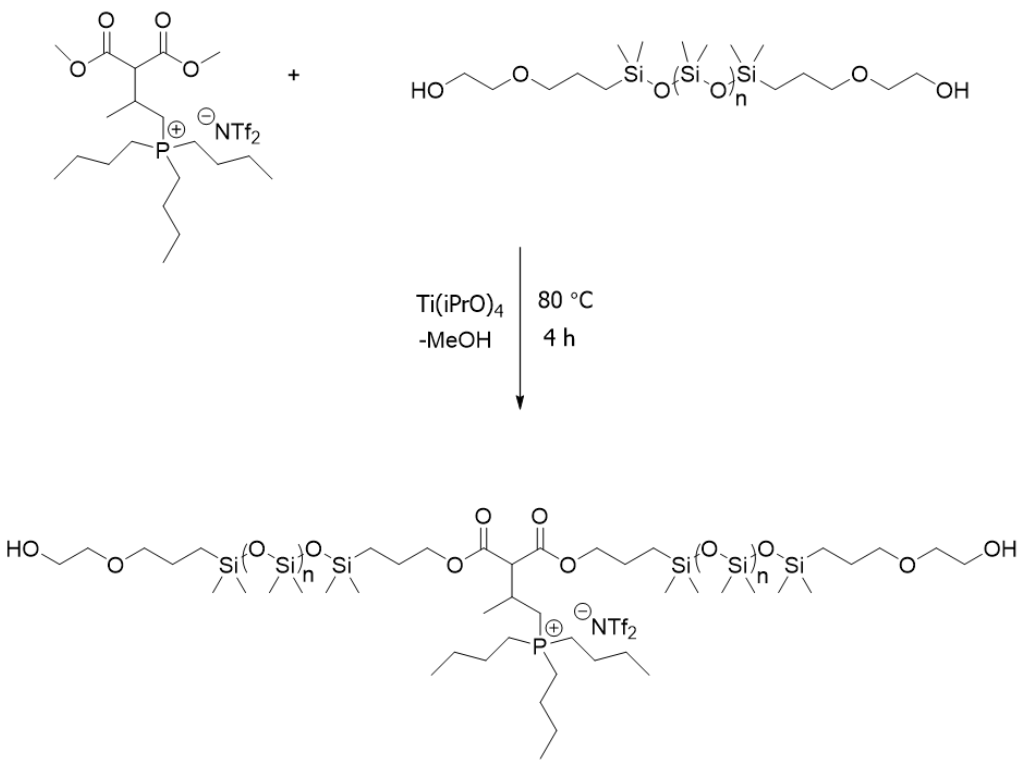


**Scheme S7.2**: Synthesis of phosphonium functionalized PDMS diol.

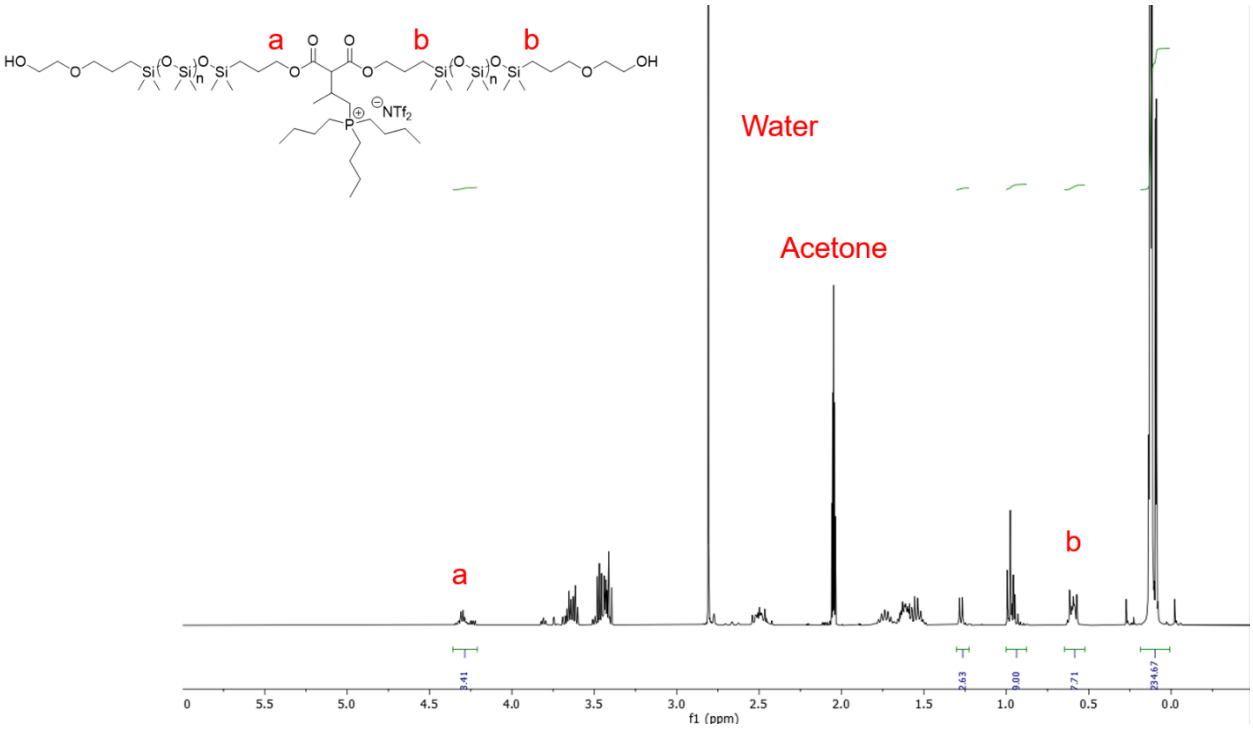


**Figure S7.3:** $^{1}$H NMR spectra of phosphonium functionalized PDMS revealing ester formation.

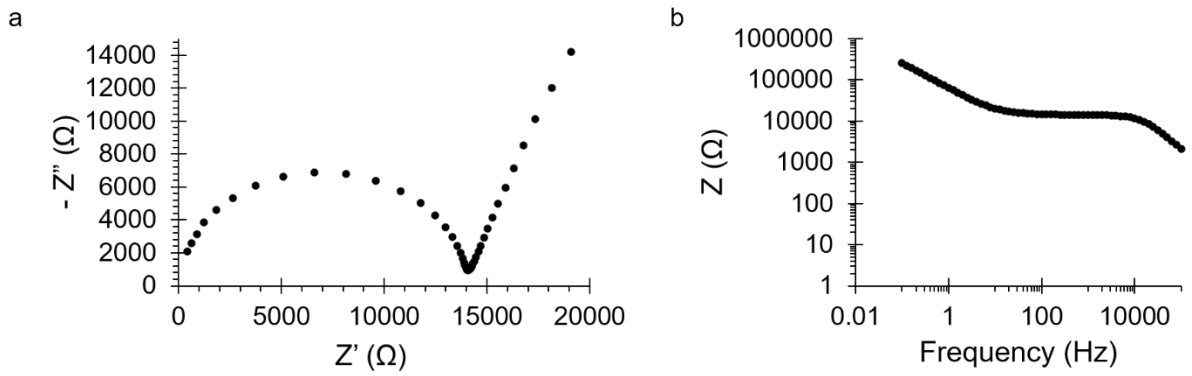


**Figure S7.4**: Representative (a) Nyquist plot and (b) Bode plot of phosphonium PSiU at 85 °C and 20% relative humidity.

# Chapter 8: **Imidazolium ionenes derived from carbonyldiimidazole**

B. Tyler White[1], Josh D. Wolfgang,[1] Jose Sintas,[2] and Timothy E. Long[2*]

[1]Department of Chemistry, Macromolecules Innovation Institute (MII), Virginia Tech, Blacksburg, VA 24061

[2]Biodesign Center for Sustainable Macromolecular Materials and Manufacturing, School for Molecular Sciences, Arizona State University, Tempe, AZ 85287

*To whom correspondence should be addressed: E-mail: Timothy.E.Long@asu.edu.

## 8.1 Abstract

Monomers formed from carbonyldiimidazole provide less toxic methods to produce polycarbonates and polyurethanes compared to current industrial standards. However, this approach has yet to be applied to the synthesis of imidazolium ionenes. This study details the preliminary synthesis of a series of imidazolium ionenes synthesized from a bis-carbonylimidazole monomer, poly(ethylene glycol) dibromide, and an optional dibromide chain extender. All the synthesized ionenes displayed water-solubility; however, the physical properties of the ionenes suggested that only low molecular weight polymers were achieved. Furthermore, thermal analysis revealed a singular $T_g$ in the segmented systems and a low $T_g$ for the homopolymer of the hard segment at 4 °C. Infrared spectroscopy measurements indicated the formation of imidazolium in some of the ionenes but did not necessarily demonstrate full conversion. *In situ* infrared spectroscopy of a small-molecule control further indicated a lack of complete conversion from the imidazole to imidazolium, which points to the need for a refined synthetic method in the future.

## 8.2 Introduction

Carbonyldiimiazole (CDI) finds use in many applications involving small-molecule synthesis especially regarding pharmaceuticals.[1-7] Specifically, CDI facilitates the formation of amide, urea,

carbamate, and thiocarbamate functionalities. CDI has also served as a monomer for polycarbonate synthesis as a replacement for the highly toxic monomer phosgene.[8-12] A recent example comes from Olsson and Malkoch *et al.* where the authors reacted various diols with CDI to liberate imidazole and produce monomers with two reactive carbonylimidazole functionalities.[11] Step-growth polymerization of these bis-carbonylimidazole monomers with aliphatic diols yielded polycarbonate materials with number-average molecular weights ($M_n$) reaching 20 kg $mol^{-1}$. Rannard and coworkers expanded this chemistry to polyurethanes when they used CDI as a coupling agent to form hyperbranched and dendritic polyurethanes in the absence of isocyanates.[13-15] Most recently, Wolfgang and Long *et. al.* capitalized on this chemistry to synthesize linear thermoplastic non-isocyanate polyurethanes from a butanediol-based bis-carbonylimidazole monomer.[16] They showed that the polymers formed creasable films through melt processing and demonstrated the ability to tune the thermal and thermomechanical properties of the polyurethanes based on the selection of diamines used in the polymer synthesis. While these methods show significant promise for replacing hazardous chemicals in the synthesis of commonly used polymers, one major drawback lies in the release of two equivalents of imidazole per equivalent of bis-carbonylimidazole during the reaction. The removal of the imidazole byproduct requires solvent extraction with water or sublimation, both of which prove expensive on an industrial scale.

Leveraging the structure of the bis-carbonylimidazole monomer should provide a route towards the synthesis of imidazolium ionenes through an atom-efficient reaction. Moreover, the properties of these ionenes may rival those of polyurethanes synthesized from CDI chemistry if properly designed.[17] Though relatively less studied than their ammonium-based analogues, imidazolium ionenes show promise for biological applications, solar cells, electrospinning, and $CO_2$ separation, which warrants their continued exploration.[18-21] Williams and Long *et al.*

described the synthesis of a series of segmented imidazolium ionenes with poly(tertamethylene oxide) (PTMO)-based soft segments (SS) and chain extended hard segments (HS).[22] They demonstrated the ability to tune the thermomechanical properties of the ionene based on the amount of HS present in the polymer. Schreiner and Green *et al.* studied a similar family of ionenes with non-chain-extended HSs and measured the effect of changing the PTMO molecular weight on mechanical properties.[20] The imidazolium ionenes exhibited excellent mechanical properties with strains at break exceeding 1000% and ultimate stresses reaching >30 MPa largely due to the strain-induced crystallization of the PTMO segments. These studies suggest that forming ionenes from bis-carbonylimidazole monomers could provide a unique route towards making polymers with interesting properties. Although previous literature has demonstrated the ability to quaternize substituted carbonyl imidazoles to the corresponding imidazolium,[23] to the best of our knowledge no examples exist of imidazolium ionenes synthesized from CDI or its derivatives. Herein, we report preliminary experiments into the synthesis of imidazolium ionenes from a bis-carbonylimidazole monomer with an eye towards producing ionically conductive materials. Poly(ethylene glycol) of varying molecular weights served as a SS for these ionenes, which contained a HS comprised of a butanediol-based bis-carbonylimidazole monomer with an optional chain extender.

## 8.3 Experimental

### 8.3.1 Materials

1,4-Butanediol (ReagentPlus®, 99%), 1,1′-Carbonyldiimidazole (CDI, 97%), 1-iodobutane (99%), poly(ethylene glycol) (PEG, BioReagent, 400 g $mol^{-1}$), potassium carbonate ($K_2CO_3$, ACS reagent, ≥99.0%), 6-bromohexanoyl chloride (>97%), and acetonitrile (anhydrous, 99.8%) were purchased from Sigma-Aldrich and used as received. Ethyl Acetate (HPLC), anhydrous ethyl

ether, ethanol (200 proof) and PEG (Bioreagent, 2,000 g $mol^{-1}$) were purchased from Fisher Scientific and used as received. 1,12-dibromododecane (DBD, 98%) was purchased from Sigma-Aldrich and was recrystallized from ethanol before use. N,N-dimethylformamide (DMF, extra dry, 99.8%) and dichloromethane (DCM, extra dry, 99.9%) were purchased from Acros Organics. Ultra-high purity nitrogen gas (99.999%) was purchased from Praxair.

### 8.3.2 Synthesis of 1,4-butyl(bis-carbonylimidazolide) (BBCI)

The synthesis of BBCI followed the procedure reported by Wolfgang and *Long et al*.[16] 1,4-butanediol (10.000 g, 111 mmol) was added via powder funnel to a three-necked round bottomed flask equipped with a magnetic stir bar. Ethyl acetate (220 mL) was added to the flask and the mixture was stirred until the butanediol dissolved completely. CDI (44.981 g, 277 mmol) was added slowly to the solution to allow for easier dissolution. The reaction was allowed to proceed for 2 h at room temperature while stirring. The BBCI product precipitated from the clear solution as it was formed resulting in a white slurry. The product was filtered with a fritted filter and washed twice with additional ethyl acetate (~50 mL) to remove any unreacted reagents. The resultant white powder was dried *in vacuo* at 60 °C for 18 h to give a >95% yield. The melting point of the pure white powder measured between 135 -137 °C). $^{1}$H NMR ($CDCl_3$, δ, **Figure S8.1**) 8.12-8.14 (t, 2H), 7.41-7.43 (t, 2H), 7.07-7.09 (m, 2H), 4.47-4.52 (t, 4H) 1.94-2.00 (m, 4H).

### 8.3.3 Synthesis of PEG dibromide

The synthesis of $PEG_{400}$ and $PEG_{2k}$ dibromide proceeded as follows. In a general procedure, $PEG_{400}$ (9.963 g, 358 mmol) and $K_2CO_3$ (11.524 g, 83.4 mmol) were added to an oven dried three-necked round bottomed flask equipped with a magnetic stir bar and a glass addition funnel. The septum-sealed reactor was subjected to a constant nitrogen purge for 5 min before anhydrous DCM

(18 mL) was added via syringe. The heterogeneous mixture was allowed to cool to 0 °C in an ice bath while stirring. 6-bromohexanoyl chloride (13.054 g, 61.1 mmol) was added to the addition funnel and diluted with an addition 10 mL of anhydrous DCM before adding dropwise to the reaction mixture. The reaction proceeded for 16 h before quenching with 0.1 mL of DI $H_2O$. The mixture was filtered through a fritted filter equipped with filter paper to remove the $K_2CO_3$ and the resultant solution was stirred with basic alumina for 48 h to remove any residual acid. The solvent was removed by rotary evaporation and the product was dried *in vacuo* at 60 °C to yield a pale-yellow liquid product. $^1$H NMR ($CDCl_3$, δ, **Figure S8.2**) 1.36 (m, 4H), 1.53 (m, 4 H), 1.78 (m, 4H), 2.30 (m, 4H), 3.49 (m, 30H), 3.57 (m, 4H), 4.10 (m, 4H).

### 8.3.4 Synthesis of imidazolium ionenes

The synthesis of segmented and non-segmented ionenes were carried out using the following general procedure. For a segmented ionene containing 30 wt% HS, BBCI (2.128 g, 7.65 mmol), $PEG_{400}$ dibromide (2.518 g, 3.52 mmol), and DBD (1.353 g, 4.12 mmol) were added to a three-necked round bottomed flask equipped with a condenser and a magnetic stir bar. Anhydrous DMF was added via syringe and the flask was purged with $N_2$. The solution was heated at 80 °C for 48 h under constant nitrogen flow. The heterogeneous solution became homogeneous within min of heating. The polymer solution was precipitated in ether and dried *in vacuo* at 60 °C to afford a viscous pale-yellow liquid.

### 8.3.5 Synthesis of BBCI ionic liquid

BBCI (5 g, 18 mmol) and1,4-iodobutane (6.61 g, 36 mmol) were added to a three-necked round bottom flask with a magnetic stir bar and dissolved in acetonitrile. The reaction was allowed to

react under reflux at 80 °C for 30 hours. An in-situ FTIR probe was inserted into the reactor and was used to monitor reaction times.

### 8.3.6 Analytical methods

Nuclear magnetic resonance (NMR) spectroscopy was carried out on an Agilent U4-DD2 spectrometer operating at 400 MHz and 23 °C. All NMR samples were prepared from a either a DMSO-$d_6$ or $CDCl_3$ solution at approximately 10 mg $mL^{-1}$. A TA instruments Q2000 facilitated differential scanning calorimetry (DSC) measurements under nitrogen flow and cooled with a refrigerated cooling system. The glass transition temperatures ($T_g$) were taken as the inflection point of the step transition that occurred during the second heating step. FTIR was performed on a Nicolet iS5 spectrometer equipped with an iD7 ATR stage at room temperature. A Mettler Toledo ReactIR 15 allowed for the *in situ* monitoring of imidazolium formation. The spectra were taken 2 min apart from each other and consisted of 16 scans each.

## 8.4 Results and Discussion

The facile synthesis of BBCI provided a route towards novel imidazolium ionenes with unique backbone structures. Specifically, the inclusion of a carbamate group into the imidazolium ionene structure provides a hydrogen bond acceptor, which may impart interesting bulk morphology or

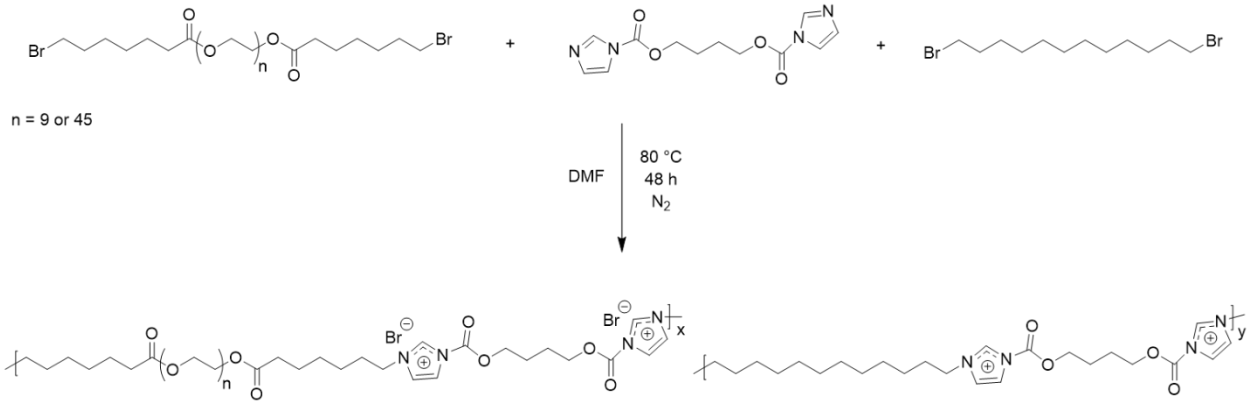


**Scheme 8.1**: Imidazolium ionene synthesis derived from the BBCI monomer and PEG dibromide.

solution properties. **Scheme 8.1** details the synthesis of imidazolium ionenes based on PEG dibromide and BBCI with an optional dibromide chain extender. In this case, the SS consists of the PEG dibromide reacted with the BBCI while the HS comprises of DBD reacted with BBCI. **Table 8.1** summarizes the compositions of the five polymers targeted in this study. Prior literature demonstrated that incorporating lower molecular weight, amorphous PEG enhanced the ionic conductivity of the ionene compared to higher molecular weight, semi-crystalline PEGs.[24] The synthesis of ionenes based on $PEG_{400}$ (n = 9) resulted in highly viscous liquids, which suggested the formation of polymers in both the segmented and non-segmented compositions. However, the inability of these polymers to form free-standing films suggests that their molecular weights remain below the critical molecular weight required for mechanical performance. Next, $PEG_{2k}$ (n = 45) was utilized for this reaction using the rationale that starting with a higher molecular weight precursor should result in higher molecular weight polymers at similar conversions to the $PEG_{400}$ system. However, attempts to cast films of these polymers resulted in waxy, brittle solids reminiscent of $PEG_{2k}$ itself. In a final attempt to achieve high molecular weight ionenes, BBCI and DBD reacted to form a homopolymer of the proposed HS. This reaction yielded a solid powder when precipitated, and solvent casting resulted in a free-standing film. Upon removing all solvent from the film in a vacuum oven, the film exhibited some flexibility, but snapped when attempting to crease the film. Furthermore, exposing the film to atmosphere overnight resulted in a sticky polymer that no longer maintained mechanical integrity. This suggests that the polymer absorbed a significant amount of water from the atmosphere, which plasticized it and lowered the $T_g$. This ionene, as well as all the others synthesized, displayed complete water solubility in an excess of DI water, which supports the hypothesis of atmospheric water uptake. Further experimentation such as TGA sorption analysis (TGA-SA) is needed to quantify the degree of water uptake.

**Table 8.1**: Compositions of synthesized ionenes and measured $T_g$s

| | Targeted HS content (wt.%) | PEG mol% | BBCI mol% | DBD mol% | $T_g$ [a] (°C) |
|---|---|---|---|---|---|
| $PEG_{400}$ | 0 | 50 | 50 | 0 | -25 |
| | 30 | 23 | 50 | 27 | -21 |
| $PEG_{2k}$ | 0 | 50 | 50 | 0 | n/a |
| | 30 | 18 | 50 | 32 | n/a |
| DBD | 100 | 0 | 50 | 50 | 4 |

[a]

DSC provided one method of examining the properties of these ionenes. Namely, segmented ionenes should exhibit two distinct $T_g$s for the hard and soft segments. **Figure 8.1** shows the DSC thermograms for the two $PEG_{400}$ ionenes as well as the HS homopolymer. The 0 wt.% HS ionene (i.e., the homopolymer of $PEG_{400}$ and BBCI) presented a $T_g$ at -25 °C, which correlates exactly with the $T_g$ of pure $PEG_{400}$. There was no indication of an increase in $T_g$ related to the inclusion of imidazolium units into the polymer backbone or the appearance of a melting peak up to 150 °C, which appears in the BBCI monomer. Extending the HS to 30 wt.% appears to increase the $T_g$ of the PEG phase slightly to -21 °C; however, there is no indication of a distinct second $T_g$ or $T_m$ for the HS up to 150 °C. The thermogram of the dried 100 wt.% ionene provides a reference for where the $T_g$ of the HS

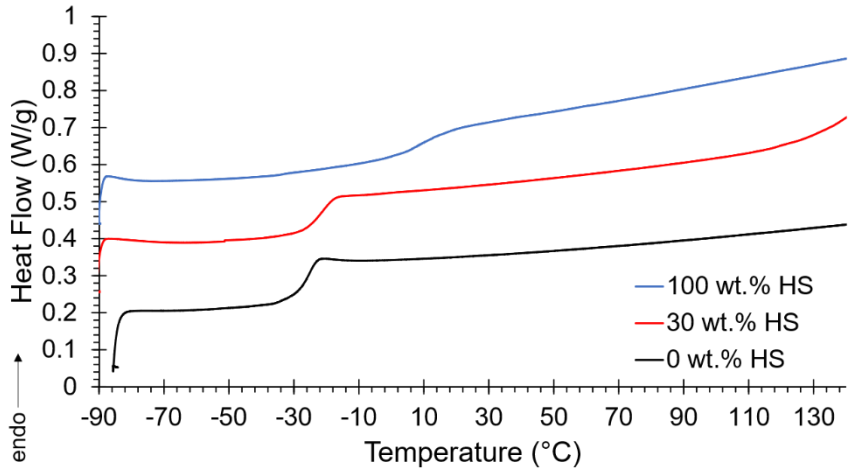


**Figure 8.1**: DSC thermograms of $PEG_{400}$ ionenes containing 0 (black) and 30 (red) wt.% HS compared to the 100 wt.% HS ionene (blue). Data is shifted vertically for clarity.

should appear in segmented systems. In this case, the film exhibited a broad $T_g$ centered around 3 °C. This $T_g$ appears significantly lower than expected for polymers containing intermolecular ionic interactions, and points to the poor mechanical properties exhibited by both the 100 wt.% HS homopolymer as well as the segmented systems. The low $T_g$ may indicate low molecular weight in the HS, but SEC analysis is required to confirm this hypothesis. However, measuring SEC of ionenes remains difficult due to ionic aggregation and polymer-column interactions. DSC analysis of the $PEG_{2k}$-based polymers showed only a melting temperature at 43 and 41 °C for the 0 wt.% and 30 wt.% HS ionenes, respectively. These melting temperatures measured ~10 °C lower than the $PEG_{2k}$ (54 °C) and the ionenes also displayed lower enthalpies of melting than the pure PEG as summarized in **Table S8.1**.

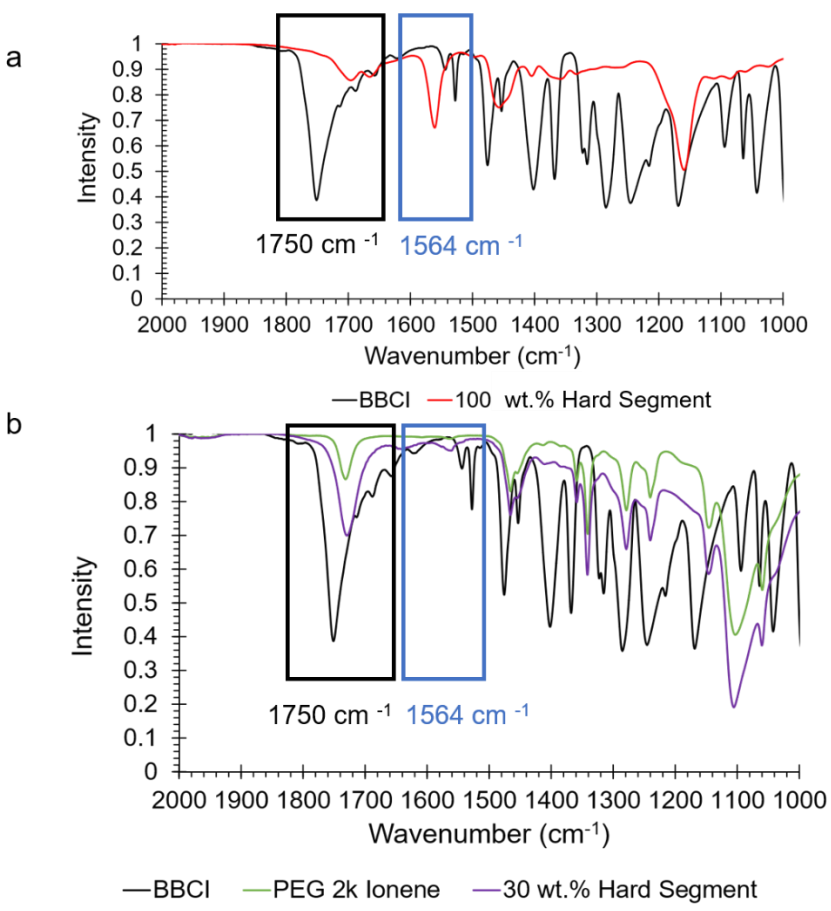


**Figure 8.2**: FTIR spectra of (a) BBCI (black) and 100 wt.% HS ionene (red) and (b) BBCI compared to $PEG_{2k}$ ionenes containing 0 (green) and 30 wt. % (purple) HS.

FTIR spectroscopy was employed as a means of providing more evidence for ionene formation. **Figure 8.2a** shows the IR spectrum of BBCI compared to that of the 100 wt.% HS ionene. The peak at approximately 1750 $cm^{-1}$ in the BBCI spectrum represents the carbonyl stretching from the carbonylimidazole group. After the reaction occurs,

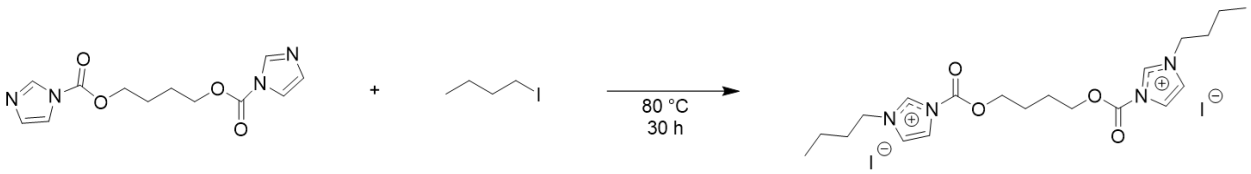


**Scheme 8.2**: Reaction of BBCI with a monofunctional iodobutane.

this peak disappears and gives rise to a new peak at 1564 $cm^{-1}$, which likely represents a shift in the frequency of the carbonyl now attached to the imidazolium. Conversely, **Figure 8.2b** shows the IR spectra of $PEG_{2k}$-based ionenes compared to BBCI. In this case, the intensity of the carbonylimidazole peak decreased, but did not disappear completely. Furthermore, no new peak was observed at 1564 $cm^{-1}$ to indicate the formation of imidazolium. This may indicate an incomplete reaction and explains the physical properties of the polymer.

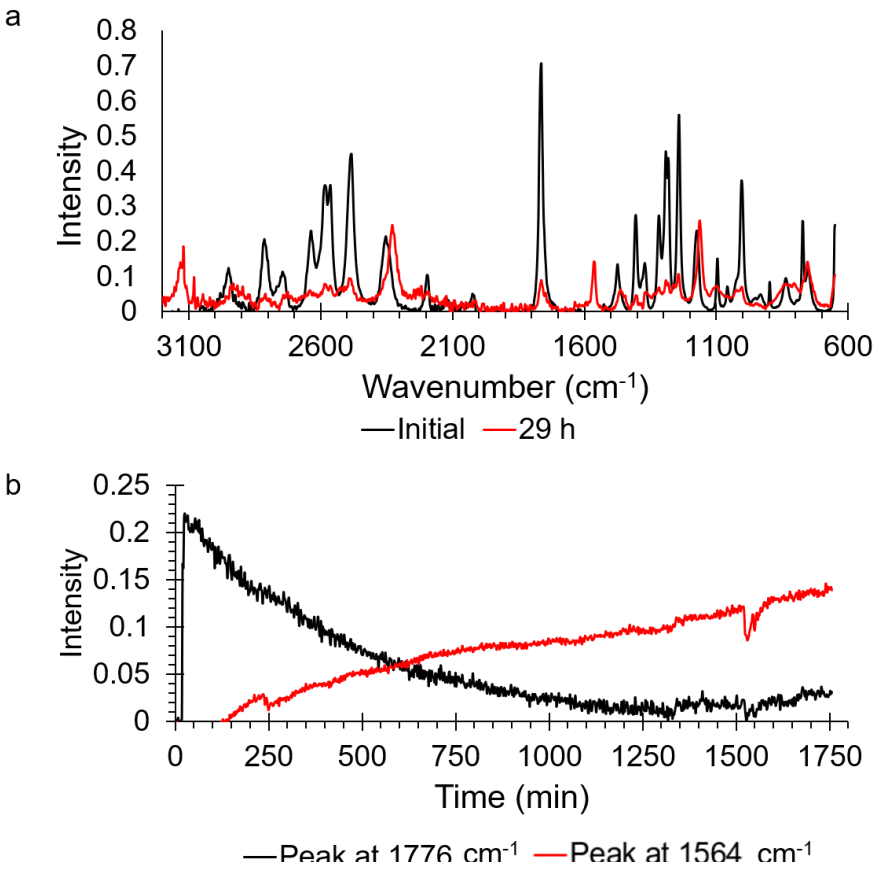


**Figure 8.3**: *In-situ* FTIR data showing (a) the spectra before (black) and after (red) the reaction occurred and (b) the intensity of two peaks as a function of time.

Carrying out the quaternization of BBCI with a monofunctional bromide helped elucidate the reaction kinetics between as shown in **Scheme 8.2**. The insertion of an IR probe into the reaction vessel allowed for *in situ* monitoring of the imidazolium formation. **Figure 8.3a** reveals the IR spectra of the

reaction mixture at the beginning of the reaction and 29 h later. As with the ionene IR spectra, a carbonyl stretching peak at 1776 $cm^{-1}$ disappeared over time and gave rise to a new peak at 1564 $cm^{-1}$. Furthermore, the appearance of a peak at 3120 $cm^{-1}$ may indicate the formation of an imidazolium ring;[25] however, this peak remained absent in the previous FTIR spectra for the ionenes. **Figure 8.3b** further demonstrated this by plotting the intensity of each peak as a function of time. Each plot reveals evidence that some of the initial imidazole remained after the reaction ended. The difficulty in reaching full conversion from the imidazole to the imidazolium likely results in the apparent low molecular weight of the ionenes. Future efforts to synthesize imidazolium ionenes from BBCI will require a more detailed examination of the polymer structure and molecular weight, as well as methods to work around the incomplete conversion of the imidazole to imidazolium.

## 8.5 Conclusions

BBCI provided a new diimidazole monomer for the potential synthesis of imidazolium ionenes. The functionalization of PEG with 6-bromohexanoyl bromide produce dibromide oligomers of varying molecular weight for segmented ionenes. The reaction of $PEG_{400}$ dibromide with BBCI yielded viscous liquids, while $PEG_{2k}$-based ionenes manifested as brittle, waxy solids. The ionene formed from the reaction of BBCI with DBD yielded a free-standing film; however, the film quickly took up water and resulted in a tacky material with no mechanical properties. DSC analysis revealed a singular $T_g$ in all of the $PEG_{400}$-derived ionenes and revealed a low $T_g$ of 4 °C for the ionene comprised of 100% HS. FTIR spectroscopy provided evidence of imidazolium formation in the $PEG_{400}$ ionenes, but little evidence for the formation of imidazolium in the $PEG_{2k}$ systems. Finally, *in situ* FTIR spectroscopy monitored the formation of imidazolium during the

reaction of a monofunctional alkylhalide with BBCI and revealed incomplete conversion of the reactants to the imidazolium species.

## 8.6 Acknowledgements

The authors would like to acknowledge Ryan Carrazzone from the John Matson research group and Ben Stovall for assistance with FTIR measurements.

## 8.7 References

1. Montalbetti, C. A.; Falque, V., Amide bond formation and peptide coupling. *Tetrahedron* **2005,** *61* (46), 10827-10852.
2. Padiya, K. J.; Gavade, S.; Kardile, B.; Tiwari, M.; Bajare, S.; Mane, M.; Gaware, V.; Varghese, S.; Harel, D.; Kurhade, S., Unprecedented "in water" imidazole carbonylation: paradigm shift for preparation of urea and carbamate. *Organic letters* **2012,** *14* (11), 2814-2817.
3. Paul, R.; Anderson, G. W., N, N'-Carbonyldiimidazole, a New Peptide Forming Reagent1. *Journal of the American Chemical Society* **1960,** *82* (17), 4596-4600.
4. Vaidyanathan, R.; Kalthod, V. G.; Ngo, D. P.; Manley, J. M.; Lapekas, S. P., Amidations using N, N '-carbonyldiimidazole: Remarkable rate enhancement by carbon dioxide. *The Journal of organic chemistry* **2004,** *69* (7), 2565-2568.
5. Verma, S. K.; Ghorpade, R.; Pratap, A.; Kaushik, M., Solvent free, N, N′-carbonyldiimidazole (CDI) mediated amidation. *Tetrahedron letters* **2012,** *53* (19), 2373-2376.
6. Verma, S. K.; Ghorpade, R.; Pratap, A.; Kaushik, M., CDI-mediated monoacylation of symmetrical diamines and selective acylation of primary amines of unsymmetrical diamines. *Green chemistry* **2012,** *14* (2), 326-329.
7. Woodman, E. K.; Chaffey, J. G.; Hopes, P. A.; Hose, D. R.; Gilday, J. P., N, N′-Carbonyldiimidazole-Mediated Amide Coupling: Significant Rate Enhancement Achieved by Acid Catalysis with Imidazole· HCl. *Organic Process Research & Development* **2009,** *13* (1), 106-113.
8. Fréchet, J. M.; Bouchard, F.; Eichler, E.; Houlihan, F. M.; Iizawa, T.; Kryczka, B.; Willson, C. G., Thermally depolymerizable polycarbonates V. Acid catalyzed thermolysis of allylic and benzylic polycarbonates: a new route to resist imaging. *Polymer Journal* **1987,** *19* (1), 31-49.
9. Houlihan, F.; Bouchard, F.; Frechet, J.; Willson, C., Thermally depolymerizable polycarbonates. 2. Synthesis of novel linear tertiary copolycarbonates by phase-transfer catalysis. *Macromolecules* **1986,** *19* (1), 13-19.
10. Hult, D.; García-Gallego, S.; Ingverud, T.; Andrén, O. C.; Malkoch, M., Degradable high T g sugar-derived polycarbonates from isosorbide and dihydroxyacetone. *Polym. Chem.* **2018,** *9* (17), 2238-2246.
11. Olsson, J.; Hult, D.; Garcia-Gallego, S.; Malkoch, M., Fluoride-promoted carbonylation polymerization: a facile step-growth technique to polycarbonates. *Chemical science* **2017,** *8* (7), 4853-4857.

12. Scheel, A.; Komber, H.; Voit, B. In *Hyperbranched thermolabile polycarbonates derived from a A2+ B3 monomer system*, Macromolecular Symposia, Wiley Online Library: 2004; pp 101-110.
13. Feast, W. J.; Rannard, S. P.; Stoddart, A., Selective convergent synthesis of aliphatic polyurethane dendrimers. *Macromolecules* **2003,** *36* (26), 9704-9706.
14. Rannard, S. P.; Davis, N. J.; Herbert, I., Synthesis of Water Soluble Hyperbranched Polyurethanes Using Selective Activation of AB2 Monomers. *Macromolecules* **2004,** *37* (25), 9418-9430.
15. Stoddart, A.; Feast, W. J.; Rannard, S. P., Synthesis and thermal studies of aliphatic polyurethane dendrimers: a geometric approach to the Flory–Fox equation for dendrimer glass transition temperature. *Soft Matter* **2012,** *8* (4), 1096-1108.
16. Wolfgang, J. D.; White, B. T.; Long, T. E., Non-Isocyanate Polyurethanes from 1,1'-Carbonyldiimidazole: An Activated Carbamate Approach. *Submitted for Publication* **2021**.
17. Bara, J. E.; O'Harra, K. E., Recent Advances in the Design of Ionenes: Toward Convergence with High-Performance Polymers. *Macromolecular Chemistry and Physics* **2019,** *220* (13), 1900078.
18. Anderson, E. B.; Long, T. E., Imidazole- and imidazolium-containing polymers for biology and material science applications. *Polymer* **2010,** *51* (12), 2447-2454.
19. Kammakakam, I.; Rao, A. H.; Yoon, H. W.; Nam, S.; Park, H. B.; Kim, T.-H., An imidazolium-based ionene blended with crosslinked PEO as a novel polymer membrane for selective CO 2 separation. *Macromolecular Research* **2014,** *22* (8), 907-916.
20. Schreiner, C.; Bridge, A. T.; Hunley, M. T.; Long, T. E.; Green, M. D., Segmented imidazolium ionenes: Solution rheology, thermomechanical properties, and electrospinning. *Polymer* **2017,** *114*, 257-265.
21. Suzuki, K.; Yamaguchi, M.; Hotta, S.; Tanabe, N.; Yanagida, S., A new alkyl-imidazole polymer prepared as an inonic polymer electrolyte by in situ polymerization of dye sensitized solar cells. *Journal of Photochemistry and Photobiology A: Chemistry* **2004,** *164* (1), 81-85.
22. Williams, S. R.; Salas-de la Cruz, D.; Winey, K. I.; Long, T. E., Ionene segmented block copolymers containing imidazolium cations: Structure–property relationships as a function of hard segment content. *Polymer* **2010,** *51* (6), 1252-1257.
23. Batey, R. A.; Santhakumar, V.; Yoshina-Ishii, C.; Taylor, S. D., An efficient new protocol for the formation of unsymmetrical tri- and tetrasubstituted ureas. *Tetrahedron Letters* **1998,** *39* (35), 6267-6270.
24. Lee, M.; Choi, U. H.; Salas-de la Cruz, D.; Mittal, A.; Winey, K. I.; Colby, R. H.; Gibson, H. W., Imidazolium polyesters: structure–property relationships in thermal behavior, ionic conductivity, and morphology. *Advanced Functional Materials* **2011,** *21* (4), 708-717.
25. Haddad, B.; Mokhtar, D.; Goussem, M.; Belarbi, E.-h.; Villemin, D.; Bresson, S.; Rahmouni, M.; Dhumal, N. R.; Kim, H. J.; Kiefer, J., Influence of methyl and propyl groups on the vibrational spectra of two imidazolium ionic liquids and their non-ionic precursors. *Journal of Molecular Structure* **2017,** *1134*, 582-590.

## 8.8 Supplemental Information

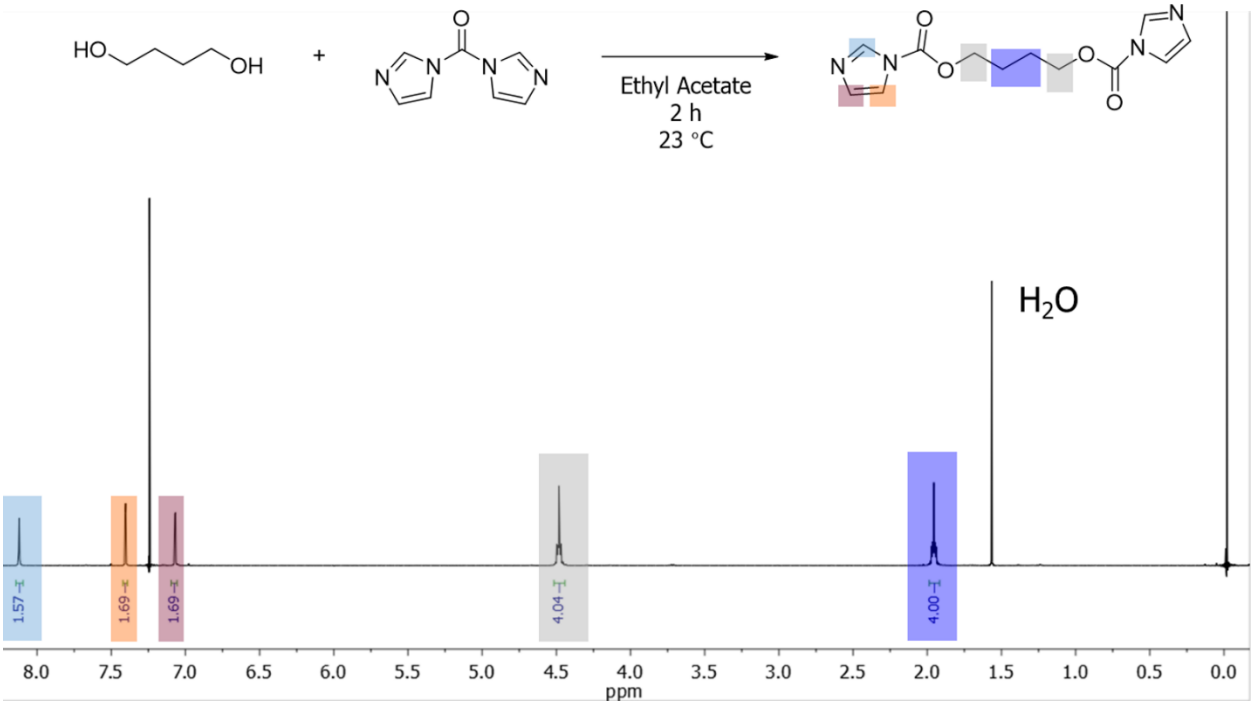


**Figure S8.1**: $^{1}H$ NMR spectrum of BBCI taken in $CDCl_3$.

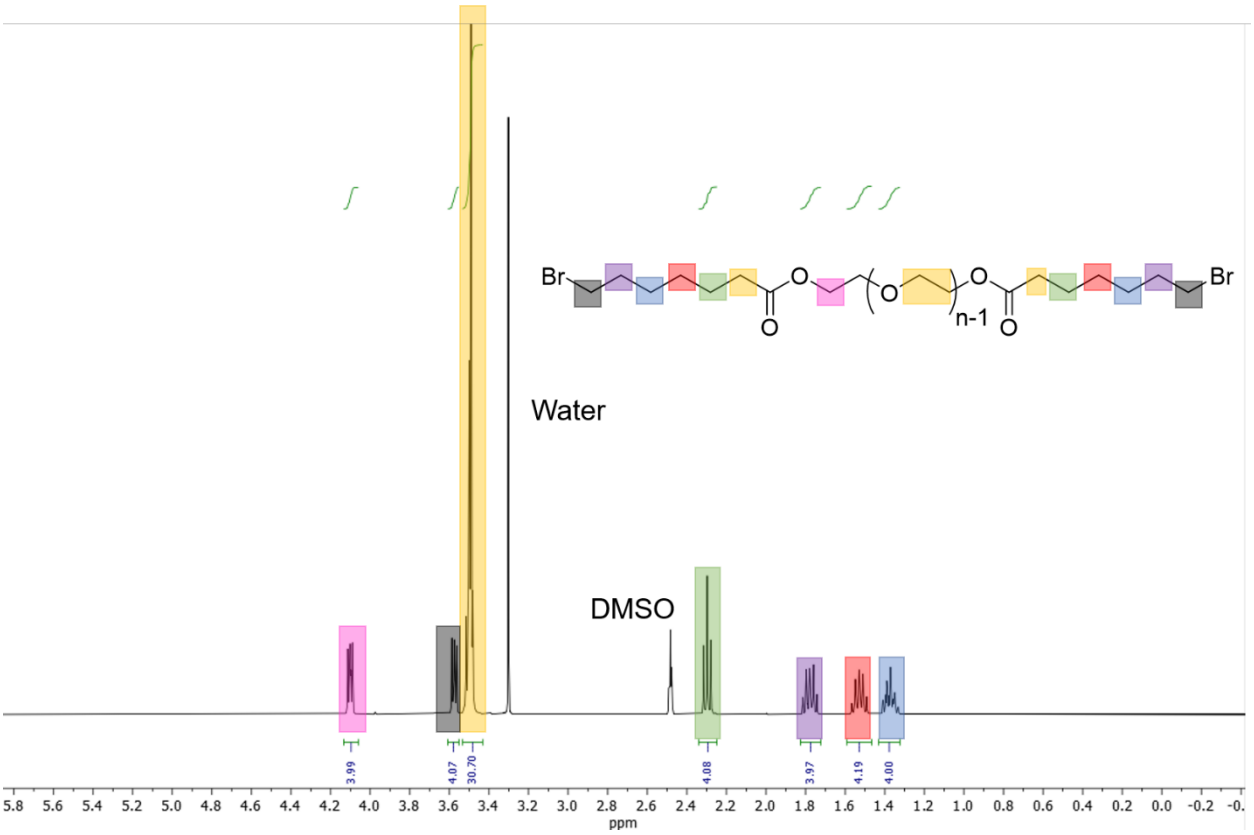


**Figure S8.1**: $^{1}$H NMR spectrum of BBCI taken in d6-DMSO.

**Table S8.1**: Thermal properties of $PEG_{2k}$ and $PEG_{2k}$-based ionenes.

| Sample | $T_m$ (°C) | $\Delta H_m$ (J/g) |
|---|---|---|
| **$PEG_{2k}$** | 54 | 179 |
| **$PEG_{2k}$ Ionene** | 43 | 110 |
| **$PEG_{2k}$ 30 wt.% HS** | 41 | 71.0 |

# Chapter 9: **Overall Conclusions**

The use of industrially relevant chemistries, both new and old, allowed for the synthesis and characterization of novel step-growth polymers for use in modern technologies such as additive manufacturing and electromechanical transducers. Urea serves as a bio-derived replacement for toxic isocyanates in the synthesis of polyureas. The melt polycondensation of urea with poly(tertamethylene oxide) (PTMO) and a small molecule chain extender afforded a family of segmented polyurea (PUr) elastomers in the absence of solvent or catalyst. Varying the hard segment (HS) content resulted in tunable thermal, mechanical, and thermomechanical properties. The PUrs all exhibited soft segment (SS) melting peaks near room temperature, and PUrs containing 20 and 30 wt.% HS displayed two endothermic transitions near 120 °C for the melting of the HS. Dynamic mechanical analysis (DMA) revealed the presence of phase separation at all compositions and showed an increase in the plateau storage modulus with increasing HS content. Varying the HS content led to tunable mechanical properties, and the high stains at break (between 340 and 770% strains) suggested that high molecular weight as achieved across the range of PUr compositions. The storage modulus and ultimate stress increased with increasing HS, which correlated well with literature examples of isocyanate-based PUrs. These isocyanate-free PUrs exhibited high dielectric permittivities that reached values as high as 10.6. Although this high permittivity also correlated with high dielectric loss, this data suggests that careful modification of the PUr design in the future may lead materials suitable for dielectric elastomer applications. This represents a new application for polyurea elastomers that has been previously unexplored

This isocyanate-, solvent-, and catalyst-free approach to PUr synthesis was expanded to produce water-soluble poly(ether urea)s (PEUs) for extrusion additive manufacturing (AM).

Utilizing a series of commercially available, water-soluble polyether diamines of varying molecular weight enabled the determination of structure-property relationships in the resultant PEUs. Polyethers with melting points below room temperature resulted in amorphous PEUs at room temperature that displayed little to no mechanical stability as films. PEU 2000 displayed a melting temperature above room temperature at 35 °C, which facilitated the formation of mechanically robust films. Tensile analysis revealed thermoplastic yield behavior in this material and a strain at break that exceeded 500%. The slow crystallization behavior of this PEU made extrusion AM difficult when depositing layers onto a room temperature build stage. However, cooling the build stage with dry ice increased the crystallization rate of the PEU enough to allow for the printing of a water-soluble hollow cube as a proof of concept.

Another AM technique, vat photopolymerization (VP), permitted 3D printing of liquid unsaturated polyester resins (UPR). The incorporation of a phosphonium polymerizable ionic liquid (PIL) into the resin allowed for the exclusion of the classically-used reactive diluent styrene. The synthesis of the unsaturated polyester (UPE) oligomers closely followed an industrial process, and the concentration of crosslinking sites was varied through the incorporation of phthalic anhydride into the backbone. The inclusion of dimethoxyethane as a non-reactive diluent helped to solubilize the resin while maintaining a low volatility. A series of photorheological experiments screen the potential UPR compositions to determine their viability for VP. The UPE saturation content, PIL concentration, and solids content were all varied individually to determine that the UPR containing 60 wt.% UPE-23 and 40 wt.% PIL at a concentration of 70 wt.% solids in dimethoxyethane showed the most promise for VP. Thermal analysis of the cured UPRs revealed that the $T_{d,5\%}$ of the polymers increased linearly with an increase in PIL content. VP produced high-resolution 3D structures and scanning electron microscopy confirmed that pores did not form in

the printed part throughout the solvent removal process. Parts produced from VP demonstrated ionic conductivities that reached $10^{-5}$ S $cm^{-1}$ at 150 °C, suggesting that these cured UPRs may find use in high-temperature electronic applications.

The synthesis of a novel phosphonium ionic liquid (IL) provided a route for incorporating a phosphonium motif into the low $T_g$ poly(dimethyl siloxane) phase of a poly(siloxane urethane) (PSiU). We hypothesized that incorporating the ionic unit into the extremely low $T_g$ phase would enhance the ionic conductivity compared to poly(urethanes) with other charged soft segments (i.e., sulfonated poly(ethylene glycol)). A PSiU containing 70 wt.% of the phosphonium-functionalized SS formed an optically clear and flexible film when solution cast. Differential scanning calorimetry revealed an identical $T_g$ between the charged PSiU and an uncharged control, which proved that the incorporation of ionic interactions into the SS did not negatively impact the thermal properties of the PSiU. DMA confirmed these thermal transitions and suggested that microphase separation occurred between the SS and HS as indicated from the plateau modulus after the SS $T_g$. Small angle x-ray scattering confirmed that strong microphase separation occurred and revealed that the domain size in the charged PSiU measured slightly higher than that of the control. Conductivity measurements indicated a room temperature ionic conductivity of 3.0 x$10^{-8}$ S $cm^{-1}$ with the temperature dependence showing Arrhenius behavior. The comparable conductivity to sulfonated poly(ethylene glycol)-based polyurethanes despite having a 40 °C lower $T_g$ suggests that continuing to decrease the $T_g$ results in a diminishing return on the ionic conductivity. Despite this, the charged PSiU exhibited conductivity values comparable to literature examples for ionic polymer transducers, which indicates that this polymer may prove suitable for these applications.

A biscarbonylimidazole monomer reported recently from our group (BBCI) provided the basis for a study into the synthesis of novel segmented imidazolium ionenes. Poly(ethylene glycol)

(PEG) oligomers served as telechelic macromonomers in the ionene synthesis. Ionenes formed from 400 g $mol^{-1}$ PEG became viscous liquids while those formed form 2 kg $mol^{-1}$ PEG formed brittle, waxy solids similar to pure $PEG_{2k}$ suggesting that these materials do not reach high molecular weights. The ionene containing 100 wt.% of the HS formed a solid film that absorbed a significant amount of atmospheric water overnight. All the synthesized ionenes displayed water solubility in excess DI water. DSC analysis did not reveal any evidence of phase separation in any of the ionenes but did show a decrease in the melting point and enthalpy of $PEG_{2k}$-based ionenes. FTIR spectroscopy provided some evidence of imidazolium formation in the 100 wt.% HS ionene; however, FTIR of the $PEG_{2k}$ ionenes remained inconclusive. Finally, *in situ* FTIR monitored the formation of the imidazolium in the reaction of BBCI with a monofunctional alkyl halide. The experiment revealed an increase in the imidazolium formation over the course of 30 h but indicated that some unreacted imidazole remained in the end. The difficulty in reaching full conversion likely relates to the presumed low molecular weight of the ionenes. From these results we conclude that the attached carbonyl on the imidazole ring reduces the nucleophilicity of the reactive nitrogen species. In order to achieve high molecular weight polymer, a different approach using preformed, reactive oligomers may prove suitable for overcoming this limitation.

# Chapter 10: **Suggested Future Work**

## 10.1 Amorphous, isocyanate-free polyureas/ polyurethanes for dielectric elastomers with high permittivity and low dielectric loss

Our group previously demonstrated the ability to synthesize isocyanate-free polyureas (PUrs) utilizing urea as a biologically derived monomer.[1-3] Chapter 3 demonstrated the ability to leverage this chemistry for the purpose of making elastomers with tunable moduli and high dielectric permittivity. However, dielectric relaxation spectroscopy revealed high dielectric losses for the compositions tested, which limits their potential use as dielectric elastomers. We theorized that the presence of crystalline domains in both the hard and soft segments resulted in the high degrees of dielectric loss. Therefore, careful synthetic design is needed to produce elastomers with high dielectric permittivity (> 3) and low dielectric loss (< 5%).

The first step in the design process involves the choice of SS oligomer. Lorenzini and Sotzing *et al.* reported that the presence of etheric oxygen atoms in the backbone enhances the dielectric permittivity of polyurethanes (PUs) and PUrs.[4] Therefore, an amorphous polyether such as poly(propylene glycol) (PPG) seems promising for producing PUrs with high permittivity. Furthermore, segmented PUrs and PUs synthesized from PPG have demonstrated elastomeric properties.[5] Next, the hard segment (HS) requires a high $T_g$ without the presence of crystallinity. The Zhang group described several examples of amorphous, high $T_g$ thermoplastic PUrs with low dielectric loss.[6-9] These studies utilized various aromatic diamine chain extenders in the PUr synthesis to produce thermoplastics with permittivities ranging from 4-6 with < 3% dielectric loss. These results suggest that incorporating aromatic diamines into the HS of a segmented PUr may result in amorphous elastomers with high permittivity and low dielectric loss.

**Scheme 10.1** shows the proposed synthesis of a novel segmented PUr. This reaction involves the combination of a 2 kg $mol^{-1}$ PPG diamine with 4,4′-(4,4′-isopropylidenediphenyl-1,1′-diyldioxy)dianiline and urea. The synthetic procedure followed the previously reported method and PUrs containing 30 and 40 wt.% HS were targeted. Both compositions resulted in a tacky, amber polymer, but only the 40 wt.% sample produced a free-standing film as shown in **Scheme 10.1**. However, this film was sticky to the touch and was not capable of supporting its own weight. Differential scanning calorimetry revealed a singular $T_g$ that increased from -33 to -6 °C for the 30 and 40 wt.% HS, respectively. The presence of a singular $T_g$ that sits well above that of PPG (-75 °C) suggests a lack of phase separation between the SS and HS. This may occur due to the bulk of the aromatic group, which dilutes the urea hydrogen bonding and prevents the formation of a percolated HS. This reaction was repeated with two smaller aromatic diamines explored by the Zhang group (i.e., m-phenylenediamine (mPD) and 4,4'-Oxydianiline (ODA)) to circumvent this issue. However, every reaction attempted with these monomers and urea resulted in a low molecular weight, waxy solid material, even with the exclusion of the PPG diamine. It remains unclear why aromatic diamines appear incompatible with this chemistry; however, these segmented PUr structures still show promise for dielectric elastomer applications.

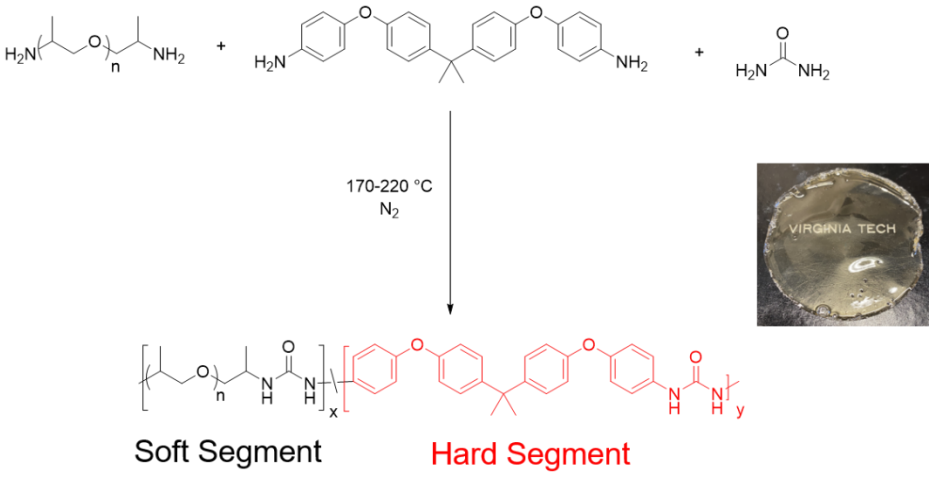


**Scheme 10.1**: Synthesis of a PPG-based polyurea with an aromatic HS. The polymer containing 40 wt.% HS formed an optically clear free-standing film.

Future work in this area should follow one or multiple of the following routes. First, other cyclic, aliphatic diamine molecules may lead to high molecular weight amorphous HSs. For example, 4,4′-methylenebis(cyclohexylamine) represents the diamine version of a commonly used diisocyanate for PUr and PU syntheses (4,4′-methylenebis(cyclohexyl isocyanate) (HMDI)), which provides an amorphous HS. Another approach is to leverage a different isocyanate-free chemistry. Our group recently demonstrated the ability to form high molecular weight PUs through the reaction of a biscarbonylimidazole monomer with a variety of diols.[10] This reaction could serve to form PUrs or PUs with the desired structures for amorphous dielectric elastomers; however, this chemistry may also prove incompatible with the aromatic diamines. **Figure 10.1** summarizes the different routes towards amorphous segmented PUrs described here.

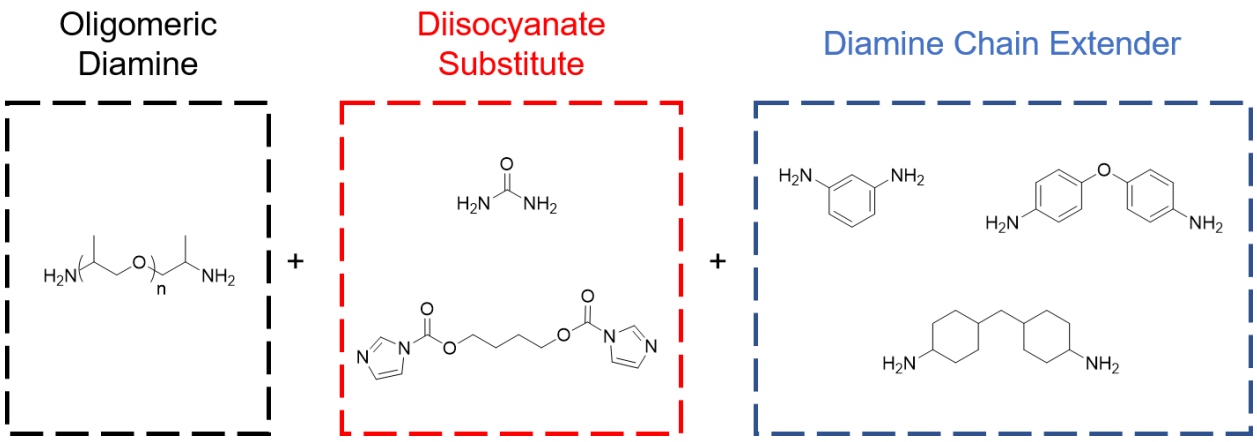


**Figure 10.1**: Proposed monomers for future research into amorphous, isocyanate-free PUrs

## 10.2 PEG-based unsaturated polyesters for vat photopolymerization

Chapter 6 presented a novel approach towards 3D printing unsaturated polyester resins (UPR) through vat photopolymerization (VP) utilizing a non-volatile polymerizable ionic liquid (PIL) and a low-volatility diluent, dimethoxyethane. This approach provides advantages over other UPRs for VP because it eliminates styrene as a reactive diluent; however, removing the dimethoxyethane remains a top priority for future UPR formulations. Moreover, the cured UPR

displays low ionic conductivities due to the relatively high $T_g$ for conductivity (36 °C). Sassmann and Weichold produced poly(ethylene glycol) (PEG)-based unsaturated polyesters (UPEs) doped with Li salt to serve as conductive resistivity sensors in concrete screws.[11] Although very little characterization was performed on the polymer, the sensor fabricated from this cured resin displayed a conductivity of 1 x $10^{-5}$ at room temperature. The results of this work suggest that combining our approach with a PEG-based UPE could enhance the conductivity of the cured resin. Also, the incorporation of PEG into the UPE backbone may increase the solubility of the polymer in the PIL similar to the VP resin studied by Schultz and Long *et al.*[12]

Initial attempts to synthesize PEG-UPEs using 400 g $mol^{-1}$ PEG and the same synthetic procedure outlined in Chapter 6 resulted in oligomers that exhibited a high degree of the cis maleate isomer (~50%). The addition of titanium (IV) isopropoxide as an esterification catalyst improved amount of trans isomer in the backbone to approximately 93% as measured from $^1$H NMR spectroscopy (**Figure 10.2**) The resultant polymer manifested as a yellow liquid at room temperature, which contrasts with the solid propylene-glycol-based UPE. Unfortunately, this PEG-UPE remained immiscible with the PIL and required dilution with diglyme. A resin was formulated with 60 wt.% UPE, 40 wt.% PIL, 2 wt.% of photoinitiator, and diluted to a concentration of 70 wt.% solids. Preliminary

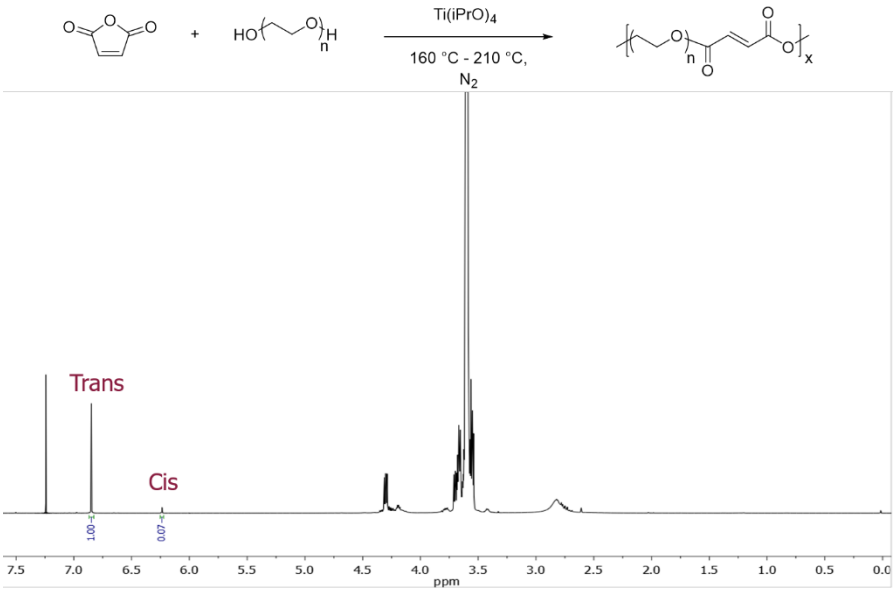


**Figure 10.2**: $^1$H NMR spectrum in $CDCl_3$ of $PEG_{400}$ -UPE

attempts to photocure this UPR with UV light led to the formation of a weak, rubbery solid. This suggests that more controlled attempts to cure this resin (e.g., photorheology) may produce materials with suitable moduli for VP. Future work should focus on developing this resin with varying PEG molecular weights, degrees of unsaturation, and PIL concentrations. Furthermore, the chemical identity of the PIL itself can be altered to try to facilitate solubility. For example, increasing the the hydrophilicity of the charged group and/or counterion may improve the solubility compared to the hydrophobic PIL utilized in Chapter 6.

## 10.3 Incorporation of fillers into UPRs for 3D printing of composites

As mentioned in Chapter 6, UPRs primarily find use in glass-fiber-reinforced (GFR) composites. For this reason, incorporating fillers such as glass fibers or silica nanoparticles into either the PEG-, or propylene-glycol-based UPR will further enhance the utility of these 3D printed materials. Dispersing an inorganic filler into the UPR will likely increase the viscosity to a degree that will prevent recoating for a VP process, so 3D printing these composite materials may require a different process. Direct ink write (DIW) and UV-assisted DIW have demonstrate the ability to print polymer nanocomposites with a variety of organic and inorganic nanofillers.[13-15] UV-assisted DIW combines the extrusion of a shear thinning paste with photocuring to produce geometrically complex three-dimensional structures. Future work should center on varying the types and concentrations of inorganic fillers in UPRs to determine suitable rheological properties for UV-assisted DIW. The mechanical properties of the resultant cured UPR should also be evaluated as a function of filler content.

## 10.4 Fabrication of ionic polymer-metal composites from segmented PUs

As discussed in Chapters 2 and 5, very few literature examples report ionic polymer-metal composites (IPMCs) fabricated from segmented PUs despite their synthetic variability and

desirable microphase separated morphologies. Gao and Long *et al.* previously described the synthesis and characterization of PUs containing either a sulfonated SS or HS.[16, 17] The sulfonated SS PU demonstrated the ability to swell with a commercial ionic liquid up to 25 wt.%, which increased the conductivity from $10^{-8}$ S $cm^{-1}$ to $10^{-6}$ S $cm^{-1}$. This PU provides a foundation for exploring charged PUs as membranes for IPMC or ion polymer-carbon composite (IPCC) actuators. Preliminary experiments focused on reproducing this PU and coating it with carbon paper electrodes as shown in **Figure 10.3**. The synthesized PU contained 70 wt.% of the sulfonated SS described by Gao. The carbon paper was first soaked in a solution of the sulfonated PU and annealed *in vacuo* to impregnate the electrode with polymer; this step helps to improve adhesion between the film and electrodes. The electrodes were then melt pressed onto the PU film to provide the final actuator. Unfortunately, the IPCCs formed from this method did not show actuation under applied voltage, even upon casting the film with 20 wt.% of a commercial imidazolium IL. A voltmeter measured a significant voltage drop across the actuator compared to the applied voltage indicating a degree of electron conduction across the film, which likely prevented actuation. This phenomenon may occur due to fibers from the edges of the carbon paper crossing over the thin polymer membrane during melt pressing. Future experiments will require modulation of pressure during the melt pressing step to avoid this issue, and fabricating a control based on Nafion™ using

the same method will further elucidate the cause of this issue. Alternatively, gold foil may replace carbon paper as electrodes to form IPMCs.

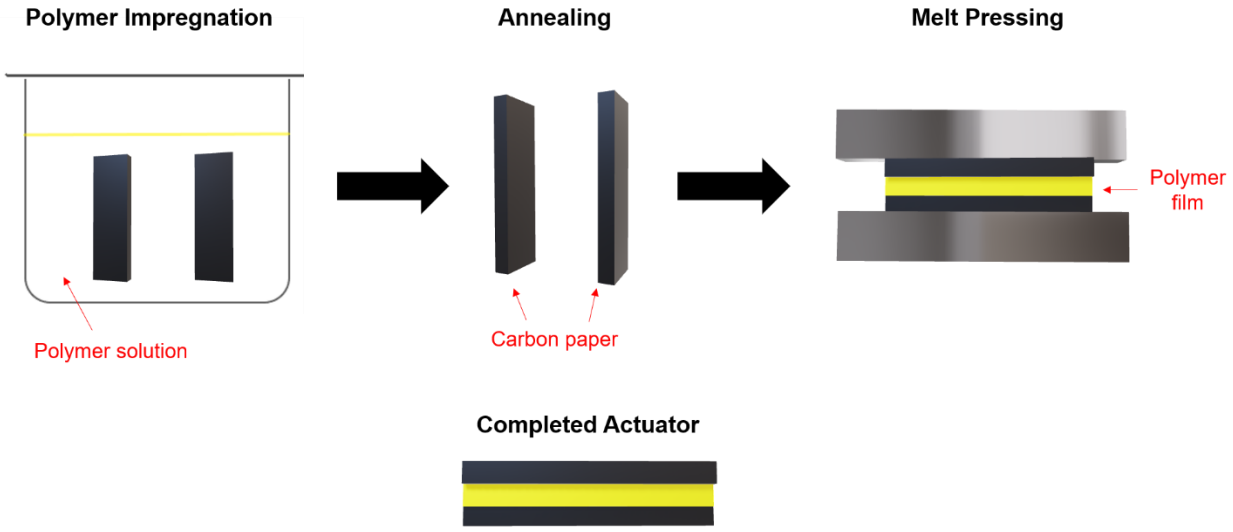


**Figure 10.3**: Fabrication of IPCCs using a sulfonated segmented PUs coated with carbon paper.

The phosphonium-functionalized poly(siloxane urethane) PSiU described in Chapter 7 may also find use in the future as a membrane for IPMCs or IPPCs. The ionic conductivity at room temperature measures relatively low at $10^{-8}$ S $cm^{-1}$, but literature examples have demonstrated the ability to produces actuators with conductivities in this range.[18, 19] Initial attempts to swell the PSiU with an imidazolium ionic liquid to improve conductivity proved unfruitful; the mass of the sample remained unchanged after soaking for 48 h in the ionic liquid. Further attempts to cast the PSiU with the IL failed due to the incompatible solubilities of the ionic liquid and PSiU with every organic solvent attempted. Attempting to swell the PSiU with a more hydrophobic ionic liquid may lead to better results, but the modulus of the swollen PSiU may drop to a level that makes actuator fabrication impossible. Increasing the amount of hard segment in the PSiU will help to improve the modulus of the material to allow for the accommodation of higher amounts of ionic liquid, however.

## 10.5 Segmented imidazolium ionenes

Current attempts to synthesize ionenes from a dicarbonylimidazole monomer (BBCI) have resulted in seemingly low molecular weight materials. However, the successful synthesis of polymer demonstrates promise for using this method to produce ionenes with unique backbone structures. Immediate future work on this project will involve attempting to measure the molecular weight of synthesized materials through size exclusion chromatography to prove that low molecular weight leads to the observed lack of mechanical properties. The lack of complete conversion as demonstrated through FTIR, especially for $PEG_{2k}$ ionenes, requires correction for the realization of high molecular weight polymers. One potential route forward involves replacing the PEG oligomers with poly(tetramethyl oxide) (PTMO). PEG is known to coordinate with anions in a crown ether effect, which may hinder the progress of the reaction, especially as the length of the PEG chain grows. Several previous studies have demonstrated the ability to form high molecular weight ionenes with PTMO SSs.[20, 21] Failure to produce high molecular weight ionenes from nearly identical starting materials as found in literature would point to a deficiency in the BBCI monomer to produce high molecular weight materials.

Another strategy to circumvent the incomplete conversion of imidazole to imidazolium in BBCI is to quaternize the imidazoles with a functional group first and then incorporate the imidazolium into a polyester or polyurethane. For example, Gao and Long *et al*. previously synthesized an imidazolium chain extender for conventional polyurethane synthesis.[22] Through this approach, reacting BBCI with an excess of 2-chloroethanol or a similar compound should provide a fully functionalized BBCI imidazolium ionic liquid (**Figure 10.4**) after purification to remove the unreacted monomer. This diol can then serve as a monomer for polyester or polyurethane synthesis. This imidazolium monomer will prove unique due to the incorporation of

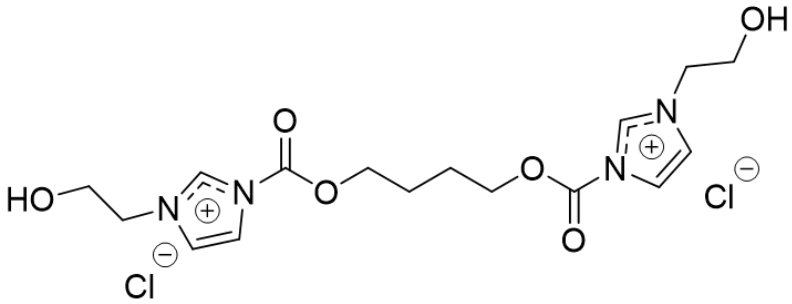


**Figure 10.4**: Structure of a proposed imidazolium diol derived from BBCI.

additional hydrogen bond acceptors (carbonyl) into the polyurethane or polyester backbone. If the solubility trends of the ionenes synthesized in Chapter 8 hold for this approach, utilizing this imidazolium monomer may impart water-solubility or dispersibility into the polymer it is incorporated into. Upon the achievement of high molecular weight polymer, the ionene should be subjected to an ion metathesis reaction to replace the counterion with a larger anion to enhance the ionic conductivity. Dependent on the modulus and electrical properties, these ionenes may prove suitable for electromechanical applications.

## 10.6 References


1. Dennis, J. M.; Steinberg, L. I.; Pekkanen, A. M.; Maiz, J.; Hegde, M.; Müller, A. J.; Long, T. E., Synthesis and characterization of isocyanate-free polyureas. *Green Chemistry* **2018,** *20* (1), 243-249.
2. Sirrine, J. M.; Schexnayder, S. A.; Dennis, J. M.; Long, T. E., Urea as a monomer for isocyanate-free synthesis of segmented poly (dimethyl siloxane) polyureas. *Polymer* **2018,** *154*, 225-232.
3. White, B. T.; Migliore, J. M.; Mapesa, E. U.; Wolfgang, J. D.; Sangoro, J.; Long, T. E., Isocyanate-and solvent-free synthesis of melt processible polyurea elastomers derived from urea as a monomer. *RSC Advances* **2020,** *10* (32), 18760-18768.
4. Lorenzini, R.; Kline, W.; Wang, C.; Ramprasad, R.; Sotzing, G., The rational design of polyurea & polyurethane dielectric materials. *Polymer* **2013,** *54* (14), 3529-3533.
5. Ertem, S. P.; Yilgor, E.; Kosak, C.; Wilkes, G. L.; Zhang, M.; Yilgor, I., Effect of soft segment molecular weight on tensile properties of poly (propylene oxide) based polyurethaneureas. *Polymer* **2012,** *53* (21), 4614-4622.
6. Wu, S.; Lin, M.; Burlingame, Q.; Zhang, Q., Meta-aromatic polyurea with high dipole moment and dipole density for energy storage capacitors. *Applied Physics Letters* **2014,** *104* (7), 072903.
7. Thakur, Y.; Lin, M.; Wu, S.; Cheng, Z.; Jeong, D.-Y.; Zhang, Q., Tailoring the dipole properties in dielectric polymers to realize high energy density with high breakdown strength and low dielectric loss. *Journal of Applied Physics* **2015,** *117* (11), 114104.
8. Thakur, Y.; Lin, M.; Wu, S.; Zhang, Q., Aromatic Polyurea Possessing High Electrical Energy Density and Low Loss. *Journal of Electronic Materials* **2016,** *45* (10), 4721-4725.

9. Cheng, Z.; Lin, M.; Wu, S.; Thakur, Y.; Zhou, Y.; Jeong, D.-Y.; Shen, Q.; Zhang, Q., Aromatic poly (arylene ether urea) with high dipole moment for high thermal stability and high energy density capacitors. *Applied Physics Letters* **2015,** *106* (20), 202902.
10. Wolfgang, J. D.; White, B. T.; Long, T. E., Non-Isocyanate Polyurethanes from 1,1'-Carbonyldiimidazole: An Activated Carbamate Approach. *Submitted for Publication* **2021**.
11. Sassmann, P. B.; Weichold, O., Preparation and characterisation of ion-conductive unsaturated polyester resins for the on-site production of resistivity sensors. *Ionics* **2019,** *25* (8), 3971-3978.
12. Schultz, A. R.; Lambert, P. M.; Chartrain, N. A.; Ruohoniemi, D. M.; Zhang, Z.; Jangu, C.; Zhang, M.; Williams, C. B.; Long, T. E., 3D Printing Phosphonium Ionic Liquid Networks with Mask Projection Microstereolithography. *ACS Macro Lett.* **2014,** *3* (11), 1205-1209.
13. Scott, P. J.; Rau, D. A.; Wen, J.; Nguyen, M.; Kasprzak, C. R.; Williams, C. B.; Long, T. E., Polymer-inorganic hybrid colloids for ultraviolet-assisted direct ink write of polymer nanocomposites. *Additive Manufacturing* **2020,** *35*, 101393.
14. Compton, B. G.; Lewis, J. A., 3D-Printing of Lightweight Cellular Composites. *Advanced Materials* **2014,** *26* (34), 5930-5935.
15. Siqueira, G.; Kokkinis, D.; Libanori, R.; Hausmann, M. K.; Gladman, A. S.; Neels, A.; Tingaut, P.; Zimmermann, T.; Lewis, J. A.; Studart, A. R., Cellulose Nanocrystal Inks for 3D Printing of Textured Cellular Architectures. *Advanced Functional Materials* **2017,** *27* (12), 1604619.
16. Gao, R. Synthesis and Properties of Ion-Containing Block and Segmented Copolymers and Their Composites. Virginia Tech, 2012.
17. Gao, R.; Zhang, M.; Dixit, N.; Moore, R. B.; Long, T. E., Influence of ionic charge placement on performance of poly (ethylene glycol)-based sulfonated polyurethanes. *Polymer* **2012,** *53* (6), 1203-1211.
18. Green, M. D.; Wang, D.; Hemp, S. T.; Choi, J.-H.; Winey, K. I.; Heflin, J. R.; Long, T. E., Synthesis of imidazolium ABA triblock copolymers for electromechanical transducers. *Polymer* **2012,** *53* (17), 3677-3686.
19. White, B. T.; Long, T. E., Advances in Polymeric Materials for Electromechanical Devices. *Macromol. Rapid Commun.* **2019,** *40* (1), 1800521.
20. Schreiner, C.; Bridge, A. T.; Hunley, M. T.; Long, T. E.; Green, M. D., Segmented imidazolium ionenes: Solution rheology, thermomechanical properties, and electrospinning. *Polymer* **2017,** *114*, 257-265.
21. Williams, S. R.; Salas-de la Cruz, D.; Winey, K. I.; Long, T. E., Ionene segmented block copolymers containing imidazolium cations: Structure–property relationships as a function of hard segment content. *Polymer* **2010,** *51* (6), 1252-1257.
22. Gao, R.; Zhang, M.; Wang, S. W.; Moore, R. B.; Colby, R. H.; Long, T. E., Polyurethanes Containing an Imidazolium Diol-Based Ionic-Liquid Chain Extender for Incorporation of Ionic-Liquid Electrolytes. *Macromolecular Chemistry and Physics* **2013,** *214* (9), 1027-1036.